KAUNAS UNIVERSITY OF TECHNOLOGY PANEVEZYS INSTITUTE
PANEVEZYS TECHNOLOGY AND SCIENCE PARK
WARSAW MOTOR TRANSPORT INSTITUTE
TALLINN UNIVERSITY OF TECHNOLOGY
RIGA TECHNICAL UNIVERSITY

INTELLIGENT TECHNOLOGIES IN LOGISTICS AND MECHATRONICS SYSTEMS

ITELMS'2009

PROCEEDINGS OF THE 4TH INTERNATIONAL CONFERENCE

EDITED BY Z. BAZARAS AND V. KLEIZA

June 04-05, 2009
Panevėžys, Lithuania

TECHNOLOGIJA
KAUNAS·2009

CONFERENCE IS ORGANIZED BY

Kaunas University of Technology Panevezys Institute
Panevezys Technology and Science Park
Warsaw Motor Transport Institute
Tallinn University of Technology
Riga Technical University

CONFERENCE IS SUPPORTED BY

State Fund of Science and Study of Lithuania

The proceedings of the 4th International Conference INTELLIGENT TECHNOLOGIES IN LOGISTICS AND MECHATRONICS SYSTEMS contain selected papers.

All papers were reviewed.

The style and language of authors were not corrected. Only minor editorial corrections have been carried out by the Publisher.

All rights preserved. No part of this publication may be reproduced, stored in retrieval system, or transmitted in any form or by any means, electronic, photocopying, recording or otherwise, without the permission of the Publisher.

© Kaunas University of Technology, 2009

CONFERENCE SCIENTIFIC COMMITTEE

CHAIRMAN
Prof. Z. Bazaras, Kaunas University of Technology, Lithuania

SCIENTIFIC SECRETARY
Prof. V. Kleiza, Kaunas University of Technology, Lithuania

MEMBERS
Dr. G. Badenes, Institute of Photonic Sciences, Spain
Prof. P. Balckars, Riga Technical University, Latvia
Prof. J. Bareišis, Kaunas University of Technology, Lithuania
Prof. P. Castro, Porto University, Portugal
Dr. J. Furch, Brno University of Defense, Czech Republic
Dr. V. Hutsaylyuk, Military University of Technology, Poland
Prof. I. Karabegović (Bosnia and Herzegovina)
Prof. J. Laugis, Tallinn University of Technology, Estonia
Prof. A. Levchenkov, Riga Technical University, Latvia
Dr. M. Litwin, Motor Transport Institute, Poland
Prof. V. Ostasevicius, Lithuania
Prof. Ribickis, Riga Technical University, Latvia
Prof. M. Sitarz, Silezian Technical University, TRANSMEC, Poland
Prof. A. Sladkowsky, Silezian Technical University, Poland
D. Sprečić (Bosnia and Herzegovina)
Dr. Ch. Tatkeu, Transport Electronics and Signal Processing Laboratory, France
Prof. V. Tilipalov, Kaliningrad State Technical University, Russia
Prof. B. Timofeev, St. Petersburg State Polytechnic Institute, Russia
Dr. D. Vinnikov, Tallinn University of Technology, Estonia

LOCAL ORGANIZING COMMITTEE
R. Bukėnas
V. Narbutas
E. Patapienė
Dr. D. Susnienė
Dr. A. Tautkus
Dr. D. Vaičiulis

4th International Conference
"INTELLIGENT TECHNOLOGIES IN LOGISTICS AND MECHATRONICS SYSTEMS"

Klaipedos str. 1, Panevezys LT-35209, Lithuania
http://internet.ktu.lt/en/scriptas1.asp?meniu=virsus3.html&pirmas=science/menu.html&antras=science/conf2009/conferences_2009.html

PREFACE

The first (2006) and second International Workshops “Intelligent Technologies in Logistics and Mechatronics Systems ITELMS” were held at Riga Technical University. The 3rd international workshop ITELMS'2008 was held at Kaunas University of Technology Panevezys Institute on 22 - 23 May, 2008. The 4th international conference ITELMS'2009 continues three year tradition and takes place at Kaunas University of Technology Panevezys Institute on 4-5 June, 2009.

The aims of the Conference are to share the latest topical information on the issues of intelligent technologies in logistics and mechatronics Systems. The papers in the Proceedings presented the following areas:

- Intelligent Logistics Systems
- Multi Criteria Decision Making
- Composites in Infrastructures
- Automotive Transport
- Intelligent applications of solid state physics
- Intelligent Mechatronics Systems
- Mechanisms of Transport Means and their Diagnostics
- Railway Transport
- Transport Technologies
- Modern Building Technologies

In the invitations to Conference, sent year before the Conference starts, the instructions how to prepare reports and manuscripts provided as well as the deadlines for the reports are indicated.

A primary goal of Conference is to present the highest quality research results. A key element in attiring goal is the evolution and selection procedure developed by the Conference Scientific Committee.

All papers presented in Conference and published in Proceedings undergo this procedure. Instruction for submitting proposals, including requirements and deadlines, are published in Call for Papers in the http://internet.ktu.lt/en/scriptas1.asp?meniu=virsus3.html&pirmas=science/menu.html&antras=science/conf2009/conferences_2009.html. Paper proposals must contain sufficient information for a trough review. All submissions to determine topic areas are directed to appropriate Topic Coordinators. The Topic Coordinators review the submissions much them to the expertise according to the interests and forward them to selected reviewers. At least two reviewers examine each submission in details.

Selection of papers for the Conference is highly competitive, so authors should assure their submissions to meet all Conference Scientific Committee’s requirements and to be of the highest possible quality.

All Conference participants prepare manuscripts according to the requirements that make our Proceedings to be valuable recourse of new information which allows evaluating investigations of the scientists from different countries.

Prof. Z. Bazaras
Prof. V. Kleiza

Contents

Proceedings of 4th International Conference ITELMS'2009

Method for Improvement of Electromagnetic Rail Brake Performance for Light Rail Vehicles

H. Hõimoja, J. Laugis, D. Vinnikov

Tallinn University of Technology, Department of Electrical Drives and Power Electronics, Ehitajate tee 5, 19086 Tallinn, Estonia, E-mail: dm.vin@mail.ee

Abstract

This paper introduces a novel solution for the performance improvement of electromagnetic rail brakes of a tramcar. The electromagnetic rail brakes are directly supplied from the onboard low-voltage power supply system (LVPS), whose reliability and operating performance becomes especially crucial from the point of view of passenger and road safety. An existing LVPS especially combined with outdated back-up batteries result in significant voltage drops, which can result in lack of the braking force available from electromagnetic brakes. This could be vital in some dangerous traffic situations, where the full braking effort should be applied. To solve these problems authors propose to implement the ultracapacitors in LVPS of light rail vehicles (and tramcars, in particular) for the compensating of voltage drops and covering the peak loads caused by applying of electromagnetic rail brakes. The method proposed could enhance the reliability of the LVPS of a city trams, resulting in performance improvement of the electromagnetic brakes. The simulations and experiments have confirmed that correctly chosen ultracapacitors integrated into existing auxiliary low-voltage supply can contribute to the significant improvement of electromagnetic rail brakes' performance.
KEY WORDS: *light rail vehicle, traction catenary, battery, ultracapacitors, control principles, efficiency analysis*.

1. Introduction

The use of ultracapacitors in electric traction power trains has not only been discussed in many papers, but also implemented in reality [1]. While this energy storage method cannot often be affordable in the main traction scale, it might contribute to enhancing the quality and reliability of the onboard low-voltage power supply system.

In the normal operation, an APS converter must ensure trouble-free operation of all the subsystems connected to it outputs. But in the case of crossing of catenary section disconnectors, when the output voltage of the APS converter drops to zero, all the secondary low-voltage systems are supplied from the tram back-up battery. After the disconnector, battery is refilled from the APS. It means that the onboard battery needs to have sufficient energy density (to provide constant power to such loads, like lighting, announcement systems, etc.) and high power density (for peak current demands, like emergency braking). Namely, the last criteria have raised many questions in several European tram- or LRV-companies. Based on the huge amount of investigations, it has been stated that namely the back-up battery is the weakest part on old and even on new trams. For instance, in winter with low outside temperatures, the productivity of the accumulator battery dramatically decreases, because of increased internal resistance, which, in turn, depends on the electrolyte's density. Further, with very low temperatures (-35 ^{0}C and lower), productivity is so low, that the battery even can not been charged. Finally it means that sometimes during section disconnectors and in the case of dangerous traffic situation, a tramcar driver is not able to stop the tram with the emergency (electromagnetic) brake because of the discharged back-up battery. Thus, rugged railway RAMS requirements are violated and it may cost sufficient penalties to the tramcar company [2].

2. Description of Existing Low-Voltage Power Supply System

Typically, the low-voltage power network of a tramcar is fed from catenary by means of a motor-generator or static DC/DC converter. Low-voltage loads comprise illumination, a passenger information system, safety, control and auxiliary drive circuits, as depicted in Fig. 1. The nominal output voltage U_{APS} of the APS is slightly higher than the predefined nominal value $U_{N,aux}$, which compensates the voltage drops caused by the long leads and allows charging of the main back-up battery. An onboard battery G1 is necessary to support some critical loads during the catenary power disruption or APS failure; these loads mainly comprise control and safety circuits like emergency lights and braking.

As the most widespread tram type in the former Warsaw Pact countries is ČKD KT4 produced between 1974 and 1997, further analysis is based on this model. With some modifications, primarily regarding traction drives and passenger information systems, these trams have not met any serious replacement plans. The standardized values for the onboard low-voltage supply system are specified in Table 1, where U_{min} is the minimum allowable short-term voltage [3].

The existing battery on a KT4 type tramcar is composed of 17 or 18 NiCd cells, 1.2 V each, as shown in Table 2. During the time of commissioning in the 1980s, these battery types were the only option with sufficient energy and power density.

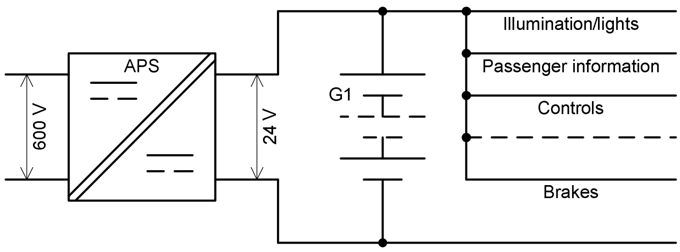

Fig. 1. Simplified representation of a low-voltage power supply system of a tramcar

Table 1

Standardized fluctuations in the secondary supply system of the KT4-type trams

$U_{N,aux}$, V	U_{APS} , V	U_{min} , V
24	26.4	17.0

Table 2

Specifications of the onboard battery of KT4-type trams

Characteristic	Cell	Battery	
Type	NK-125	17 cells	18 cells
Nominal voltage, V	1.2	20.4	21.6
Minimal voltage, V	1.0	17	18
Float charging voltage, V	1.4	24	25
Capacity, Ah	125		
Internal resistance at full charge, mΩ	0.32	5.44	5.76
Temperature range, °C	-40...+40		
Rated service life	10 years		

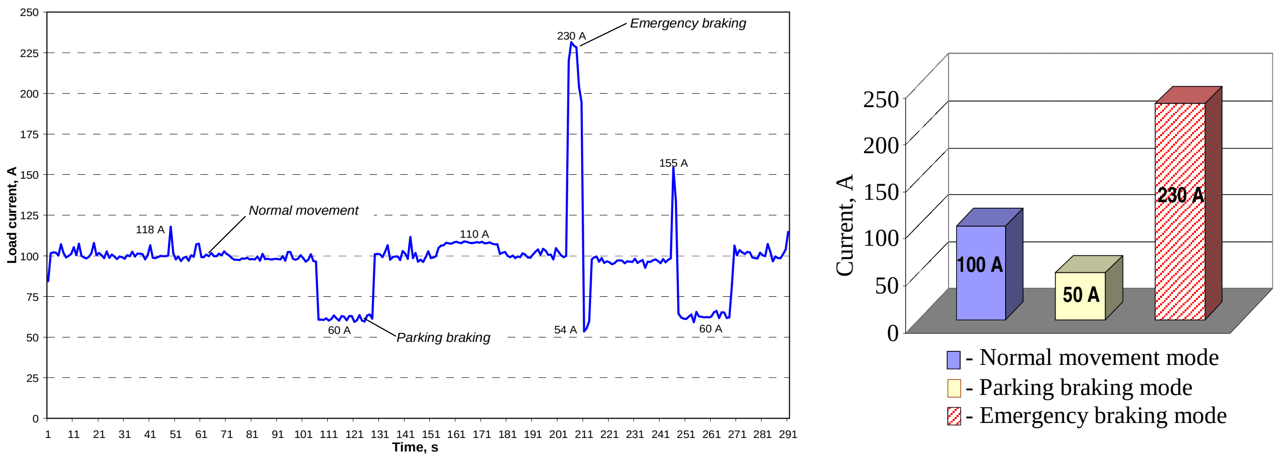

a b

Fig. 2. Low-voltage loads under different operation modes

It must be mentioned here that with few exceptions, the existing batteries were installed in Soviet times and have therefore exhausted their rated capabilities, expressed by increased internal resistance and decreased capacity. As for recently procured trolleybuses, mostly modern gel-type lead-acid batteries are used with overdimensioned capacity due to less specific power compared to NiCd. However, the properly chosen gel-type batteries show similar service time and energetic performance with approximately three times smaller cost and less environmental issues.

During the operation of a LRV in the city traffic conditions different low-voltage loads may be switched on and off very randomly. For instance, in the LRV ČKD KT4 for braking at low speeds and for the parking brake, the mechanical pad-brakes with solenoid drives are used. During normal movement, solenoids are in the involved position, consuming a current of about 40 A. When the mechanical brakes are applied, the current in the solenoids is reduced to 25-40 A, depending on the position of the braking pedal (Fig. 2*a*). To simplify the further discussion, the average operational cycle of a LRV can be divided into three most demanding operation modes (applicable to the load of the onboard APS): normal movement mode, parking braking mode and emergency braking mode. Each of those is characterized by its averaged current consumption as shown in Fig. 2*b*.

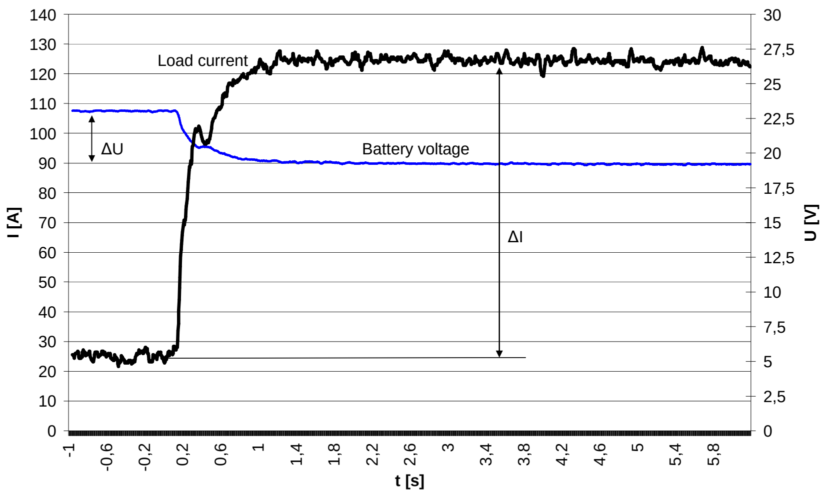

Fig. 3. Battery terminal voltage change during the emergency braking mode

Concerning a LRV, the most demanding operating mode is the emergency braking mode, when the electromagnetic rail brake is applied. At full brake effort the maximal load current in several cases could achieve 230 A, but typically the values of load current lie in the range of 120…150 A. To analyze the behavior of low-voltage power supply system at the emergency braking mode the series of measurements was performed. The terminal voltage of the onboard back-up battery as well as the load current were measured and recorded during the selected time intervals. The experimental results are presented in Fig. 3. The curves in Fig. 3 display a significant voltage drop, which is greater than might be assumed from the series internal resistance value provided in Table 2.

The voltage and current changes ΔU and ΔI, respectively, shown in Fig. 3 allow us to calculate the actual internal resistance R_{bat} of the onboard battery stack:

$$R_{bat} = \frac{\Delta U}{\Delta I} . \tag{1}$$

In our case, ΔU = 3.8 V and ΔI = 99 A, so R_{bat} = 38.3 mΩ. This value is much higher than shown in Table 2, which can only be explained by the ageing of a battery.

3. Proposed Optimization Possibility

As an optimization possibility of onboard low-voltage power supply system with back-up battery in such demanding conditions and peak power requirements, the use of ultracapacitors in the secondary low-voltage power supply bus of the tramcar in combination with the onboard back-up battery is proposed, as depicted in Fig. 4. For reliability and response time considerations, no interface converters were implemented.

Sizing of Ultracapacitors. For the maximal improvement of peak load performance the ultracapacitors should be chosen correctly. First, the necessary capacity must be derived from peak load characteristics. Secondly, a selection can be made from among the commercially available products suitable for rolling stock applications.
The emergency braking is a process with rapidly changing dynamics with a duration ≤ 6 s, depending on the initial speed and limited to safe deceleration rates. In an ideal case, the design of the onboard combined energy storage system must be coordinated so that peak loads can be supplied by the energy storage without reducing the operating voltage U_{aux} below the accepted minimum U_{min}.

The electromagnetic brake can be modeled as an equivalent RL load with resistance R_{br} and inductance L_{br}. Referring back to Fig. 3, we can calculate R_{br} including wiring:

$$R_{br} = \frac{U_2}{I_2} - R_{bat} , \tag{3}$$

where U_2 and I_2 are battery terminal voltages and current under peak load respectively. After assigning parameter values, we get R_{br} = 120 mΩ.

The ideal braking current I_{br} with eliminated internal resistance would be much higher and depend only on R_{br} and rated system voltage $U_{N,aux}$ = 24 V. Application of Ohm's law gives for I_{br} = 200 A. Inductance of electromagnetic rail brake L_{br} can be calculated by

$$L_{br} = \tau \cdot R_{br} , \tag{4}$$

where τ = 0.4 s is the time constant estimated from Fig. 2. Energy W_{br} consumed during braking is expressed by

$$W_{br} = U_{N,aux} I_{br} t_{br} , \tag{5}$$

where t_{br} is the duration of a braking event. Accordingly, the amount of energy consumed during a 6 s braking process W_{br} = 28.8 kJ. The value of capacity required from an ultracapacitor for the compensation of a random peak load can be estimated by

$$C = \frac{2W_{br}}{U^2_{N,aux} - U^2_{\min}} . \tag{6}$$

Replacing variables in (6) with numbers given in Table 1, gives C = 200 F. From the variety of vendors and different ultracapacitor types commercially available, the BMOD0500 P016 ultracapacitor modules from Maxwell Technologies were selected for the current application, whose technical specifications are presented in Table 3. For matching the operating voltage and necessary capacitance, two modules were connected in series.

With the total weight of 11.5 kg and overall dimensions of 416 mm x 134 mm x 157 mm (L x W x H), the installed module would have no serious impact on the total volume occupied by the combined onboard storage system.

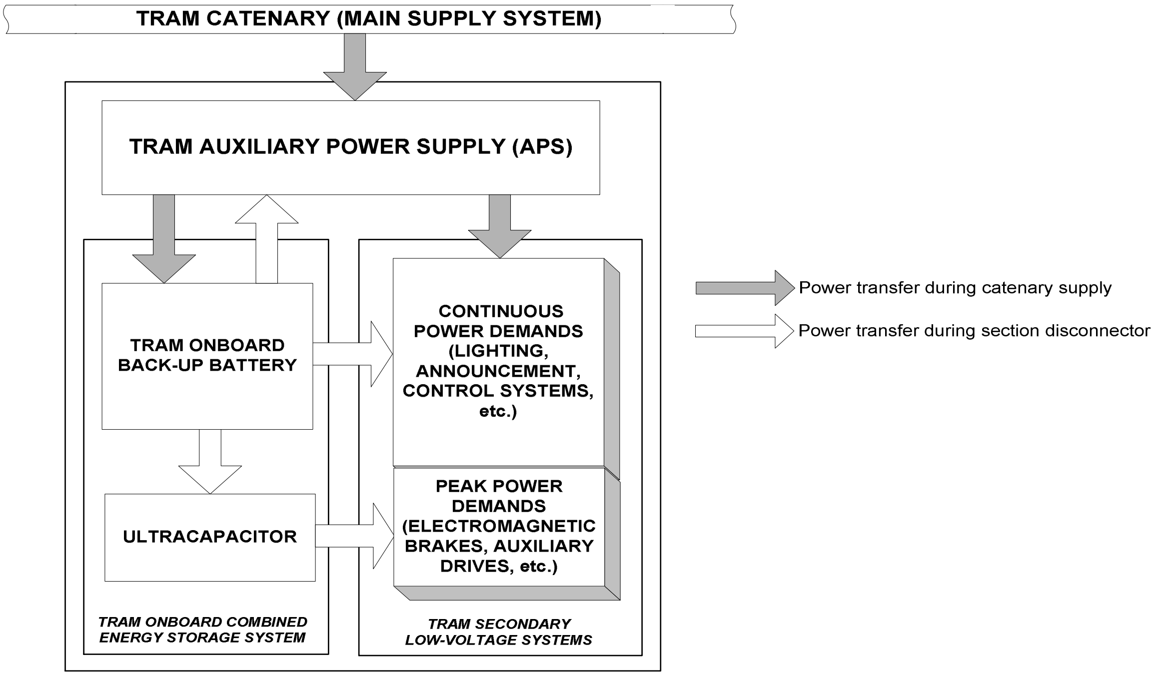

Fig. 4. Proposed structure of an upgraded auxiliary low-voltage supply system

Table 3

Specifications of selected nnnultracapacitor modules [4]

Characteristic	Module	Set
Rated voltage, V	16.2	32.4
Capacitance, F	500	250
Internal series resistance, mΩ	2.4	4.8
Energy density, Wh/kg	3.17	
Power density, W/kg	6700	

4. Simulations and Experimental Results

To verify the results of calculations, a software model was developed in *Simulink* environment. Simplifications and substitutions were made as follows:

1. the NiCd battery is modeled as a series connection of an ideal voltage source U_0 = 24 V and internal resistance R_{bat} = 38.3 mΩ [5];
2. the electromagnetic rail brake is modeled as an equivalent RL circuit with parameters R_{br} = 120 mΩ and L_{br} = 48 mH;
3. the ultracapacitor set is represented by a series connection of an ideal capacitance C and a resistor R_{UC} based on the values presented in Table 3;
4. normal loads while running and braking are represented by equivalent resistors.

The resulting simulation diagram and simulation results are shown in Fig. 5*a*. As seen from Fig. 5*b*, the low voltage system's performance increases remarkably. In the beginning, the braking current reaches 180 A and then starts slightly falling. Both storage devices are involved in energy exchange with a decreasing contribution of the ultracapacitors and an increasing load on the main battery. During 6 s emergency braking, the system voltage falls down to 20 V.

To verify the theoretical assumptions and simulation results the test system with ultracapacitor module was installed on tramcar KT4. The ultracapacitor modules used in experiment were the PCM14014 from Maxwell Technologies. The modules were connected in series with resulting terminal voltage of 28 V and capacitance 75 F. Due to limited choice of ultracapacitors available for the experiment the capacitance of installed stack was about 60% smaller than required. The ultracapacitor stack (C1+C2) was connected in parallel to the onboard back-up battery G1, as shown in Fig. 6. During the experiments the APS was disconnected from the supply grid (catenary free operation).

Although the experimental results (Fig. 7.) show that the ultracapacitors available are underdimensioned for the current application, they give some hints for further assumptions. The battery terminal voltage decrease rate during a braking with 6 s duration is no more defined only by electromagnetic brakes inductivity, but also by additional charge delivered by the ultracapacitor set. While the ultracapacitors discharge, the battery's contribution to a peak load supply increases. After the electromagnetic rail brake is released, the ultracapacitors start to recharge either from the APS or the main battery. The charging current i_C depends on the auxiliary voltage U_{aux}, total capacitance C, initial capacitor terminal voltage U_{C0} and an equivalent resistance R_{eq} including wiring, battery's and ultracapacitors internal resistances

$$i_C = \frac{U_{aux} - U_{C0}}{R_{eq}} \exp\left\{-\frac{t}{R_{eq}C}\right\}. \tag{7}$$

The differences between the experimented battery and the combined back-up supply powering the electromagnetic rail brake are summarized in Table 4. Obviously the increased current contributes to the additional braking force, depending on the brake's magnetization curve. The more limited the voltage drop, the better is emergency braking performance.

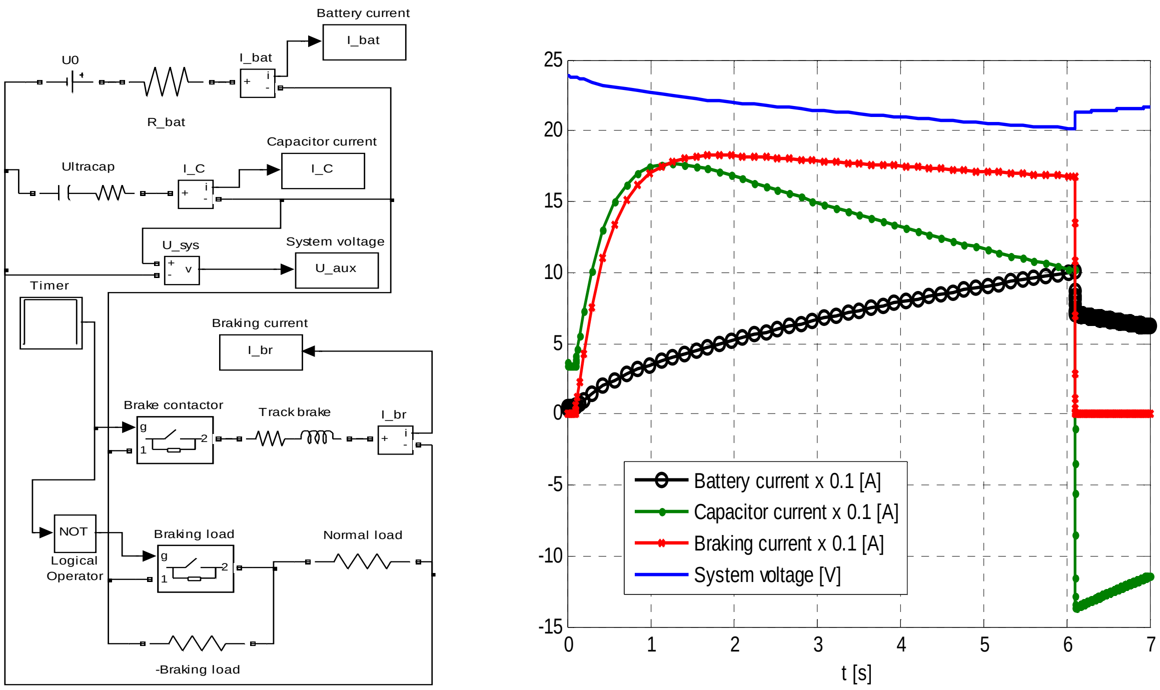

a b

Fig. 5. Battery/ultracapacitor supply simulation diagram (a) and simulated currents and battery voltage with combined battery-ultracapacitor storage (b)

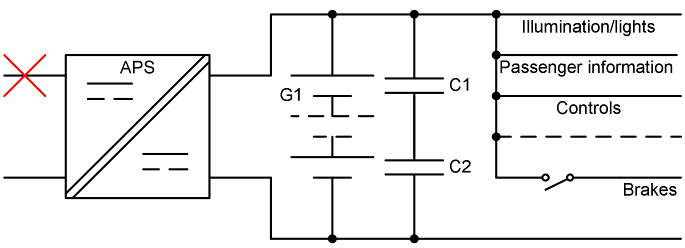

Fig. 6. Experimental setup with ultracapacitors in parallel with main back-up battery

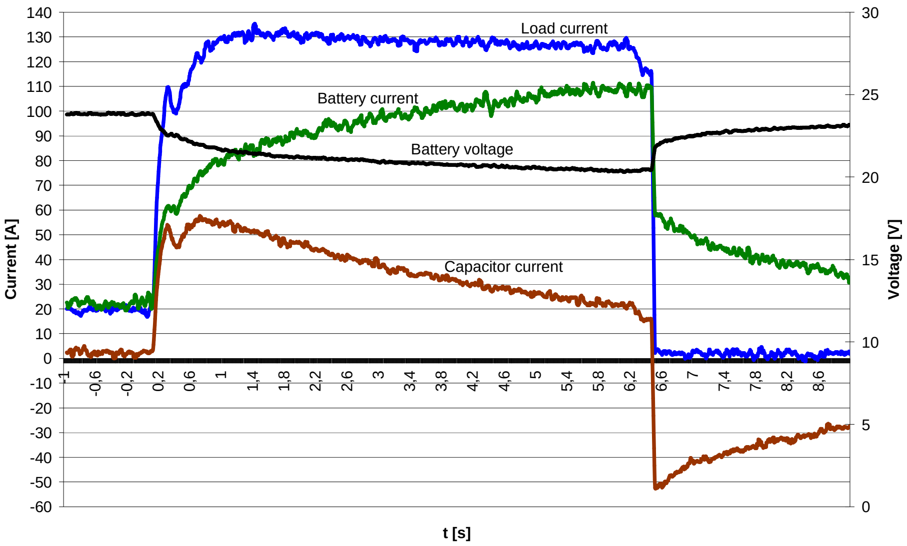

Fig. 7. Experimental results with PCM14014 ultracapacitors

Table 4

Comparison of experimented back-up energy storages

Parameter	Battery	Battery + ultracapacitor
Final voltage, V	19.2	20.3
Load current, A	125	130

5. Conclusion

The simulations showed that the performance of existing onboard low-voltage auxiliary power supply could be remarkably improved by adding an ultracapacitor module in parallel to the main battery. With a correctly chosen ultracapacitor module, the computed braking current reached its maximum value and system voltage drop was found more limited than before. With higher current, the emergency electromagnetic rail brakes provide more braking force. Moreover, the power demands of other peak loads of a tramcar, like door drives and disc brake solenoids, can be more effectively satisfied. Ultracapacitors in the low-voltage power supply (LVPS) bus of tramcars offer the following advantages:

1. improvement of efficiency and reliability of the emergency braking system especially at cold temperatures
2. better efficiency of LVPS;
3. performance optimization possibility of other onboard devices;
4. possibility of reduced main back-up battery size;
5. prolonged main back-up battery life;
6. reduced maintenance costs of the combined onboard storage system.

To minimize voltage drops and increase the efficiency of the proposed solution, the ultracapacitors should be carefully chosen and placed preferably as close to the peak load as possible. Simulations must be followed by experiments on real vehicles, after which practical results with different coupling topologies, main back-up battery minimization possibilities can be analyzed and the efficiency and feasibility analysis of the developed combined energy storage system under different climatic conditions can be made.

References

1. **M. Steiner, M. Klohr.** Energy storage system with ultracaps on board of railway vehicles, Proceedings of 2007 European Conference on Power Electronics and Applications, Sept 2-5, 2007, 10 p.
2. **D. Vinnikov.** Research, Design and Implementation of Auxiliary Power Supplies for the Light Rail Vehicles", Ph.D. dissertation, Dept. El. Drives Pow. Elec., Tallinn Univ. Tech., Estonia, 2005.
3. IDT EN 50155:2007. Railway applications - Electronic equipment used on rolling stock.
4. Maxwell Technologies Inc.: BMOD0500-16.2V Ultracapacitors, www.maxwell.com.
5. **J. V. Mierlo, P. V. D. Bossche, G. Maggeto.** Models of energy sources for EV and HEV: fuel cells, batteries, ultracapacitors, flywheel and engine-generators. Journal of Power Sources, No. 4, 2004, p. 76-89.
6. **H. Hõimoja, D. Vinnikov, R. Strzelecki.** Application of Ultracapacitors in Low-Voltage Power Supply Systems of Light Rail Vehicles. The 2009 World Congress on Electronics and Electrical Engineering, WCEEENG'09; Cairo, Egypt, April 6-8, 2009.

Classification of Rail Flaws Using Cepstral Detection

V. Gargasas, A. Knyš

Department of Control Technology, Kaunas University of Technology, Studentu str. 48-325a, LT-51367 Kaunas, Lithuania, E-mail: andrius.knys@ktu.lt

Abstract

Various ultrasonic diagnostic methods are widely used to detect internal rail flaws. Despite modern equipment implemented to examine the rail, most of the systems are not capable to run diagnostics and classification in real time. In this work an implementation of signal cepstrum analysis is surveyed and the experiments that give fast-track results are presented. This work presents experimental data of a rail diagnostic using ultrasonic signal and its cepstral analysis. The results show that it is possible not only to detect internal rail flaws using ultrasonic diagnostics, but also it is possible to determine what kind of a flaw – large and dangerous crack or a small one is present. These results show a possibility to implement a real-time diagnostic and classification system.
KEY WORDS: *rail flaws, ultrasonic diagnostics, cepstrum, detection, classification.*

1. Introduction

For a present time various ultrasonic diagnostic methods are widely used to diagnose metal construction condition and to evaluate internal defects or flaws. Several different ultrasonic diagnostic methods exist. The use of them is determined by a geometrical characteristic of an investigated object. As the computer and microprocessor units improve, more and more possibilities to measure complex signals occur allowing to implement and use more complex algorithms or functions to process the experimental data. New systems to collect and process diagnostic data are created and the hardware of defect scopes is improved, depending on a geometry/shape of an analysed object, test speed, precision of results.

One of the most important objects that ultrasonic diagnostics are used on is rail. The condition of a rail has a direct influence on a railroad safety. The rail is significantly stressed during exploitation. This causes various flaws inside the rail that may cause rail break and affect the traffic safety. The rail break is the main reason of railroad accidents and this makes up to 30% of all total accidents.

Main requirements to rail diagnostic system are:

1. A reliable detection of rail flaws. The riskiness of the flaw is described by few parameters, such as: clearance of the flaw, orientation inside the rail, character of the flaw;
2. Maximum testing speed. In order to check all the rails in use and minimizing staff and equipment, the most of the test speed is required.

The shape of the rail determines the way of testing it. The contact between the ultrasonic sensor and the rail is possible only on the top of the rail crown. In this case the method to examine the rail is called "echo method": a short ultrasonic excitation signal is transmitted from the sensor on the top of the rail and then system is switched to a reception mode and records the echo of the signal. Depending on an orientation of the flaw, the signal can be transmitted at different angle relating to the horizontal axis of the rail. Analysing the shape amplitude and delay of the received signal gives us information on parameters of the flaw and the distance to it. In order to collect information on the flaw that is greater than a critical threshold of the flaw, the ultrasonic wavelength used has to be shorter than a flaw clearance. According to this a testing frequency is assorted.

To achieve a maximum testing speed is necessary to estimate testing duration and a maximum distance between neighbouring test points. Testing duration depends on a speed of ultrasonic waves spreading inside metal construction and on a path length of transmitted and echoed signals. The distance between neighbouring test points is determined by requirements on a minimal flaw that must be detected. The step should not be longer than minimal flaw. In this case the pathway of the transmitted ultrasonic signal will travel through a flaw.

As maximal parameters of innocuous crack and travel speed of ultrasonic signal in rail (c = 3260 m/s) are known, the minimal frequency of ultrasonic signal is calculated: f_{US} = 2.5 MHz. The path length of the ultrasonic signal in a type R50 rail is q = 0.65 m and the signal travelling time is 92 μs (sometimes the pathway may be shorter, depending on detector angle or rail part investigated: the crown, neck or heart). In this case as the defect scope travels along the rail at speed of 11.1 m/s (40 km/h) and testing at 0.005 m interval, the measurement period is T_M = 450 μs (f_M = 2.2 kHz). Using digital converting system, the reflected signal is recorded in each step with analogue-to-digital converter that has a sampling frequency f_{AD} few times higher than the ultrasonic frequency used. If f_{AD} of 20 MHz is used, then each array of recorded data will consist of 1840 elements. Depending on analogue-to-digital converter resolution the data flow rate will be: $i_{8\text{bit}}$ = 32.7 Mbit/s, $i_{12\text{bit}}$ = 49.1 Mbit/s, $i_{16\text{bit}}$ = 65.4 Mbit/s. To process the data in real time the according methods have to be developed.

In practice to minimize data flow rate the convex of the reflected ultrasonic signal instead of the signal itself is analyzed. Despite this, it is not enough to automate the diagnostic process and detect rail flaws in real time, so various signal processing algorithms are implemented.

2. Rail Diagnostic Methods

The most common defect is a crack that develops in the crown of the rail, at an angle of approximately 70° relative to the horizontal axis. It is known as a kidney defect, because of its shape. Various methods have been developed to detect the defects and the most commonly used is an ultrasonic system, which transmits an acoustic signal into the rail and measures the reflection of the waves from the defect. This is a effective method, but requires scanning of the complete rail on a regular basis and so it is very labour and intensive. Motorized vehicles, equipped with such ultrasonic measurement equipment, are employed to increase the frequency and efficiency of defect detection.

Some known kind of detection system is based on three ultrasonic probes. The probes are used to detect two families of cracks in the rail. One probe, called 0° probe, is intended to find horizontal cracks and two probes, called 68° probes, are intended to find transversal cracks with a 68° theoretical mean orientation of running surface. Ultrasonic probes emit an acoustic wave which travels in the rail in a specific direction. The wave flows without reflection until the material is homogeneous. So if the crack is perpendicular to the direction of wave propagation, the reflective wave comes back to the probe which records an ultrasonic echo called A-scan. Most of industrial non destructive control systems are based on this kind of visualization. All the detection procedures of the automatic inspection train are based on this signal.

Article [1] describes a new idea is to work on an accumulation of successive A-scan signals which form in fact an image. This image is called B-scan. It keeps the geometrical coherence of the defect taken advantage during the processing and leads to a better noise immunity. So the crack is seen in its whole structure and none as a limited signal reaching a threshold.

The Radon transform is a process adapted to detect lines in an image [2]. It proceeds by projecting all the pixels onto a turning axis centred in the image. Neural networks can be viewed as a type of "black box" which can be used to take a set of inputs describing an object, such as a bolt hole, and classify these inputs as belonging to one of several possible categories. In this research, various features were selected from bolt hole transducer returns and were used as inputs to the neural networks. The networks then classified each set of inputs as representing a "good" bolt hole (BH) or a "bad" (defective) bolt hole. B-scan processing has the advantage to keep the geometrical coherence of the defect during the inspection although an A-scan signal is only a part of the global response of the defect. Cracks appear as a line in the image with different intensities, the angle corresponds to a 68° transversal crack.

The basic architecture of the neural networks used in research of bolt whole. The networks are called backpropagation networks and consist of three layers of nodes; the input layer (I), the hidden layer (H), and the output layer (O) respectively. Weighted arcs connect each node in a parent layer to each of the nodes in the following layer [3].

Features for a specific bolt hole sample are introduced to nodes in the input layer. The neural network has 45 inputs. These inputs are then pronpagated through the network to produce an output at each of the output nodes. The node with the highest output represents the decision of the network as to whether the inputs represent a good or a defective bolt hole.

Initially, each network must be "trained" to recognize good bolt holes from defective ones. This is done by taking a set of BH features for which the classification is known. Each of these features is introduced to the network and the outputs are compared with the desired outputs.

Once the network is trained, it can be used to recognize new inputs for which the classifications are not known. This is done by introducing the input features for a bolt hole at the input layer of the trained network and noting the values produced at the output nodes. The node with the highest output indicates the network classification. The value of the highest output along with the difference between the values of the output nodes are indicators of how certain the network is about the classification.

The result of the described implemented methods is that B-scan is more effective than the A-scan. This is because the attributes that describe the flaw in B-scan are classified more precisely than the A-scan ones.

Anyway, the image creation in B-scan mode and the implementation of the neural network takes quite a long time even using modern systems and is not capable to process all the data in real-time.

In [4] a new signal classification method based on a co-variation matrix is presented. Here the signal collected during analysis is taken as an accidental process. Then two kinds of covariance metrics are defined. Covariance functions are very simple to rate and to get rate set covariance functions. Identity functions can be used to compare (separate) characteristics and then the covariance metric is defined like distances.

In order to widen the possibilities to process ultrasonic signals and ways to separate informative features of the signal, a possibility to use the signal cepstrum analysis is surveyed.

3. Cepstrum Analysis to Detect Rail Flaws

The complex cepstrum $\hat{x}$ for a sequence x is calculated by finding the complex natural logarithm of the Fourier transform of x, then the inverse Fourier transform of the resulting sequence [5].

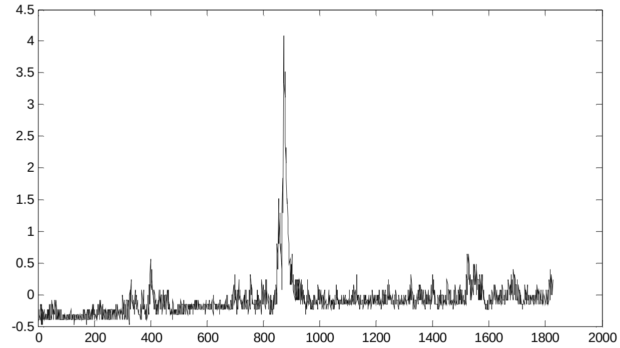

Fig. 1. Echo of the signal in a “healthy” rail

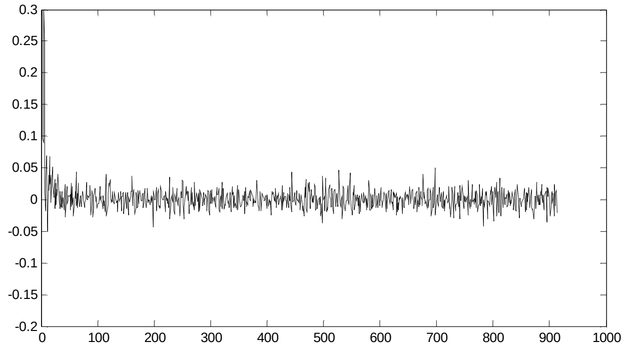

Fig. 2. Cepstrum of a signal Fig. 1

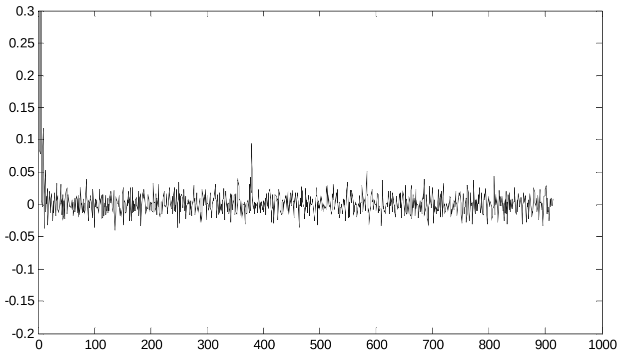

Fig. 3. Cepstrum of the reflected signal (“large” crack)

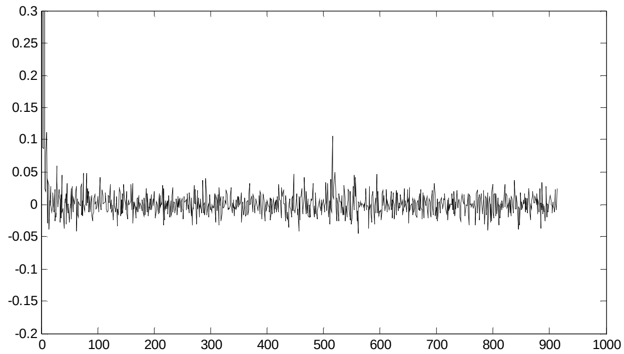

Fig. 4. Cepstrum of the reflected signal (“small” crack)

The cepstrum can be seen as information about rate of change in the different spectrum bands. It is now also used as an excellent feature vector for representing the human voice and musical signals [6].

$$\hat{x} = \frac{1}{2\pi} \int_{-\pi}^{\pi} \log\left[X\left(e^{j\omega}\right)\right] e^{j\omega n} d\omega. \tag{1}$$

In our case the recorded ultrasonic signal from a “healthy” rail is presented in Fig. 1 and the cepstrum of it is presented in Fig. 2.

We can see in Fig. 1 that there is only an echo of the transmitted signal coming from the bottom of the rail. And the cepstrum of it is almost straight line without significant peaks showing any change in spectrum bands.

Fig. 3 shows significant peak that is subject to a crack inside the rail which causes a reflection of the signal from that crack. All the energy of the signal was reflected from a large crack and none of it passed down to the bottom.

In Fig. 4 we observe peaks that are caused by an echoed signal from crack inside the rail. Here part of the signal energy reflects from the crack and another part passes the crack and reflects from the bottom of the rail.

The research shows that the cepstrum of recorded signal may help to determine whether the rail has cracks inside or not. If the cepstrum shows significant peaks it may be caused by the signal reflection from an internal rail flaw/crack. These peaks can be taken as informative marks for a further processing and determination of the flaw type. In our case if the peak is higher than 0.05 then an internal flaw is present. As the analysed data array is not big (less than 2000 elements) implementation of fast Fourier transform is possible and may provide fast and reliable diagnostic results. This gives a possibility to process the data in real time providing an improved railway inspection system.

4. Classification of a Flaw

During the experiment a set of signals, representing one of the classes of the internal flaws, were recorded:

- Class A: a signal reflection from a large dimensions internal crack;
- Class B: a signal from a healthy rail;
- Class C: a signal reflection from a small dimensions internal crack.

Having a purpose to refer an unknown signal to one of the prescribed classes, it is convenient to use a geometrical classifier. To use it an informative signs have to be determined. We chose a system with two informative signs (x_1, x_2) that describe coordinates of cepstrum peaks. In order to have the signs x_1 and x_2 of the same range, the x_1 has to be multiplied by n = 10000. In this case the plot of the investigated signals is as shown in Fig. 5.

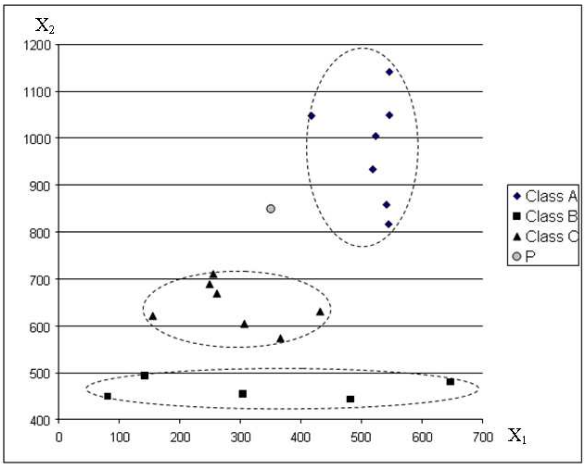

Fig. 5. Plot of the signal classes (Class B – healthy rail, Classes A and C – damaged rail)

Fig. 5 shows that peak of the signal cepstrum of a healthy rail is not significant and its position on an x1 axis is not determined. Class A signal peaks are positioned in a quiet narrow range on x1 axis, but x2 range is much wider.

Using a metric plot which describes different signal classes allows to refer a signal of an unknown class to one of the prescribed. This allows determining if it is one of the serious cracks and what a danger arises.

In a geometrical classifier to recognize an object or process and classify it a method of proximity is used (2).

$$S\left(x, y^m\right) = \frac{1}{M}\sum_{m=1}^{M} d^2\left(x, y^m\right) \tag{2}$$

where $x = \{x_1, ..., x_N\}$: coordinates of an object that is to be determined; $y^m = \{y_1^m, y_2^m, ..., y_N^m\}$: coordinates of a set of known signal class.

The investigated object is referred to a class which is the nearest one, i.e. the class that has the minimum square distance from the object investigated (3).

$$d^2\left(y_{mi}; y_{mj}\right) = \frac{1}{M_m\left(M_m - 1\right)}\sum_{i=1}^{M_m}\sum_{j=1}^{M_m} d^2\left(y_{m_i}; y_{m_j}\right) = \min \tag{3}$$

where y_{m_i} : *i*-reference of M-class.

5. Conclusions

Signal cepstrum analysis is useful to detect internal rail flaws using ultrasonic diagnostics.

Cepstrum itself does not provide information about a type of a flaw, but can be used as a significant parameter determining a class of flaw (i.e. using geometrical classifier).

As the data processing time using fast Fourier transform is minimized, it gives a possibility to implement a real-time diagnostic and classification system.

References

1. **Cygan H., Girardi L., Aknin P., Simard P.** B-scan ultrasonic image analysis for internal rail defect detection. WCRR Edinburgh Scotland, 2003, p. 57-63.
2. **Salazar A., Gosálbez J., Bosch I.** Reconstructing Ultrasonic Images and Flaw Detection in Timefrequency Domain by Matching A-scan Inspections. Eusipco 2005 - CDROM Proceedings 2005, p. 1-5.
3. **Guangde S., Xianglin Z., Hui Z.** An Intelligent Instrument for Ultrasonic Nondestructive Examination Flaw Inspection of Rails. Congress on Intelligent Control and Automation. - Hangzhou, China, 2004, p. 3632-3635.
4. **V. A. Buinevičius, V. Gargasas.** Geležinkelio objektų būklės įvertinimas atsitiktinių procesų klasifikavimo metodu // Elektronika ir elektrotechnika 2004, Nr. 4(46), p .86-89.
5. **Childers D. G., Skinner D. P., Kemerait R. C.** The Cepstrum: A Guide to Processing // Proceedings of the IEEE, 1977, Vol. 65, No. 10, p. 1428-1443.
6. **Bogert B. P., Healy M. J. R., Tukey J. W.** The quefrency analysis of time series for echoes: cepstrum, pseudo-autocovariance, cross-cepstrum, and saphe cracking. Proceedings of the Symposium on Time Series Analysis (M. Rosenblatt, Ed) Chapter 15, New York: Wiley, 1963. p. 209-243.

Proceedings of 4th International Conference ITELMS'2009

Oxygenated Diesel Fuels: Physical–Chemical Properties and Exploitation Characteristics

Z. Bazaras*, L. Raslavičius**

**Department of Transport Engineering, Kaunas University of Technology Kęstučio g. 27, LT–44025, Kaunas, Lithuania. E–mail: Zilvinas.Bazaras@ktu.lt*
***Institute of Agriculture Engineering Lithuanian University of Agriculture, Instituto str. 20, LT–54132, Raudondvaris, Kaunas region, Lithuania. E–mail: Laurencas.Raslavicius@gmail.com*

Abstract

This paper continues the presentation of complex experiment results on direct injection diesel engine (combustion chamber consists of a dished piston) which were carried out at the Institute of Agricultural Engineering LUA while using blends of mineral diesel (D) and rapeseed methyl ester (RME) with dehydrated ethanol (E) additives as a fuel. Immediately communicating with the farmers about the purpose of bio–based fuels, also preparing D–RME–E exploitation manual we deal with the lack of scientific data about physical–chemical characteristics of the mentioned blends. Thus far obtained positive on–field experiment test data about investigated three–component fuel blends motor characteristics were extended by the laboratory tests and theoretical calculations.
KEY WORDS: *D–RME–E blend, BE–diesel, physical–chemical properties, oxygenated fuels, ethanol.*

1. Introduction

The blend levels of biodiesel and petroleum diesel fuel that have been recommended by crude oil refineries in EC market suggest that no engine modifications will not be necessary if use a 5% RME additive. Increased amount of biodiesel in D/RME blend directly affects the change of combustible compound characteristics of those two types of fuel of different origin [1–3]. Schumacher [4] reported physical and chemical properties associated with the mixing of biodiesel with petroleum diesel fuel. Some of these properties were nonlinear in nature; however, the analysis conducted by Schumacher did not reveal data points that were lower than either of the parent blendstocks (biodiesel or petroleum diesel fuel). Changing these chemical and physical properties to meet the needs of the biodiesel user may be needed for some of these attributes. Issues such as cetane number, viscosity, density and solubility have only recently been investigated by biodiesel researchers. The preliminary findings are quite good; however, as pointed out by Krahl [5] variation could exist due to the fact that some engines are fueled with different biodiesel feedstocks. Krahl only examined 100% neat biodiesel from rapeseed. No attempt was made to determine if another feedstock or if blends of biodiesel and petroleum diesel would exhibit similar benefits. Krahl also observed that the size of the PM when fueling with biodiesel was larger than when fueling with petroleum diesel fuel.

Otherwise, if disregarding that biodiesel has energy values comparable to those of fossil fuels and has superior lubricity and environmentally friendly characteristics, must admit that when mixing it with mineral diesel, a cetane number has a tendency to increase [6–8]. This determines worsened quality of combustion process, which directly affects on increased fuel consumption and emission level of nitrogen oxides. One of the methods to avoid the above mentioned negative effects is the use of a dehydrated ethyl alcohol additive (hereafter – ethanol) in mineral diesel and rapeseed methyl ester blends [2; 3].

2. Testing Procedures

2.1. Cetane Number and Ignition Delay Time

Two oxygenated biofuels (biodiesel and ethanol) have received intensive attention as potential alternative fuels for vehicle engines due to their renewable property and reduction of fossil CO_2 discharge which most probably contributes to the global climate changes. D–RME–E is a new form of biofuel blend from renewable material that has energy values comparable to those of fossil fuels. On the basis of these assumptions a scientific hypothesis was formed that the use of ethanol additive in mineral diesel and RME mixtures would allow achieving their flammability characteristics close to pure mineral diesel. It was decided to assess the possibility to use three–component combustible mixture made of mineral diesel, rapeseed methyl ester and 5–10% of ethanol in heavy duty transport means driven by unmodified direct injection (combustion chamber consists of a dished piston) diesel engines [2].

Optimizing the combustion process (i.e., reducing NO_x and PM emissions without serious compromises in fuel consumption) requires profound knowledge of all formation processes involved. Biodiesel is an oxygenated fuel, approximately 10 percent by volume that exhibits cetane characteristics which exceed that of petroleum diesel fuel. Some combustion characteristics of mineral diesel and oxygenated biofuels blends are as follows:

1. Various proportions by volume rapeseed methyl ester addition to mineral diesel distinguish an increased cetane number of the blend (see Fig. 1). 5% ethanol additive (v/v) to B15 (85%D+15%RME) blend reduced combustible mixture cetane number which became equal to fossil diesel [6].
2. Fuelling diesel engine with pure rapeseed methyl ester is characterized by shortened ignition delay duration [2; 3; 10] thus distinguishing happened in advance combustion process (see Fig. 2*a*). The CN of a given compound (B15+5%E) is higher the shorter its ignition delay time is and vice versa. Cetane improvers may have another important ramification, namely the reduction of NO_x exhaust emissions. It is known for D/RME blends small quantities (v/v) of ethanol can reduce these exhaust emissions. Cetane improvers function by reducing the ignition delay (see Fig. 2*b*) and lowering the premixed fuel combustion temperature [7], thus lowering NO_x by inhibiting their formation, which occurs at high temperatures in the combustion chamber.

2.2. Density and Viscosity

Biodiesel generally display higher density than mineral diesel (see Fig. 3*a*). This difference has impacts on heating value and fuel consumption, as the amount of fuel introduced into the combustion chamber is determined volumetrically [1]. Because of much lower surface tension, the density and viscosity of alcohols comparatively with mineral diesel fuel is expected to improve several characteristics of fuel such as atomization (fineness, homogeneity of fuel spray cone), fuel mixing (more homogeneous thermal field in cylinder) and heat release that increases the cycle indicated efficiency [10].

Fuel viscosity has impacts on injection and combustion. Higher viscosity leads to a higher drag in the injection pump and thus causes higher pressures and injection volumes, especially at low engine operating temperatures [1]. As a direct consequence the timing for fuel injection and ignition tends to be slightly advanced for biodiesel, which might in turn lead to increased nitrogen oxide exhaust emissions due to higher maximum combustion temperature [1, 2, 9, 10].

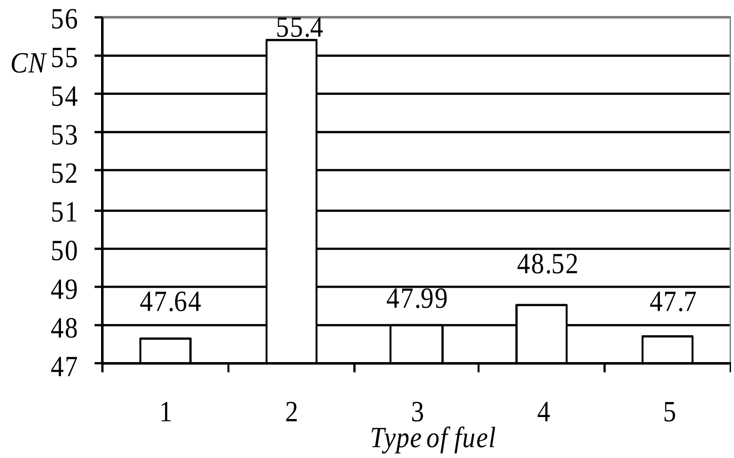

Fig. 1. Cetane number variation subjected to the type of fuel: 1 – D; 2 – RME; 3 – B10 (90%D+10%RME); 4 – B15 (85%D+15%RME); 5 – B15+5%E

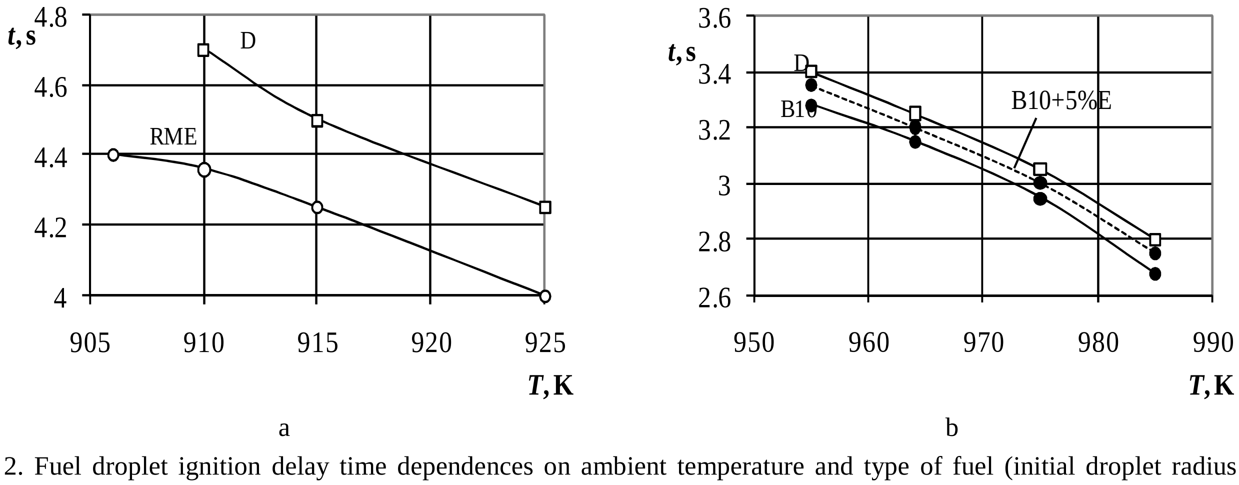

Fig. 2. Fuel droplet ignition delay time dependences on ambient temperature and type of fuel (initial droplet radius r_0=1±0.05 mm)

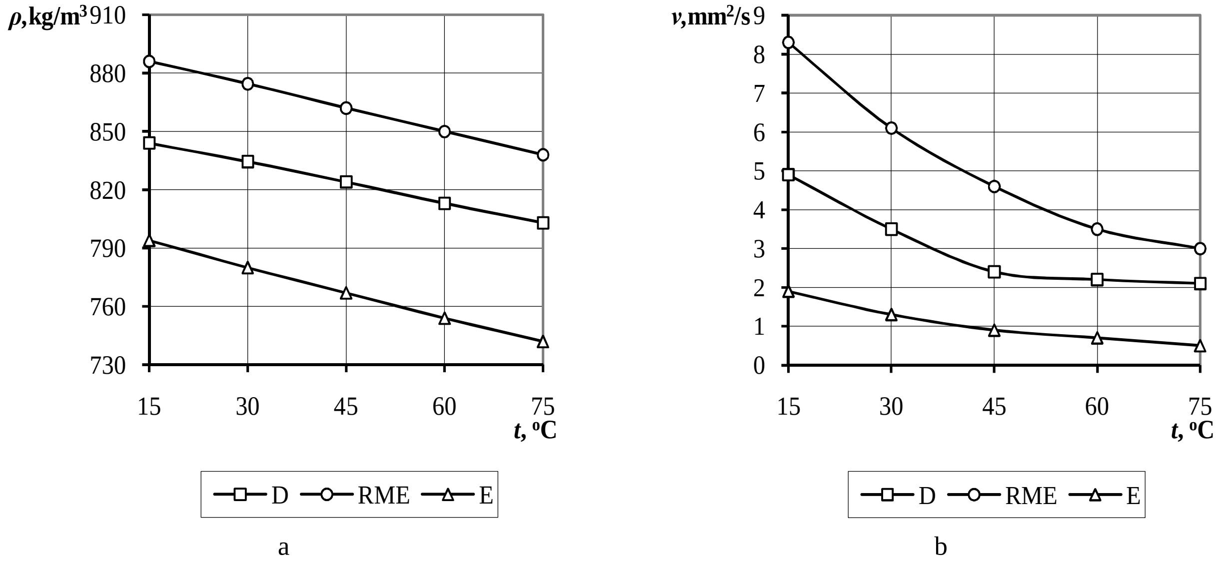

Fig. 3. Density (a) and kinematic viscosity (b) variations subjected to the temperature and type of fuel

2.3. Lubricity

With the advent of low–sulfur petroleum–based diesel fuels, the issue of diesel fuel lubricity is becoming increasingly important. Desulfurization of conventional, petroleum–derived diesel fuel reduces or eliminates the inherent lubricity of this fuel, which is essential for proper functioning of vital engine components such as fuel pumps and injectors [11]. As a remedy the routine addition of a small amount of biodiesel seems feasible. Fatty acid methyl esters do not pose any operational problems, even if they are used in higher concentrations [11]. Unfortunately, alcohols characterizing the difficulties of applying them as diesel fuels are as follows: low lubricating properties, aggression to non–ferrous metals and high flushing [10].

2.4. Solubility

Comparing different types of oxygenated fuel additives to fossil diesel we must admit that the intersolubility of components in the D–RME–E system was substantially high and show the optimal results. Using absolute ethanol (99.8%) stable three–component biodiesel mixtures in a relatively wide range of component concentrations could be produced [2, 12].

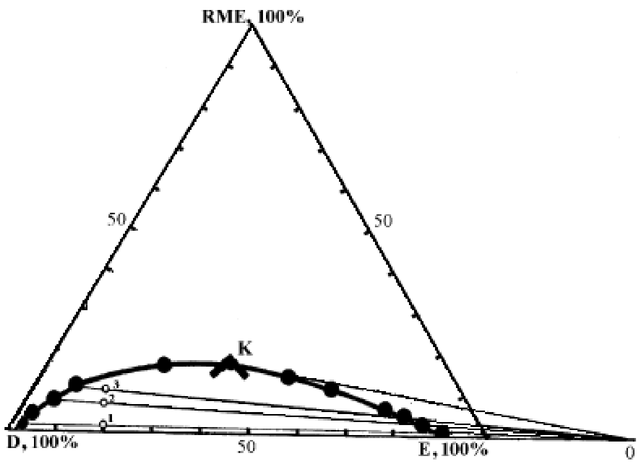

Fig. 4. Solubility of D–RME–E system at 20 °C [12]: 1, 2, 3 – nodes, K – critical point of solubility

2.5. Chemical Behavior

Biodiesel has solvent properties. This type of fuel does not work well with traditional rubber parts found in most vehicles today. Hoses and other rubber parts wear down over time with biodiesel use. Mixing RME, ethanol and regular diesel into a blend will help to rectify this common issue. Due to more aggressive chemical behavior of bio–based additives to rubber and plastic parts of fuel supply system, gaskets and fuel tank cap, it is recommendable to replace them with the ones that resist degradation.

When first using bio–based additives (especially – biodiesel) it is recommended to replace the fuel filter on tractors engine. Because of the solvent properties in biodiesel, it may cause the release of accumulated deposits inside the fuel tank and fuel lines from years of fossil diesel use. These deposits can flow down the fuel line and may plug the fuel filter.

3. Conclusions

The above discussion shows that properties of oxygenated diesel fuels, containing RME and ethanol are strongly influenced by the quantity (v/v) of fatty esters in the D/RME blend. Both biodiesel and dehydrated ethyl alcohol can have considerable influence on fuel properties such as cetane number with relation to combustion and exhaust emissions, viscosity, density and lubricity. Generally, cetane number and viscosity of D–RME–E fuels increase with increasing volume of neat fatty compounds. It therefore appears reasonable concept to enrich certain fatty ester and fossil diesel blend with ethanol having desirable properties in order to improve the exploitation characteristics of the whole fuel. Ethanol has oxygen participating in combustion process, the atoms of which are of a much lesser mass compared with hydrocarbon compounds. That conditions a better combustion reaction and lesser amount of open–ended combustion products is emitted.

A recommendation for using D–RME–E fuel blend in unmodified direct injection (combustion chamber consists of a dished piston) diesel engines was prepared.

References

1. **Mittelbach, M., Remschmidt, C.** Biodiesel – the Comprehensive Handbook. 1 st. Editon, Boersedruck Ges. m.b.H., Vienna, 2004, 330 p.
2. **Raslavicius, L.** Research into three component combustible mixture application for fuelling diesel engines. Doctoral Thesis, 2009, 121 p.
3. **Bazaras, Ž., Raslavičius, L.** Investigation of Three–Component Biodiesel Fuels Using a Single Droplet Technique. *Vibroengineering – 2008*: proceedings of the 7 th international conference, October 9–11, 2008, Kaunas University of technology, Lithuania. p. 109–112.
4. **Schumacher, L.G.** Physical and Chemical Characteristics of Biodiesel Blends. *Commercialization of Biodiesel: Environmental and Health Benefits Conference*, 1996. Mammoth Hot Springs, WY.
5. **Krahl, J., Baum, K., Hackbarth, U., Jeberien, H.–E.** et al. Gaseous Compounds, Ozone Precursors, Particle Number and Particle Size Distributions, and Mutagenic Effects Due to Biodiesel. ASAE Paper 996136, 1999.
6. **Kwanchareon, P., Luengnaruemitchai, A., Jai–In, S.** Solubility of a Diesel–Biodiesel–Ethanol Blend, its Fuel Properties, and its Emission Characteristics from Diesel Engine. *Fuel*, 2007, vol. 86, Iss. 7–8, p. 1053–1061.
7. **Ulman, T.L., Spreen, K.B., Mason, R.L.** Effects of Cetane Number, Cetane Improver, Aromatics, and Oxygenates on Heavy Duty Diesel Engine Emissions. SAE Technical Paper # 941020, 1994.
8. **Akasaka, Y., Sakurai, Y.** Effects of Oxygenated Fuel and Cetane Improver on Exhaust Emission from Heavy–Duty DI Diesel Engines. SAE Paper 942023, 1994.
9. **Yuan, Y., Mei, D., Wang, Z., Zhang, T.** Combustion and Emissions of the Diesel Engine Using Bio–Diesel Fuel. Front. Mech. Eng. China, vol. 3 (2), 2008, p. 189–192.
10. **Lebedevas, S., Lebedeva, G.** Maišytų spirito biodyzelinų Lietuvos transporto sektoriuje panaudojimo problematika. *Transport*, vol. 24(1), p. 58–65.
11. **Knothe, G.** Dependence of Biodiesel Fuel Properties on the Structure of Fatty Acid Alkyl Esters. Fuel Processing Technology, vol. 86, 2005, p. 1059–1070.
12. **Makareviciene, V., Sendzikiene, E., Janulis, P.** Solubility of Multi–Component Biodiesel Fuel Systems. Bioresource Technology, vol. 96, 2005, p. 611−616.

Proceedings of 4th International Conference ITELMS'2009

Main Types of Corrosion Damages during Operation NPP With WWER and RBMK Reactors

J. Bazaras*, Z. Bazaras, B. Timofeev*****

**Lithuanian University of Agriculture, Instituto str. 20, LT–54132 Raudondvaris, Kaunas region, Lithuania*
***Kaunas University of Technology Panevezys Institute, Daukanto str. 12, LT–35212 Panevezys, Lithuania. E–mail: Zilvinas.Bazaras@ktu.lt*
****St. Petersburg State Polytechnic University, Russia, E-mail: prometey@pop3.rcom.ru*

1. Introduction

World statistical data show that 31 to 41% of the total number of cases of degradation of pressure vessels and piping during operation of water-cooled NPPs is associated with various types of corrosion damages. Because, of this concern, various corrosion issues commonly experienced in Russian Reactors (WWER and RBMK). They include:

- pitting corrosion in un-clad WWER-440 reactor pressure vessel (RPV);
- corrosion cracking at the transition welding joints of RPV nozzles and piping;
- corrosion issues in PGV-440 steam generator collectors;
- steam generator heat exchanged tube corrosion
- intergranular stress corrosion cracking (IGSCC) in RBMK low carbon steel piping Du-800 with clad metal on inner surface;
- IGSCC in RBMK downcomers Du-300 from austenitic stainless steel.

Thus the operating experience of Russian NPP indicates that corrosion and mechanical damage may occur in various components of equipment and piping. These types of damages are presented in Fig. 1.

The world statistical data show that more distributed damages of NPP equipment and piping is intergranular stress corrosion cracking (IGSCC). The general information is presented in Fig. 2 for different types of RPV and data base for piping are given in Table 1.

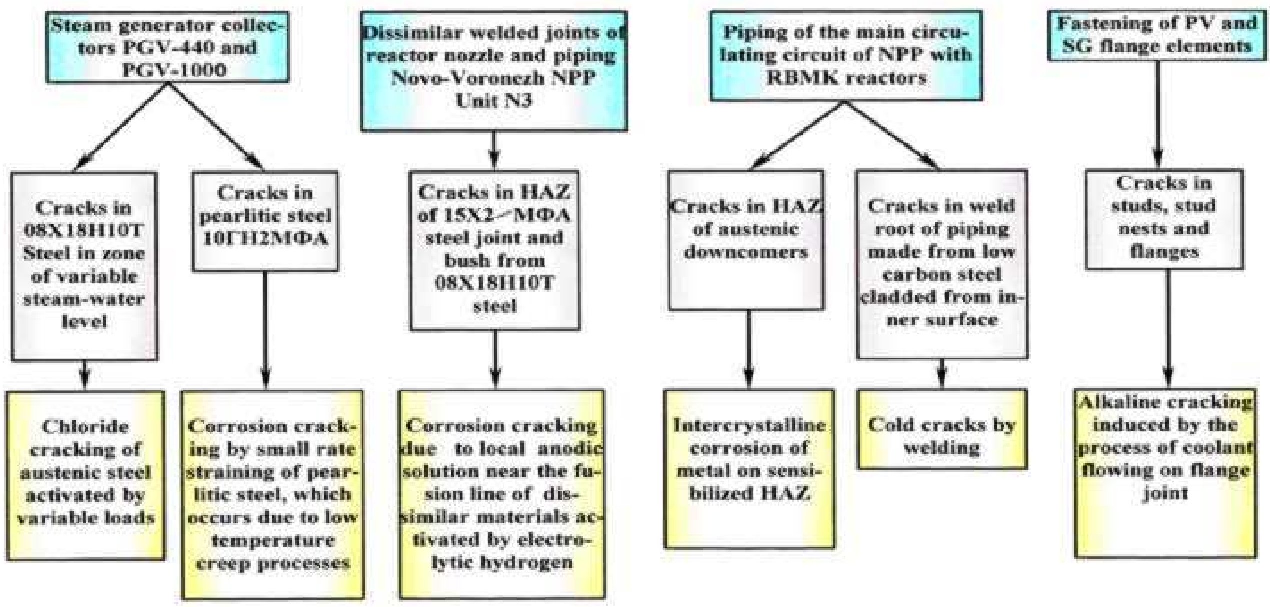

Fig. 1. Main cases of metal damages during NPP equipment operation

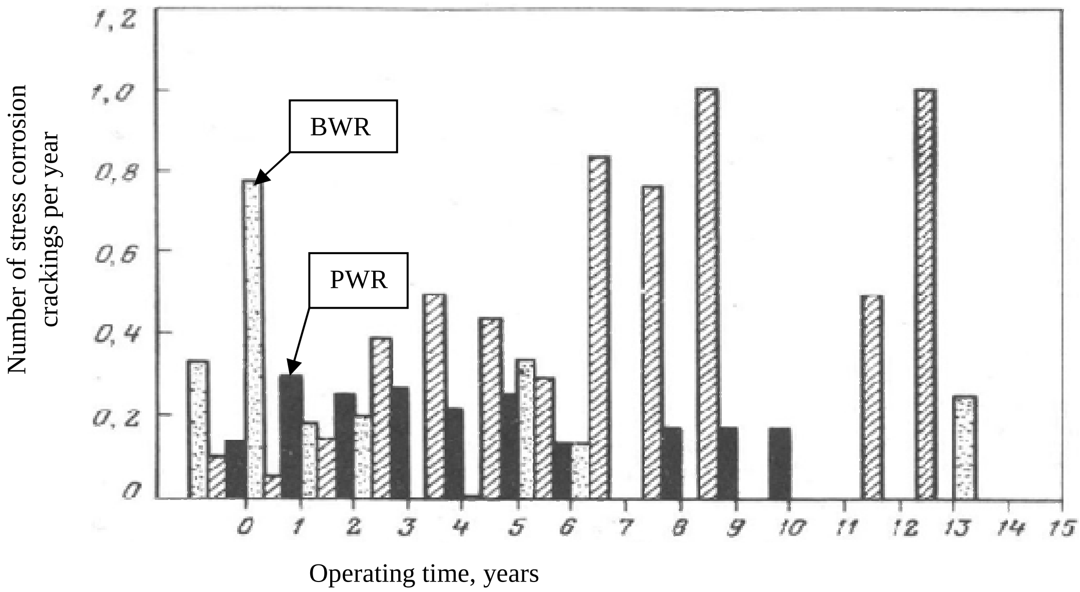

Fig. 2. Stress corrosion cracking for different types of reactor

Table 1

Data base of piping failures in various countries

Country or region	Total number of failures	Cracks	Leakage's	Breaks
Asia	8	0	3	5
Eastern Europe	235	61	142	32
Finland	26	10	14	2
France	128	47	73	8
Germany	186	113	68	5
Japan	46	7	33	6
Other	132	19	90	23
Sweden	278	153	106	19
Switzerland	48	36	10	2
USA	2627	658	1839	136
Sum total	3714	1104	2372	238

2. Corrosion Damages of WWER-440 RPV

The ten WWER-440 reactors (see Table 2) were manufactured from ferrite steel of type 15Cr2MoVA without anticorrosive cladding at the inner surface and they were in operation for a long time (more than 30 years) at various NPPs.

Table 2

The WWER reactors without anticorrosive cladding

NPP name	Unit	Type of reactor	BOL	EOL
Novo-Voronezh	2	V-3M	1969	1992
	3	V-179	1971	2016
	4	V-179	1972	2017
Kola	1	V-230	1973	2018
	2	V-230	1974	2019
Nord	1	V-230	1973	1990
	2	V-230	1975	1990
Kozloduy	1	V-230	1974	2004
	2	V-230	1975	2004
Mezemor*	1	V-270	1976	2015

* The tenth RPV of V-270 without anticorrosive clad metal in inner surface (NPP Mezamor in Armeniya) was not in operation for some years after earthquake, though since 1996 it is operation again.

During the operation these RPV reactors some corrosion damages (pits and pitting) were arise in the inner surface of vessel. The typical corrosion damages and distribution of their density are presented in Fig. 3.

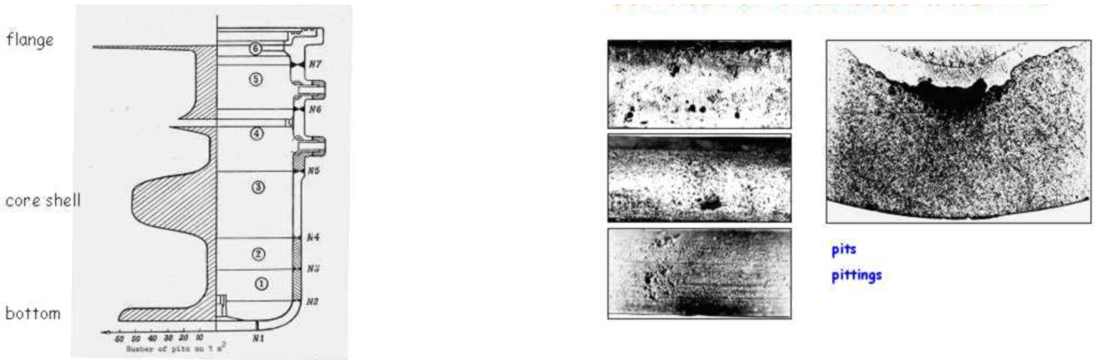

Fig. 3. Typical corrosion damages after prolonged operation time

As can you see from Fig. 3 the three areas of RPV have more density of damages, namely:

- surface of flange;
- core shell;
- bottom.

The second type of corrosion damages is the crack at the transition welding joints of WWER-440 RPV nozzle shell from heat resistant 15Cr2MoVA steel and piping of main circulation circuit (pipe Du-500 from austenite stainless 08Cr18Ni10Ti steel. During operation (5-10 years) we had a lot of damages of such type in circular direction along fusion line of heterogeneous welded joint. The typical cracks are presented in Fig. 4 and the variant of repair – in Fig. 5.

These procedures were performed for the third unit of Novo-Voronezh NPP.

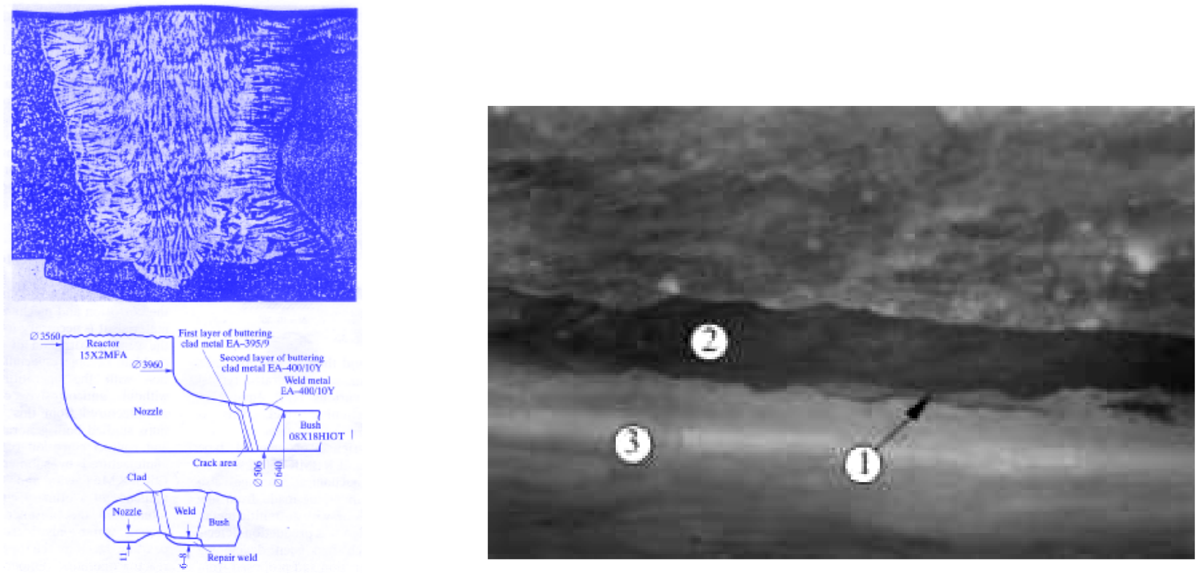

Fig. 4. Damages of dissimilar welded joint between the nozzle shell and austenite pipes Du-500: 1 – crack; 2 – buttering clad metal produced by MAW EA-395/9 electrode ; 3 – base metal (15Cr2MoVA steel)

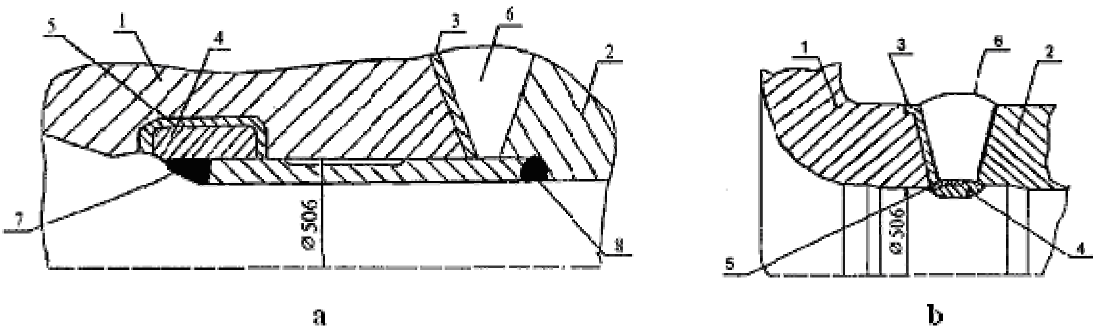

Fig. 5. Two variants of unit of joint the WWER-440 RPV nozzle shell with main circulation circuit (piping Du-500): 1- RPV; 2 - sleeve; 3, 4, 5 - technological cladding; 6, 7, 8 - welds

3. Corrosion Damages of Steam Generators

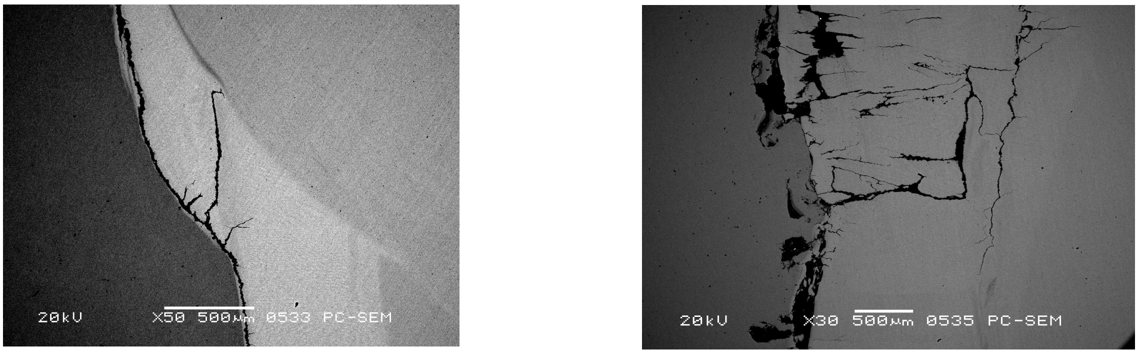

a b

Fig. 6. View of corrosion damages of PGV-440 of the first unit of Novo-Voronezh NPP: a) 5 mm from inner surface, b) 20 mm from inner surface

Fig. 7. View of crack in heat exchanged piping ∅16x1.5 mm

3. Corrosion Damages of RBMK Reactors

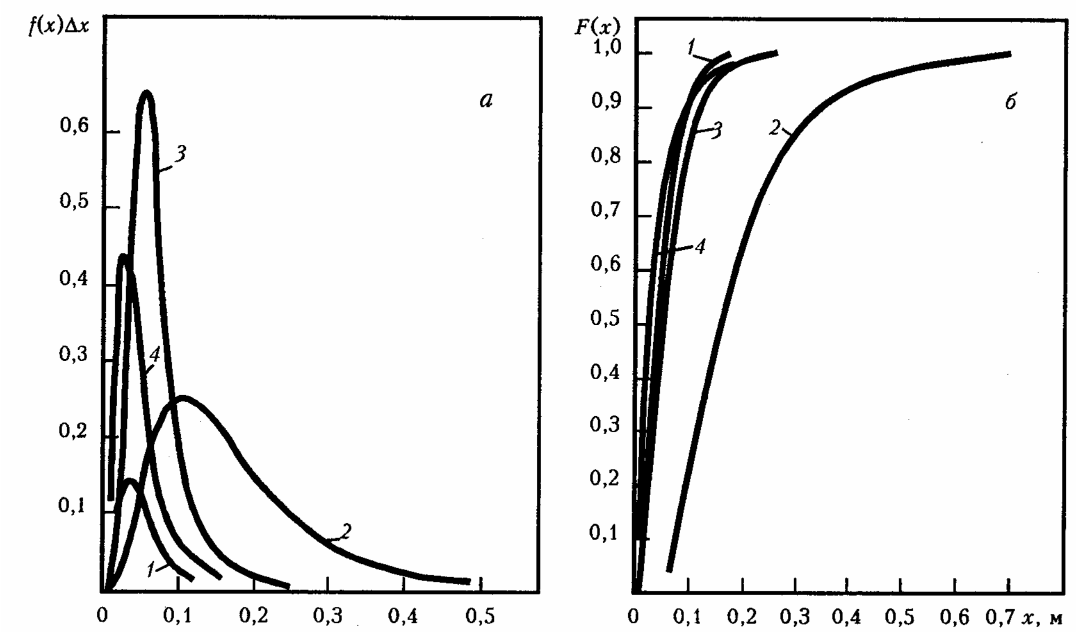

Fig. 8. IGSCC damage statistics of welded joints of downcomers on RBMK reactors in Ignalina NPP (1), Sosnovy Bor NPP (2), Smolensk NPP (3), Chernobyl NPP (4)

Fig. 9. Typical character and topography of damaged austenite piping Du-300 of RBMK reactors

5. Conclusion

Thus the various types of corrosion damages we can see during operation of nuclear power equipment. It is necessary to assess of mechanism of each type of corrosion damage and then using some measurements to exclude the reasons of these defects nucleation.

Proceedings of 4th International Conference ITELMS'2009

Development of Industrial Logistics Functions for Manufacturing Process Quality Improvement

A. Bargelis*, A. Stasiškis**

**Kaunas University of Technology, Kęstučio str. 27, Kaunas, Lithuania, E-mail: algirdas.bargelis@ktu.lt*
***Kaunas University of Technology, Daukanto str. 12, Panevezys, Lithuania, E-mail: andrius.stasiskis@ktu.lt*

Abstract

The paper deals with Hybrid manufacturing systems (HMS) that consists of CNC machine tools, robotics, computers with appropriate software logistics functions and high skilled employees in the technological sector of HMS. The quality problems are very urgent in HMS when production is oriented in high variety and low production volume business. The aggregate logistics function for manufacturing process quality improvement have been developed on the activity analysis performed in HMS operating with traditional processes as plastic parts molding, sheet metal parts stamping, CNC laser cutting and other high tech CNC and information technologies. The developed research has been tested and adopted in two manufacturing companies. It furnishes the possibility to estimate the manufacturing process quality index and to foreseen ways for quality improvement with minimum manufacturing cost.
KEY WORDS: *Product, process, quality index, aggregate function, quality increase, cost minimization*

1. Introduction

1.1. Competitive Manufacturing Environment

Manufacturing competitiveness of the 21st century is associated with the rapidly changing products and shortening life time. Manufacturing emphasised new challenges and difficulties [1]. Quality and costs are the main factors leading to survival or successful business. Rapid design and manufacturing procedures could not have been possible without aggregate logistics function for manufacturing process quality improvement. When part quantity is big and traditional stamping is used, part quality depends on die condition. If die design is suitable and the right material is used then part quality is right. The problem arises only when die wears and part becomes unusable. In case of plastic part moulding, part quality depends on mould condition and used material. If die or mould is in good condition there should be no problems with quality. In low production volume, the plasma cutting or CNC laser cutting and bending operations in HMS often are applied. Applying mentioned operations, part quality depends on right material and machine selection, employs skill and so on. In some cases when relevant part is produced, the flexible machine stations (FMS) could be used. Last case requires highest level of investment and employees' skills.

Conceptual design phase greatly influences the resulting cost, quality, product manufacturability and its life cycle parameters [2, 3]. During the product concept design phase product and process design are prepared. The best product and process design means the lowest cost of the product design and manufacturing [4].

1.2 Quality Problems in HMS

The research of this paper is to find the best solution considering the capability of various processes, machine tools and suppliers located in different companies and countries.

Aggregate function could help to find and evaluate each product and process alternative to the process capability when dimensions accuracy of a part are strongly related with low production cost [5-6]. The manufacturing systems modelling and engineering widely applied in virtual prototyping environment searching best alternative [7]. Computer integrated manufacturing approach used in all stages of product development cycle to appraisal and control quality parameters and process capability sustains it right in all stages [8]. This activity is available overlapping different functions as consideration of customer requirements, product and process design and manufacturing. Process capability is strictly related to the product quality and manufacturing cost. When process capability indices are insufficient, problems related with quality arise [9]. Aggregate function enables to find new process with sufficient capability for each product and process alternative and with minimal production costs. It is adopted to estimate and increase the process capability at the early product and process design stage.

2. Aggregate Logistics Function for Manufacturing Process Quality Improvement

As mentioned above manufacturing process is evaluated by its capability indices. The decisive factor for process manufacturing cost and capability is product design feature (DF), in particular, geometrical form and qualitative-quantitative parameters (QQP).

Quantitative parameters are:

- Quantity of different DF in product design.
- Dimensions.
- Number of manufacturing operations.
- Production volume.

Qualitative parameters are:

- DF quality requirements (tolerances, surface roughness).
- Surface quality requirements (damage of surface lateness, painting quality etc.).
- Machine tool capability C_p and process capability C_{pk} indices.
- Process standard deviation σ .

QQP depends on part/product 3D CAD requirements, material, used technology and manufacturers traditions. Designer must evaluate product manufacturing cost at the early design stage and vary DF geometrical form and QQP if necessary. The best product design and process is defined by two criterions – cost and capability.

Contradictions among the product cost, quality and delivery time arises in rapid product design. Tight product design features tolerances increases manufacturing costs and time and introduce more variation and product defects. In most cases, product implementation costs are directly related to process capability. The most popular process capability indices are C_p and C_{pk} [10]. Machine tool capability C_p and process capability C_{pk} are used to determine the work efficiency [11]. If these indices are less than 1.0, the process capability is insufficient. When both C_p is more than 1.0 and C_{pk} is less than 1.0 process needs to be adjusted. When both C_p and C_{pk} are more than 1.0, process variation fits to tolerance limits. Process capability indices equal to 1.0 are minimal requirement for each producer, however indices equal to two, are accepted by many companies.

In piece and serial production often $C_p = 1 \div 1.33$, because companies are using a cost-of-poor-quality strategy that attempts to bring costs to everyone's attention as a basis for corrective action. In mass and high-run production is used to keep $C_p = 2$, because investments to quality costs quit for big production volume of parts.

C_p and C_{pk} are defined by the following equations [10]

$$C_p = \frac{USL - LSL}{6\sigma}, \tag{1}$$

and

$$C_{pk} = \min\left\{\frac{USL - \overline{X}}{3\sigma}, \frac{\overline{X} - LSL}{3\sigma}\right\} \tag{2}$$

where USL – upper specification limit, mm; LSL – lower specification limit, mm; σ is the process standard deviation or overall process variability, mm; X is the mean value of the whole process parameter, mm.

The value of process capability indices is calculated for each operation. $C_p^{\min} = 1$ and $C_p^{\max} = 2$ are the minimal and maximal values of the acceptable capability indices seeking the minimal process costs. The critical operation is that which has the minimum value of C_p index. On the other hand the means of process capability indices with process costs are related:

$$\begin{cases} 0 < S \le S_{\max}, & S \to \min, \\ C_p^{\min} \le C_p \le C_p^{\max}, & C_p \to \max \end{cases} \tag{3}$$

where $S_{\max}$ is the biggest acceptable costs of an operation, money units; $C_P^{\min} = 1.33$ and $C_p^{\max} = 2$ are the minimal and maximal value of the acceptable capability indices [10].

Contradictions between DFA and DFM approaches arise at aiming reducing manufacturing costs. Simplifying the assembling process designer reduces the number of product parts inducing the other parts to become more complicated. And in other hand, simplifying manufacturing part shapes invokes more complicated product assembly process.

The solution of this conflict situation and search of the best version require generating a vital number of product and process alternatives checking their C_p and S acceptability. Manufacturing costs S forecasting method of product P_j applying research [4] has been used.

Product's parts manufacturing and assembly operation time forecasting is related with statistical data [12]. The fabricating and assembling operation time in developed DB is statistically defined by process charts and appropriate machines and tooling are fixed by considered companies. Designer having process capability and manufacturing cost data is able to compare each product and process alternative and make a true decision.

Today's marketplace raises specific requirements to manufacturer. New product should be not only better, but also it should be cheap. In some cases collaboration brings better results than working alone. Seeking best results in this area, the aggregate logistic function should be employed. To have good relationship among partners (Fig. 1) some rules should be obtained:

1. Every partner must create the add value;
2. Partnership must be based on reciprocal trust and benefit;
3. Must be minimal investment to have utmost gain;
4. The relations among partners should be based on logic.

In case that SME1 produces products from sheet metal parts, it could have relationship with SME4 that produces auxiliary equipment. If manufacturing volume is big, for some parts manufacturing could be involved SME2. For painting operation and packaging SME1 and SME2 have relations with SME3.

When specific part (TV plastic case) and processes are needed the SME5 with specific process could be involved. In this case SME1 arranging relationships has some possibilities:

1. both part and mould manufacturing consign to SME5;
2. only moulding consign to SME5 and design and produce mould by itself;
3. moulding consigns to SME5, by used mould from second-hand and repairs it in SME4.

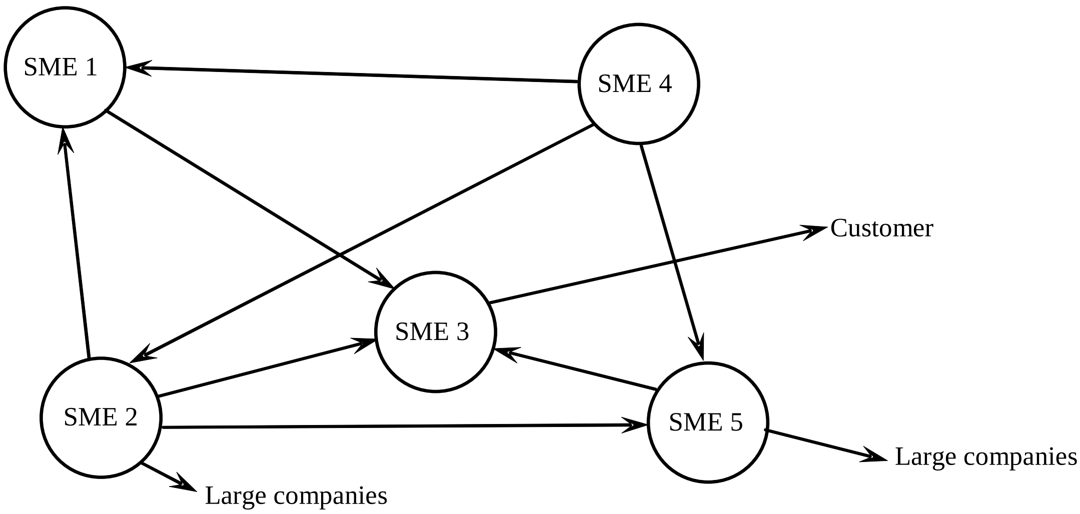

Fig. 1. SME network: SME 1 – Product manufacturer; SME 2 – sheet metal stamping; SME 3 – Powder painting, packaging and transportation; SME 4 – auxiliary equipment producer; SME 5 – Plastic parts molding

When selecting partners, the process capability indices and manufacturing costs should be checked. If any machine tool has acceptable index C_p and any manufacturing process has acceptable index C_{pk}, but both have unacceptable cost S, it means they are not competitive for the considered part or component. In such a case, it is necessary to look for other more competitive process, exchange component design or select other partner.

The developed industrial logistics functions have been tested in two Lithuanian manufacturing companies with different products and parts. Both companies are producing sheet metal products and components.

3. Results and Discussion

Ten similar products of low carbon sheet metal (thickness 1-2 mm) designs with various geometrical form, size, dimensions, parts tolerances and surface powder painting has been considered. Some of these products and their basic data are shown in Table 1.

Considered processes were traditional stamping and the modern CNC Laser cutting, punching and bending machines. The products assembling applying riveting and welding operations in specialized manually and robotics operating work places have been arranged.

The problems arise not only in part manufacturing, but also in painting, assembling and packaging processes. Table 1 shows the data of critical operations defined during research. CNC Laser cutting operation of slots and holes has bad C_p values (less than 1) for considered parts while the rest operations have suitable indices of machine tool capability. The reason of insufficient process capability indices is operators and engineers' low skill and random errors of cutting process. The necessity of the application of CNC Laser cutting operation in small volume production is defined by part geometrical form and design features peculiarities.

Table 2 shows the manufacturing cost of most complicated parts produced by CNC Laser cutting, CNC Punching and CNC Bending machines. These machines are used when production volume is up to 1500-2500 pieces per year. When production volume exceeds 2500-3000 pieces per year, then the purposive consideration is necessary to carry out selecting traditional presses and dies or CNC laser cutting, punching and bending machine tools. The part material, size, complexity of geometrical form, tolerances is main factors for decision making applying a developed aggregate function. The manufacturing time and delivery deadline are decisive criterion selecting one from available two options. When production volume is greatly bigger then 2500-3000 pieces per year, it is better to use traditional technologies applying presses and dies. Such conclusion overlaps with the research of other investigators [13] that worked in sheet metal industry of Finland. Their research shoes that employee empowerment in HMS has a substantial meaning in all product and process development cycle, in particular, when CNC machine tools dominate.

Table 1

Basic principal data of considered products

No.	Product type	Different Part number	Most complicated part feature		Operation Accuracy, mm	C_p
1	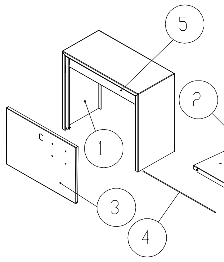	5	Part No 130	Holes and slots	Laser cutting ±0.1 Punching ±0.1	0.92 2.1
				Contour and Positioning	Laser cutting ±0.3 Punching ±0.3	1.3 1.8
				All operations	Stamping ±0.1	2.3
					Bending ±0.3	2.4
2	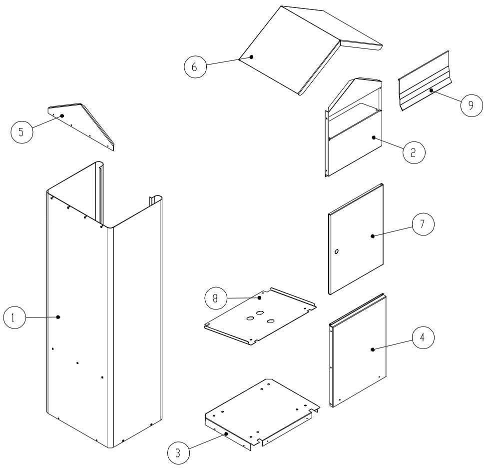	10	Part No 120	Holes and slots	Laser cutting ±0.1 Punching ±0.1	0.96 2.2
				Contour and Positioning	Laser cutting ±0.3 Punching ±0.3	1.3 2.4
				All operations	Stamping ±0.1	2.4
					Bending ±0.3	2.3
3	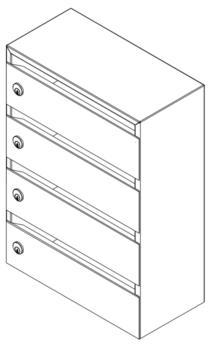	6	Part No 151	Holes and slots	Laser cutting ±0.1 Punching ±0.1	0.97 2.25
				Contour and Positioning	Laser cutting ±0.3 Punching ±0.3	2.2 2.5
				All operations	Stamping ±0.1	2.3
					Bending ±0.3	2.3

Table 2

Manufacturing cost of considered parts produced by various CNC machines

No.	T, h	Perimeter	Number of bends	Punching cost, €	Laser cutting cost, €	Bending cost, €	Total cost (punching & bending), €	Total cost (laser cutting & bending), €
130	0.011	1038	5	0.450	-	0.712	1.162	-
120	0.027	1720	4	0.531	1.84	0.572	1.103	2.412
151	0.015	2192	8	0.613	2.34	1.139	1.752	-

4. Conclusions

The growing complexity of new products and stiff competition in marketplaces enhance the demand to minimize product and process development costs and delivery time to customer in all stages of product life cycle.

The proposed aggregate functions will reduce the risk of implementing new products, processes and operations. It was shown that capability and manufacturing cost analysis helps to determine the ability for manufacturing between tolerance limits and engineering specifications. Capability and manufacturing cost analysis gives the needed information to choose the right partner.

The developed approach, unfortunately, has some limitations; the main of them being a relative narrow consideration area of manufacturing systems, products and processes to which it could be applied. Future work will focus on the expansion of the variety data and features in the developed aggregate functions, in particular, the number of product types, processes and operations aiming to overcome the existing limitations of proposed approach.

References

1. **Myint S.** Concurrent engineering (CE) in product design: a multi-criteria decision – making approach. Concurrent Engineering: Research and Applications, 1999, 7, p. 2-9.
2. **Bargelis A.** The modelling structure of intelligent manufacturing system for mechanical components. Proceedings of the 2nd International Conference on Integrated Design and Manufacturing in Mechanical Engineering (IDMME'98), Compiegne, France, 25-28, May 1998, p. 1145-1153.
3. **Gebresenbet T., Jain P. K., Jain S. C.** Preliminary manufacturability analysis using feature-function resource considerations for cylindrical machined parts. Int. J. Computer Integrated Manufacturing, 2002, 15, p. 361-378.
4. **Bargelis A., Hoehne G., Česnulevičius A.** Intelligent functional model for costs minimization in hybrid manufacturing systems. Informatica, 2004, 15, p. 3-22.
5. **Chua C. K., The S. H., Gray R. K. L.** Rapid prototyping versus virtual prototyping in Product design and manufacturing. The International Journal of Advanced Manufacturing Technology, 1999, 15, p. 597-603.
6. **Wiendahl H. P, Fiebig T. H.** Virtual factory design – a new tool for a co-operative planning approach. Int. J. Computer Integrated Manufacturing, 2003, 16, p. 535-541.
7. **Buede D. M.** The Engineering Design of Systems: Models and Methods. John Wiley & Sons, Inc., New York, 2000, 462 p.
8. **Rehg, A., Kreaber H. W.** Computer Integrated Manufacturing. Columbus, Ohio, 2001, 512 p.
9. **Dudek-Burlikowska M.** Quality estimation of process with usage control charts type X-R and quality capability of process Cp and Cpk, Journal of materials processing technology, 2005, 162-163, p. 736-743.
10. **Oakland, J. S.** Statistical Process Control, 4th ed. Butterworth-Heinemann, UK, 1999, 238 p.
11. **Motorcu A. L., Gullu A.** Statistical process control in machining, a case study for machine tool capability and process capability. Materials and Design, 2006, 27, p. 364-372.
12. **Bargelis, A., Stasiskis, A.** IDEF0 modelling technique to estimate and increase the process capability at the early product design stage, Mechanika, 2008, no 3 (71), p. 45-50.
13. **Ollikainen M., Varis J.** Employee empowerment in reducing production error amount in sheet metalworking, Mechanika, 2006, no 6 (62), p. 39-45.

Axle Renewing Characteristics Quality Estimation Methodic

Z. Bazaras*, D. Somov**

**Kaunas University of Technology, Department of Transport engineering, Kęstučio str. 27, LT-44312 Kaunas, Lithuania, E-mail: Zilvinas.Bazaras@ktu.lt*
***Kaunas University of Technology, Department of Transport engineering, Kęstučio str. 27, LT-44312 Kaunas, Lithuania, E-mail: dmitrij.somov@gmail.com*

Abstract

Axle's quality renewing estimation methods are reviewed in this article. New axles renewing method parameter counting system is offered according to this system.
KEY WORDS: *wheel renewing, quality estimation method.*

1. Introduction

Possibilities of axles renewing increase were searched to evaluate various axles renewing type quality method usage perspectives. That why various works of different organizations and axles renewing type quality estimation methods were analyzed.

2. Axle Renewing Quality Level Estimation

Comparisons and renewing type quality level estimation after axles renewing method classification were made. Rational renewing choosing method is shown in Fig. 1. In the first stage comparisons are made in experimental way. Piece P_i indexes were used, which allows using this method in other wheel renewing fields (P1), thermo-renewing to 600 HB (P2), to 350 HB (P3), economical renewing of wheel with run surface defects (P4), physico-mechanical wheel rim character renewing (P5), constructional tool simplicity (P6), tool constructing and adjusting heaviness (P7), formation of comfortable and transportable shaving (P8), shaving remaking necessity (P9). Total indexes are formulated:

$$Q = \sum_{i=1}^{n} P_i k_i \tag{1}$$

where: P_i - piece index in grades; k_i - piece index ponder ability coefficient; n - number of used piece indexes.

There are 3 types of estimating every total index quantity: estimation of all piece indexes; not estimating hardened wheels to 600 HB renewing; not estimating physical-mechanical wheel rim quality renewing.

According to recommendations of standard GOST16431-79, total value index is equated to 0 if at least one piece index is equal to 0.

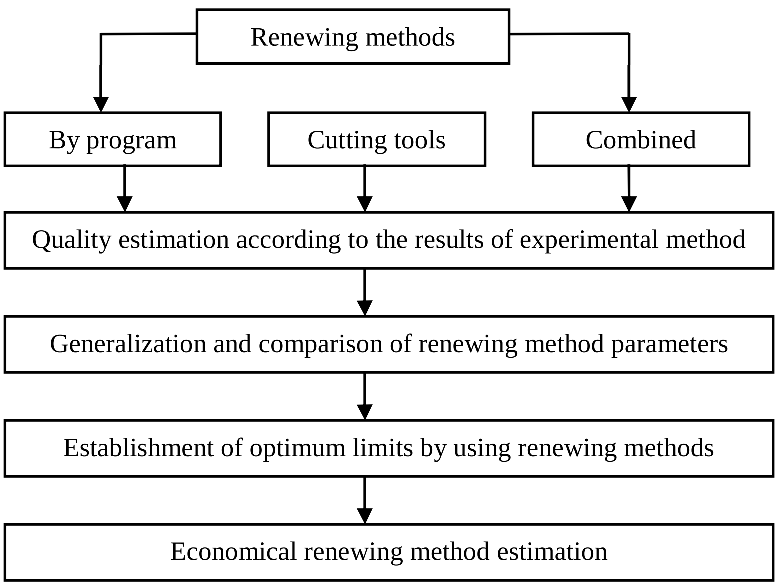

Fig. 1. Scheme of choosing wheel working renewing methods

3. Renewing Method Parameter Counting

Renewing method parameter counting is made by the kinematical analysis processing method base. Basic time given for the wheel run surface geometric profile renewing could be formulated (2):

$$T_0 = \frac{W}{a_1 bV} \tag{2}$$

where T_0 – basic time; W – cut metal thickness; V – cutting speed; a_1 – mean off-cut thickness; b – total off-cut thickness.

Cutting speed V and average off-cut thickness a_1 which describes cutting edge length unit average strain are main cutting process physical parameters. Va_1 product describes cutting edge length unit possibilities of analyzed process. Total off-cut width b defines detail ant tool parameters.

Va_1 product size depends on various tool work conditions shaving processing and system strain. Tool work conditions and shaving processing which affects tool wear off and allowable off-cut thickness could be described with track length l_1 which every cutting edge point goes through with detail unit erupting cutting and general track length l_n which one cutting edge during all the processing period goes through. Off-cut width describes strain system condition. It is known that for all processing methods main cutting power P_z is proportional to a_1 in degree y and to b in degree which is close to one (3):

$$P_z = ca_1^y b \tag{3}$$

Comparing methods while working with equal thickness off-cut the processing system strain conditions will be found by all the time working total off-cut width b.

Earlier mentioned processing indexes to the basic time T_0 and T_0 expression trough these indexes reflects in wheel run surface profile processing scheme comparison analysis methodology. Usually finding basic time the out point is the push size. Even using the same processing methods depending on cutting edge geometry tool of pushing side has different opportunities. For example, when there are the same cut speed and the same width off-cuts, grinding knife of which φ = 15° can work 3.3 times bigger push than knife of which φ = 60°. Push can have different physical meanings and can differ from real size very much when there are different processing methods.

Investigating and comparing different processing methods it's necessary to know three main physical process parameters (a, b, v) dependency of technological parameters push S, cutting depth t, detail turn frequency n_q, tool n_u.

Later the total length of all at the same time working cutting edges is taken instead of total off-cut width when this size changes during cutting process it is necessary to take average meaning (4):

$$b = b_1 Z \tag{4}$$

where Z – number of at the same time working cutting edges; b_1 – off-cut width.

Average off-cut thickness

$$a_1 = \frac{W}{l_{av} m_1} \tag{5}$$

where l_{av} – the way which all the cutting edges goes during all the processing time; m_1 – detail cutting surface length.

This investigation and optimization of amount parameters was done before evaluating them by comparing method. Economical valuation is being made in two levels:

- conditional wheel department;
- girandole.

4. Axles Renewing Method Quality Comparing Results in the Way of Experimental Method

There are shown meaning of coefficients which are attached to piece indexes (Table 1).

Counting concentrating indexes in 3 ways showed that only 9 of all the methods can be used in processing axles which have strength of 600 HB. The methods of second and third groups are included too.

At the same time account of such piece index as physical – mechanical rim metal property regeneration, reduces number of used methods to 4, where all they are from the third group. The biggest concentrating index meaning is got during shape willing with the mill, which has very hard material (milling – grinding) with thermo processing (3.5 method, Table 2) which helps regenerate physical – mechanical run surface property and cut-in profile high speed grinding shape with outside wheel touch with thermo processing (3.6 method, Table 2) which helps regenerate physical – mechanical run surface property.

Table 1

Ponder ability coefficient meanings

Types of establishing concentrating indexes	Column number from Table 2 and corresponding meaning of concentrating coefficients K_i								
	3	4	5	6	7	8	9	10	11
The first (with all indexes)	0.5	1.0	1.5	2.0	2.5	0.5	0.5	1.0	0.5
The second (without 4-th column)	0.5	-	1.5	2.5	3.0	0.5	1.0	1.0	0.5
The third (without 4-th and 7-th columns)	0.5	-	2.5	3.5	-	0.5	1.0	1.5	0.5

Table 2

Methods of establishing concentrating indexes

Number and group name	Number and processing method name	Piece value indexes which describe opportunity									Total value index Q account		
		P1	P2	P3	P4	P5	P6	P7	P8	P9	All indexes	Indexes without 4^{th} column	Indexes without 4^{th}, 7^{th} column
		Grade estimation of piece indexes									Estimation of all indexes in grades		
1	2	3	4	5	6	7	8	9	10	11	12	13	14
Processing with the program or with the template	1.1 Grinding with the template one or few knifes installed consecutive to the axles	5	0	3	3	0	5	5	4	3	0	0	35,5
	1.2 Grinding with the template one or few turning knife heads	3	0	4	4	0	3	5	4	3	0	0	39,5
	1.3 Milling with the template one or few mills installed consecutive to the axles	3	0	3	3	0	4	4	5	5	0	0	35,5
	1.4 Milling with the template transversal knifes	3	0	3	3	0	4	4	5	5	0	0	35,5
	1.5 Grinding with the template few knifes installed on different axles sides	5	0	3	3	0	5	5	4	3	0	0	35,5
	1.6 Grinding with the template few turning knife heads	3	0	4	4	0	3	5	4	4	0	0	40,0
	1.7 Milling with the template few disc mills installed on different axles sides	3	0	3	3	0	4	5	5	5	0	0	36,5
	1.8 Milling with the template few transversal mills installed on different axles sides	3	0	3	3	0	4	5	5	5	0	0	36,5
Processing with shaping tools	2.1 Grinding with one or few long knifes in ray direction	3	0	3	0	0	3	3	3	3	0	0	0
	2.2 Grinding with one or few long knifes in tangent direction	3	0	3	0	3	3	3	3	3	0	0	0
	2.3 Outside spiral grinding	3	0	3	0	0	3	3	3	3	0	0	0
	2.4 Inside spiral grinding	3	0	3	0	0	3	3	3	3	0	0	0
	2.5 Outside milling with one or few shaping mills	5	0	3	0	0	3	3	5	5	0	0	0
	2.6 Milling with shaping mills which have hard material – mill-grinding	4	5	5	5	0	4	4	5	4	0	0	47,5
	2.7 Inside milling with shaping mill	3	0	3	0	0	3	3	5	5	0	0	0
	2.8 High speed cut-in profile outside grinding	5	5	5	5	0	4	4	5	4	0	0	48
	2.9 High speed cut-in profile inside grinding	3	5	5	5	0	4	4	5	4	0	0	47
	2.10 Cut-in profile outside grinding	5	5	5	5	0	4	4	5	4	0	0	48
	2.11 Milling with the mill set (angular, shaping, transversal) fixed in different axles sides	3	0	0	3	0	3	3	5	5	0	0	34
	2.12 Run profile processing with processing tools	0	0	0	0	0	4	4	3	3	0	0	0

1	2	3	4	5	6	7	8	9	10	11	12	13	14
Combined processing	3.1 Grinding with the template one or few knifes fixed into axles consecutively using preliminary thermo processing with inductive heating to increase processing	5	0	3	5	0	5	5	3	3	0	0	41
	3.2 Outside milling with one or few shaping mills with preliminary inductive heating	5	0	3	5	0	3	3	5	5	0	0	42
	3.3 Grinding with the template one or few knifes fixed into axles consecutively using preliminary and after processing thermo processing which helps to increase physical – mechanical run surface property	5	5	5	5	5	3	5	3	3	46	48	45
	3.4 Outside milling with one or few shaping mills using thermo processing after processing which regenerates physical – mechanical run surface property	5	5	5	5	5	3	3	5	5	48	49	47
	3.5 Milling with shaping mills which have hard material – mill-grinding using thermo processing after processing	5	5	5	5	5	4	4	5	5	49	50.5	48.5
	3.6 High speed cut-in profile outside grinding using thermo processing after processing which regenerates physical – mechanical run surface property	5	5	5	5	5	5	4	5	5	49	50.5	48.5
	3.7 Grinding with the template one or few knifes fixed into axles consecutively using plasmatic heating for the surface which is being cut	5	5	5	5	0	3	3	3	3	0	0	43

Results of counting concentrating results allowed further analysis choose only these methods which are better than other methods and now are used regenerating axles run surface profiles. This is used for grinding (1.1), milling (2.5) renewing methods and also cut-in profile high speed methods (2.8) which all are of the third group it means all that is combined processing.

5. Conclusion

1. Axles renewing method quality estimation methodic is offered which connects next main stages:
   - Type quality estimation using experimental estimation method;
   - Renewing type parameter optimization and comparing;
   - Determining rational edges of renewing type using;
   - Economical renewing type estimation.
2. Carried out profile renewing quality method comparing actually is estimation of experimental method. Methods chosen for further analysis are better and more practical that are grinding, milling methods also cut-in profile high speed grinding method and combined processing methods with sourcing extra energy. The preference goes to the cut-in profile grinding method with thermo processing which has the biggest manufacturing process regeneration and allows processing axles with defects more economic and regenerates physical – mechanical axles run surface metal property which allows increase axles resources.

References

1. **Bhateja P. C., Chisholm A. W., Paltinson E. I.** A computer-dided study of the texture of the working surface of grinding wheels / Proc. 12^{th} MTDK conf. 1991.P.72-78.
2. **Furuichi R., Narayama M., Doi T.** Influence of dressing conditions of grinding wheels on grinding fluid performance / Bull.ISME.1997.№10 (38). 58p.

Proceedings of 4th International Conference ITELMS'2009

Public Transport System from Stakeholder Management Perspective

D. Susnienė

Kaunas University of Technology Panevežys Institute, Klaipėdos str. 1, 35209 Panevėžys, Lithuania,
E-mail: dalia.susniene@ktu.lt

Abstract

Efficient transport system increases safety, improves network efficiency and stimulates intermodality which reduces transport impact on environment and makes cities more attractive. In order to be and successfully operate in the market it is necessary for public transport companies to look for and implement new management models in their system. Involvement of stakeholders in supply of public transport services, i.e. what level of relationships are needed between a transportation company and its various stakeholders is necessary in order to meet the main stakeholder – passenger – needs. Consequently, as to supply the passenger with best service, relationships between different stakeholders (municipality. public transport company. state. road maintenance service. etc.) are of vital importance.
KEYWORDS: *public transport, management, stakeholders, service, satisfaction of needs.*

1. Introduction

New global challenges have pushed public transport into the front line. In several European countries, bus networks recorded strong growth in ridership during 2008 [1]. Therefore cater for demands on two fronts: firstly, expectations of quantitative and qualitative service improvements, which call for a rapid response in the short term; secondly, in the medium term, a quickening of the pace in terms of, research efforts.

How carefully does a public transport organization listen to its customers and other stakeholders? Everyone says they listen but do they actually hear what your customer is saying? Or do they tend to filter customer needs and expectations through old paradigms, twisting what customers say they want to fit what you thought they wanted, or what you hoped they wanted, or perhaps what you already provide?

2. Management of Public Transport Organizations

When faced with the necessity to travel, an individual's natural desire is for a personal mode of transport that is flexible, independent and that is perceived as fast. The only reasonable way in which to reconcile individual aspirations and the will of all stakeholders in public transport, is to provide public transport services of the highest possible quality in a way that will persuade a large number of inhabitants to resist the temptation to use individual modes, to resist the temptation to use individual modes, to give public transport a try and become regular public transport users. The improvement of quality presents positive stakes for all the stakeholders concerned: the public authority, the clients, the operators, the community and others. Any such action to improve quality naturally comes at a price of all stakeholders. However, it must be seen as an investment whose beneficial spin-offs for the community, passengers and operators will easily justify the commitment. Competing with other modes of transportation, especially the personal car, requires understanding what good public transport service is and why it is important [2, 3]. The first question is, "What is customer service and how can public transport service meet customers' and other stakeholders' needs? Clearly, customer service means more than putting vehicles on the street. In the broadest sense, customer service is doing whatever it takes to satisfy passengers. Service quality is more elusive than product quality. Because human behavior plays such an important role in service quality, it cannot be dealt with as much rigor and precision as one would engineer a manufacturing process so as to produce consistent products [4, 5]. However, as consumers and users of both products and services, we have no trouble identifying what is important to us. Customer satisfaction or the lack thereof, is the difference between the services customer expect from public transport system and the services they perceive they are getting, all the time comparing public transport services to alternative modes of travel. While most passengers do not expect public transport services to be as convenient as a personal car, they often expect them to be more affordable. They have every right to expect that buses will arrive on time, be clean, comfortable, safe, and that the whole process of using public transport will be understandable and responsive to them as users.

The second important question is the one this paper intends to answer, "How can public transport system/company be managed to ensure stakeholder satisfaction? If there is a problem in organization, there should be a tool that could help to design, build, or retool a product or service to precisely align with what stakeholders wants and expects? A tool which takes stakeholder demands as its energy source, and focusing those demands so intently that it can cut through old modes of thinking and operating, to pinpoint a product or level of service that truly will satisfy your customer [6, 7].

The problem can be solved expanding the paradigm of customer and satisfaction of its needs by converting it into paradigm of stakeholders and satisfaction of their needs, i.e. organization's customers should be considered all important stakeholders and their needs should be met in the way as not to violate their interests [8,9]. This is quite a complicated task because the wide range of stakeholders brings together different interests but harmonization aspects of them are not analyzed enough by scholars and there is no consensus on methodology how to incorporate different interests into organization's goals and how satisfying customer needs to satisfy important stakeholder needs.

The example can be set on this matter. ISO 9001:2000 standard, the requirements of which are obligatory, is only orientated to customers and necessity of satisfaction of their needs. ISO 9004:2000 standard already specifies, that „the success of the organization depends on understanding and satisfying the current and future needs and expectations of present and potential customers and end-users, as well as understanding and considering those of other interested parties" (ISO 9004:2000). However, this standard provides only guidelines for performance improvement, and is not obligatory only because of the absence of stakeholder satisfaction methods.

Methodology of meeting stakeholder needs must be grounded on organizational management that should frame the premises for creating value to stakeholders and eventually meeting their needs [10, 11, 12]. Satisfaction of stakeholder needs is a multidimensional process therefore certain criteria must be identified and adapted to organization's processes to ensure efficient organizational management in the context of satisfaction of stakeholders needs. These criteria will allow to collect and analyze data on the quality of organizational processes pertinent the capacity of stakeholder value creation and to identify the need and ways for process improvement. However, there is a lack of criteria that could cover the most important stakeholder management aspects and allow developing this complicated, multidimensional relationship network effectively harmonizing and integrating stakeholder interests in unison with the implementation of organizational goals.

Involvement of stakeholders into provision of public transport services is necessary to assure that a passenger as an important stakeholder would be satisfied [13, 14]. Therefore, it is necessary to implement new management models in order to achieve good results and create value to stakeholders. It is necessary to identify and structure the criteria of meeting stakeholder needs, and to adapt them to organizational management and activity processes. Thereby the issue of satisfaction of stakeholder needs is viewed from organizational aspect and is confined to organizational management and activity processes. The position is taken up that in order to create value for stakeholders it is necessary to identify criteria that organization could follow in its activity and consequently generate premises for efficient management of stakeholder relationships and for satisfaction of stakeholder needs.

Particular stakeholders or their groups could be distinguished in public transport enterprises. A very large impact on the decisions of the public transport enterprises has not only typical stakeholders (customers and end users, employees, owners and investors, suppliers and partners, community) but state institutions and local authorities (municipalities) as well. Unlike other organizations public transport enterprises experience great influence from state institutions and local authorities in their decision taking, organizational management and performance. Therefore, public transport enterprises have particular stakeholders with the specific relationships and influence, and it is important to know how to align and satisfy their interests. Consequently, the research carried out on the example of public transport enterprises will help to solve the analogical problems of other organizations, which have smaller number of stakeholders and their groups.

3. Empirical Study

After thorough analysis of academic literature criteria and their indicators were identified. They will generate the premises for satisfaction of stakeholder needs at public transport companies and can precondition the validity and reliability of assessment of organizational processes and activity in the aspect of stakeholder satisfaction and reveal strengths and weaknesses of these processes.

In accordance with identified criteria and their indicators the questionnaire was designed and chosen as a research tool at four successfully operating public transport companies. The questionnaire comprises 48 statements (indicators) which are derived from ten criteria concerning the satisfaction of stakeholder needs:

1. Senior management belief that relationship building with stakeholders is important to bottom-line success (9 indicators).
2. Time spent by managers communicating about building relationships with stakeholders and shared information (4 indicators).
3. Employee readiness to keep relationship with key stakeholders and responsibility (5 indicators).
4. Organization's culture support for personal values and needs (8 indicators).
5. Organization's orientation to satisfaction of stakeholder needs (4 indicators).
6. Organization's actions ensuring stakeholder satisfaction (7 indicators).
7. Organizational systems set up or redesigned to support the mission (5 indicators).
8. Organization's policies geared to long-term success (2 indicators).
9. Care for environmental issues (1 indicator).
10. General assessment of stakeholder approach in an organization (3 indicators).

The questionnaire is designed in such a way that the higher point for statement reflects the more efficient satisfaction of stakeholder needs and vice versa the lower point for statement reflects lower efficiency of organization's activity concerning stakeholder satisfaction. Four biggest public transport companies in Vilnius and Kaunas were chosen to carry the survey.

The research data was statistically processed by statistic programme SPSS 12.0 and by Microsoft Office Excel 2003. Data is analyzed according to the results of every indicator separately taking into account the opinion of employees and senior management. Later the same procedure was done to the categories/dimensions the research was carried out in four public transport enterprises.

Comparing all the nine dimensions/categories of the questionnaire the highest percentage from employees got these category: organization's orientation to satisfaction of stakeholder needs (54,4 percent). The highest rank from senior management got following categories: organizational culture support for personal values and needs, organization's policies geared to long-term success (100%). However, the highest ranked employee category - organization's orientation to satisfaction of stakeholder needs - was evaluated by the managers relatively high too (96.9%).

The lowest percentage of the positive answers from the point of employees got the categories –organizational systems set up or redesigned to support the mission (33.1%) and organization's policies geared to long-term success (40.8%).

It is necessary to say that employees and senior management's opinion on this position was different, because from the managers this position got the highest percentage of the positive answers and from employees the lowest percentage of the positive answers. The lowest percentage of the positive answers from managers got categories: employee readiness to keep relationship with key stakeholders and responsibility (82.5%) and time spent by managers communicating about building relationships with stakeholders and shared information (84.4%).

When analyzing and comparing the indicators (questions), the highest evaluation got organization's care for its reputation in society ($\overline{x}$ = 4.04; M_e = 4; M_0 = 5). Actually, it was the only indicator that got more then four points from the employees. There were more indicators relatively ranked high: employee knowing the organization's mission and goals ($\overline{x}$ = 3.97; M_e = 4; M_0 = 5) and two other indicators that got the same results: organization's aspiration is to keep relationships with the stakeholders and organization's goal is to satisfy the needs of stakeholders ($\overline{x}$ = 3.91). Senior management's opinion was different again, they ranked the highest other indicators: analysis of the customers' complaints ($\overline{x}$ = 4.88), care for employees, employee training, permanent update of company's range of services, employee motivation to keep relationships with the stakeholders and organization's policies geared to long-term success indicators were ranked equally ($\overline{x}$ = 4.75).

The lowest ranking from employees got these indicators: transparency of pay system ($\overline{x}$ = 2.69; M_e = 2.5; M_0 = 1) and employee granting and initiative stimulation ($\overline{x}$ = 2.79; M_e = 3; M_0 = 1).

Senior management again had different opinion and ranked the lowest these indicators: manager‘s pay dependency on the success of the relationship with the stakeholders ($\overline{x}$ = 3.13) and following indicators as funding relationships with the stakeholders, including cooperation with the stakeholders into the functions regulations, and settling accounts with the suppliers in time were ranked equally ($\overline{x}$ = 3.25).

4. Conclusions

Efficient public transport system and its management play a very important role in increasing safety, improving network efficiency and stimulating intermodality which reduces transport impact on environment and makes cities more attractive. Even with the constantly increasing number of private cars public transport can play a very important role as efficient management of public transport system is vital to rapid economic growth and people welfare:

When analyzing and improving the operations of public transport companies under the research they should pay attention to the ranked lowest indicators and categories as well as find reasons for this and for different opinions of employees and senior management.

When pursuing the goal of the empirical research, i.e. to reason the premises for satisfaction of stakeholder needs in organizational management, the research results revealed that the questionnaire can assure validity, representativity and reliability because relative score mean error is significantly lower then 10 percent with 95 percent of the fiducial probability. This means that identified criteria and their indicators concerning the satisfaction of stakeholders' needs (on the basis of which a questionnaire was designed) allows to reliably, objectively and validly assess organization's process orientation to stakeholders' needs satisfaction and to disclose its strengths and weaknesses.

References

1. UITP, International Association of Public Transport, A UITP position paper, http://www.uitp.com
2. **Kennedy, C. A.** A comparison of the sustainability of public transport and private transport systems. Transportation, 29 (4), 2002, p. 459-493.
3. **Richard, M.** Quality and customer's satisfaction. 52 nd International Congress, Stuttgart 1997.
4. **Eden, C.** Making strategy: The Journey of Strategic Management / C. Eden,.F. Ackermann. London: Sage Publications, 1998, 117 p.

5. **Mopin P.** 2000. Customer Defined Quality Standards. Presentation to Union of Public Transport International Conference. www.publ./lit45_html
6. **Elias A. A.** 2000. Stakeholder analysis for systems thinking and modelling / A.A.Elias, R.Y.Cavana. www.esc.auckland.ac.nz/organizations/ORSNZ/conf35/paper/BobCavana.pdf
7. **Fley J. K.** From quality management to organization excellence: Don‘t throw the baby out with the bath water // Proceedings of the fourth international and seventh national research conference on quality management, Sydney. 2001. p. 154-177.
8. The High Performance Organization Group (the HPO). 2006. http://www.the-hpo.com/
9. **Viegas J. M.** Public transport in the sustainable urban transport policy package: taking an integral policy approach. ECMT/OECD Workshop on implementing strategies to improve public transport for sustainable urban travel. Athens, Greece, 1999.
10. **Ackermann F.** 2001. Stakeholders Matter: Techniques for Their Identification and Management/ F. Ackermann, C. Eden// Department of Management Science Research Paper No. 2001/20, Strathclyde Business School, Glasgow.
11. European Multi Stakeholder Forum on CSR. 2003. http://europa.eu.int/comm/enterprise/csr/forum.htm
12. **Svendsen A.** The stakeholder strategy: profiting from collaborative business relationships. 1998.
13. **Carnell Don. S.** Performance Excellence System at Public Transport Companies. 2003. www.atco.org
14. **Vinck S.** 2000. Quality and Customer Satisfaction in Public Transport – 52nd International Congress Stuttgart’2000. www.art.man.ac./transres/lect6.htm

Proceedings of 4th International Conference ITELMS'2009

Approximation of Static Tensile Curves

A. Bražėnas*, D. Vaičiulis**

Kaunas University of Technology, Daukanto 12, 35212 Panevėžys, Lithuania, E-mail: algis.brazenas@ktu.lt
**Kaunas University of Technology, Daukanto 12, 35212 Panevėžys, Lithuania, E-mail: dainius.vaiciulis@ktu.lt*

Abstract

The paper presents results analytical investigations of static loading curves approximation. Dependencies for of the static tensile curves approximated by power function accuracy improving are proposed in this work.
KEY WORDS: *tensile curve, linear approximation, piecewise-linear, approximation by power function.*

1. Introduction

Test curve of material at static tension are obtained by automatically it recording in coordinates $\sigma - e$. This curve may be divided in two intervals: elastic loading, when $\sigma \le \sigma_{et}$ and elastic plastic loading – $\sigma = f(e)$. When $\sigma_i > \sigma_{et}$, $\sigma = f(e)$ may be expressed by polynomial or power type function. Because at elasto-plastically deformed zone the parameter of material hardening $E_1 \ll E$ strain intensity strongly depends on limit elasticity of materials σ_{et}. Therefore relative stresses $\overline{\sigma} = \sigma / \sigma_{et}$ and strains $\overline{e} = e / e_{et}$ are frequently used ($e_{et} = \sigma_{et} / e$). In this case stress and strains values may be determined by dependencies $\sigma = \sigma_{et}\,\overline{\sigma}$ and $e = e_{et}\,\overline{e}$.

For stresses and strains calculation the linearly, piecewise-linearly approximated curves and curves approximated by power function are frequently used [1-3].

2. Analysis of the Approximated Curves

The parameters of material hardening in elastic plastic zone depends on type of approximation depends and accepted maximum strain value $\overline{e}_{sn} = e_{sn} / e_{et}$ of approximation curve. For stress strain state calculated under static loading and determination of cyclic elastic plastic loading diagrams parameters, when rate of cyclic properties changing is not large, $e_{ns} = 0.025 – 0.03$ can be accepted. When rate of cyclic properties changing is large for cyclic softening materials $e_{ns} = 0.025 – 0.03$ and for cyclic hardening materials – $e_{ns} = 0.5 e_{ut1}$ (e_{ut1} is the minimum value of tensile strain which corresponds σ_{ut}) [3]. For stress strain state calculation at static loading, when $e > 0.03$, the parameters of approximated curves mast be determined by accepting $e_{ns} = e_{ut1}$.

The most exactly parameters of test curve corresponds piecewise-linearly approximated curve (Fig. 1). In this case, when $\overline{e}_i < \overline{e} \le \overline{e}_{i+1}$,

$$\overline{\sigma} = a_i + b_i \overline{e} \tag{1}$$

where a_i and b_i are parameters of materials calculated by formulas: $b_i = \dfrac{\overline{\sigma}_{i+1} - \overline{\sigma}_i}{\overline{e}_{i+1} - \overline{e}_i}$ and $a_i = \overline{\sigma}_i - \overline{e}_i b_i$ [2, 3].

From Eq.(1) follows that parameter b_n in initial stage of elastic plastic deforming decreases more intensively with increasing $\overline{e}$. Therefore, in this loading stage lesser values of difference $\overline{e}_i - \overline{e}_{i-1}$ must be accepted.

In this case value elastic stress of approximated curve is equal to experimentally determined value σ_{et} which corresponds $e_{et} = \sigma_{pr} / E + 0.003$. Values of strains $\overline{e}$ = (1; 1.25; 1.5; 2.0; 3.0; 4.0; 5.0; 7.0)$\cdot \overline{e}_{sn}$ may be recommended.

Stress strain state determination by using piecewise-linearly approximated curves is sufficiently complicated. Therefore, this curve often used in finite element method (FEM). For simplifying stress determination linear approximation and approximation by power function of dependence $\sigma = f(e)$ are frequently used. In this case approximated diagrams rather approximately correspond to tension curve of material.

Linearly approximated diagram may be obtained from Eq.(1) when $\overline{e}_i = 1$, $\overline{e}_{i+1} = \overline{e}_{sn}$ and $b_i = \overline{E}_1 = \dfrac{E_1}{E} = \dfrac{\overline{\sigma}_{sn} - 1}{\overline{e}_{sn} - 1}$ (Fig. 2, line 1). Then stress in elastic plastic zone $1 < \overline{e} \le \overline{e}_{sn}$ is determined by dependence

$$\overline{\sigma} = 1 + \overline{E}_1 (\overline{e} - 1) \tag{2}$$

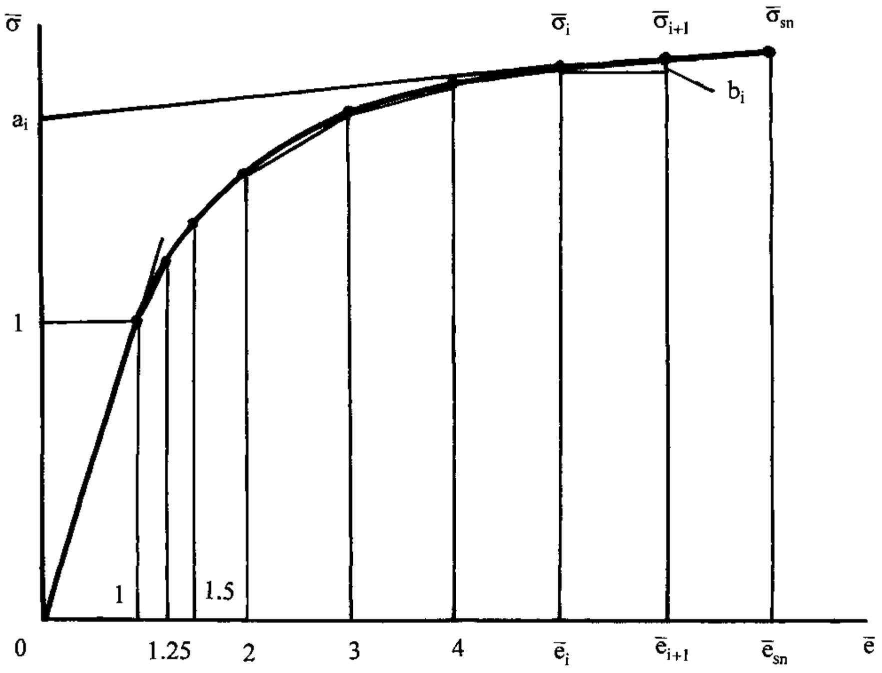

Fig. 1. Scheme of piecewise-linear polygonal approximation

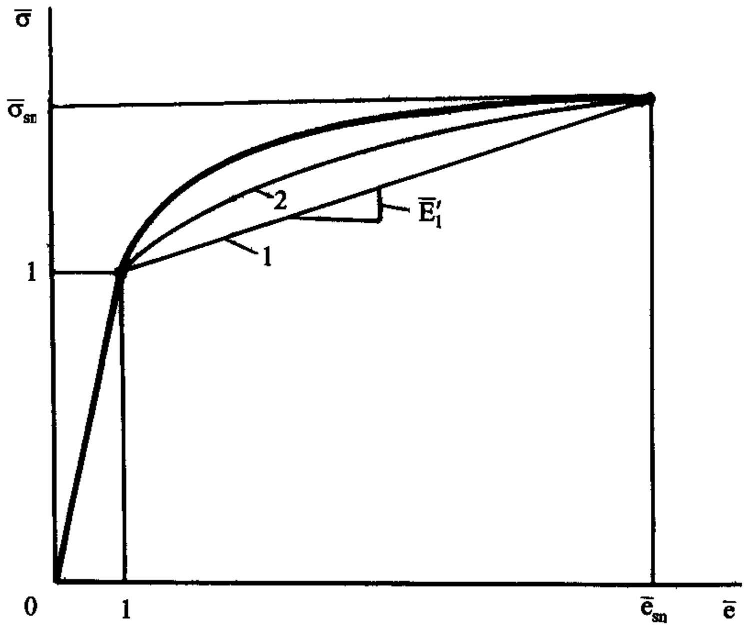

Fig. 2. Tensile curves approximated linearly (line 1) and by power function (curve 2) in coordinates $\bar{\sigma}-\bar{e}$

When test curve is approximated by power function (Fig. 2 curve 2) stress in elastic plastic zone is determined by dependence

$$\bar{\sigma}=\bar{e}^{m_0} \tag{3}$$

where $m_0=\lg\bar{\sigma}_{sn}/\lg\bar{e}_{sn}$ is parameter of material [2, 3].

Curve approximated by power function (3) better correspond test curve than the 1st line. From Eq.(3) follows that in coordinate system $\lg\bar{\sigma}-\lg\bar{e}$, that stress $\bar{\sigma}$ linearly depends on $\bar{e}$.

From Fig. 2 follows that maximum error in relative coordinates $\bar{\sigma}-\bar{e}$ is in initial zone of approximated curve when elastic plastic strain is small. This error may be decreased by increasing limit elasticity $\sigma_e>\sigma_{et}$ of approximated curve. The parameters of approximated tensile curve may be determined from conditions:

1. Work of the internal forces calculated by using test and approximated curves is the same;
2. The summary areas in interval of strain $1<\bar{e}'<\bar{e}'_{sn}$ between test and approximated curves, displaced lower and upper approximated curve, must be equal ($\bar{e}'=e/e_e$; $\bar{e}'_{sn}=e_{sn}/e_e$) (Fig. 3).

Limit elasticity of approximated curve $\sigma_e > \sigma_{et}$ and $e_e = \sigma_e / E$ is determined from the 2nd condition by approaching method [1]. In the 1st approaching may be accepted $\sigma_e^{(1)} = (\sigma_{et} + \sigma_{0.2})/2$. Then from Eq.(2) dependence

$$\overline{\sigma}' = 1 + \overline{E}_1'(\overline{e}' - 1) \tag{4}$$

is obtained, where $\overline{\sigma}' = \sigma / \sigma_e$ and $\overline{E}_1' = \dfrac{\overline{\sigma}_{ns}' - 1}{\overline{e}_{ns}' - 1}$.

Linearly approximated curve in coordinates $\overline{\sigma} - \overline{e}$ satisfactory correspond material test curve (Fig. 3).

Stress and strain in coordinates $\sigma - e$ may be calculated by dependencies $\sigma = \sigma_e \overline{\sigma}'$ and $e = e_e\, \overline{e}'$.

When $\overline{E}_1 = 0$ and $0 \le e \le e_{sn}$ by Eq.(2) is obtained Prandtly's diagram

$$\sigma = \sigma_Y = const \text{ when } e \ge e_Y \tag{5}$$

where σ_Y is yield strength.

In the 1st approaching may be accepted $\sigma_Y \approx \sigma_e^{(1)}$. For external force determination at elastic plastic loading σ_Y may be determined from the 1st condition. Then $\sigma_Y \approx (\sigma_{0.2} + \sigma_{ut})/2$ [4].

Analyses of deforming curves approximated by power function showed that it may be more exact when approximation is made in such manner:

- strain zone $0 \le e \le e_{sn}$ is divided into tree intervals: 1) $0 \le e \le e_{et}$; 2) $e_{et} < e \le e_1$ and 3) $e_1 < e \le e_{sn}$;
- $\overline{e} = e / e_{et}$, $\overline{e}_{et} = 1$, $\overline{e}_1 = e_1 / e_{et}$ and $\overline{e}_{sn} = e_{sn} / e_{et}$ are determined;
- $\overline{\sigma} = \sigma / \sigma_{et}$, $\overline{\sigma}_{et} = 1$, $\overline{\sigma}_1 = \sigma_1 / \sigma_{et}$ and $\overline{\sigma}_{sn} = \sigma_{sn} / \sigma_{et}$ are determined;
- stress

$$\overline{\sigma}_{cal} = \overline{e}^{\,m_{0\,cal}} \tag{6}$$

when $\overline{e}_1 < \overline{e} \le \overline{e}_{sn}$ is calculated

where $\overline{e}_1$ minimum value of strain when Eq.(5) valued (Fig. 4); $m_{0\,cal} = \lg \dfrac{\overline{\sigma}_{sn}}{\overline{\sigma}_{0.2}} / \lg \dfrac{\overline{e}_{sn}}{\overline{e}_{0.2}}$;

- parameter $C_\sigma = 0.5(\overline{\sigma}_{0.2} / \overline{\sigma}_{0.2\,cal} + \overline{\sigma}_{sn} / \overline{\sigma}_{sn\,cal})$ is determined;

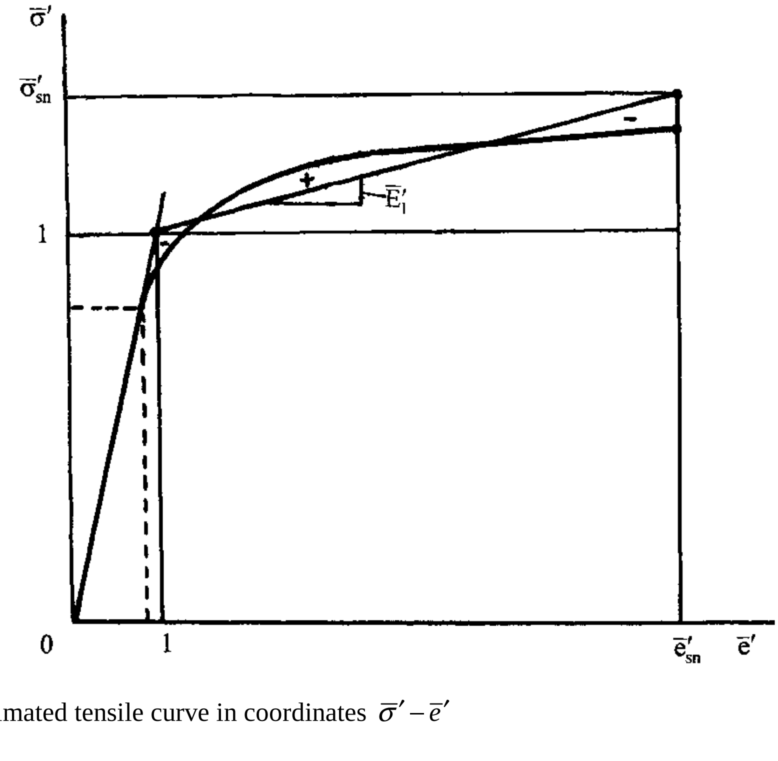

Fig. 3. Linearly approximated tensile curve in coordinates $\overline{\sigma}' - \overline{e}'$

- stress

$$\overline{\sigma} = C_{\sigma}\, \overline{e} \tag{7}$$

when $\overline{e}_1 < \overline{e} \le \overline{e}_{sn}$ is calculated. When for stresses determination criterion of deformation is used accuracy of Eq.(6) may be increased by using the variable parameter

$$C_{\sigma} = C_{\sigma\,0.2} + m_{C\sigma} \lg \frac{\overline{e}}{\overline{e}_{0.2}} \tag{8}$$

where $m_{C\sigma} = m_{C\sigma\, m} = \left(C_{\sigma\, sn} - C_{\sigma 0.2}\right) / \lg \dfrac{\overline{e}_{sn}}{\overline{e}_{0.2}}$;

- when $\overline{\sigma}_1 < \overline{\sigma} \le \overline{\sigma}_{sn}$ and $C_{\sigma} = const$ strain $\overline{e}$ is determined by dependence

$$\overline{e} = \left(\frac{\overline{\sigma}}{C_{\sigma}}\right)^{1/m_{0\,cal}} \tag{9}$$

where $\overline{\sigma}_1$ is relative stress which corresponds strain $\overline{e}_1$. When parameter $C_{\sigma} \ne const$, $\overline{e}$ is determined by approaching method. In the 1st approaching may be accepted $C_{\sigma}^{(1)} = C_{\sigma\, m}$;

- when $\overline{e} \le \overline{e}_1$ stress and strains are calculated from equations:

$$\overline{\sigma} = \overline{e}^{\,m_{01}} ;\ \overline{e} = \overline{\sigma}^{\,1/m_{01}} \tag{10}$$

where $m_{01} = \lg \overline{\sigma}_1 / \lg \overline{e}_1$.

Scheme approximation of the grade 15Cr2MoVA steel tensile curve by using Eqs.(7)-(10) in coordinates $\lg \overline{\sigma} - \lg \overline{e}$, when σ_e = 490 MPa, e_e = 0.00256, $\sigma_{0.2}$ = 560 MPa, $e_{0.2}$ = 0.00456, $\sigma_{sn} = \sigma_{ut}$ = 725 MPa, $e_{sn} = e_{ut}$ = 0.12, is shown in Fig. 4. Minimum strain value, when Eq.(5) valued, $\overline{e}_1 = 1.25$. From Fig. 4 follows that tensile curve approximated by using Eqs.(7)-(10) showed a good agreement with test curve. This curve more exactly correspond the 1st condition when values $\overline{\sigma}'_{0.2}$ and $\overline{\sigma}'_{ut}$ in coordinates $\lg \overline{\sigma} - \lg \overline{e}$ are determined by using method of least squares.

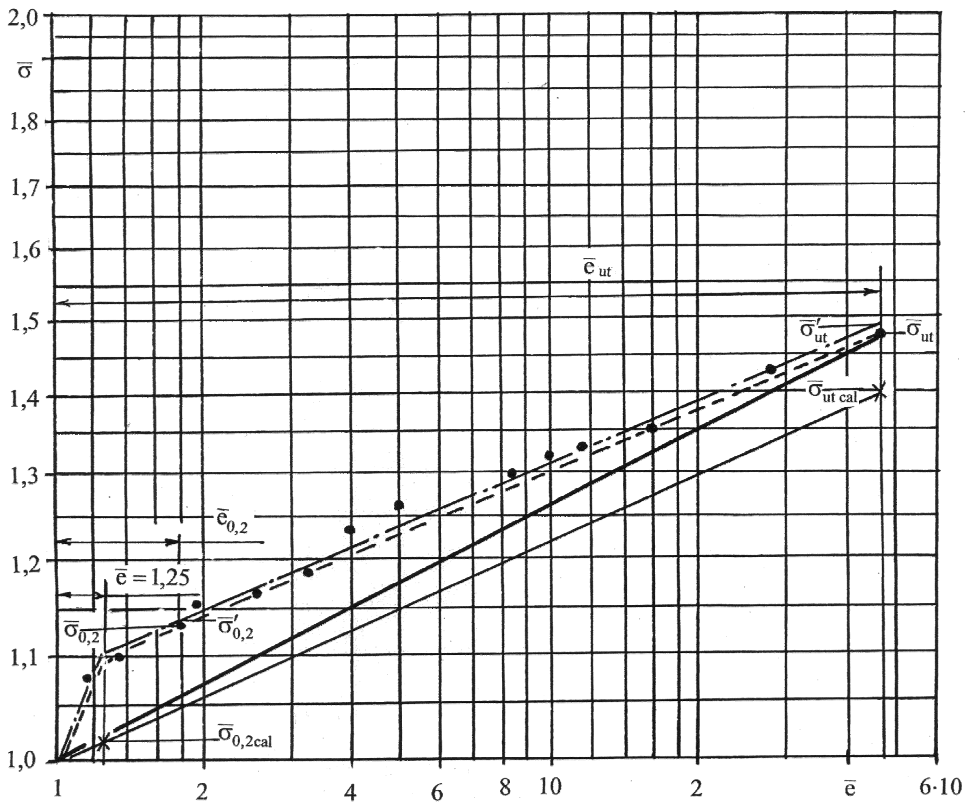

Fig. 4. Scheme of tensile curve approximation by power function Eq. (3) and Eqs.(6)-(10): ━━ Eq(3); ——— Eq(6); – – – Eqs.(7) – (10); — · — · — Eqs. (7) – (10), when $\overline{\sigma}'_{0.2}$ and $\overline{\sigma}'_{ut}$ are determined by using the method of least squares

Accuracy of this curve is negligible less then accuracy of piecewise-linearly approximated one. Therefore, this curve is recommended for analytical stress strain state calculation at elastic plastic loading.

In tensile curves, approximated by using Eqs.(1)-(10), is accepted $\sigma = F / A_0$ and $e = \Delta l / l$ (A_0 is initial cross-section of specimen). In mechanics of plastic deformation in metal processing tensile curve of true stress σ^t and true strain $e^t = \ln(1+e)$ are used [4]. The true stress σ^t is determined by estimating decreasing area of specimen cross-section A_i at static tension ($\sigma^t = F_i / A_i$). In this case $\sigma^t_{sn} = s_K$ and $e^t_{sn} = e^t_{\lim} = \ln[1/(1-\psi)]$ (s_K is fracture stress at static tension; ψ is relative decreasing of cross-section area at tensile loading).

Approximated tensile curves $\bar{\sigma}^t - \bar{e}^t$ may be determined analogically as tensile curves $\bar{\sigma} - \bar{e}$ by substituting $\bar{\sigma}^t_{sn}$, $\bar{e}^t_{sn}$ instead of $\bar{\sigma}_{sn}$, $\bar{e}_{sn}$. For construction of curve $\bar{\sigma}^t - \bar{e}^t$ when $e \le 0.035$ may be accepted $\bar{e}^t \approx \bar{e}$. In this case for approximation Eq.(3) and Prandtly’s type curve frequently used.

3. Tensile Curves Approximation by using Mechanical Properties of Materials Presented in Standards

From Eqs.(2)-(10) follows that for tensile curve approximation the parameters σ_e, e_e, $\sigma_{0.2}$, $e_{0.2}$, σ_{ut}, e_{ut1}, ψ, s_K must be known. But parameters σ_e, e_e, $e_{0.2}$, e_{ut1}, s_K there are not presented. Its values approximately may be calculated by equations:

$$s_K \approx \sigma_{ut}(1+1{,}4\psi); \quad \sigma_e \approx \left[\frac{\sigma_{0,2}}{(400+\sigma_{0,2})^{m_0}}\right]^{1/(1-m_0)}; \quad e_{ut2} \approx \ln\left[1/\left(1-\psi\frac{\sigma_{ut}-\sigma_{0.2}}{s_K-\sigma_{0.2}}\right)\right] \tag{11}$$

where e_{ut2} is maximum values of the homogeneous strain which corresponds σ_{ut}; $m_0 \approx \dfrac{0{,}75\lg(s_K/\sigma_{0,2})}{\lg\left(\dfrac{1}{\sigma_{0,2}/2\cdot 10^5+0{,}002}\ln\dfrac{1}{1-\psi}\right)}$.

These equations are obtained in work [2] for grade steels when $E = 2\cdot 10^5$ MPa. Strain $e_{ut1} = e_{ut\,\min} \approx 0.8e_{ut2}$ [3]. Grade 15Cr2MoVA steel calculated parameters, presented in Table 1, satisfactory correspond its experimental values.

Table 1

Experimentally determined and calculation parameters of grade 15Cr2MoVA steel

Parameters	σ_{et}	s_K	e_e	$e_{0.2}$	e_{ut2}	e_{ut1}
	MPa					
Experimentally determined	419	1600	0.00256	0.00456	0.150	0.125
Calculated by Eq.(11)	518	1420	0.00259	0.00459	0.175	0.140
Disagreement, %	23	11	1.2	0.7	17	12

For curve $\bar{\sigma} - \bar{e}$ construction the modified method of approximation is recommended. In this case $\bar{e}_1 = 0.5(1+\bar{\sigma}_{0.2})$ and $C_\sigma = C_{\sigma\, m}$ may be accepted.

4. Conclusions

The modified method of tensile curves approximation by power function is proposed.
Tensile curves approximated by using this method showed a good agreement with the test curves.
Accuracy of this curve is negligible less then accuracy of piecewise-linearly approximated one.

References

1. **Kogaev, V. P., Makhutov, N. A., Gusenkov, A. P.** Strength and durability calculations of structures and machines elements. – Moscow: Mashinostrojenijie, 1985, 223p. (in Russian).
2. **Makhutov, N. A.** Deformation criteria of fracture and strength analysis of structural elements. – Moscow: Mashinostrojenijie, 1981, 272p. (in Russian).
3. **Bražėnas, A.** Strength and low cycle fatigue of mechanically heterogeneous butt welded joints. – Kaunas: Technologija, 2002, 283p.
4. **Thomsen, E. G., Yang, C. T., Kobayashi , S**. Mechanics of plastic deformation in metal processing. – New York: MacMikllan, 1965, 486p.

Proceedings of 4th International Conference ITELMS'2009

Hydrogen Using in Transport

A. Jurkauskas*, D. Kalisinskas**

**Kaunas Technological University, Kęstučio Str. 27 LT-35209, Kaunas, Lithuania, E-mail: algirdas.jurkauskas@ktu.lt*
***Kaunas Technological University, Kęstučio Str. 27 LT-35209, Kaunas, Lithuania, E-mail: dalius.kalisinskas@stud.ktu.lt*

Abstract

Hydrogen can be abstracted by help of water and electric current. Its transformation into heat or electric current usually is simple and clean. While burning with oxygen hydrogen does not discharge any pollution, except water, that after the reaction could be turned back into environment. But hydrogen, as the element very often found in the planet, does not exist in a pure form, and in all cases is found in constitution of chemical compounds in the environment. In order to abstract pure hydrogen from water electrolysis is used, and correspondingly other chemical reactions are used to abstract pure hydrogen from bicarbonates or other compounds. Electric power for electrolysis could be obtained from clean, renovating energy sources, such as solar collectors, wind power-plants, geothermal energy and so on. So hydrogen could be an important element enabling accumulate and transfer clean energy.

KEY WORDS: *hydrogen, fuel, transport, energy*.

1. Introduction

Hydrogen (lot. hydrogenium) is a chemical element in the periodic law, with the sign H. Hydrogen atomic number - one, it is the lightest and predominant element in the universe.

In these days world hydrogen energy might be one of the most effective means to solve global environmental problems emerged. Now it is realized, that global warming effect is related to increased emission of exhaust (carbonic compounds, mostly CO_2) [1]. During the last century global surface temperature was increasing 0.6°C/century [2]. This tendency was developing dramatically during the last 25 years. With reference to three well known atmospheric appearances research centers – Princeton (USA), Hamburg (Germany) and IPCC (Great Britain) –temperature during the last 25 years was increasing at 2.3, 1.3 and 1.7°C rate correspondingly. As well, it was found out, that since 1995 temperature of the Atlantic, the Pacific and the Indian oceans increased 0.06°C (US National Oceanic and Atmospheric Administration).

With reference to data of USA energy department (DOE), in 2015 world emission of carbonic compounds will increase 54% from the level of 1990 and in 1990–2100 global surface temperature will increase 1,7–4,9°C [3].

Hydrogen amount in atmosphere is rather small - just about 5×10^{-5}% of volume, a little larger it is in upper atmospheric layers. At height 2500 km, where atmosphere is especially thin, almost just single hydrogen atoms are found. Hydrogen makes up 90% of atoms of whole the universe or 70% of mass. According to number of compounds, in which hydrogen could be detected, it is considerably ahead compared with any other element.

2. Hydrogen and Energy

While excavated fuel reserves are sinking, hydrogen is one of the most attractive energy accumulation and transport materials. Hydrogen is a fuel of big energetic value, without environmental pollution when burns. Liquid hydrogen is a perspective fuel. Using of this light fuel would extend possibilities of supersonic aircrafts and spaceships.

Unfortunately, cheap hydrogen abstraction and reliable storage methods are not known by now.

Hydrogen could be produced by help of electrolysis of salt water, but this requires cheap electric power. This method would be proper, if it was success in development of thermonuclear power stations.

Hydrogen is obtained by thermolysis of water, but even at temperature 2000°C just about 1% of water fissions. By use of laws of thermodynamics this obstacle could be driven through. Transformation, difficult to perform directly, can be performed by indirect reactions. It is important, that each of those reactions runs at not very high temperature, and by summing up equations of all reactions we should obtain water fission equation: $2\ H_2O(s) \longrightarrow 2\ H_2(d) + O_2(d)$. Scientists examine the problem, how to disintegrate water photo-chemically, i.e. by help of solar light.

Now an electrochemical device is designed, it is called fuel element, in which hydrogen and oxygen connection reaction runs, and emission energy immediately is transformed into electric energy, but not to heat. Efficiency of such devices is much bigger than of traditional electric power producing methods. Fuel elements now are used in spaceships.

Hydrogen storage problem is not lesser one. Very big vessels are necessary to store gasiform hydrogen, and its liquefaction is rather difficult. Hydrogen boils at α_τ=253°C temperature, so vessels with liquid hydrogen have to be very cool. Besides, it is important not to forget that hydrogen together with oxygen and air makes explosive mixtures. Some scientists propose to dissolve hydrogen in metals or their alloys, for example, in an iron and titan alloy, and then abstract by slight warming. In future vehicles instead of petrol tank there could be metal pig absorbing hydrogen. To abstract hydrogen heat of exhaust gas would be used.

At inside temperature and under pressure hydrogen density is such low, as amount of volume unit energy to come up to 1/300 of amount of petrol energy. In order to contain hydrogen into proper for use capacity, hydrogen has to be compressed to enlarge its density. Some hydrogen driven vehicles have got fuel tanks, where hydrogen is compressed to unbelievable large 10000 psi. *The Sequel*, *General Motors* produced vehicle contains 8 kg of such compressed hydrogen, enabling to drive a distance about 500 km. Refueling is conditionally simple, but even compressed hydrogen needs large fuel tanks, occupying correspondingly four-, five-fold more room, than conventional petrol tanks. Vehicles driven by fuel elements could contain larger fuel tanks, because their engines are more compact.

Some chemical compounds have got a feature to suspend hydrogen molecules at inside temperature and under pressure, and then, under some circumstances to release them. By now most promising researches were performed with metal hydrits. These metals are steady, but heavy: fuel tank with weight about 400 kg would hold energy sufficient for about 2-hours for vehicle driving. At present 'exotic' chemical compounds examined could demonstrate that there is possible really practical hydrogen storage. We base at high pressure fuel tanks, before we will invent materials allowing effectively keeping hydrogen in hard state, says Dan O'Connell, director of hydrogen driven vehicles program in General Motors.

If all mentioned problems were solved, hydrogen would be able to replace natural gas used for dwelling heating, in metallurgy - coal and carbonite. Surely, as now, as in the future, huge hydrogen amounts would be used to synthesize ammonia. With development of economically efficient hydrogen production methods, human life would change greatly and hydrogen century would start [5].

3. Hydrogen Using in Transport

Hydrogen using in transport can be divided into several directions: a) as fluid fuel – for transport vehicles, b) as electric energy source - for electro-mobiles.

One-material H_2 can be obtained just from few compounds. One of hydrogen stocks is the most common its compound - water. In order to abstract hydrogen, it is necessary to reduce oxidation rate of H from +1 in the water H_2O up to 0 in H_2.

At present hydrogen is produced using various technologies:

1. Hydrogen production from natural gas.
2. Hydrogen is obtained as secondary product in production of chlorine and sodium.
3. Water electrolysis:
   - 3.1. Using energy of any renovating sources (wind, solar, hydro- and other);
   - 3.2. Using nuclear energy (high temperature reactors). This is the most proper high extent technology for hydrogen centralized production.
   - 3.3. Using water electrolysis $2H_2O(s) \rightarrow 2H_2(d)+O_2$ (d). During water electrolysis electric current goes through water, which disintegrates into oxygen and hydrogen gas. During this process 100% of electric energy is not transformed into chemical hydrogen energy. Energy loss appears, because ions transferring electricity have to move thus heating water. Some researchers claim having achieved 50–70% efficiency, while the other - 80–94%. These numbers do not mean energy, consumed for electricity production, loss. Including energy, consumed for electricity production, hydrogen abstraction efficiency would make up 25–45%.
   - 3.4. When methane is under action of H_2O vapor CH_4 (d)+$H_2O(s) \rightarrow CO+3H_2$ metal which is above H in metal activity table under action of acid $Zn+2HCl \rightarrow ZnCl_2+H_2$
4. Experimental hydrogen abstraction methods:
   - 4.1. Using microorganisms;
   - 4.2. Disintegrating water in high-temperature plasma;
   - 4.3. Photo-dialysis.

Hydrogen fuel cell is an electrochemical device, which produces electric energy, using hydrogen and oxygen. Fuel cells structure is close to chemical elements one. It does not need charging and does not „discharge“, works supplying sufficient amount of hydrogen and oxygen. In this equipment hydrogen conversion into energy goes without burning process, it is highly efficient, does not pollute environment, does not create any noise and vibrations. Hydrogen fuel cells are known in science more than 160 years. In 1838 William Grove developed battery, which was called „Grove cell“. In this cell there would go reverse water electrolysis process. Ceramic fuel cells appeared in 1899, when Nernst invented hard oxide electrolytes. Since 1945 three scientific groups (in the USA, Germany and former USSR) worked intensely in the field of hydrogen fuel cells. As the result of this work – Siemens and Pratt & Wittney fuel cells conceptions. Hydrogen fuel cells were adapted in NASA Apollo program in 1960. Since 1980 governments of the USA, Canada and Japan increased greatly sponsorship of hydrogen energy programs. Now hydrogen energy technologies, enabling to use hydrogen, as energy source, in stationary electric energy production systems and all kinds of transport, are created intensely.

Cell consists of three active elements: anode or fuel electrode, hard oxide electrolyte, cathode or air electrode (Fig. 1).

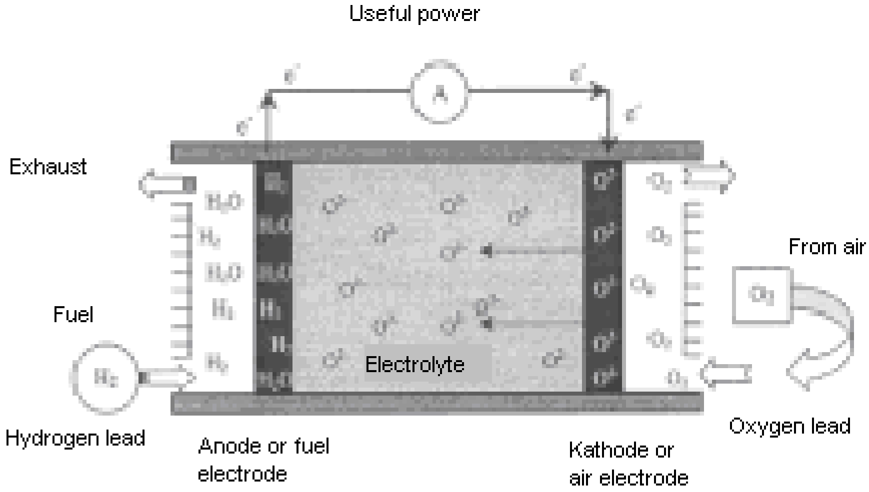

Fig. 1. Working principle of hard oxide hydrogen fuel cells

During operation hydrogen is supplied to an anode, oxygen (usually from air) – to a cathode. Oxygen molecules at electrode area are reduced and oxygen ions are obtained. These ions migrate through hard electrolyte at fuel electrode, where due to reaction with H_2 or CO, H_2O or CO_2 and electrons appear.

Anodic reactions:

$$2H_2 + 2O^{2-} \rightarrow 2H_2O + 4e^-$$

or

$$2CO + 2O^{2-} \rightarrow 2CO_2 + 4e^- ,$$

or

$$CH_4 + 4O^{2-} \rightarrow 2H_2O + CO_2 + 8e^- .$$

Catholic reaction:

$$O_2 + 4e^- \rightarrow 2O^{2-} .$$

4. Fuel Improvement with Hydrogen

There is an investigation of internal combustion engine efficiency increase in the use of hydrogen. Hydrogen is supplied to the intake manifold.

Fuel improvement with hydrogen increases of efficiency of internal combustion engine by adding hydrogen into fuel. This is achieved by injection of hydrogen or fuel mixture with hydrogen into the engine fuel collector or using prepared in filling stations mixtures of hydrogen and compressed natural gas.

In the mixture of hydrogen and compressed natural gas there is 4–9% of hydrogen (when calculated by amount of emissive energy). Danger of leakage and combustibility caused by gas mixture in which hydrogen amount does not exceed 50%, is the same as of unmixed compressed natural gas. The use of such mixtures is not required to protect against hydrogen cleavage. Hydrogen gas mixtures are prepared in hydrogen filling stations.

Hydrogen and compressed natural gas filling stations are in Norway and Canada.

Vehicle hydrogen injection systems inject fuel mixture with hydrogen or unmixed hydrogen into the engine fuel collector.

In some cases at the same time air-fuel ratio and injection times are changed. Small amounts of hydrogen to the engine intake air and the fuel portion allows the engine to operate with leaner air and fuel mixture. When mixture reaches the ratio 30:1, the combustion temperature significantly reduces, leading to reduction of nitrogen oxides formation.

In the case of majority charges of gasoline engines, the normal acceleration needs nearly stechiometric air-fuel mixtures, but at empty run, with reduced loads or at moderate acceleration, hydrogen added to the lean fuel mixture ensures the normal operation of the engine, at the same time reducing exhaust and fuel consumption. Engine efficiency increase exceeds energy costs to hydrogen production; it is valid when using hydrogen generators mounted in a vehicle.

Summarizing comparison of hydrogen and gasoline properties, exclusive feature of the engine operating on hydrogen improved fuel is to work with lean (or lean in particular) fuel mixture, thereby reducing exhaust and reducing fuel consumption. Systems operating on fuel improved with hydrogen are superior to the pure hydrogen-powered internal combustion engines, because they need the smaller changes of engine and fuel supply (and storage) system.

To create lean or lean in particular combustion mixture modified electronic injection system or carburetor is needed.

Hydrogen production by electrolysis using the vehicle battery or electricity supplied by generator and diesel fuel improvement with hydrogen in the older diesel tows can help to save up to 4% fuel and so many reduce exhaust amount. This method is applied in Canada and the USA [6].

New vehicles will be equipped with wire – aluminum, magnesium or boron. This wire in filling stations will be directly winded out from huge coil into vehicle inside, and then electro- motor will wind it onto a coil, replacing petrol tank – everything will go simply and elegantly.

When vehicle needs some energy, this wire automatically will be directed to metal and vapor internal combustion chamber. There wire will be heated up to high temperature and then its reaction with water vapor will start, as result of the reaction will be obtained hydrogen and metal oxide.

Hydrogen will be directed to internal combustion engines or fuel elements, and metal oxide will be accumulated in a vehicle. During next filling in the petrol station it will be taken from the vehicle and sent to process. For example, such metal oxide may be used as stock material in chemical and metallurgy industry or after obtaining metal from it may be returned back to filling stations.

It is interesting, that in the case of internal combustion engine, energy of water vapor from system outlet together with hydrogen flow will be utilized, thus increasing total system coefficient of efficiency.

Actually, innovation has got a disadvantage –for the same distance to drive, a coil with wire weighing several times more than petrol tank, ensuring the same energy amount, will be needed. Supposedly, 100 kg of wire instead of 33 kg conventional fuel. But for most vehicles extra 70–80 kg is just inconsiderable weight increment.

Anyway, this is by a long way less than, let's say, weight of batteries, equaling by energy volume or balloon with gasiform hydrogen. Walls of gasiform hydrogen balloon have to be thick due to high pressure, and balloon with liquid hydrogen weighs much because of thick heat insulation.

The company „Engineuity" is looking for investors and supposes in three years to demonstrate an operating example of vehicle with new fuel supply system.

Hybrid vehicles. In this case an engine of vehicle consists of two engines with different features: electromotor and heat-engine. Maximum power and torque in electromotor characteristic are reached with low rpm, and with high rpm - its power is minimum. Meanwhile in the case of heat internal combustion engine - on the contrary: power is minimum with low rpm. Maximum power is obtained, when rpm reaches 80% of maximum rpm. That is why gearbox is necessary for heat-engines. According to such scheme the car TOYOTA PRIUS with 40 HP electromotor and 60 HP internal combustion engine, consuming up to 4 1 gasoline to every 100 km has been in exploitation in Japan and Europe for several years. This is obtained using characteristic features of both engines, by boosting only an electromotor and returning energy during braking back to a battery. According to the pollution standards this car meets Eupopean ecological requirements, valid since 2005. If spark ignition engine in this car, is replaced with compression ignition one, consumption of diesel fuel might decrease to 21/100 km. It is enviable result for total 100 HP car power, almost five times less than in the case of normal gasoline engine of the same power and as many times less pollute exhausted and oxygen burnt.

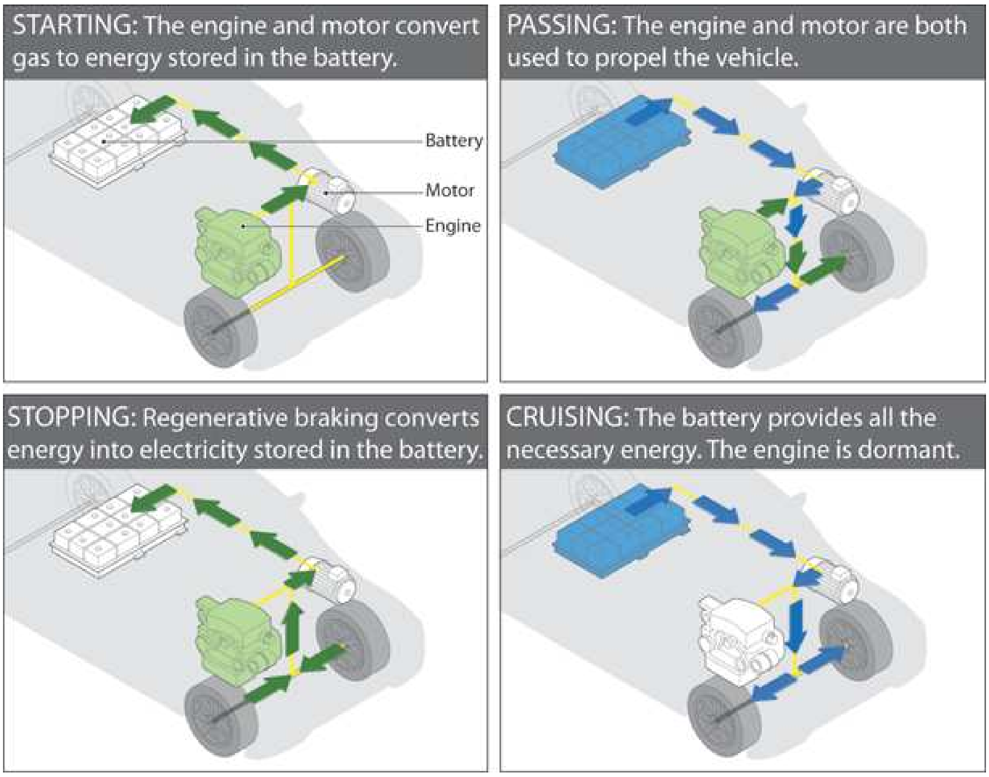

Fig. 2. Hybrid vehicle scheme

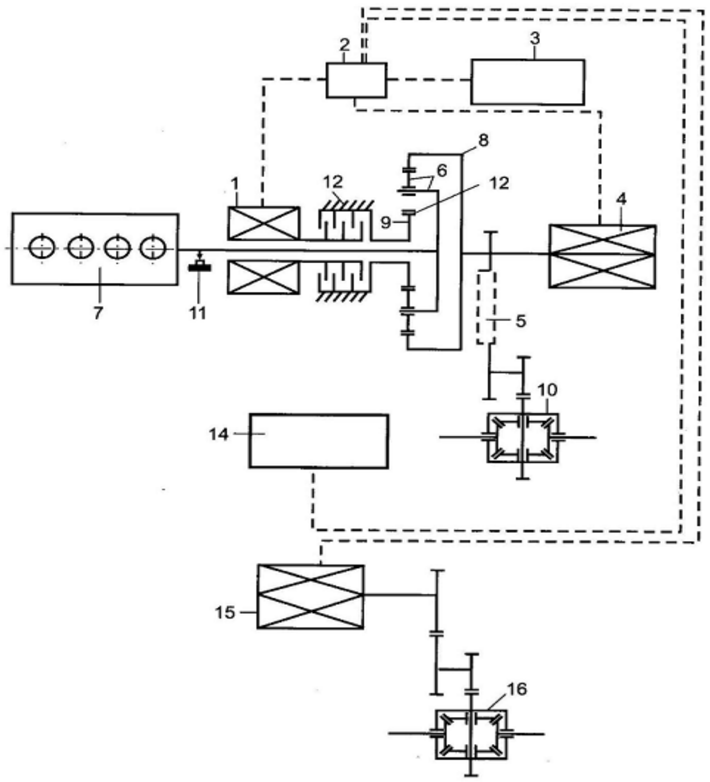

Fig. 3. “Lexus RX 400h” transmission principled scheme: 1 – generator – electro- motors; 2 – current converter; 3 – high voltage regulator; 4 and 15 – electro-motors – generators; 5 – reducer; 6 – wizard and satelite; 7 – internal combustion engine; 8 and 9 coronary and central gears; 10 and 16 – fore and rear axle; 11 – single direction coupling; 12 – planetary reducer; 13 – brake; 14 – electric control block.

By using hydrogen and oxygen, electric energy is produced. This electric energy might be used in a hybrid vehicle, as an energy source. Fuel elements – it is not fuel and not an engine. They are complex devices, where hydrogen during electrochemical process joins together to air oxygen supplied to fuel element, thus forming simple water. Electric power produced during this reaction is used to drive an electro- motor of transport vehicle. So any vehicle using fuel elements technology we without doubt could call electro-mobile, because it has no an internal combustion engine and does not use petroleum products to obtain energy.

5. Conclusions

Hydrogen ensures more efficient energy production and almost zero pollution.

Hydrogen as fuel use in internal combustion engines: it burns perfectly, so can replace natural gas, and it would not be necessary even to change engines structure - it would be enough to solve its storage in a car problem and develop the light as possible and as safe as possible an engine supply structure.

References

1. Worldwatch paper 157. Hydrogen Futures: Toward a Sustainable Energy System, August 2001.
2. National Center for Atmospheric Research. News release, July 2001.
3. Energy Information Agency (EIA), October 2001.
5. Word Energy Council (WEC). Survey of Energy Resources, 1998.
6. http://images.katalogas.lt/maleidykla/ene41/E-62.pdf
7. http://lt.wikipedia.org/wiki/Degal%C5%B3_pagerinimas_hydrogen
8. **Das L. M.** Hydrogen Engines. “Research and Development Programmes in Indian Institute of Technology, Delhi”. International Journal of Hydrogen Energy. 2002, Vol. 27, No 9, p. 953-965.
9. **Das L. M., Milton P.** “Experimental evaluation of a Hydrogen Added Natural Gas (HANG) Operated SI engine,” Symposium on International Automotive Technology SAE Paper No 2005-26-29 (January 2005)

Proceedings of 4th International Conference ITELMS'2009

Stability and Optical Properties of Adenine and Thymine Pairs

M. L. Balevičius*, J. Tamulienė**

** Vilnius University, Sauletekio av. 9,10222 , Vilnius, Lithuania, E-mail: Mindaugas.Balevicius@ff.vu.lt*
*** Institute of Theoretical Physics and Astronomy of Vilnius University, A. Gostauto str. 17, 08110, Vilnius, Lithuania, E-mail: gicevic@itpa.lt*

Abstract

The paper presents an investigation of canonical and non-canonical dimers of adenine (A) and thymine (T) basis. We compared stability and optical properties of these derivatives. Several different places of the T in respect of A were obtained and changes of the electronic structure of the investigated dimers were presented. The results proved that the stability of non-canonical dimers is similar to that of a canonical AT pair. Moreover, it is should be difficult to recognize non-canonical AT base pairs by using optical measurements.
KEY WORDS: *quantum mechanical investigation, Adenine, Thymine, base pairs, non-canonical base pairs.*

1. Introduction

Today a structural model of natural or synthetic nucleic acid polymer revealed the existence of a number of different non-Watson Crick arrangements occurring as single, tandem or consecutive base pairs. The guanine-uracil, guanine-adenine, adenine-adenine, uracil-uracil are often encountered [1]. Recent investigations indicating that single-stranded DNA or double-stranded DNA has the potential to adopt a wide variety of unusual duplex and hairpin motifs in the presence (trans) or absence (cis) of ligands [4]. The principles for the formation of the unusual structures have been established through the observation of a number of recurring structural motifs associated with different sequences. It is emphasized, that now using the definition of "unusual duplex" has a very broad meaning; i) the non-canonical sequence, i.e. two or four consecutive mismatched base pairs the stability of which is only slightly less than that containing canonical GC or AT base pairs; ii) shared base pairs; iii) a slightly disordered canonical base pair due to an additional hydrogen bonding in the loops. These unusual base pairs are established experimentally, i.e. it is established what can be possible, however, the other possible base pairings different from those known today are not presented. Thus, the thorough study of non-canonical base pairs and their location in the sequence are very useful and should be performed theoretically aiming to establish the non-observed pairs that nave not beeen investigated or observed today.

The newest investigations showed a possibility to design and synthesize a novel conformationally constrained pyridazinone E^{ag} -base peptide nucleic acid (PNA) -monomer 2 capable of binding thymine in a triplex motif [6]. The adenine analogue, 2-aminopurine (2-AP) can also form a Watson-Crick-type base pair, thus, maintaining the overall structural integrity of duplex DNA [7]. Moreover, a PNA-PNA-PNA triplex construct is also possible from one purine and two pyrimidine decamers, as it is evidenced from circular dichroic measurements. The PNAs conjugation with complementary DNA and RNA forms hybrids, too. A PNA duplex containing L-Iysinyl amide attached to the carboxyl terminal of the PNAs can demonstrate a handedness resulting the helicity of the structure. As a solution, the PNA monomer exists as both the *cis* and *trans* rotamers about the tertiary amine bond, slightly favouring the *trans* conformation [8]. It was early demonstrated that PNA-T can form a right-handed PNA/*DNA* triple helix with poly(dA) [9]. These investigations allow us to foresee the capability to form various duplex and/ or triple structures of a base pair different from a Watson-Crick-type, i.e. non-canonical base pairs.

Hence, the general aim of our investigations is to establish the stability of all possible base pairs. In this paper we present the results of investigations on stability and optical properties of AT pairs.

2. Results and Disscussion

The structural origin of described derivatives has been studied by using the generalized gradient approximation for the exchange-correlation potential in the density functional theory (DFT) as it is described by Becke's three-parameter hybrid functional, using the non-local correlation provided by Lee, Yang, and Parr. The DFT method is commonly referred to as B3LYP [9], - a representative standard DFT method. The TVZ basis set has been used as well [10]. The structures of the investigated derivatives have been optimized globally without any symmetry constraint, in order to determine the lowest energy structures of each cluster. The optical spectra of these molecular structure was investigated by the CIS (method (singly excited configuration interaction) [11]. This method is the simplest way to treat excited states and provides the possibility to pick up both singlet and triplet excited states. GAMESS program suites were used for all simulations here [13, 14].

The view of the investigated AT basis pairs is shown in Fig. 1. We indicated thesystems as I, II and III to simplify the discussion.

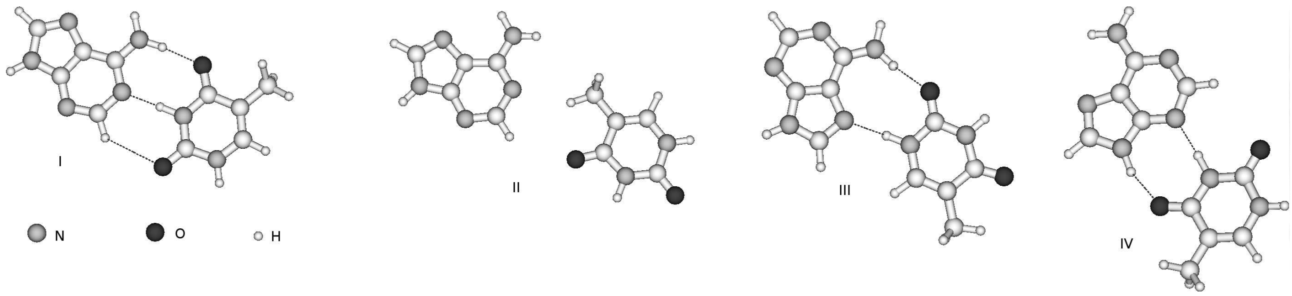

Fig. 1. The view of Adenine and Thymine basis pairs under investigation

The difference of total energy of these dimers in the equilibrium state is calculated folowingly:

$$\Delta E = E_i - E_j \ ,$$

where E_i and E_j is the total energy of the dimers (Table 1).

Table 1

Difference of total energy of the investigated dimmers

E_j \ E_i	I	II	III	IV
I	–	0.680	0.027	-0.082
II	0.680	–	-0.708	-0.762
III	0.027	-0.708	–	-0.109
IV	-0.082	-0.762	-0.109	–

It is necessary to mention, that pair I is the canonical base pair of adenine thymine. So, it is possible to see that non-canonical base pair IV is more stable than canonical base pairs. Additionally, the total energy of the pair III is only 0.027 eV higher than that of pair I. It implies the difficulty to recognize which pair is more preferable to be detected. On the other hand, the results of these trial investigations allow us to speculate that the surrounding of the adenine-thymine pairs in the DNR or PNR sequence could influence the stability of this pair remarkably. It is predicted, that in some cases the large stability of non-canonical basis pairs could not allowe to form the above sequences, while accidental occurrence of the pairs should lead to a large tension. So, it is no doubt that pairs I and III could be obtained in a DNR or PNR sequence, thus we intend to obtain some optical properties of these pairs. Further, the property of pair II has not been investigated because the total energy of formation is much higher than that of other pairs what proves very small possibility to obtain such a pair.

The density of the states of the investigated pairs is shown in Fig. 1. It is necessary to mention, that the influence of both environment and surrounding what would have to influence optical properties of these pairs, are not included into this research. Obviously, the density of states of these pairs is similar. So, the obtained optical spectra of these pairs should be similar. Thus, it should be suspect difficult to distinguish these pairs in complicated systems.

More unococcupied states in the energy region [0-1] a.u. indicate the possibility of greater transition rates and, therefore, higher levels of absorption. Increasing of excitation energy leads to decreasing of the level of absorption. The phenomena obtained in all the investigated molecules and support the above results on similarities of the optical spectra. On the other hand, these results exhibit clearly, that optical properties of Adenine and Thymine pairs are independent of their placement with respect to each other. In addition, we speculate that the recognition of the described pairs, when methods of chemical analyze are applied, would be also impossible. Hence, it is necessary to have molecular devices to obtain non-canonical basis pairs in the DNR or PNR sequences that could be important when explaining possible mutations or creating new polimers for molecular electronics.

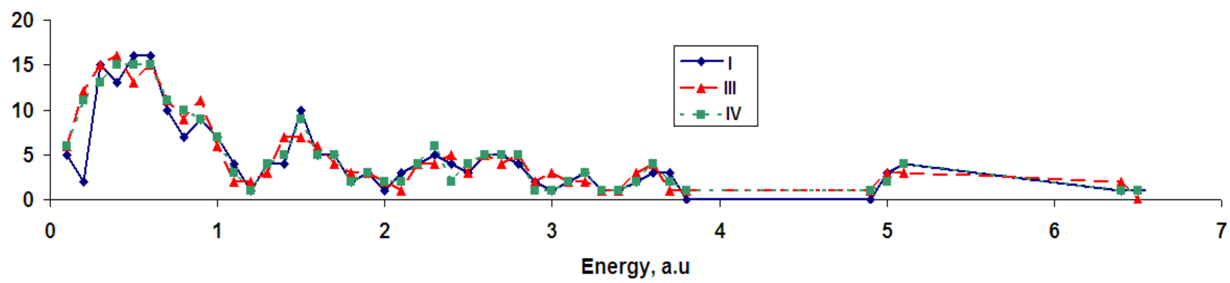

Fig. 2. Density of states of the investigated pairs obtained by CIS method

3. Conclusions

The research of possible Adenine and Thymine pairs has shown that stability of some non-canonical base pairs could be larger than that of canonical bases pairs. The total energy of some non-canonical base pair is only 0.027 eV smaller than that of canonical. It implies that the stability the above pairs is similar to the canonical one. The above structures are exhibited in Fig 1.

The investigation of the density of states of these pairs allow us to foresee, that optical spectra of these derivatives is similar, thus it is impossible to optically recognize of these pairs. So, a new molecular device or method must be created to obtain non-canonical basis pairs and explain possible mutations and create new polimer for molecular electronic.

Acknowledge

This work is performed in the frame of COST MP0802 activity.

References

1. **Chandrasekhar K., Malathi R.** Non-Watson Crick base pairs might stabilize RNA structural motifs in ribozymes – A comparative study of group-I intron structures, J. Biosci, 2003,ol.28, p. 547-555.
2. **Yuko Ito, Mizutani T.** Evidence of G-A/A-G pair, not A-G/G-A pair in SECIC element, Nucleic Acids research Supplement 2001, 1, Oxford university press.
3. **Jayasena S. D., Jolmston B. H.** Oligonucleotide-directed triple helix formation at adjacent oligopurine and oligopyridine DNA tracts by alternate strand recognization, Nucleic Acids Res. 1992, 20 (20), p.5279-5288.
4. **Shan – HoChou, Ko-Hsin Chin, Andrew H.-J. Wang.** Unusual DNA duplex and hairpin motifs, Nucleic Acids Research, 2003, Vol. 31, No. 10, p. 2461-2474
5. **Ray A., B. Norden B.** Peptide nucleic acid (PNA):its medical and biotechnical applications and promise for the future” FASEB Journal, 2000, Vol. 14, p.p.1041-1060.
6. **Eldrup A. B., Dahl O., Neilsen P. E.** A novel peptide nucleic acid monomer for recognition of thymine in triplex-helix structures, J. Am. Chem. Soc., 1997, Vol. 119, p.p. 11116-11117.
7. **Raney K. D., Sowers L. C., Millar D. P., Benkovic S. J.** A fluorescence-based assay for monitoring helicase activity, Proc. Natl. Acad. Sci. USA, 1994, Vol. 91, p.p. 6644-6648.
8. **Eriksson M., Neilsen P. E.** PNA-nucleic acid complexes: Structure, stability and dynamics, Q. Rev. Biophys., 1996, vol. 29, p.p. 369-394.
9. **Norden B., Kubista M., Kurucsev T.** Linear dichroism spectroscopy of nucleic acids, Q. Rev. Biophys. 1992, vol. 25, p.p. 51-170.
10. **Becke A. D.** Density-functional thermochemistry. iii. the role of exact exchange”,J. Chem. Phys. ,1993, 98, p. 5648.
11. **Godbout N., Salahub D. R., Andzelm J., Wimmer E.** Optimization of Gaussian-type basis sets for local spin density functional calculations. Part I. Boron through neon, optimization technique and validation. Can. J. Chem. 70, 560, 1992.
12. **Schmidt M. W., Baldrige K. K., Boatz J. A., Elbert S. T., Gordon M. S., Jensen J. H., Koseki S., Matsunaga N., Nguyen K. A., Su S. J., Windus T. L., Dupuis M., Montgomery J. A.** General Atomic and Molecular Electronic Structure System, Journal Computational Chemistry 1993, 14, 1347,1993.
13. Advances in electronic structure theory: GAMESS a decade later" **Gordon M. S., Schmidt M. W.** pp. 1167-1189, in "Theory and Applications of Computational Chemistry: the first forty years" **Dykstra C. E., Frenking G., Kim K. S., Scuseria G. E.** (editors), Elsevier, Amsterdam, 2005.

Proceedings of 4th International Conference ITELMS'2009

Ability to Control Swinging of Payload during the Movement of the Rotary Cranes Mechanism

T. Čampara*, H. Bukvić, D. Sprečić*****

**University of Tuzla, Faculty of Mechanical Engineering, Univerzitetska 4, 75000 Tuzla, Bosnia and Herzegovina, E-mail: tarek@bih.net.ba*
***Fa KFS GmbH, 85757 Karlsfeld, Germany, E-mail: husref_bukvic@yahoo.com*
****University of Tuzla, Faculty of Mechanical Engineering, Univerzitetska 4, 75000 Tuzla, Bosnia and Herzegovina, E-mail: esprecic@bih.net.ba*

Abstract

The main objective of this work is to develop useful computer model of tower cranes which could be used to design practical controllers for tower cranes. The computer model allows us to simulate and analyze motions of crane very quickly. In this work, we presented computer model of tower crane developed using MATLAB software and its module SIMMECHANIC. The computer model is a block scheme and is very flexible in a sense of changing structure of crane and including additional variable. Presented model includes feedback control based on the output values of swinging angle of payload. Swinging angles of payload were observed on the model with feedback control.
KEY WORDS: *rotary cranes mechanism, tower crane, computer model, simulation.*

1. Introduction

In this work, we present computer model which is developed using SIMMECHANIC in order to develop controller based on this model. The nonlinearities are included as well [2]. Therefore, controllers designed based on these models are applicable to real systems like controllers based on linear models with friction compensation [1, 2]. We used the tool of MATLAB - SIMMECHANIC to model the tower crane and to analyze the motions of tower crane. Our task using SIMMECHANIC to model the crane is to define the bodies and its joints, drivers and constrains. [5] To simulate the moving of crane we should put the inputs such as forces, velocities, masses and inertias. To get the results in a form of diagram we put different scopes on places witch we analyze [5]. We observed the position of payload in global XYZ-coordinate system and angles of cable in tangential and radial plane in local xyz-coordinate system of carriage [3, 4, 5]. Output values of α_T and α_R achieved by simulation on computer model with feedback control [1].

2. Introduction

Fig. 1 shows the system configuration under investigation. The jib structure of a tower crane is represented by a cantilever beam of length L, which is attached to a rotating rigid hub with radius d. The beam is assumed to be uniform and slender, and satisfies Euler-Bernoulli beam assumption that the rotary inertial and shear deformations can be ignored [6]. A rotation reference frame *xyz* is attached to the rotating hub. The axis *x* is identical to the neutral axis of the beam when it has no deflection.

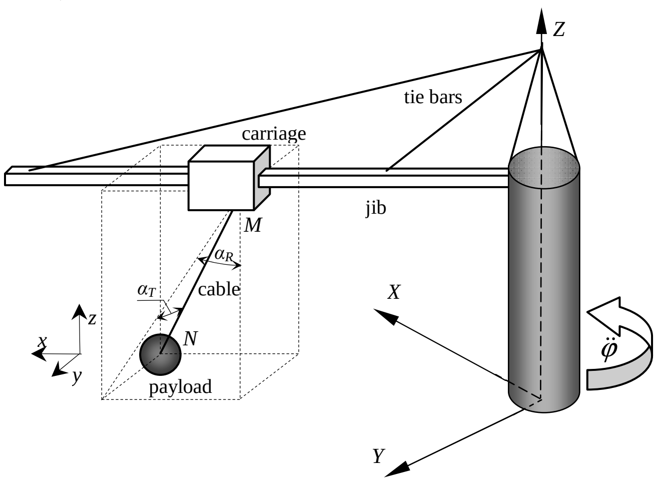

Fig. 1. Slewing flexible beam with moving payload pendulum

3. Tower Crane Computer Model with Feedback Control

The start point is developing adequate computer model based on the structure of tower crane we will analyze. In this work as observed crane we took tower crane additional weight on an opposite site of carriage [7]. Fig. 2 shows the general block scheme of controlled dynamic system.

Equivalent computer model for the tower crane is shown on Fig. 3 [8]. As we can see that is a block scheme with its structure. Beam, jibs, tie bars and cable with payload are represented as rigid bodies.

The carriage is represented as point masses moving along the jib 2. Driving of crane and carriage is represented using input signal 1 and 2, respectively [8]. Fig. 3 shows the computer model of the same tower crane with feedback control. This feedback control contains sensors, switches and gains. Feedback control takes action in a case if values of two angles α_T and α_R arise over given limits.

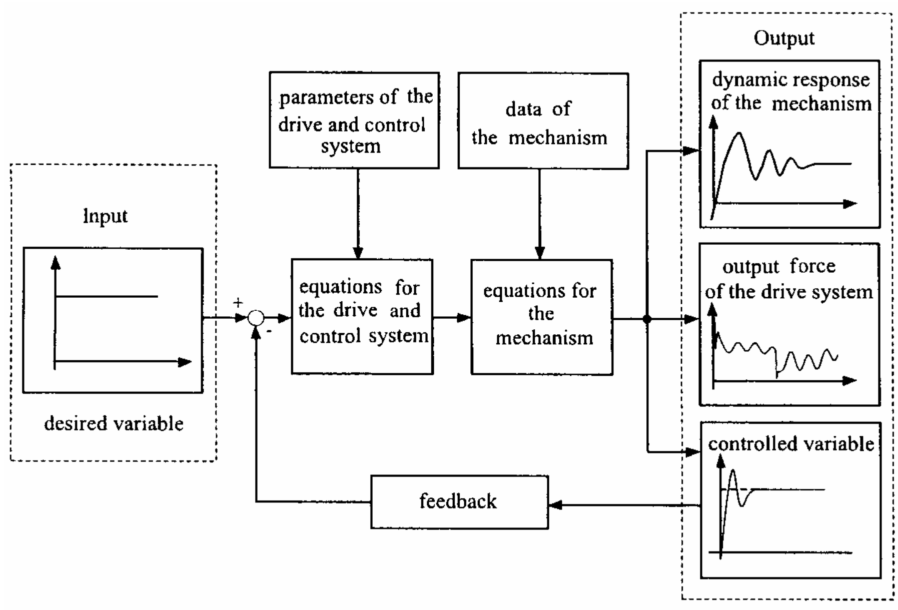

Fig. 2. The general block scheme of controlled dynamic system

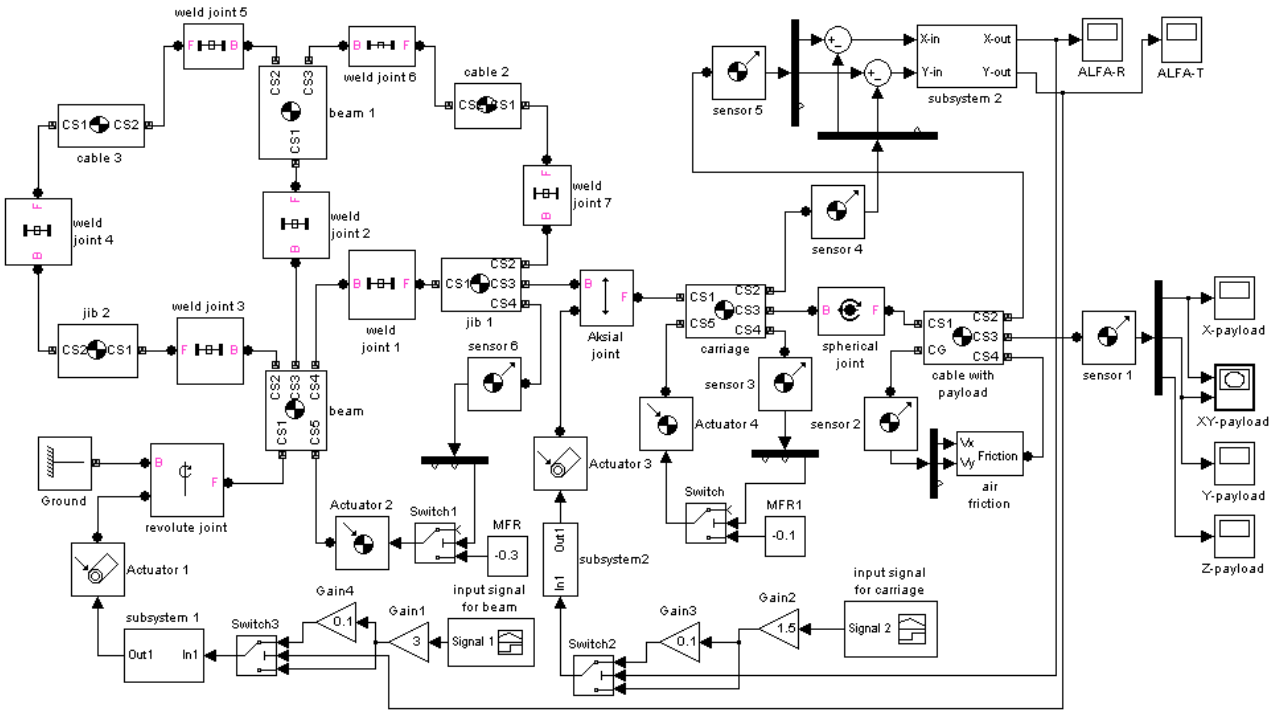

Fig. 3. Tower crane computer model with feedback control

4. Simulation on Computer Model

On Fig. 4 and Fig. 5 are shown input driving signals used in the simulation on computer models. The *x*-axis is time axis and *y*-axis is signal value axis [7]. As input signals we used the velocity. In order to get all needed parameters, we had to derivate and to integrate the velocity input signal. This procedure has been made in block subsystem 1 and block subsystem 2, respectively.

On Fig. 6 and Fig. 7 are shown the angles of cable with payload in local *xyz*-coordinate system of carriage obtained by simulation on computer model shown on Fig. 3. The *x*-axis is time axis and *y*-axis is value of angle α_T in tangential and α_R in radial plane in local coordinate-system of carriage. The angle values are given in degrees.

Table 1

Simulation parameters

Simulation parameters on computer model			
crane height	2.00 m	mass of beam	16.00 kg
jib 1 length	2.00 m	mass of payload	51.66 kg
jib 2 length	1.00 m	mass of additional weight	51.66 kg
cable length	1.50 m	mass of carriage	12.40 kg
moment of inertia of beam	4.27 kgm^2	simulation time	100 sec
friction moment MFR	0.30 Nm	α_T - max	0.1 deg
friction moment MFR1	0.10 Nm	α_R - max	0.5 deg

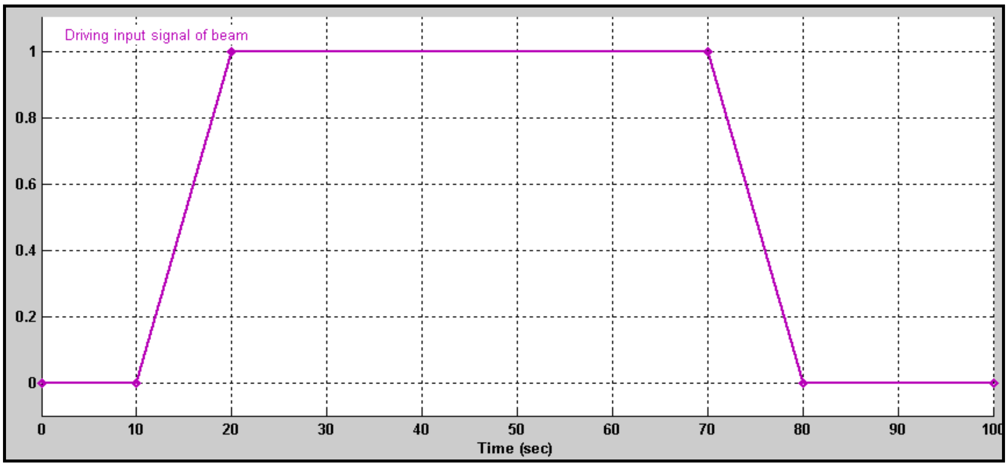

Fig. 4. Driving input signal of beam

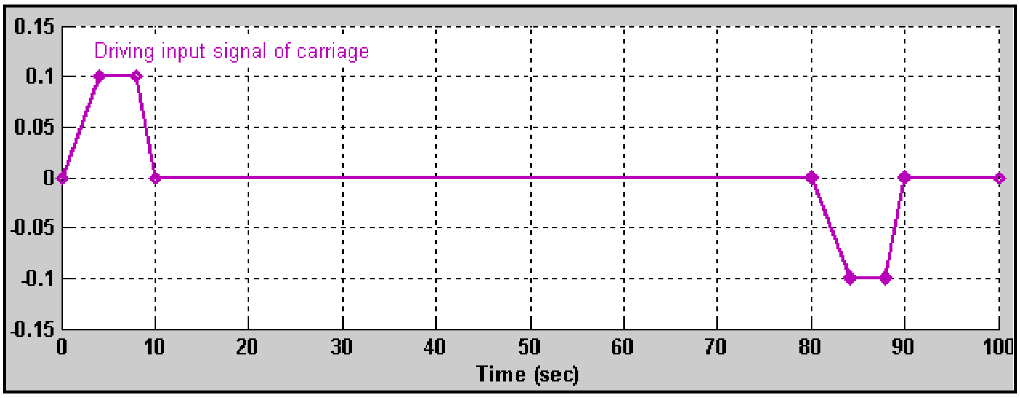

Fig. 5. Driving input signal of carriage

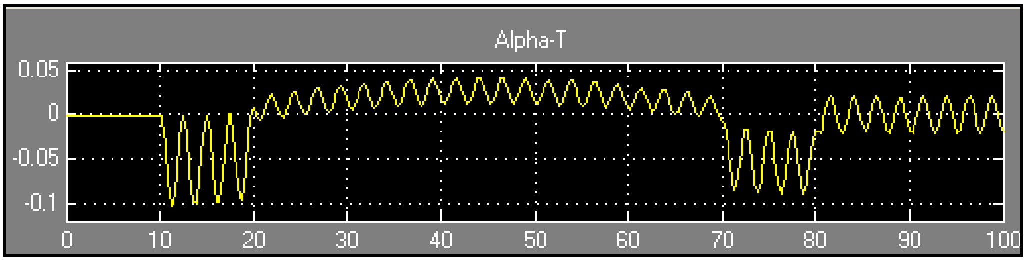

Fig. 6. Output value for α_T of cable with payload with feedback control in local coordinate system of carriage

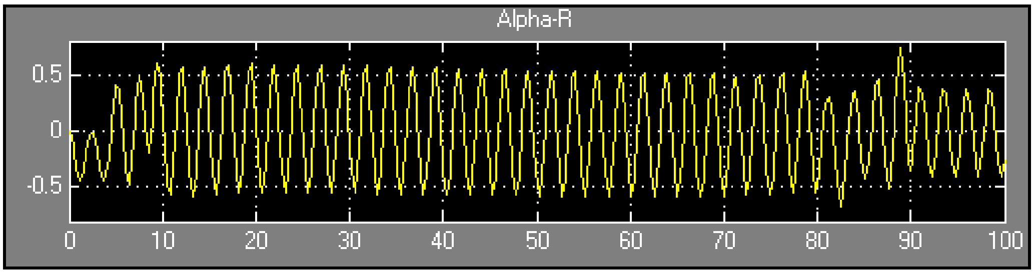

Fig. 7. Output value for α_R of cable with payload with feedback control in local coordinate system of carriage

5. Conclusions

The main idea in this paper was to show how it is possible to develop useful computer model of tower crane which could be used for simulation and analysis. The computer models shown in this paper have been used to simulate motions on a tower crane with the parameters given on the beginning of part 4 this papers. On the results of first simulation we added feedback control based on output values of angles α_T and α_R to develop adequate controller and to check it directly in SIMMECHANIC. Presented computer models include friction effects as well. We think that our paper shows models and simulation as one possible and fast way how to find out motions of tower cranes. Computer models shown in this paper give us enough information about motions we are interested in.

References

1. **Abdel-Rahman E. M., Nayfeh A. H., Masoud Z. N.** Dynamics and control of cranes: A Review, to appear in Journal of Vibration and Control 9, 2002.
2. **Lee H.P.** Dynamic response of a beam with moving mass, Journal of Sound and Vibration, 1996, 191 (2), p. 289–294.
3. **Oguamanam D. C. D., Hansen J. S., Heppler G. R.** Dynamics of a three-dimensional overhead crane system, Journal of Sound and Vibration, 2001, 242 (3), p. 411–426.
4. **Ridout A. J.** Anti-swing control of the overhead crane using linear feedback, Journal of Electrical and Electronics Engineering, 1989., 9(1/2), p. 17–26.
5. **Sun G., Kleeberger M.** Dynamic responses of hydraulic mobile crane with consideration of the drive system, Mechanism and Machine Theory, 2003, 38 p. 1489-1508.
6. **Yang W., Zhang Z., Shen R.** Modeling of system dynamics of a slewing flexible beam with moving payload pendulum, Mechanical Research Communications, 2006, 34, p. 260–266.
7. **Armstrong B., Dupont P., Canudas C.** A survey of models, analysis tools, and compensation methods for the control of the machines with friction. – Automatica, 1994, 30(70), p. 1083-1138.
8. MATLAB Tutorial.

Selection of Optimal Worm Gear Mechanism Dimensions using Evolutionary Strategy

T. Čampara*, H. Bukvić, D. Sprečić*****

**University of Tuzla, Faculty of Mechanical Engineering, Univerzitetska 4, 75000 Tuzla, Bosnia and Herzegovina, E-mail: tarek@bih.net.ba*
***Fa KFS GmbH, 85757 Karlsfeld, Germany, E-mail: husref_bukvic@yahoo.com*
****University of Tuzla, Faculty of Mechanical Engineering, Univerzitetska 4, 75000 Tuzla, Bosnia and Herzegovina, E-mail: esprecic@bih.net.ba*

Abstract

The objective of this paper is to use an evolutionary optimization method for the determination of the optimal worm gearing mechanism dimensions, such that the optimized dimensions are within realistic manufacturing constraints and the gearing power loss is minimized. The design of worm gearing mechanism has to satisfy various constraints, e.g. the geometrical, kinematics and the strength, while delivering excellent performance, minimum of power loss, long life and high reliability. This invokes the need of an optimal design methodology to achieve these objectives collectively, i.e. the multi-objective optimization. These objectives are hard to satisfy, thus making it a numerically challenging problem. The numerical toughness and a need to optimize them collectively warrant an application of the evolutionary multi-objective optimization. Objective function for optimization is gearing power loss ratio.
KEY WORDS: *worm gear, mechatronic, power loss, design, nondeterministic optimization, genetic algorithm.*

1. Introduction

Worm gears provide a normal single reduction range of 5:1 to 75-1. The pitch line velocity is ideally up to 30 m/s. The efficiency of a worm gear ranges from 98% for the lowest ratios to 20% for the highest ratios. As the frictional heat generation is generally high the worm box is designed disperse heat to the surroundings and lubrication is and essential requirement. Worm gears are quiet in operation and at the higher ratios are inherently self locking - the worm can drive the gear but the gear cannot drive the worm. The worm gear action is a sliding action which results in significant frictional losses. A number of factors influence efficiency, including ratio, input speed, tooth geometry, and lubrication. By far, the most important of these is ratio. A lower-ratio unit (5:1 for example) has more threads on the worm and a higher helix angle compared to a high-ratio unit. Higher helix angles mean less sliding friction and hence, higher efficiency. The purpose of this work is also to introduce the continuous genetic algorithms. Most sources call this version of the GA a real-valued GA. We use the term continuous rather than real-valued to avoid confusion between real and complex numbers [1].

2. Problem Statement

Gear-reducer inefficiency converts power to heat. AGMA (American Gear Manufacturers Assn.) guidelines for worm-gear, helical, and other types of reducers limit the maximum allowable operating temperature to 40 °C above ambient, not to exceed 90 °C. To stay within these guidelines, worm-gear reducers must be considerably larger than equivalent-rated helical reducers (to dissipate more heat) or rely on auxiliary cooling devices. Efficiency of worm gear drives depends to a large extent on the helix angle of the worm, ratios of the worm gear and center distance. Multiple thread worms and gears with higher helix angle prove 25% to 50% more efficient than single thread worms. The mesh or engagement of worms with worm gears produces a sliding action causing considerable friction and greater loss of efficiency beyond other types of gearing. The purpose of the optimization is to determine such a set of worm gear characteristic dimensions – z_1 (number of worm teeth), i (worm gear ratio) and d_{m1}/a (ratio between mean diameter of worm and center distance of worm gear pair) that satisfy the limitation equations and balance the conflicting objectives. The worm gear parameters must be selected so that the gear power loss (P_z/P_2) is minimized to the greatest possible extent. Fig. 1 shows selected parameters.

$$\min_{(z1,\,i,\,dm1/a)} \eta_Z = F\left(z_1, i, \frac{d_{m1}}{a}\right)_{\min} \tag{1}$$

Gearing power loss ratio (P_z/P_2) is calculated according to:

$$\frac{P_Z}{P_2} = \frac{1}{\eta_Z} - 1 \tag{2}$$

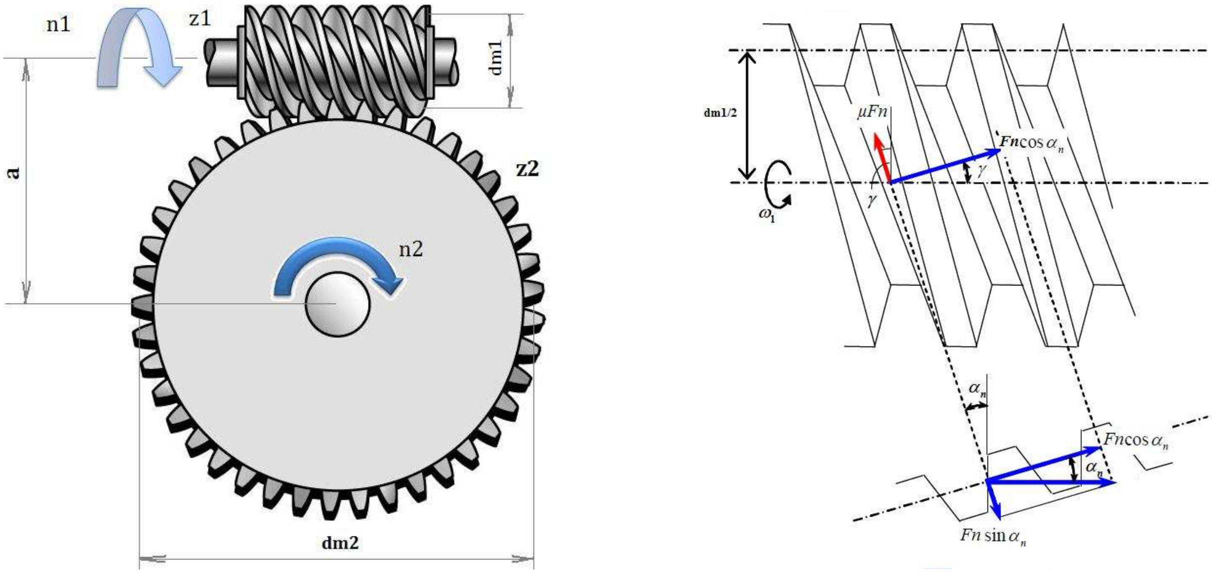

Fig. 1. Worm gear characteristic dimensions, z_1 (number of worm teeth), i (worm gear ratio) and d_{m1}/a (ratio between mean diameter of worm and center distance of worm gear pair)

Efficiency of gearing η_Z is a function of z_1 (number of worm teeth), i (worm gear ratio) and d_{m1}/a (ratio between mean diameter of worm and center distance of worm gear pair):

$$\eta_Z = \frac{1-\mu_Z \tan\gamma_m}{1+\mu_Z/\tan\gamma_m} \tag{3}$$

where μ_z is gearing coefficient of friction, γ_m is pitch angle at mean diameter calculated as follows:

$$\mu_Z = \mu_1 + \frac{\mu_o - \mu_1}{(1+v_F)^P}; \quad \mu_1 = \frac{(Y_M\ Y_Z)}{\sqrt{a}}; \quad p = \sqrt{\frac{0.072}{\mu_1}} \tag{4}$$

μ_0 is basic coefficient of friction, μ_1 mean coefficient of friction, Y_M =1 is material factor for steel alloy structural steel 16MnCr5 case-hardened and bronze (centrifugal cast) CuSn12Ni2-C-GZ (DIN EN 1982). Y_Z is pitch angle factor obtained from recommended values as function of γ_m. v_F is sliding velocity calculated as follows:

$$v_F = \frac{d_{m1}\omega_1}{2\cos\gamma_m} \tag{5}$$

where $\omega_1 = 2\pi n_1/60$, n_1 =1500 rpm of worm, γ_m is pitch angle calculated as follows:

$$\tan\gamma_m = \frac{z_1}{z_F}; \quad z_F = \frac{d_{m1}}{m}; \quad m = \frac{d_{m2}}{z_2}; \quad d_{m2} = 2a - d_{m1} \tag{6}$$

where z_F is factor of the worm shape, m is axial module, d_{m2} is mean diameter of worm wheel.

3. Constraints

There are several factors limiting the worm gearing dimensions. Those factors usually originate from technical specifications and technological considerations. The following constraints are taken into account:

1. Permissible range of worm gearing dimensions:

$$z_{1\min} \le z_1 \le z_{1\max}; \quad i_{\min} \le i \le i_{\max};$$

$$d_{m1\min}/a \le d_{m1}/a \le d_{m1\max}/a; \quad \gamma_{\min} \le \gamma \le \gamma_{\max} \tag{7}$$

$$2 \le z_1 \le 4; \quad 10 \le i \le 22; \quad 0.3 \le d_{m1}/a \le 0.55; \quad 15^\circ \le \gamma \le 25^\circ \tag{8}$$

2. Permissible stress limitations:

$$g_1(x) = \frac{F\,t_2}{b_{m2}\,m\,z_2} 2.5 - 3.6 \le 0\,, \quad \text{linear pressure worm gear tooth} \tag{9}$$

$$g_2(x) = \frac{F\,t_2}{b_{m2}\,m\,\pi} - 30 \le 0\,, \quad \text{bending stress of gear tooth} \tag{10}$$

$$g_3(x) = \frac{d_{m1}}{1000} - \frac{F_{tR1}\,L^3}{48\,E\,I} \le 0\,, \quad \text{acceptable deflection of worm shaft} \tag{11}$$

where, F_{t2} is axial force of worm gear, b_{m2} is width of worm gear at mean diameter of worm wheel and F_{tR1} is total radial force. Equations for F_{t2} and F_{tR1} are well known so they are not presented in this paper.

4. Genetic Algorithm

Genetic algorithm (GA) maintains a population of individuals (encoded solutions), and guides the population towards the optimum solutions [2]. Fitness function provides a measure of performance of an individual how fits. Rather than starting from a single point solution within the search space as in traditional optimization methods, the genetic algorithm starts running with an initial population which is coding of design variables. GA selects the fittest individuals and eliminates the unfit individuals in this way. The flow chart of genetic algorithm is shown in Fig. 2. An initial population is chosen randomly at the beginning, and fitness of initial population individuals is evaluated.

Then an iterative process starts until the termination criteria have been run across. After the evaluation of individual fitness in the population, the genetic operators, selection, crossover and mutation are applied to breed a new generation. Other genetic operators are applied as needed. The newly created individuals replace the existing generation and reevaluation is started for fitness of new individuals. The loop is repeated until acceptable solution is found.

5. Numerical Results

Table 1 illustrates the outcomes that were obtained by applying the GA method. The first row shows the best solution of given problem for population of 200 chromosomes, 3 generations and mutation ratio 0.0001. The optimal calculated solution of the gearing power loss ratio (P_z/P_2) is 0.06650.

Table 1

Results obtained in this work compared to the other authors

z_1	d_{m1}/a	i	(P_z/P_2)	γ	tan $g\ \gamma$	z_2	d_{m1}	d_{m2}	μ_z	η_z
3	**0.31**	**15**	**0.06650**	**20.83419**	**0.36344**	**45**	**62**	**338**	**0.02119**	**0.93764**
3	0.43	11	**0.07045**	19.02748	0.33192	33	86	314	0.02092	0.93418
3	0.48	10	**0.07271**	18.15287	0.31667	30	96	304	0.02079	0.93222
3	0.49	10	**0.07408**	17.66541	0.30816	30	98	302	0.02072	0.93103
3	0.34	16	**0.07459**	17.49251	0.30515	48	68	332	0.02069	0.93059
4	0.50	10	**0.07549**	17.19745	0.30000	40	100	300	0.02065	0.92981
4	0.47	11	**0.07619**	16.96460	0.29594	44	94	306	0.02060	0.92921

Fig. 3 shows the plots of gearing power loss ratio (P_z/P_2) values during the working of GA for different number of population. Design variables have different values and take searched minimum value of objective function at 200-th generation shown in Fig. 4.

It has been shown that design variables take values as: number of worm teeth is 3, friction coefficient is 0.02119, and helix angle is 20.8°. Fig. 4 shows the plots of the best fitness function values in each generation as optimization proceed for worm gear ratio i is 15 and d_{m1}/a ratio between mean diameter of worm and center distance of worm gear pair for 200 populations is 0.31. The overall results show that the best design converge 200-th generation. Refining the design is possible by adapting GA parameters such as mutation rate, crossover rate and population size. The GA application developed in Visual Basic for Application has been run several times for different values of design variables. The results obtained are given in Table 1.

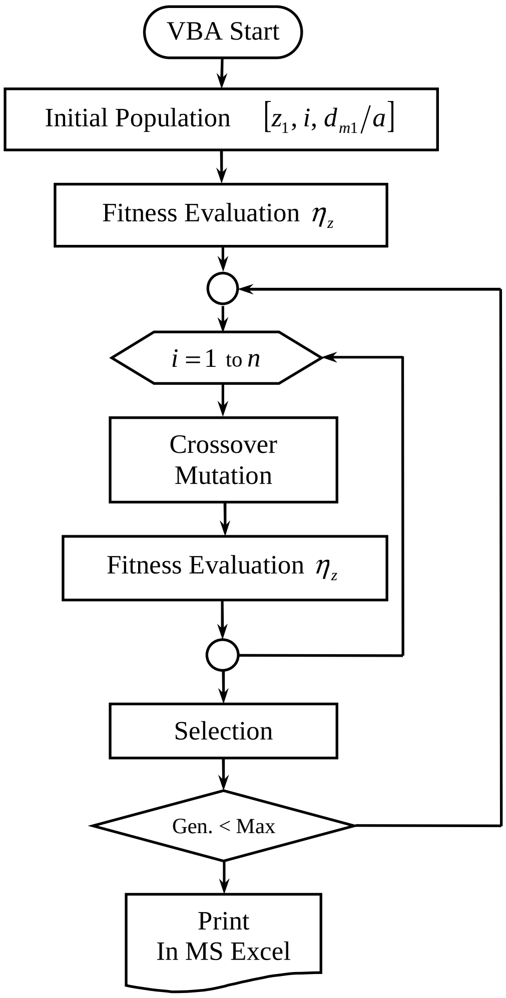

Fig.2. A flowchart for the GA optimization process

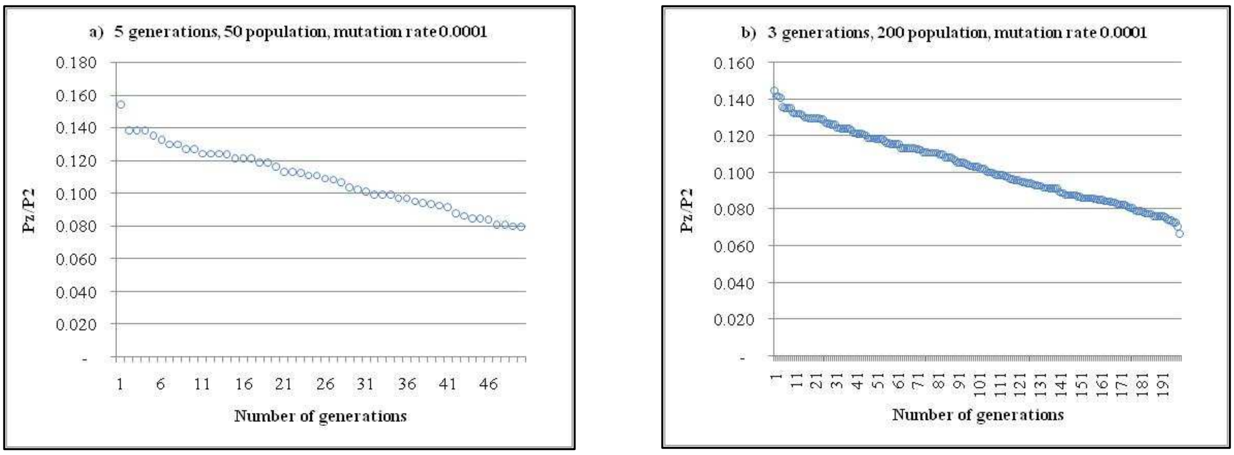

Fig. 3. Calculated gearing power loss ratio regarding number of generation

Genetic algorithms do not have many mathematical requirements and can handle all types of objective functions and constraints. Because of their evolutionary nature, genetic algorithms can be used to search for solutions without regard to the specific inner workings of problem. Therefore, it is hoped that many more complex problems can be solved using genetic algorithms than using conventional methods. Because genetic algorithms, as a kind of metaheuristics, provide us with great flexibility to incorporate conventional methods into the main framework, we can exploit the advantages of both genetic algorithms and conventional methods to establish much more efficient implementations to problems. The growing research on applying genetic algorithms to multi-objective optimization problems presents a formidable theoretical and practical challenge to mathematical community [3].

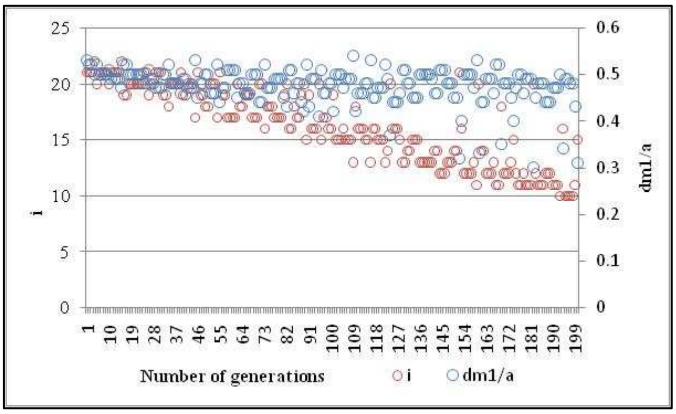

Fig. 4. Numerical results of GA for worm gear ratio i and d_{m1}/a ratio between mean diameter of worm and center distance of worm gear pair for 200 population

6. Conclusions

Worm gear comprises combination of threaded gear (worm) and mating gear (worm wheel). The worm gear can be classified into various types based on gear type of worm and worm wheel, and angle of two axes. Gear ratio of worm gear is determined by the proportion of number of threads of worm (number of gears) and number of gears of worm wheel. As the number of threads of worm can be 1, one gear shift can achieve a couple tenths to a couple hundredth of large reduction, which translates into high torque with less space. On the contrary, it has a disadvantage that transmission efficiency is not good due to friction from contact gears. The worm is always the driver in speed reducers, but occasionally the units are used in reverse fashion for speed increasing. Worm-gear sets are self-locking when the gear cannot drive the worm. This occurs when the tangent of the lead angle is less than the coefficient of friction [4].

The objective of this work is to apply the genetic algorithm optimization procedure for the determination of optimal worm gearing dimension so that the gearing power loss ratio (P_z/P_2) is minimized. In addition the same method can be easily extended to the five dimensional cases with a constraint upon the maximum permissible mass of the worm gear mechanism. No knowledge about the derivatives is needed and only a fitness function needs to be defined. This is a key benefit of such a genetic algorithm; it converges towards the global minimum every time. Downside of genetic algorithms is that since they incorporate random elements, they don't always yield the same solution each time. On the other hand, genetic algorithms are robust and don't require gradient-based computations plus, they can handle very nonlinear problems in many cases better than a gradient-based approach can [5].

References

1. **Randy L. H., Sue E. H.** Practical genetic algorithms, John Wiley & Sons, Inc., 2004, p. 51.
2. **Mitsuo G., Runwei C.** Genetic Algorithms and engineering Optimization, John Wiley & Sons, Inc., 2000, p. 18.
3. **Bjorndal M., Caprara A., Cowling P., Croce F., Lourence H., Malucelli F., Orman A., Pisinger D., Rego C., Salazar J.** Some thoughts on combinatorial optimization, Europian Journal of operational Research, 1995, vol 83, p. 253-270.
4. **Joseph E. S., Charles R. M.** Standard handbook of machine design, McGraw-Hill, 1996, p. 2-3.
5. **David M. B.** Excel Scientific and Engineering Cookbook, O'Reilly, 2006, ch. 13.
6. **John G., Stephen B., Rob B., Michael A.** Excel® 2007 VBA Programmer's Reference, 2007, Wiley Publishing, Inc.

Proceedings of 4th International Conference ITELMS'2009

The Research on the Models of Dynamic Controllers

V. Januševičius, O. Fiodorova, J. Valickas

Kaunas University of Technology Panevezys Institute, Daukanto str. 12, LT-35209 Panevezys, Lithuania,
E-mail: jonas.valickas@ktu.lt

Abstract

In this paper the investigation of the influences of the various controllers to given plant control system is qualitative characteristics presented, and also the characteristics of the sensitivity of a system for uncertainty and variation in the controlled plant parameters are analyzed. In order to compare and contrast the results of the study, all cases used the same performance criterion for selecting and the tuning of each controller. The sensitivity of the system characteristics to errors in the plant transmittance is measured by using root loci approach. MATLAB software is appropriately used in the entire analysis.

KEY WORDS: *controllers, sensitivity, performance criterion.*

1. Introduction

Solving the control systems design problems, one confronts the following two critical questions: what type of feedback controller should be used to control a given plant (or process), and how to select the best values for the adjustable parameters of the chosen controller in order to achieve an "optimum" response for the controlled plant?

In addition, in the practical implementation of control systems it is important not only to achieve of the static and dynamic control process performances, but also to ensure that the characteristics have to be the less dependent on the plant parameters and their variations. These problems are particularly relevant to the design, for example, intelligent cruise control of the car systems characteristics: vehicle parameters (tire pressure, tire wear, etc.), road conditions (rain, ice, bumps, crowns, etc. or external factors (for example, wind) which vary during the operation. In the control systems practice, these tasks are usually resolved by comparing and reconciling the results of alternative design decisions. This work studied the effects of the different controllers to the plant control features, as well as, the influence of this variation to these characteristics. Two methods of the compensation were used to compensate the plant characteristics:

- in the process control widely used compensator – PID controller;
- using the algebraic compensators - a standard [1] and robastic [3] controllers.

PID controller has a fixed dimension and model regardless of the application. As compared to an algebraic PID controller PID controller has a smaller number of closed-loop poles but it is generally easier to produce.

The model (i. e. the number poles and zeros) of an algebraic controller will vary according to the problem type to fit the dimensional requirement of each problem.

The performance criterion for the tuning of each controller was considered for the exact placement of closed-loop poles.

To facilitate the comparison of the various controllers and to aid in design, each is applied to a virtual third-order type 1 plant model that possesses the dominant closed-loop poles. All the controllers that will be considered may be implemented by means of cascade-compensated configuration (Fig. 1).

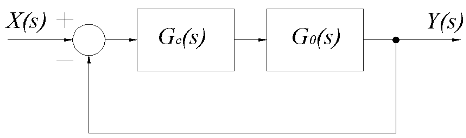

Fig. 1. Cascade compensated system

2. Selecting the Transfer Function $G_C(s)$

Suppose the transfer function of the plant and controller in the cascade compensated system (Fig. 1) are given by

$$G_0(s) = \frac{N_0(s)}{D_0(s)} \tag{1}$$

and

$$G_C(s) = \frac{N_C(s)}{D_C(s)}, \tag{2}$$

so, the placement of the compensated system closed-loop poles can be found by solving the characteristic equation

$$A(s) = D_C(s)D_0(s) + N_C(s)N_0(s)\,. \tag{3}$$

The order of the equation (3) (i. e. the order of compensated system) is the order of used plant plus the order of the transfer functions of the controller. The number of the closed-loop poles that can be placed is equal to the number of adjustable factors in the controller. In general, if the compensated system is order w and the controller has m adjustable factors, then the designer can exactly place m closed-loop poles as desired. The remaining $n – m$ closed-loop poles plus the m controller adjustable factors become dependent variables that must be computed from the equations arising from the characteristic polynomial. These equations are always linear and may possibly be simultaneous.

The third-order type 1 system

$$G_0(s) = \frac{1}{s(s^2+5s+6)} \tag{4}$$

is to be compensated so that the closed-loop poles (that means the desired transient response performance specification) become at –1 and $-1 \pm j1$. Then from equation (3) we find the form of desired equation

$$A(s) = (s+1)(s+1-j1)(s+1+j1) = s^3+3s^2+4s+2 = 0\,. \tag{5}$$

This characteristic equation implementing the three transfer function of controllers can be found:

a. PID controller transfer function. Including classical ideal PID controller

$$G_C(s) = \frac{k_d s^2 + k_p s + k_i}{s} \tag{6}$$

the closed-loop systems characteristic equation becomes fourth order (n = 4):

$$A(s) = (s+a)(s+1)(s+1+j1)(s+1-j1) = s^4+(3+a)s^3+(4+3a)s^2+(4a+2)s+2a = 0\,. \tag{7}$$

Since there are only m=3 adjustable constants in the PID controller, only three of four closed-loop poles can be placed exactly. It is convenient to call the fourth pole $– p$, so that desired characteristic equation (5) becomes

$$A(s) = (s+a)(s+1)(s+1+j1)(s+1-j1) = s^4+(3+a)s^3+(4+3a)s^2+(4a+2)s+2a = 0\,. \tag{8}$$

The three adjustable factors of the PID controller can be calculating by equating power-of-s coefficients in (7) and (8)

$$\begin{cases} 3+a=5 \Rightarrow a=2 \\ 4+3a=6+k_d \Rightarrow 10=6+k_d \Rightarrow k_d=4 \\ 4a+2=k_p \Rightarrow k_p=10 \\ 2a=k_i \Rightarrow k_i=4 \end{cases}$$

The required transfer function of PID controller is

$$G_C(s) = \frac{4s^2+10s+4}{s} = \frac{4\cdot(s^2+2.5s+1)}{s}\,. \tag{9}$$

The closed-loop poles of compensated system with PID controller are at *–1*, *–2* and $-1 \pm j1$ (see Table 1).

Table 1

Summary of compensation

Controller	Closed loop poles	Steady state error $e_s(t)$	Overshoot M_p, %	Settling time t_s, s	Rise Time t_r, s	Steady State $y(\infty)$
Algebraic	$-1, -1\pm j1, -2, -3$	2	0	4.3	2.5	1
PID	$-1, -1\pm j1, -2$	0	32,8	4.85	0.834	1
Robust	$-1, -1\pm j1$	2	0	4.3	2.5	1

b. Transfer function of the algebraic controller. The transfer's function of the algebraic controller $G_C(s)$ can be calculated using simple algebra to create a desired closed-loop transfer function $W(s)=\dfrac{Y(s)}{X(s)}$ (Fig. 1).

$$W(s)=\frac{B(s)}{A(s)}=\frac{B(s)}{a_3s^3+a_2s^2+a_1s+a_0}. \tag{10}$$

If *W(s)* is given, the required controller can be found, so that

$$G_C(s)=\frac{W(s)}{G_0(s)\cdot[1-W(s)]}. \tag{11}$$

Suppose the same three closed-loop poles with algebraic controller are to be placed as before –1 and $-1 \pm j1$. To obtain type 1 operation, the numerator *B(s)* and denominator $A(s)$ s^0 coefficients must be equal, so

$$W(s)=\frac{2}{(s+1)(s+1+j1)(s+1-j1)}=\frac{2}{s^3+3s^2+4s+2}. \tag{12}$$

From equation (11), the algebraic controller would be

$$G_C(s)=\frac{2\cdot(s^3+5s^2+6s)}{s^3+3s^3+4s+2-2}=\frac{2(s^2+5s+6)}{s^2+3s+4}. \tag{13}$$

The closed-loop poles with algebraic controller are at –1. –2, –3, $-1 \pm j1$ (see Table 1).

c. Transfer function of robust controller. In the robastic control scheme (Fig. 2) the plant transfers function $G_0(s)$ is divided into two parts, so that

$$G_0(s)=G_{01}(s)G_{02}(s), \tag{14}$$

where $G_{01}(s)$ – contains the part of the plant that may be uncertain; $G_{02}(s)$ – is most likely to be correct.
The desired closed-loop transfer function *W(s)* is divided into two parts:

$$W(s)=W_1(s)W_2(s), \tag{15}$$

where $W_1(s)$ – contains poles that may move under uncertainty $G_{01}(s)$; $W_2(s)$ – contains poles that should not change.

The controller $G_{C1}(s)$ is chosen to force the inner most loop to have closed-loop transfer function $W_1(s)$ so that

$$G_{C1}(s)=\frac{W_1(s)}{G_{01}(s)\left[1-W_1(s)\right]}. \tag{16}$$

The other two controllers are chosen to be

$$H(s)=W_2(s) \tag{17}$$

and

$$G_{C2}(s)=\frac{W_2(s)}{G_{02}(s)}. \tag{18}$$

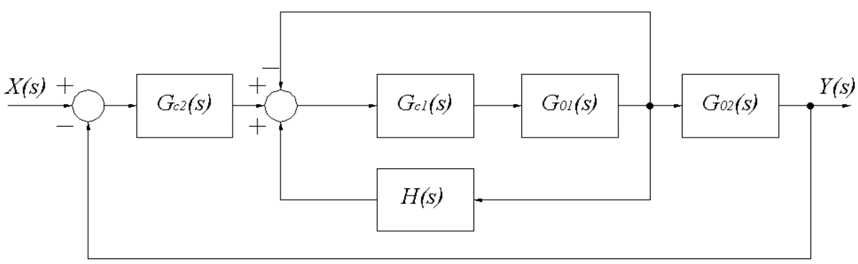

Fig. 2. Robust algebraic controller scheme

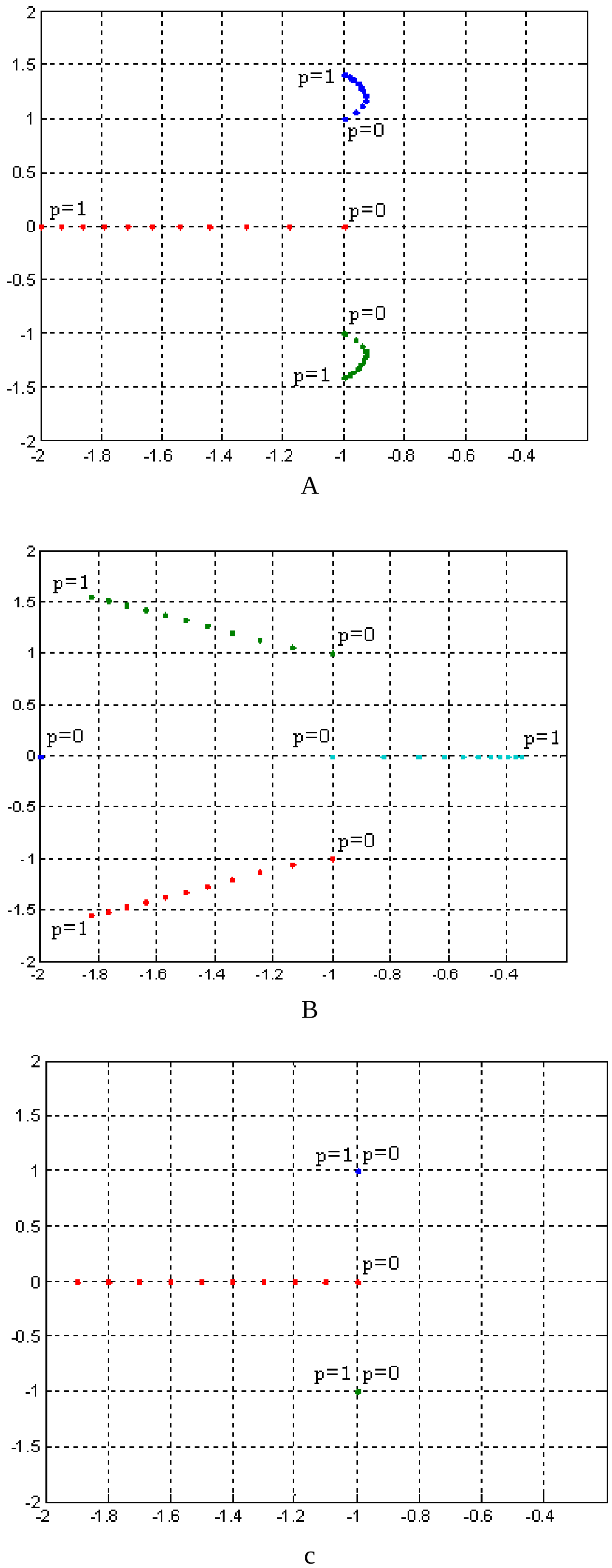

Fig. 3. The root loci with respect to the variation in pole *p*: a – for the system with algebraic controller, b – for the system with PID controller, c – for the system with robust controller

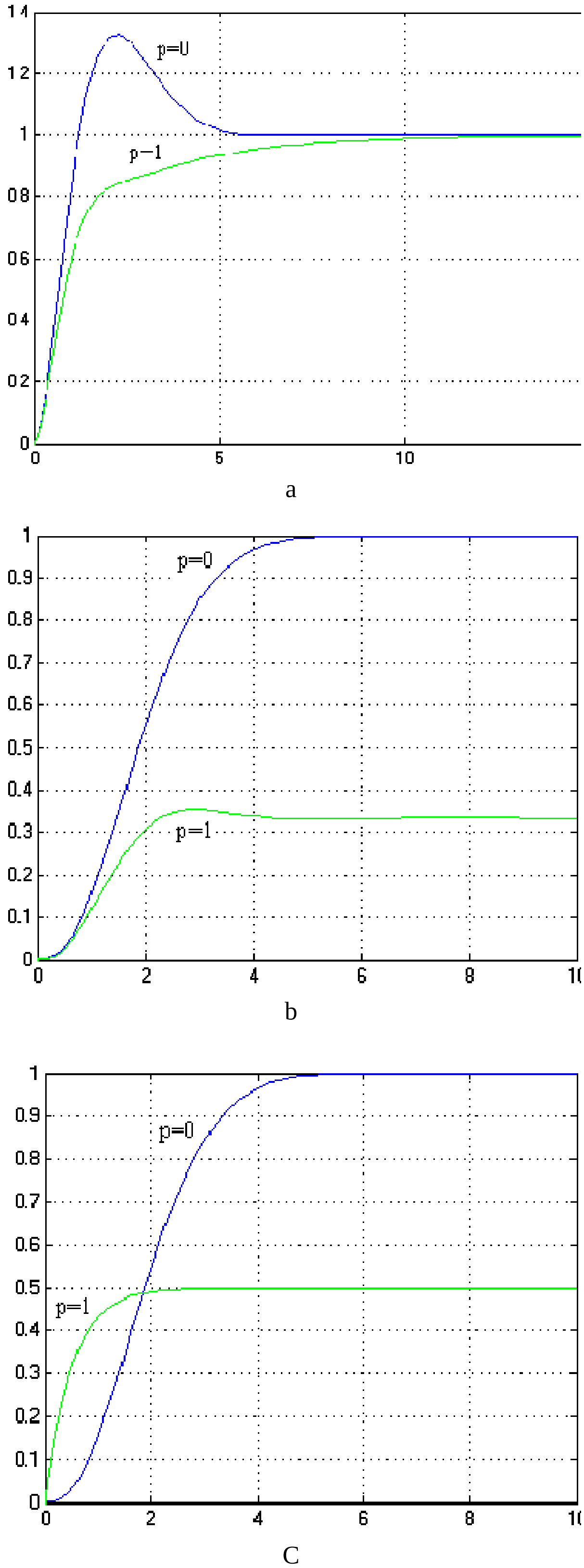

Fig. 4. Step responses of the system with: a – PID controller, b – algebraic controller, c – robust controller when the pole of the plant varies

Suppose that the closed loop poles are to become –1 and $-1 \pm j1$, and a designer is confident in the location of the open-loop plant poles *–2* and *–3*, but less confident that the third pole is actually at *0*.

Further, it is important to ensure that the complex conjugate closed-loop poles are at $-1 \pm j1$, while the third desired closed-loop pole should be at *–1*, but that pole could vary if the plant pole at *0* is uncertain. Then

$$G_{01}(s) = \frac{1}{s}, \quad G_{02}(s) = \frac{1}{s^2 + 5s + 6}, \quad W_1(s) = \frac{1}{(s+1)}, \quad W_2(s) = \frac{2}{s^2 + 2s + 2}, \tag{19}$$

and the robust algebraic controller's functions should be

$$G_{C1}(s) = 1, \quad G_{C2}(s) = \frac{2(s^2 + 5s + 6)}{s^2 + 2s + 2}, \quad H(s) = \frac{2}{s^2 + 2s + 2}. \tag{20}$$

The closed-loop poles with robust controller are at –1 and $-1 \pm j1$ (see Table 1).

3. Closed – Loop Poles Sensitivity Measures

Solving the sensitivity analysis problem of compensated system it is necessary to estimate the sensitivity of every closed-loop pole and every component of transient response to variation of the plant parameter *p*. The root loci technique [4] permits to estimate the effect of variation of the parameter *p* on the all closed-loop poles.

The characteristic equation of compensated system (Fig. 1) applicable for construction of root locus when variable parameter *p* = [0, 1] has the form

$$A(s, p) = 1 + p\frac{N_C(s)N_0(s)}{D_C(s)D_0(s)} = 0. \tag{21}$$

This equation when three different controllers are implemented becomes:

- with PID controller: $1 + a\dfrac{s^3 + 5s^2 + 6s}{s^4 + 5s^3 + 10s^2 + 10s + 4} = 0$,
- with algebraic controller: $1 + a\dfrac{s^2 + 3s + 4}{s^3 + 3s^2 + 4s + 2} = 0$,
- with robust controller: $1 + a\dfrac{s^2 + 2s + 2}{s^3 + 3s^2 + 4s + 2} = 0$.

The Fig. 4 illustrates the diagrams with the step response (that match the systems with the different controllers).

4. Conclusions

1. A PID controller leads to achieve the higher steady-state accuracy of compensated system. The faster response with PID controller comes at the expense of higher maximum deviations.
2. An algebraic and robust controller produces nonzero steady-state error. While the speed of response of compensated system is rather fast.
3. The sensitivity of compensated system with respect to uncertain pole *p*=0 of the plant is higher with PID controller. The response of system with this controller is very sluggish.
4. The variation of the pole of the plant from its nominal *p*=0 value greatly reduces the steady-state accuracy of compensated system with algebraic and robust controller. At the same time this greatly increases the speed of response of the system with robust controller.

References

1. **Schmid C.** Course on Dynamics of multidisplicinary and controlled Systems. http://www.atp.ruhr-uni-bochum.de/rt1/syscontrol/node73.html. May 2009.
2. **Byrne R., Dorato P., Abdallah Ch.** Experimental results in robust lateral control of highway vehicles // IEEE Control Systems Magazine. 1998. Vol. 18, No. 2. p. 70-76.
3. **Maffezzoni C., Schiavoni N., Ferretti G.** Robust design of cascade control // IEEE Control Systems Magazine. 1990. – Vol. 10. p. 21-25.
4. **Januševičius V. S., Dervinienė A.** Sensitivity measures of feedback system // The 3rd International Conference on Electrical and Control Technologies. 2008. p. 101-104.

Proceedings of 4th International Conference ITELMS'2009

Intelligent Technologies in Development of Leadership Competence

S. Bekešienė*, R. Smaliukienė**

** Gen. J. Žemaitis Military Academy of Lithuania, Šilo 5A, LT-10322 Vilnius, Lithuania, E-mail: svajone.vosteriene@lka.lt*
*** Gen. J. Žemaitis Military Academy of Lithuania, Šilo 5A, LT-10322 Vilnius, Lithuania, E-mail: rasa.smaliukiene@lka.lt*

Abstract

This article describes the evolution of intelligent technology based leadership test program from its origin. The program was designed to overcome two widely prevalent challenges in leadership development programs. Firstly, multidimensional character of leadership competence was evaluated by introducing meta-analysis of a self-assessment program and highly individualized recommendations were enabled. Secondly, the significance of different leadership qualities in the practice was bounded with the assessment results and high level of flexibility of leadership assessment program was reached. The article includes a description of the algorithm structure of the leadership test program.
KEY WORDS: *Maple 12, multidimensional database, leadership competence, test program.*

1. Introduction

The use of information technology in the development of leadership competence is one of the new directions in leadership research and practice. Cases of technology-mediated leadership development initiatives abound online and on the intranets of military educational institutions. However the main challenge in leadership development programs remains the holistic (as opposed to isolated) approach to the competence of leadership.

The leadership development models in military are based on two main ideas. The first idea puts forward the educational impact towards the development of the leadership competence. From this point of view, the leadership competence is not innate gift but acquired during the process of learning and practicing [1]. Therefore the specific job for leadership educational programs deals with a development of a set of deliverables, outputs and roles that each creates a number of individual qualities [2]. To asses this multidimensional competence of leadership new approach that connects this variety of elements into one system is needed. In this article the employment of intelligent technologies we propose as a solution for this challenge.

The room for intelligent technologies in leadership development program is even increasing when we are focusing on the second idea of leadership development. It represents the clear distinction between leadership development and leader development. At the core of this distinction is the orientation toward a developing either human capital (leader development) or social capital (leadership development) [3]. Education in military is orientated toward social capital and emphasizes the development of mutual obligations and commitments built on a foundation of organizational trust and respect. From this perspective the set of changing objectives for the leadership development program, as well as the specific knowledge and skills that should be developed by the completion of the program are set. As the leadership in military is associated with high flexibility versus control and high compatibility with organizational changes versus stability of the system, the objectives for the leadership development is changing constantly [4]. Therefore we need tough connections between the changing requirement of the military and leadership development programs. To overcome this challenge the individual learning approach based on information technologies can be used. The detailed overview of the solutions and activities that deals with this problem are discusses in a broader way. Herewith the purpose of this report is to describe the evolution of one information technology based leadership development program from its origin.

2. The Competence of Leadership and the Methods for it's Research

As was stated in the introduction many researchers have advocated the need for a holistic (as opposed to isolated) approach to the study of qualities that would describe the level of leadership. Hence, the multivariate assessment of the leadership qualities was introduced. The leadership qualities in this study were examined using self-report method.

Additionally looking for more specific qualities of leaders in military, the research in the Lithuanian military academy in 2008 was performed [5]. The research was designed to find out what is participants' attitude towards leadership in military and how do they evaluate the significance of the characteristics that describes leadership in military. Only small part of this research was used for the development of the information system that we are describing there. The study diagnosed that seven competencies are most valuable for leaders in military: Each of this competence was evaluated and became their weight. Following weights where used in computing the values of leadership competence: communicability – 0.12, ability to organize group work – 0.18; task orientation – 0.16; self management – 0.10; capability of social integration – 0.02; clarity of goals related to crew – 0.09; ability to influence – 0.33; which accounts total 1.

3. The Test Algorithm Structure

The testing process is coherent with learning process. So, the testing is used in many areas for keeping a close watch on student advancement and this type testing is known as broad-brush testing. The other kind of testing is the formative influence, when the students want to examine personality his knowledge or progress of recourse for learning. In either way the testing interconnects with formally learning area with clear determined intents by which are evaluated abilities. Regularly are creating the own test systems that afford desirable possibilities and meet the individual requirements more effective and productivity.

In this intense the tests program was developed in Lithuanian Military Academy. The specifically leadership testing program for cadets was realized on personal computers on the top of UBUNTU 8.10 LINUX operating system [10]. The program was realized by Maple 12 version [8].

The test algorithm schema is presented in Fig. 1 below. The specifically program for leadership is constructed to draw the individual recommendations for tested cadet after get test results deep analyzing.

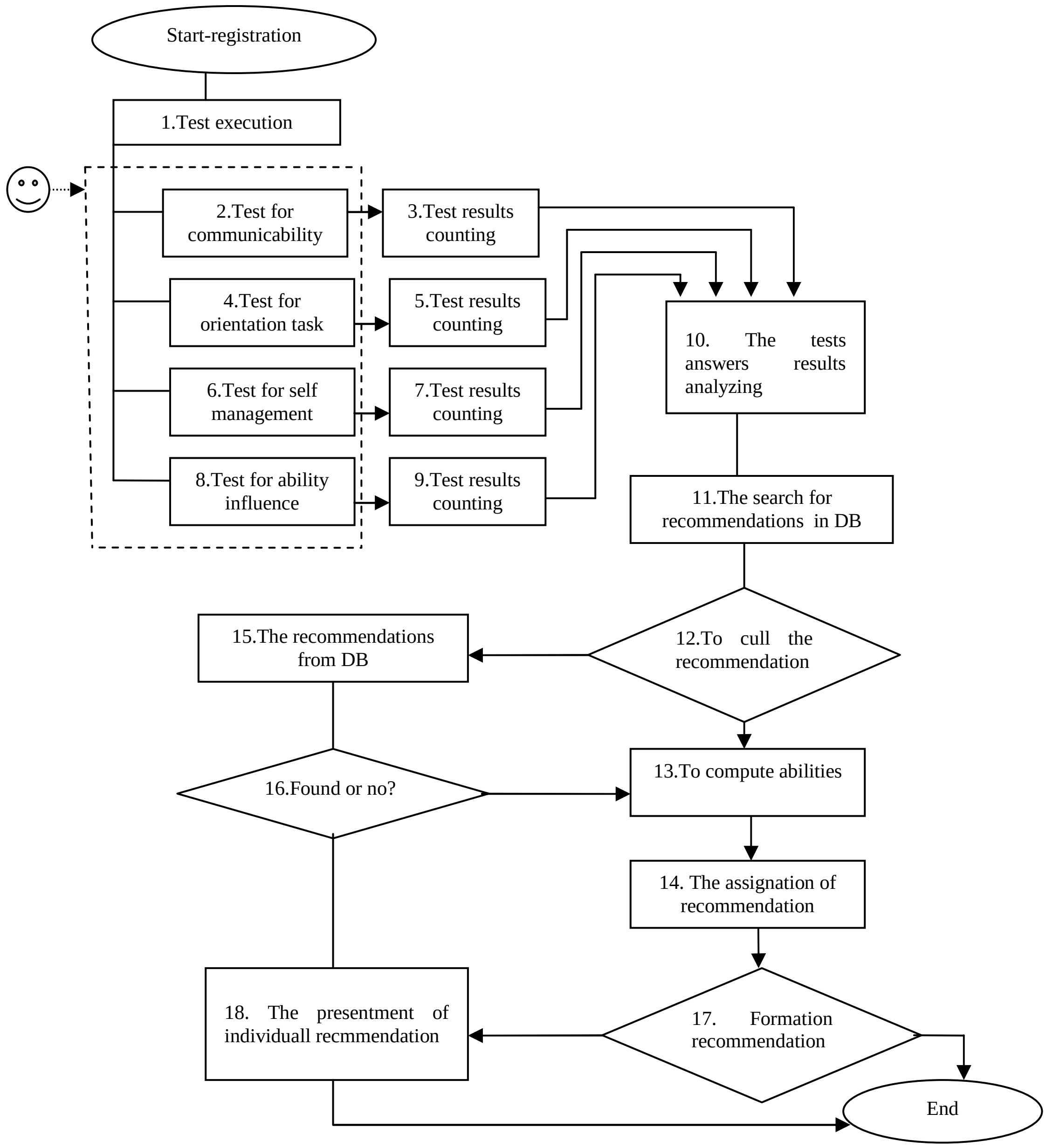

Fig. 1. The algorithm schema presented in blocs for test program of individually recommendation extraction.

The algorithm schema, presented in blocs for test program of individually recommendation extraction (Fig. 1), was expanded by deep analyzing of get results and constructed to draw the individual recommendation for tested participant. Traditionally existing tests are limited in first 10 blocs (1-10 blocs), where the test user is tested by 2-th, 4-th, 6-th and 8-th then 3-th, 5-th, 7-th and 9-th blocs analyzing and counting the answers and result can be presented by 10-th bloc. The test can inform participant about the get scores of tested factors, but to solve the problem in this easy way nowadays is not popular, because this type the get information is not easy to understand for user, and he can't correctly to form individual recommendations for himself. So, for constructing the not ambiguity recommendation in this test program was realized multiplex intellectual task solving schema as presented in Fig.1.

To examine the cadet's abilities in leadership was designed the multidimensional test program of four factors, which are presented as: test for communicability (2-th bloc), test for orientation task (4-th bloc), test for self management (6-th bloc) and test for ability influence (8-th bloc). The get results after investigative factors analysis was placed as values to the data sets (10-th bloc). The all results of each item were included to the individual analysis in the 13-th bloc. The competences were extracted by using the data sets of test program results. The 14-th and 15-th blocs were used for individual recommendation assortment. In additionally, as result for each tested cadet this test program presents the individual recommendations and suggests the individual solution to get the better results as was (18-th bloc). Such recommendation is placed to text file "rekomendacija.txt".

In the Fig. 1 schematically are shown the direct work of user and test program in the personal computer system. This area is marked as the box of dotted line, which including the 2-th, 4-th, 6-th and 8-th blocs.

4. The Test Program Analyzing

In our demands was to construct the test program, which generally shows students not only the results of their answers (i.e., correct or incorrect), but also why they got those results, which enhances their understanding of the leadership principles. This approach was used in our test program, because fits very well with the goals of the self-assessment program; it is important to not only tell cadets whether their abilities were assessed very well, but also to make available to tell how to correct missing attributes and, where relevant, the rationale for that streaks.

Nowadays is not popular to solve the problem in narrow-gauge way, because the get information after testing must be clear and easy to understand for the tested user. In other way such user can't correct to form future tasks for him. The test program design was constructed for new demands. The introduced new program is expanded by forming special individual recommendations. This is the one of advantages of this test program.

The specifically leadership testing program for cadets leadership analyzing was realized by Maple 12 version possibilities as maplets on personal computers [7, 9]. The maplet is a reusable object which contains one or more than one transformation which is used to populate the data from source to target based on the business logic and we can use the same logic in different mappings without creating the mapping again.

The test program starts at the "Start-registration" field. To construct this window was chosen the text field of thirty symbols and variable "kariunas". The button "OK" is the confirmation for completed information. In Maple 12 version programming area it looks as presented below:

```
maplet := Maplet([["Įveskite savo vardą ir pavardę: ", TextField['IB1'](30)],
[Button("OK", Shutdown(['IB1']))]]);Maplets[Display](maplet);kariunas := op(%);
```

For the testing cadet the test program's start window appears such as presented in Fig. 2.

Fig. 2. The test program start-registration window.

This start is important in some directions: at first in such as let us indicate the tested person after finishing all testing, at the second the test program is designed to present the scores for somebody, who started the registration, and the last if someone starts the registration he can't to stop the test program before end.

Below are described the four choice factors that are the core of realized program.

Factor I- communicability test derived from the morality, integrity and dutifulness sub-scales. Thus, factor I was the 40-item, computerized test (2-th bloc). This test results analyzing consist of two steps. The firs all chooses was compare with answers and computed singly the congruencies by communicative and organizational dispositions abilities. The second was determine the communicative (K_k) and organizational (K_o) coefficients by formulas below

$$K_k = \frac{K_x}{20} \quad \text{and} \quad K_o = \frac{O_x}{20},$$

where K_x – the computed congruencies of communicative abilities and O_x – the computed congruencies of organizational abilities. The get results were analyzed by evaluation scale presented in the Table 1.

The test answer can be represented by the fix outcome agree or disagree (Yes or No). The outcomes of fixed answers indicate the communicative and organizational dispositions in our examination. The generalized graded unfolding model, which is perhaps the most flexible model available for personality statements, was utilized. For deep analyzing of get results each bloc of two of communicability test blocs was computed and evaluated like two tests.

After results computation and evaluation as presented in the Table 1, the get result follows to one of five evaluation groups. Then test program is constructed to follow the procedure, which includes multiplication by special picked coefficient 0.12.

In this way was determining the congruencies of communicative (the high score can be 12 points) and organizational dispositions (the high score can be 12 points) abilities.

Table 1

Evaluation scale of coefficients and points

Coefficient K_k	Coefficient K_o	Evaluation scale in points
0.10-0.45	0.20-0.55	1
0.45-0.55	0.56-0.65	2
0.56-0.65	0.66-0.70	3
0.66-0.75	0.71-0.80	4
0.75-1.00	0.81-1.00	5

Factor II- the orientation task consisted of 22-item computerized test (4-th bloc) for the self-efficacy, assertiveness and intellect sub-scales. The items were selected to depict a confident and persuasive individual with good intellectual capacity, which typically takes charge of tasks and delivers results. Such individuals could be expected to assume roles with managerial responsibility and authority.

Table 2

Evaluation scale of motivation score in points

	The motivation level									
Group	Low level			Middle level				High level		
Subgroup	1	2	3	4	5	6	7	8	9	10
Points	2-9	10	11	12	13	14	15	16	17	18-22

The motivation is the dependence or ambitions that take the impulse and energy to affect and apply to aching goal. After results computation and evaluation as are presented in the Table 2, the result follows to one of three evaluation group’s subgroup. Then follows the procedure that includes multiplication by special picked coefficient 0,16. In this way was determining the congruencies of motivation (the high score can be 16 points) abilities. The motivation was included to control for any possible relationships between the motivation to become a commander and leadership perceptions. Factor II was thus labeled as dominance.

Factors III - the self-management task consisted of 20-item computerized test (6-th bloc) for determinate the professional motivation, interest area, character and other. This 4-item factor was therefore interpreted as diligence and consisted wholly of items reflecting the openness to experience construct. Factor III was comprised primarily of items from the conscientiousness sub-scale of self-discipline. This test structured from propositions, which has three different ends. The test answer can be represented as agreement by the fix one of outcome (A or B or C). In Maple 12 version, programming area it looks as presented below:

```
Maplet1 := Maplet(Window('title' = cat(pav, " - pavyzdziai"),
[Label(Image(cat(currentdir(),"/Images/", p, "0.JPG"))),
[Button("Pradėti testą", Shutdown())]]));
Maplets[Display](maplet1);

NULL;
rez := 0;
for k while k<n+1 do
maplet1 := Maplet(
   Window( 'title' = cat(pav, " – užduotys:"),
      Label(Image(cat(currentdir(), "/Images/",p,k,".JPG"))),
          BoxCell( "Pasirinkite:" ),
          GridLayout
          ([
             ["A", RadioButton[ChB1]( 'group' = 'BG1' )],
             ["B", RadioButton[ChB2]( 'group' = 'BG1' )],
             ["C", RadioButton[ChB4]( 'group' = 'BG1' )]
          ]),
          [Button( "Pirmyn", Shutdown( ['ChB1', 'ChB2', 'ChB3'] ) ),
           Button( "Baigti", Shutdown("true") )]
       ]
   ),
   ButtonGroup['BG1']()
):
Maplets[Display](maplet1);
```

As you can see, to programming the test example windows were used the prepared images, such as the image 0.JPG, that program found it in “Images” directory. The window of self-management test is shown in Fig. 3. There is the brief representation of this entire test, the explanation how to get the best score, and the example of task.

The tasks windows of the test program are forming as two areas. In one area are displaying the prepared task as image and the other area displaying the outcomes, such as A, B and C. Such window is shown below in Fig. 4.

For deep analyzing of get results from each item of 4-items of the self management test was computed and evaluated like four tests. After results computation and evaluation the result follows to one of four evaluation groups. There is the specification of calculating test results, because the number of motives of each group is not the same. For equalization process of all groups, the first and second groups are multiply by 2, the third and fourth groups are multiply by 3, only then all groups can be compare with each other. Then follows the procedure that includes multiplication by special picked coefficient 0,1. In this way was determining the congruencies by four groups: 1-th individual contribution to work’s motives, 2-th social importance of work’s motives, 3-th the personality fixate in the work motives and 4-th professional mastership motives. The high score of abilities in each group can be 10 points.

Factor IV – the ability influence consisted of 50-item computerized test (8-th bloc) for intercourse determine. Factor IV was identified as Sociability. After results computation and evaluation, the result follows to one of three evaluation group. Then follows the procedure that includes multiplication by special picked coefficient 0.33.

The four factors, their component variables and the variance accounted for by each rotated factor are given in preparation of individual recommendation for tested cadet. The above analysis was repeated on the data set of complete cases. The investigative factor analysis results are presented.

5. Results and Discussions

Our first step in designing the test program was to find out what others do for similar purposes. Consequently to identify the best practices in the area, we looked at the preparation programs of the other Lithuanian armed services as was indicated in the introduction field of this article. The literature about leadership also provided several ideas that we incorporated into the overall process.

The prepared test program practical use confirms the cadet’s concentration in leadership improvement. For testing leader abilities were included two first year groups (25-ty cadets in all). This groups where included because they have a time to consummate leadership abilities.

groups (25-ty cadets in all). This groups where included because they have a time to consummate leadership abilities.

On this test program proceeding time before starting the testing for cadet was proposed windows with test example such as shown in Fig. 3, where was the recommendations and samples how correct to pass the whole test. This procedure was repeated before each test. At the end of all work the test program constructed the text file “rekomendacija.txt” with the individual recommendation and get test scores. This information file is saving in the personal computer to the particularized place and can be printed. This was doing for cadet and others convenience.

As sample one of such recommendations of the presented test program we want to analyze in full of meanings. As was sad above, the test program assignment was to calculate points by special scheme. Consequently, one of the tested cadet’s result presented overall 69-th points and where collected in between 65-84 points area. In this case the announcement for a test program user appears: “You appear to possess all of the qualities of leaders, but not all of them are developed sufficiently”. After that goes the text, which shows identified strength and provides with additional recommendations for leadership development in the future. Four tests identify 7 integrated competencies and 82 single qualities of leadership. Strongly expressed qualities are identified as strengths. In the presented case four strengths are identified: “organized, duty bounded, practical, and reliable. Additionally, the leadership style is identified and the essences of it shortly described: You lead by devoting attention to what needs doing, you make decisions based on: facts, guidelines, procedures, and rationale analysis. You enjoy measuring progress and managing schedules”. Short encouragement on these strengths appears: “It is very important, that you will use all of theses strength in your leadership duties”.

The qualities that collected low sum of points are compounded into competencies and recommendations are provided. In our chosen example two of such competencies were detected: “communicability and ability to influence”. The system provides this kind of information:

“Your (1) communicability is 5 points from 12, it scores low. The results suggest that you are not comfortable initiating conversations and activities in the group. You only sometimes are advancing your ideal within group or taking a competitive stance. (2) Ability to influence scores 16 points from 33 and is high not enough. The results suggest that you are avoiding yourself as exemplary leader”.

The following recommendations regarding learning recourses and strategies are given for the development of leadership competence:

“Take elective course on: (1) Psychology; (2) Organizational Behavior

Request to be promoted as a cadets platoon commander deputy or member of cadets council

Ask librarian to provide a list of the literature for self-study in leadership and focus on the chapters dealing with: communication and group management

In the everyday activities focus on: (1) learn and advise subordinators; (2) be enthusiastic about your duty and role as a leader”.

.

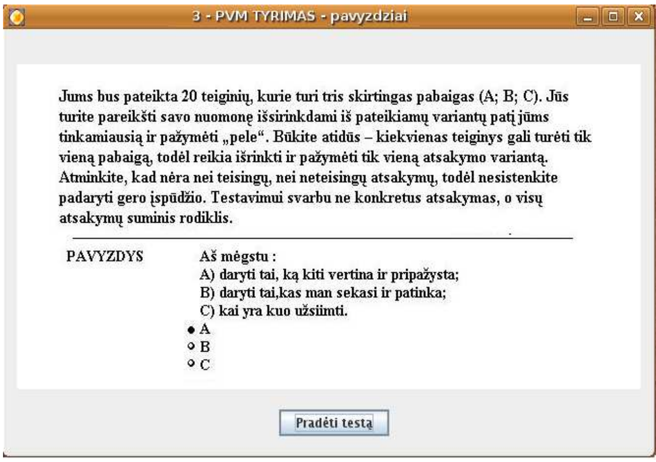

Fig. 3. The window of self-management test recommendations and example

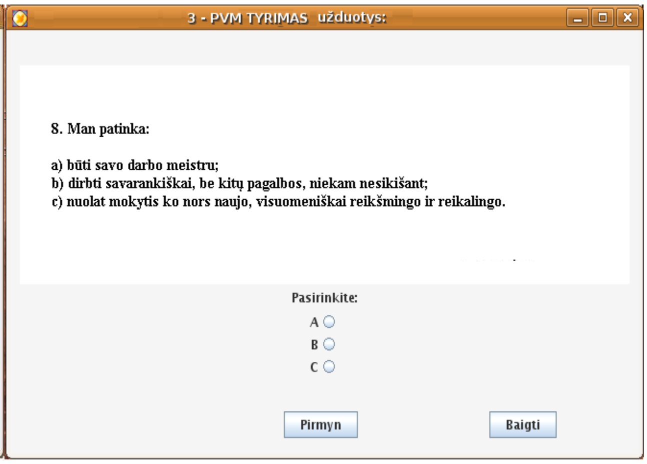

Fig. 4. The window of self-management test task

At the end the evidence of learning are presented:

- Successful interactions with cadets from different courses.
- Ability to organize group work and achieve a task

As the description of the test program above indicates, our assessment framework draws on several key concepts. Firstly, it provides individualized recommendations where each point of advice is connected with the program test results. Secondly, the recommendations are highly related to learning curriculum and leadership development program at the Academy. Thirdly, the recommendations are provided on the bases of discretion in this way the negative reaction toward the prescriptions in learning

6. Conclusions

This paper presents the leadership test program results of studies that were conducted to evaluate the viability of the recently proposed model for multidimensional preference items for prepared use. It was found that it was not necessary to have all possible pairings dimensions to accurately estimate trait scores and a minimal “circular” linking design was sufficient. Taken together, results indicated that scale length and linking requirements do not pose serious constraints on the development of tests with higher dimensional. The multivariate analysis of individual 82 qualities was tested and 7 integrated competencies where evaluated, rather than the contribution of each separate variable on its own. It should be noted that qualities in this context are seen as multidimensional construct too. Weakly expressed competencies were interpreted as weaknesses and highly individualized recommendations were provided in each case of testing. Presented leadership test program is based on intelligent technologies and allow overcoming such specific challenges in leadership development as insufficient motivation of the participants and individual differences in leadership experience. In addition, the test preparation that allows cadets to demonstrate what they know produces learning that is generalization to contexts outside of performance on the test, and test scores will take care of themselves. Effective practice exposes cadets to a variety of assessment approaches and formats, allowing them to apply their knowledge in a variety of learning situations, and taking advantage of the fact that individuals have different learning styles.

References

1. **Johansen B**., Leaders Make the Future. Berrett-Koehler Publishers, 2009. 194 p.
2. **Young M., Dulewicz V**. A Model of Command, Leadership and Management Competency in the British Royal Navy. Leadership & Organization Development Journal, Vol. 26 No. 3, 2005. p. 228-241.
3. **Popper M**. Main Principles and Practices in Leader Development. Leadership & Organization Development Journal, Vol. 26 (1), 2005. p. 62-75.
4. **Wong L., Bliese P., McGurk D**. Military Leadership: A Context Specific Review. The Leadership Quarterly. Vol. 14 (6), 2003, p. 657-692.
5. Leadership and its impact towards the development of commanders (in Lithuanian). Lithuanian Military Academy. Research report, 2008.63 p.
6. **Puzinavičius B**. Asmenybės ir grupės psichosocialinė diagnostika: anketų, klausimynų ir testų rinkinys. Lithuanian Military Academy, 2005. 283 p.
7. Maplets Beginner‘s Guide. Available at: http://valle.fciencias.unam.mx/~hector/mapletsguide.pdf
8. Maple 12. Available at: http://www.bu.edu/systems-support/software/maple.html
9. **K. Geddes, G. Labahn, M. Monagan.** Maple 12 Introductory Programming Guide, Maplesoft, 2008.
10. Linux-based operating system. Available at: http://www.ubuntu.com/

Proceedings of 4th International Conference ITELMS'2009

Stress Strain State of the Two-Layer Mechanically Inhomogeneous Pipe at Elastic Loading Subjected to Internal Pressure

A. Bražėnas*, N. Partaukas**

**Kaunas University of Technology, Daukanto 12, 35212 Panevėžys, Lithuania, E-mail: algis.brazenas@ktu.lt*
***Kaunas University of Technology, Daukanto 12, 35212 Panevėžys, Lithuania, E-mail: n.partaukas@gmail.com*

Abstract

The stress state of two-layer pipe which is subjected to internal pressure is analyzed in this paper. There is assumed that materials of both layers are isotropic, homogeneous, linearly elastic and longitudinal stress on the contact plane of layers does not appear. Equations for determination of stress state component are obtained by using these assumptions and Lame's dependencies. Comparison stress state components of the two-layer inhomogeneous pipe calculated analytically and determined by FEM showed that obtained solution is sufficiently exact. There was determined that stresses depend on the elasticity modules, relative walls thickness and layout of layers.

KEY WORDS: *two-layer pipe, reinforced pipes, stress state, contact pressure, internal pressure, elastic loading.*

1. Introduction

Multilayer structures today are replacing many of the traditional one material structure. Stress strain state of multilayer structures depends on the contact pressure arising between the layers. The main reason for the contact pressure is radial stretcher [1].

Two-layer metal plastic structures with range shape cross-section are frequently used [1, 4]. The external plastic rust preventive cowers are applied in metal pressure vessels and pipelines. Plastic tubes have such properties: little price and mass, negligible turbulent friction, high endurance to cracking, resistance to corrosion and others. They can by exploited even after micro cracking in its internal surface. But they also have such negative properties: insufficient strength and stiffness, ageing and low temperature stability. Therefore, in pipelines are widely used the reinforced tubes [3]. For reinforcing of plastic tube two-layer constructions with the external metal layer are frequently used. Due to acting internal pressure in these structures the contact pressure p_c appears.

Research of multilayer structures often is carried out by FEM [2]. FEM has been successfully used for stress state determination of multilayer structures. But FEM results have certain amount of methodological errors to determine it is not easy.

Stress strain state of homogeneous pipe subjected to internal pressure may be determined by Lame's equations [5-7]. The contact pressure p_c of interference fit was calculated from Lame's equations by estimating interference of hole and shaft $\delta_{12} = r_{12} - r_{21}$ [5]. An analytical model for two-layer cylindrical bar subjected to axial compression stress strain determination is presented in works [8,9]. It has been determined that relative stresses in contact zone of layers depend on modulus of elasticity, the radial dimensions, cross-sectional layer areas ratios and layout of materials. Contact pressure in two-layer pipe subjected to internal pressure appears on the contact surface of layers ($\rho = r$) due to increasing displacement $u = \int_{r_1}^{r} \varepsilon_r dr$ (Fig. 1). The analytical methods that could facilitate the solution of multilayer structures, subjected to internal pressure of the issue are in general, either still not created. Therefore, multilayer structure properties are not exploited to the maximum. In this paper dependencies for stress strain determination of two-layer inhomogeneous pipe at elastic loading subjected to internal pressure are obtained.

2. Stress Strain State of Inhomogeneous Two-Layer Pipe Determination

The mechanically inhomogeneous two-layer pipe may be divided in two pipes with different mechanical properties: internal pipe 1 with modulus of elasticity E_1, Poisson's ratio ν_1 limit of elasticity σ_{e1} and external pipe 2 with E_2, ν_2 and σ_{e2} (Fig. 1). Material with modulus of elasticity E is major than one of other pipe is called hard material H and in opposite case – material M. When $E_1 > E_2$ structure is denoted H-M and in opposite case – M-H. Due to acting internal pressure p radial stretch and contact pressure p_c on the contact surface of H and M materials appears. Stress state components are determined by estimating internal pressure p, contact pressure p_c and equality of circular strains $\varepsilon_{\theta H}$ and $\varepsilon_{\theta M}$ on the contact surface of H and M materials.

The stress strain state of two-layer pipe subjected to internal pressure is determined by assuming these assumptions:

1. radius $r = r_{12} = r_{21}$ when $p = 0$;
2. layer 1 and layer 2 are not connected;

3. circular strains on the surface of layers $\varepsilon_{1\theta|\rho=r} = \varepsilon_{2\theta|\rho=r}$ ($r_1 \le \rho \le r_2$ is radius of composite pipe);
4. stress intensity $\sigma_{i1} \le \sigma_{e1}$ and $\sigma_{i2} \le \sigma_{e2}$.

From these assumptions follows:

- $\sigma_{z1} = \sigma_{z2} = 0$;
- stress on the internal surface pipe $\rho = r_1$ may be determined by Lame‘s dependences. Then in internal layer

$$\sigma_{r1|\rho=r} = -p_c \tag{1}$$

$$\sigma_{\theta 1|\rho=r} = p\frac{2r_1^2}{r^2 - r_1^2} - p_c\frac{r^2 + r_1^2}{r^2 - r_1^2} \tag{2}$$

and in external layer

$$\sigma_{r2|\rho=r} = -p_c \tag{3}$$

$$\sigma_{\theta 2|\rho=r} = p_c\frac{r_2^2 + r^2}{r_2^2 - r^2} \tag{4}$$

- strains in the both layers may be determined by Hooke’s law:

$$\varepsilon_\theta = \frac{\sigma_\theta - \nu\sigma_r}{E} \qquad \text{and} \qquad \varepsilon_r = \frac{\sigma_r - \nu\sigma_\theta}{E} \tag{5}$$

Then from the (1-3) assumptions and Eqs.(1) – (5) follows:

$$\frac{1}{E_1}\left[\frac{2r_1^2 p - \left(r^2 + r_1^2\right)p_c}{r^2 - r_1^2} + \nu_1 p_c\right] = \frac{1}{E_2}\left[\frac{\left(r_2^2 + r^2\right)p_c}{r_2^2 - r^2} + \nu_2 p_c\right] \tag{6}$$

Contact pressure p_c on the surface of materials H and M may be determined by Eq.(6). Then for structure H-M

$$p_c = \frac{C_1^{H-M}}{\dfrac{C_2 + \nu_M}{E_M} + \dfrac{C_3 - \nu_H}{E_H}}\, p \tag{7}$$

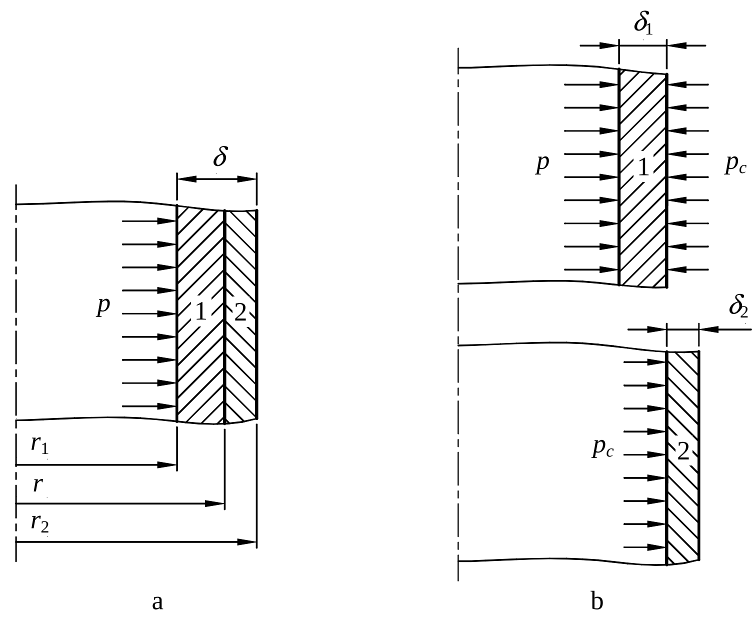

Fig. 1. Scheme of stress strain state determination of two layer pipe: a – scheme of pipe; b – distribution of pressures in internal layer 1 and external layer 2

and for structure M-H

$$p_c = \frac{C_1^{M-H}}{\dfrac{C_2+\nu_H}{E_H} + \dfrac{C_3-\nu_M}{E_M}}\, p \tag{8}$$

where $C_1^{H-M} = \dfrac{2r_1^2}{E_H\left(r^2-r_1^2\right)}$, $C_1^{M-H} = \dfrac{2r_1^2}{E_M\left(r^2-r_1^2\right)}$ $C_2 = \dfrac{r_2^2+r^2}{r_2^2-r^2}$, $C_3 = \dfrac{r^2+r_1^2}{r^2-r_1^2}$.

The contact pressure p_c as follows from Eqs. (7) – (8) is proportional to internal pressure

$$p_c = C_p\, p \tag{9}$$

where for H-M structure $C_p = \dfrac{C_1^{H-M}}{\dfrac{C_2+\nu_M}{E_M} + \dfrac{C_3-\nu_H}{E_H}}$ and for structure M-H $C_p = \dfrac{C_1^{M-H}}{\dfrac{C_2+\nu_H}{E_H} + \dfrac{C_3-\nu_M}{E_M}}$

Stress strain state of layers, when p_c is known, is more convenient to calculate in relative coordinates: $r_1 / r_1 = 1$, $s_1 = \delta_1 / r_1$, $s_2 = \delta_2 / r_1$, $s = \delta / r_1 = s_1 + s_2$, $r / r_1 = 1 + s_1$, $r_2 = 1 + s_2$, $\xi = (\rho - r_1) / r_1 = \rho / r_1 - 1$. Then stresses of internal layer, when $0 \le \xi \le s_1$

$$\left.\begin{matrix}\sigma_{r1}\\ \sigma_{\theta 1}\end{matrix}\right\} = p\left[\frac{1-C_p\left(1+s_1\right)^2}{s_1\left(2+s_1\right)} \mp \frac{\left(1-C_p\right)\left(1+s_1\right)^2}{s_1\left(2+s_1\right)\left(1+\xi\right)^2}\right] \tag{10}$$

and of external layer, when $s_1 \le \xi \le s$

$$\left.\begin{matrix}\sigma_{r1}\\ \sigma_{\theta 1}\end{matrix}\right\} = pC_p\,\frac{\left(1+s_1\right)^2 \mp \left(1+s_1\right)^2\left(1+s\right)^2/\left(1+\xi\right)^2}{\left(1+s\right)^2-\left(1+s_1\right)^2} \tag{11}$$

Eqs.(1) – (11) valid when material 1 and material 2 are absolutely elastic. For real ductile material this condition may by expressed by dependence

$$\sigma_i = \sqrt{\sigma_\theta^2 + \sigma_r^2 - \sigma_\theta\sigma_r} \le \sigma_e \tag{12}$$

The most heavily loading zone in two-layer pipe of material 1 is on internal surface of pipe ($\xi = 0$). Maximum internal pressure value when material 1 is deformed elastically may be determined from Eqs.(10) and (12) when $\xi = 0$. Then

$$p_{\max 1} = \frac{\sigma_{e1}}{\sqrt{\left[\dfrac{1-\left(1+s_1\right)^2\left(1-2C_p\right)}{s_1\left(2+s_1\right)}\right]^2 + \dfrac{1-\left(1+s_1\right)^2\left(1-2C_p\right)}{s_1\left(2+s_1\right)} + 1}} \tag{13}$$

From Eqs.(11) and (12) follows that elastic plastic strains in material 2 appears on the contact surface of layers when $\xi = s_1$ and $p = p_{\max 2}$

$$p_{\max 2} = \frac{\sigma_{e2}}{C_p\sqrt{\left[\dfrac{\left(1+s\right)^2+\left(1+s_1\right)^2}{\left(1+s\right)^2-\left(1+s_1\right)^2}\right]^2 + \dfrac{\left(1+s\right)^2+\left(1+s_1\right)^2}{\left(1+s\right)^2-\left(1+s_1\right)^2} + 1}} \tag{14}$$

The maximum value of internal pressure when Eqs.(1) – (12) valid may be determined from condition

$$p_{\max} = \min\left(p_{\max 1},\quad p_{\max 2}\right) \tag{15}$$

Elastic properties of two-layer mechanically homogeneous pipe at elastic loading subjected to internal pressure are exploited maximum when $p_{\max 1} = p_{\max 2}$.

3. Results of Analytical Investigations

Contact pressure p_c on the contact surface of materials H and M, as follows from Eqs.(1) – (11), depends on modules of elasticity E_1, E_2, Poisson's ratio ν_1, ν_2, geometrical parameters of cross-section and location of materials H and M. Value of the contact pressure p_c is proportional to internal pressure p. Ratio $C_p = p_c / p$ depends on E_M / E_H (Fig. 2) and ν_1, ν_2 (Fig. 3), relative thickness of layers s_1, s_2 (Fig. 4, Fig. 5) and location of materials H and M. In structure H-M with decreasing E_M / E_H and s_2 the contact pressure quickly decreases. With increasing E_M / E_H ratio p_c / p also increases. When $E_2 / E_1 = 1$ the contact pressure may be determined by Eq.(10). When $E_2 = E_1$ and $\nu_2 = \nu_1$ value on contact pressure $p_c = -\sigma_{r1|\rho=r}$ may be determined by Lame's equation [5].

In M-H structure ratio p_c / p decreases, with increasing E_M / E_H. In this case when $E_M << E_H$ and s_1 is small $p_c \approx p$.

Dependence p_c / p on ν_M when $\nu_H = 0.3$ is shown in Fig. 3. Ratio p_c / p in structure M-H increases and decreases in structure H-M with increasing ν_M. From Fig. 3 follows that p_c / p negligibly depends on $\nu_2 - \nu_1$. Therefore, when $|\nu_2 - \nu_1| \le 0.1$ may be accepted $\nu_2 = \nu_1$. In this case miss calculation of p_c / p does not exceed 1.5 %.

Ratio p_c / p when $s_H = 0.25$ increases with increasing s_M and E_M / E_H by parabola law (Fig. 4). When relatives stiffness of the mild external layer when E_M / E_H is small ratio p_c / p increases moderately with increasing s_M. With increasing E_M / E_H ratio temp increasing of p_c / p rises.

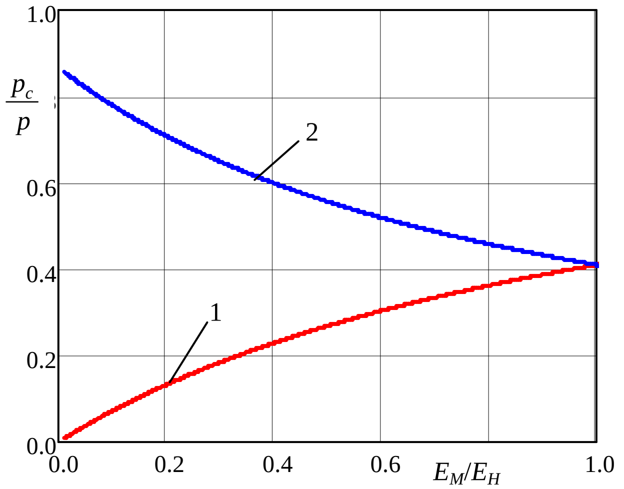

Fig. 2. Dependence p_c / p on E_M / E_H when $E_H = 21 \cdot 10^4$ MPa, $r_1 = 50$ mm, $r = 60$ mm, $r_2 = 72$ mm, $\nu_H = \nu_M = 0.3$. Curves: 1 – structure H-M; 2 – structure M-H

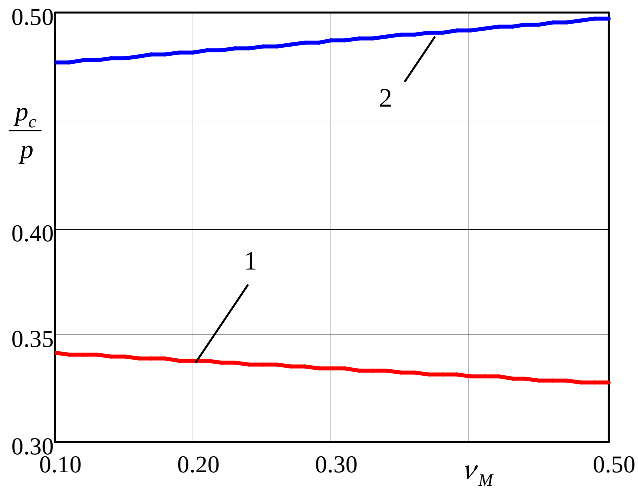

Fig. 3. Dependence p_c / p on ν_M when $E_H = 21 \cdot 10^4$ MPa, $r_1 = 50$ mm, $r = 60$ mm, $r_2 = 72$ mm, $\nu_H = 0.3$, and $E_M = 0.7 E_H$. Curves: 1 – structure H-M; 2 – structure M-H

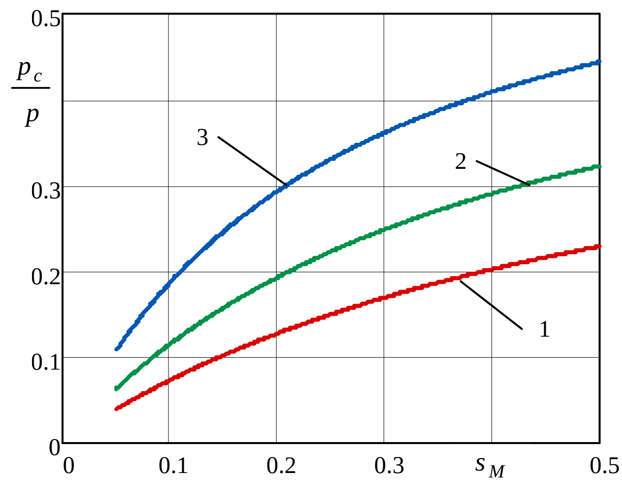

Fig. 4. Dependence p_c / p on s_M and E_M / E_H in structure H-M when $E_H = 21 \cdot 10^4$ MPa, $s_H = 0.25$, $\nu_H = \nu_M = 0.3$, $r_1 = 50$ mm. Curves: 1 – $E_M = 0.3 E_H$; 2 – $E_M = 0.5 E_H$; 3 – $E_M = 0.9 E_H$

The obtain solution for real materials valid when $\sigma_{1i} \le \sigma_{e1}$ and $\sigma_{2i} \le \sigma_{e2}$. The maximum internal pressure $p_{\max}$, when this condition valid may be determined by Eq.(15). Dependence $p_{\max}^{H-M}$ on s_H and E_M / E_H in structure H-M when $s_M = 0.25$ and $\nu_H = \nu_M = 0.3$ is shown in Fig. 5. Maximum internal pressure when Eqs.(1) – (15) valid with increasing s_H and E_M / E_H increases also.

Elastic plastic deforming in structure M-H begins in mild metal (Fig. 6). When $s_M = 0$ then $p_c = 0$ and $p_{\max}$ in material H may be determined by Lame's equations [5]. $p_{\max}$ in this case determined by Eq.(13) increases by increasing s_M and E_M / E_H. With increasing E_M / E_H temp increasing of $p_{\max}$ rises. When $E_M / E_H = 0.9$ and $\sigma_{eM} \approx \sigma_{eH}$ then $p_{\max}^{M-H} \approx p_{\max}^{H-M}$ (curves 3 in Fig. 5 and Fig. 6).

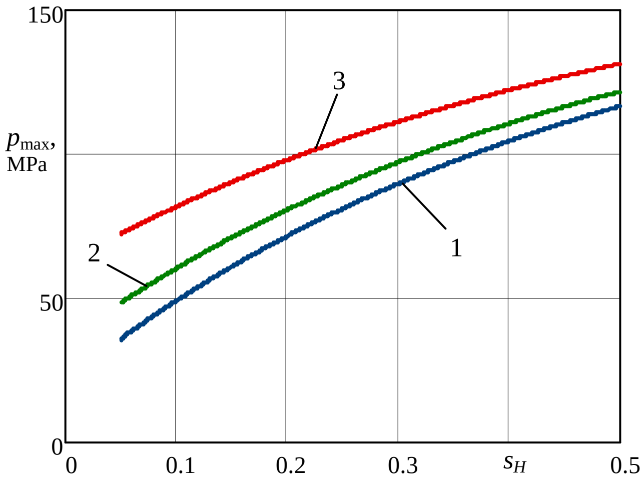

Fig. 5 Dependence $p_{\max}$ on s_H and E_M / E_H in structure H-M when $E_H = 21 \cdot 10^4$ MPa, $s_M = 0.25$, $\nu_H = \nu_M = 0.3$, $r_1 = 50$ mm, $r = 62.5$ mm, $\sigma_{eH} = 350$ MPa.
Curves:
1 – $E_M = 0.3 E_H$, $\sigma_{eM} = 100$ MPa;
2 – $E_M = 0.5 E_H$, $\sigma_{eM} = 200$ MPa;
3 – $E_M = 0.9 E_H$, $\sigma_{eM} = 300$ MPa

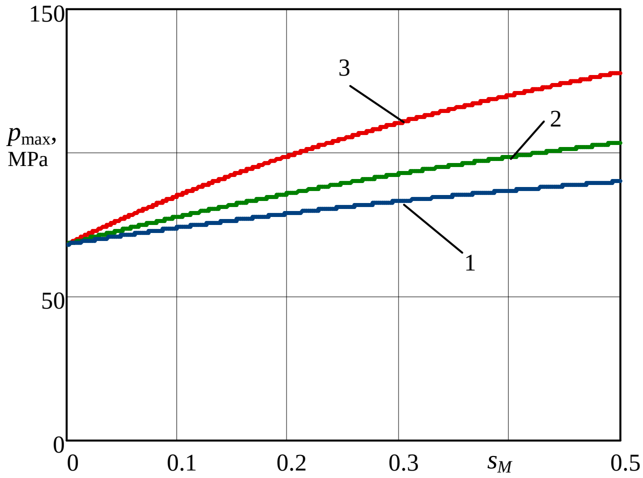

Fig. 6 Dependence $p_{\max}$ on s_M and E_M / E_H in structure M-H when $E_H = 21 \cdot 10^4$ MPa, $s_H = 0.25$, $\nu_H = \nu_M = 0.3$, $r_1 = 50$ mm, $r = 62.5$ mm, $\sigma_{eH} = 350$ MPa.
Curves:
1 – $E_M = 0.3 E_H$, $\sigma_{eM} = 100$ MPa;
2 – $E_M = 0.5 E_H$, $\sigma_{eM} = 200$ MPa;
3 – $E_M = 0.9 E_H$, $\sigma_{eM} = 300$ MPa

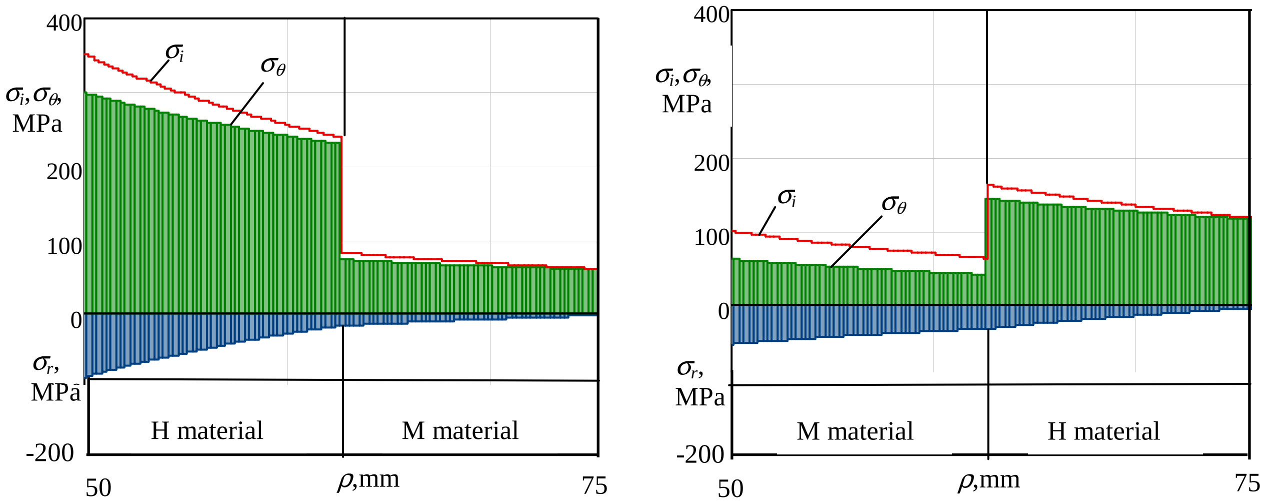

Fig. 7. Distribution of stress intensity σ_i and stresses σ_θ, σ_r in the pipe wall thickness when: $r_1 = 50$ mm, $r = 62.5$ mm, $r_2 = 75$ mm, $\nu_H = \nu_M = 0.3$, $\sigma_{eH} = 350$ MPa, $\sigma_{eM} = 100$ MPa, $E_H = 21 \cdot 10^4$ MPa, $E_M = 7 \cdot 10^4$ MPa: a – H-M, $p_{\max} = 82.6$ MPa; b – M-H, $p_{\max} = 48.5$ MPa

Internal pressure as a rule is major than $p_{\max 2}$ in structure M-H. Strain of structure H-M is more than of structure M-H one, when $s_H > 0.15$ (Fig. 5). For inhomogeneous pipe, which shown in Fig. 7, $p_{\max}^{H-M}$ of structure H-M is 1.7 times major than $p_{\max}^{M-H}$ of structure M-H.

Stress intensity σ_i and circular stress σ_θ on the contact surface of H and M materials varies saltatory (Fig. 7).

Ratio $\dfrac{\sigma^H_{\theta|\rho=r}}{\sigma^M_{\theta|\rho=r}}$ on the contact surface of materials H and M, as follows from Eqs.(10) – (11), may be determined by dependence

$$\frac{\sigma_{\theta 1|\rho=r}}{\sigma_{\theta 2|\rho=r}} = \frac{\left(r_2^2 - r^2\right)\left[2r_1^2 - C_p\left(r_2^2 + r_1^2\right)\right]}{C_p\left(r_2^2 + r^2\right)\left(r^2 - r_1^2\right)} \tag{16}$$

It is determined that on the contact surface of materials H and M: $\dfrac{\sigma_{\theta 1|\rho=r}}{\sigma_{\theta 2|\rho=r}} \approx \dfrac{E_H}{E_M}$.

The assumption $\sigma_z = 0$ at the contact surface of H-M materials in this solution is made. The stress state components in two-layer mechanically in homogeneous pipe, subjected to internal pressure at elastic loading, determined by FEM, showed that $\left|\sigma_z\right| \approx 0.002\sigma_i$. In model, which is used for stress state determination by FEM, layers on the contact surface are connected. The real deforming conditions of materials H and M on its contact surface are intermediate. Therefore, real value $\left|\sigma_z\right|$ may be lower than $0.002\sigma_i$. Values of the maximum stress σ_θ calculated analytically and determined by FEM differs less than 0.5 %. Therefore, obtained dependencies sufficiently exactly describe behavior of two-layer pipes.

4. Conclusions

The dependencies for stress strain state of two-layer inhomogeneous pipe, subjected to internal pressure, determination at elastic loading are presented. Comparison of stress state components calculated analytically and determined by FEM showed that obtain dependencies are sufficiently exact.

Ratio p_c / p in structure H-M whit increasing E_M / E_H and s_M also increases. It negligible depends on $\nu_1 - \nu_2$.

Stress state of inhomogeneous pipe depends on ratio E_M / E_H, relative thickness of layers s_1, s_2 and its layouts.

The maximum internal pressure $p_{\max}$, when both materials are deformed elastically, as a rule realizes in structure H-M. Only when ratio $E_M / E_H << 1$, $\sigma_{eM} \approx \sigma_{eH}$, $s_M >> s_H$ and both materials are deformed elastically $p_{\max}$ realizes in structure M-H. For the real materials: $\sigma_{eM} \approx \sigma_{eH}\, E_M / E_H$. Therefore, such material M practically does not exist.

Obtained dependencies may be used for calculation of the compound two-layer pipes with different mechanical properties of internal and external layers.

References

1. **Wolters M., Wessing W., Dalmolen B., et.al.** Reinforced thermoplastic pipeline (RTP) systems for gas distribution, 2006, 23rd World Gas Conference.
2. **Wang X., Li M. D., Yu Z. Y.** Self-Strengthening Research of Fiber Reinforced Pressure Vessel with Metallic Liners, Journal of Reinforced Plastics and Composites, 2001,Vol. 20, No. 16, p. 1390-1413.
3. **Ivanov S.G., Strikovski L. L., Gulyaeva M. A., Zuiko V. Yu.** Modeling the mechanical behavior of metal-reinforced thermoplastic pipes under internal pressure. –Mechanics of Composite Materials, 2005, vol. 41, no. 1, p. 57-70.
4. **Majzoobi G. H., Ghomi A.** Optimization of compound pressure cylinders. –Journal of Achievements in Materials and Manufacturing Engineering, 2006, vol. 15, issue.1-2, p.135-145.
5. **Bražėnas A.** The principles of theories elasticity and plasticity. – Shauliai: ShU publisher. 2003. – 194 p. (in Lithuanian).
6. **Kaminskas, V., Bražėnas, A.** Stress strain determination of mechanically heterogeneous welded pipelines at elastic loading. Mechanika, 2004, No. 6(51), p. 5-13.
7. **Kaminskas V., Bražėnas A.** Stresses and strains determination of welded pipelines with the mild interlayer at plane stress state under elastic-plastic loading. Mechanika, 2005, No. 3(53), p. 5-11.
8. **Partaukas N., Bareišis J.** The stress state in two-layer hollow cylindrical bars. Mechanika, 2009, No.1 (75), p. 5-12.
9. **Partaukas N., Bareišis J.** The stress state in two-layer solid cylindrical bars. Proceedings of the 14th International Conference Mechanika-2009, Kaunas, p. 301-306.

Proceedings of 4th International Conference ITELMS'2009

Equivalent Dose Rate Field Structure Investigation Using Optimum Interpolation Method

L. J. Gustas*, J. Kleiza, D. Styra*****

**Vilnius Gediminas Technical University, Saulėtekio str. 11, LT-10223 Vilnius, Lithuania, E-mail: linasg@dtiltas.lt*
***Vilnius Gediminas Technical University, Saulėtekio str. 11, LT-10223 Vilnius, Lithuania,*
E-mail: kleizajonas@gmail.com
****Vilnius Gediminas Technical University, Saulėtekio str. 11, LT-10223 Vilnius, Lithuania, E-mail: styra@fm.vgtu.lt*

Abstract

The paper presents an investigation of equivalent dose rate (EDR) field structure at the Baltic seacoast. EDR measurements were carried out near Juodkrantė July 7, 9 and 12 of 2008. Average extreme values were 41 and 98 nSv/h, and in individual cases 40 and 130 nSv/h. EDR was measured in 63 points and its field structure was obtained by optimum interpolation method. Measurement number was decreased up to 33 and 18 to get EDR field structure. The coincidence between measured and calculated values was satisfactory.
KEY WORDS: *radon decay products, optimum interpolation method, equivalent dose rate.*

1. Introduction

Natural radionuclides penetrate into environment from soil; also they are formed by the cosmic rays interaction with nuclei of air molecules. Radon and it‘s decay products exhalate from soil, and those radionuclides form the main part of radioactive materials in the surface layer of atmosphere [6]. Among 27 radon isotopes (from ^{200}Rn to ^{226}Rn) only ^{222}Rn has significance with respect to contaminating the environment and due to its individual migrating possibilities [4]. ^{222}Rn is widely distributed throughout the earth‘s crust. Radon emanates from soil, rock and water and becomes dispersed in air. Being a noble gas it migrates by diffusion and convection without any significant interaction with the constituents of air or any airborn particulates.

Epidemiological studies have indicated that the presence of radon and its decay products in inhaled air causes a health risk of lung cancer [1]. The radon content in soil gas exhaling from the ground surface as well as in underground waters (i.. e. in waters from wells that are hundreds of meters deep and springs along active fault zones) is one of the few important earthquake precursors [3]. The observed radon anomalies correlated with geophysical events may be considered as having two possible origins. Radon anomalies were related to mechanical crack growth in the rocks or to changes in flow rate of groundwater. An alternative mechanism is the stress corrosion theory. The anomalous radon concentration may be due to an increase in crustal compression, impending an earthquake that squeezes out the soil gas into the atmosphere at an increased rate [2].

These reasons show the environmental radioactivity must be under control. Huge territories like Northern sea or Baltic Sea must be controlled. Also the continent regions must be under control, and relief and soil structure in these regions must be evaluated. Significant amount of experimental information about situation in environment is needed. Also this information is needed to forecast environmental situation changes in space and time.

Collection of experimental information in huge territories is long and expensive process. When number of measurements is small the same information can be obtained by using theoric model-optimum interpolation. This model calculates element concentration in territories where measurements were not carried out, also this model calculates an error of experimental results [8]

In this research, a radiation situation possible in huge territories is decreased and used in small territories.

A 0.4 km^2 area at the Baltic Sea coast near Juodkrantė was chosen for equivalent dose rate (EDR) measurement (Fig. 1).

The objective of this research is checking of theoric model and restoration of EDR field structure in small territory when number of measurements is minimal.

2. Materials and Methods of Equivalent Dose Rate (EDR) Measurements

Equivalent dose rate (EDR) in surface layer of atmosphere was measured by scintillation radiometer SRP–88N. This device is used for working in field conditions, portable, charged by electric batteries. The main parameters are: threshold of energy registration–30 keV, relative measurement error–10%, time of one measurement–10 s, dimensions of NaI (Tl) sensor crystal - (25×40) mm.

EDR values were obtained from natural and man-made sources (asphalt). These values have a concentration of heterogeneous fields. Measurements were carried out in three ways: along seacoast (wet sand), above asphalt way and along forest (dry sand). Experimental results were obtained in 63 points, i.e., vertices of regular network, distance between them is 100 m. Measurements were carried out in 2008-07-07, 2008-07-09 and 2008-07-12 when wind velocity and direction were different. The diverse variants of obtained results were used in theoric model.

The method of optimum interpolation was chosen for mathematical modeling in this research. Using this method, the equivalent dose rate can be calculated in places where measurements were not carried out.

The main characteristics of the method of optimum interpolation, is the normalized autocorrelation function $\mu_k = \mu_k\left(\rho_{k,k+1}\right)$, which depends on equivalent dose rate in the points, where the distance between them is limited within $\rho_k < \rho \leq \rho_{k+1}$. This function depends also on the coordinates of these points. Then, before calculating the autocorrelation function $\mu(\rho_k)$, the measurement points should be divided into groups according to the distance between them. Then the normalized autocorrelation function is calculated for each group of the points:

$$\mu(\rho_k) = \frac{1}{\mu_0 N_k} \sum_{i,j=1}^{N_k} C_i^{'} C_j^{'} \tag{1}$$

where $C_i^{'} = C_i - \frac{1}{N}\sum_{j=1}^{N} C_j$, $\mu_0 = \frac{1}{m_k}\sum_{i=0}^{m_k}\left(C_i^{'}\right)^2$, N – the number of the measurement points, C_i – equivalent dose rate in the i point, m_k – the number of points between them, if the distance is limited by interval $[(k-1)\Delta\rho; k\Delta\rho)$, $\rho_k = (k-0{,}5)\Delta\rho$; k=1, 2, 3,... – the number of groups; N_k – the number of all possible products of $C_i^{'}C_j^{'}$.

When the values $\mu(\rho_k)$ are calculated in the points ρ_k, autocorrelation function $\mu(\rho) = e^{-\alpha\cdot\rho}$ is approximated by the least squares method [8].

Another part of the problem is the solution of a system of linear equations. If this system is solved, the unknown weights are calculated:

$$\sum_{j=1}^{n} \mu_{i,j} P_j^{(\theta)} = \mu_{j,\theta}\text{, } i=1,2,...,n \tag{2}$$

where: $\mu_{i,j} = \mu(\rho_{i,j})$, $P_j^{(\theta)}$ – unknown weights, $\rho_{i,j}$ – the distance between the i and θ points in which the EDR is obtained.

After solving the system of equations (2), the weights P_1, P_2,..., P_n are known, and the unknown equivalent dose rate values $C_{i,\theta}$ can be calculated:

$$C_{i,\theta} = C_{i,\theta}^{'} + \frac{1}{N}\sum_{j=1}^{N} C_j = \sum_{j=1}^{N} P_j^{(\theta)} C_j^{'} + \frac{1}{N}\sum_{j=1}^{N} C_j \tag{3}$$

In this method, the reproduced concentration field should be stationary and isotropic, and the efficiency of the method depends on fulfillment of these preconditions [7].

Then the concentrations calculated by the method of optimum interpolation should be chosen; for them, the variance of the calculated values should be less than or equal to the variance of measurement results (Стыро, 1989).

3. Results

EDR measurements were carried out at the Baltic Sea coast (Fig. 1) when wind direction and velocity were different. The map of territory where measurements were carried out is presented in Fig. 1.

Radon ant it‘s decay products exhalation from a soil depends on structure of ground surface. Radionuclides exhalation into atmosphere was different. Heterogeneous ground surface formed different EDR field structure in the surface layer of atmosphere. Measurement results are presented in Table 1.

Results of this Table show that EDR average values vary from 41 to 98 nSv/h. The greater EDR values were obtained near the ground surface. It means that the main source of natural radionuclides is a soil. Concentration of radionuclides is changing in space and time. Extreme EDR values of individual measurements were 40 and 130 nSv/h.

The method of optimum interpolation was used to analyse the EDR field’s structure and their change. Condition of stationarity was accepted. This method was used having a full experimental information (63 results), and some parts of it.

EDR field structure in July 7, 9 and 12 of 2008 near ground surface and 1 meter from ground surface are presented in Fig. 2, 3. EDR field structures near ground surface and 1 meter above it have similar form. EDR value increase near center of territory is observed. Asphalt way is an additional man-made source of radionuclides. EDR slower increases near center of territory if the distance from ground surface is 1 meter.

EDR value differences in July 7, 9 and 12 can be explained by different wind velocity and direction. When wind velocity is small the intensivity of admixture transfer decreases, and radionuclides accumulation increases near the ground surface.

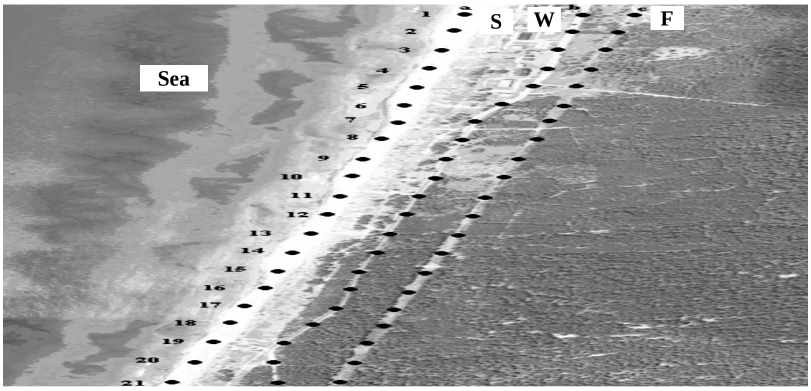

S – sea coast
W – asphalt way
F – forest

Fig. 1. Territory of EDR measurement (http://www.maps.lt/lt/zemelapis)

Table 1

EDR (nSv/h) measurement results at the Baltic sea coast near Juodkrantė in July 7, 9 and 12 of 2008

Date	2008.07.07						2008.07.09						2008.07.12					
Number of measure-ment point	EDR at sea coast, nSv/h		EDR at asphalt way, nSv/h		EDR at forest, nSv/h		EDR at sea coast, nSv/h		EDR at asphalt way, nSv/h		EDR at forest, nSv/h		EDR at sea coast, nSv/h		EDR at asphalt way, nSv/h		EDR at forest, nSv/h	
	Distance from ground, m		Distance from ground, m		Distance from ground, m		Distance from ground, m		Distance from ground, m		Distance from ground, m		Distance from ground, m		Distance from ground, m		Distance from ground, m	
	0	1	0	1	0	1	0	1	0	1	0	1	0	1	0	1	0	1
1	80	90	120	100	80	70	60	40	80	80	60	50	80	70	120	90	70	60
2	80	60	120	120	80	70	50	40	100	80	60	50	50	50	130	110	70	70
3	60	60	100	100	70	70	50	40	80	80	60	60	60	50	90	90	70	60
4	60	60	80	90	70	70	60	40	80	70	60	50	60	50	80	80	80	70
5	50	50	90	80	70	70	40	40	70	70	60	60	60	60	80	70	60	60
6	60	50	90	90	70	80	50	40	70	60	70	60	60	60	80	60	60	60
7	70	60	80	80	70	70	40	40	70	70	50	50	60	50	80	70	70	60
8	60	50	80	70	80	70	40	40	90	70	60	50	50	50	80	70	70	60
9	60	50	90	80	80	70	50	40	80	70	70	60	50	50	80	80	70	60
10	60	60	100	90	70	80	50	40	80	80	60	50	60	50	90	80	70	60
11	60	50	90	80	80	70	50	40	80	70	60	60	50	50	80	80	70	70
12	60	60	100	90	80	80	40	40	80	70	70	50	50	50	90	80	70	70
13	60	50	100	80	70	70	60	40	70	70	70	60	50	50	90	80	70	60
14	60	50	90	90	70	70	50	40	80	70	100	70	50	50	80	80	80	70
15	50	50	100	80	70	70	50	40	70	60	60	50	50	50	90	70	70	60
16	60	50	100	90	70	70	50	40	80	70	70	60	50	50	90	80	70	60
17	70	60	90	90	80	80	50	50	80	70	60	50	60	50	90	80	70	70
18	60	50	100	90	80	70	50	40	80	70	70	60	50	50	90	80	70	60
19	60	60	100	90	80	70	40	50	80	80	70	50	50	50	90	80	70	60
20	60	50	110	100	70	70	50	40	90	70	60	60	50	50	100	90	70	60
21	60	50	120	100	70	70	50	40	80	80	70	50	50	50	110	90	70	60
EDR average value, nSv/h	62	55	98	90	74	72	49	41	80	72	65	55	55	52	91	80	70	63
Wind velocity, m/s	2		1		2		6		2		2		3		3		1	
Wind direction	Eastern		Eastern		Eastern		South-western		Western		Western		Western		Western		Western	

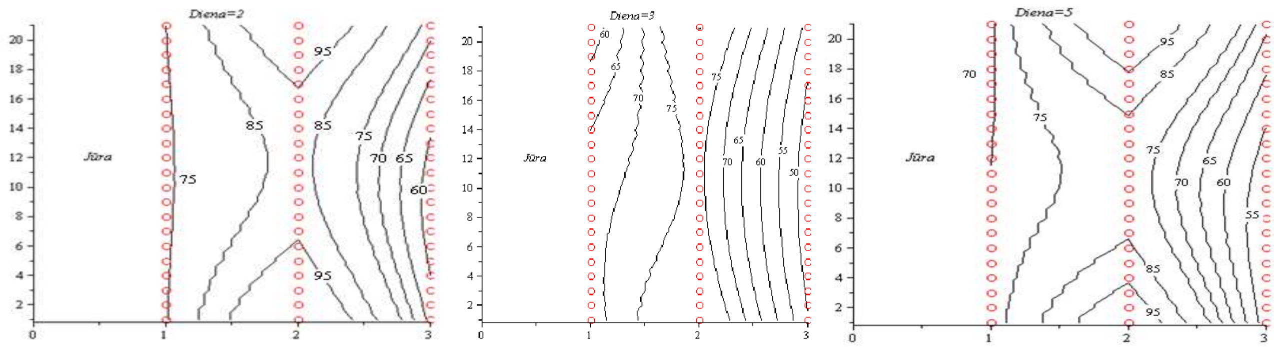

a b c

Fig. 2. EDR (nSv/h) field structure near ground surface: a – July 7 of 2008; b – July 9 of 2008; c – July 12 of 2008 (63 measurement points)

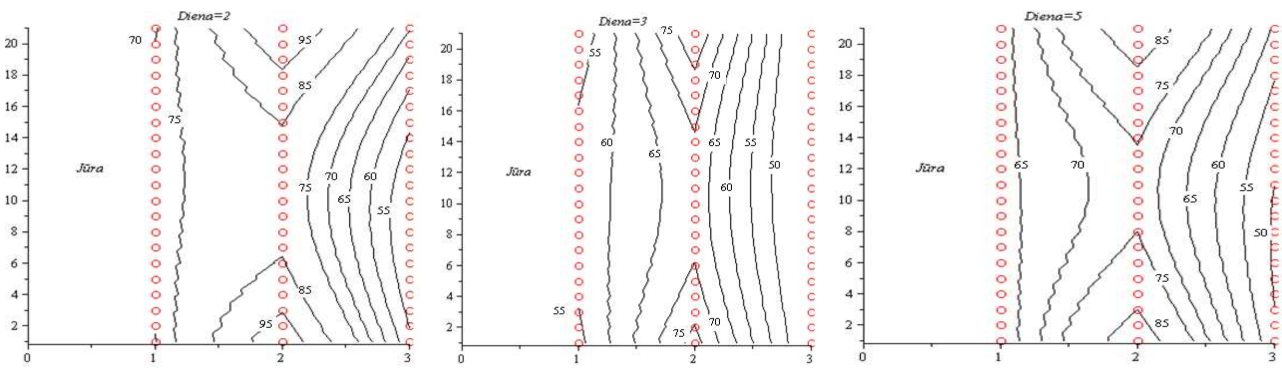

a b c

Fig. 3. EDR (nSv/h) field structure 1 meter above ground surface: a – July 7 of 2008; b – July 9 of 2008; c – July 12 of 2008 (63 measurement points)

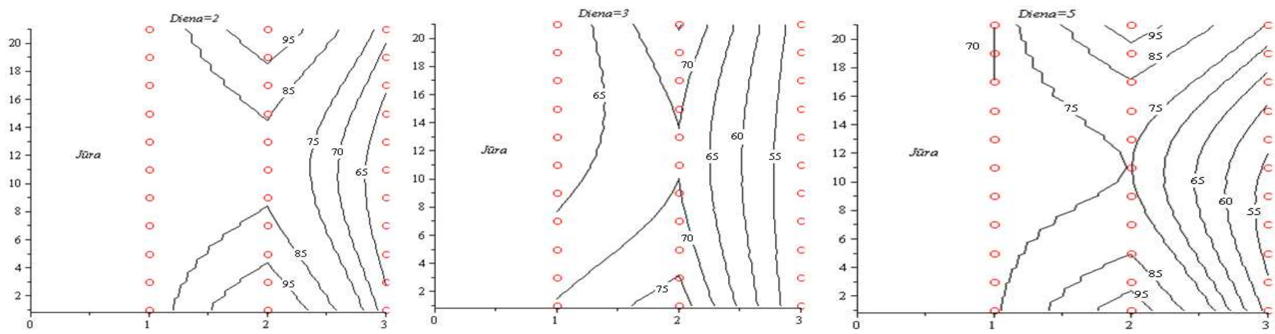

a b c

Fig. 4. EDR (nSv/h) field structure near ground surface: a – July 7 of 2008; b – July 9 of 2008; c – July 12 of 2008 (33 measurement points)

The objective of this research is restoration of EDR field structure in small territory when number of measurements is minimal. 33 measurement points are used, 30 measurement points are removed, and EDR values are calculated by optimum interpolation method. Obtained results are presented in Fig. 4, 5.

Comparison of EDR field structures calculated with 63 experimental values (Fig. 2, 3) and with 33 values (Fig. 4, 5) confirmed that the last one can restore the EDR field structure for every presented situation. The coincidence of the calculated results was satisfactory in above stated figures. EDR values increase near the central part of territory is observed. In every case a similar structure of EDR field near the ground surface and at the one meter distance from it were obtained.

Numerical results of the same situation are presented in Table 2. Here the difference between theoretic and experimental EDR values does not exceed 15%.

18 measurement results were used to restore EDR field structure over the same territory by optimum interpolation method (Fig. 6, 7).

Here the form of isolines differs from analogical curves in Fig. 2, 3, when 63 experimental results were used.

The difference between average values of measured and calculated results of EDR does not exceed 15 %, however this difference in individual points (Fig. 1) sometimes is greater and in particular over artificial surface (Table 3).

In the 9 cases from 63 results the difference between measured and calculated values exceeds 20 %.

Comparison of EDR field structures when 63 and 18 experimental results were used show that 18 measurement points can restore EDR field structure for every day. The coincidence between measured and calculated EDR values was satisfactory. EDR value increase near center of territory is observed. EDR increases less near center of territory when distance from the ground surface is 1 meter.

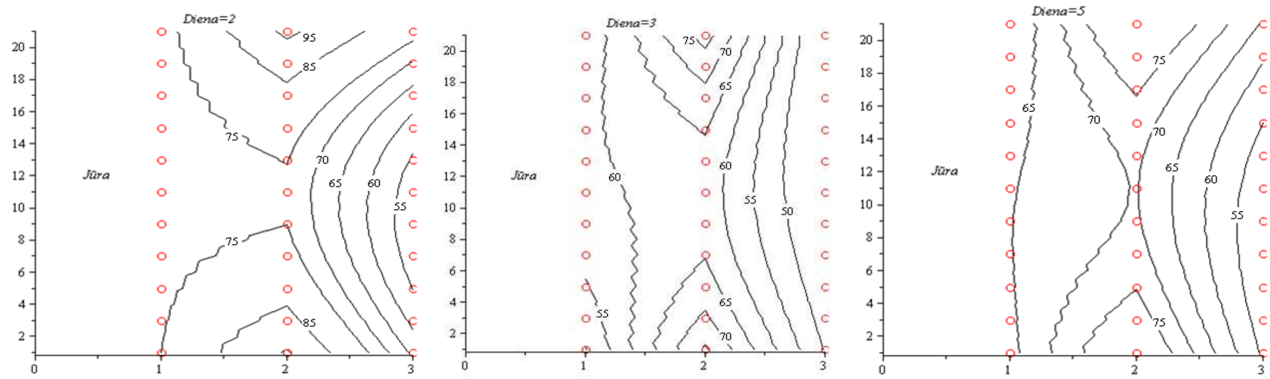

a b c

Fig. 5. EDR (nSv/h) field structure 1 meter above ground surface: a – July 7 of 2008; b – July 9 of 2008; c – July 12 of 2008 (33 measurement points)

Table 2

Comparison of the theoric and experimental values (nSv/h) 2008-07-07 1 meter above ground surface when 33 measurement points were used

Number of measurement point	EDR at sea coast, nSv/h		EDR at asphalt way, nSv/h		EDR at forest, nSv/h	
	Measured EDR value	Calculated EDR value	Measured EDR value	Calculated EDR value	Measured EDR value	Calculated EDR value
1	90	90	100	100	70	70
2	60	80	120	90	70	77
3	60	60	100	100	70	70
4	60	61	90	78	70	74
5	50	50	80	80	70	70
6	50	59	90	73	80	72
7	60	60	80	80	70	70
8	50	59	70	73	70	73
9	50	50	80	80	70	70
10	60	55	90	72	80	73
11	50	50	80	80	70	70
12	60	55	90	72	80	73
13	50	50	80	80	70	70
14	50	54	90	71	70	72
15	50	50	80	80	70	70
16	50	60	90	77	70	78
17	60	60	90	90	80	80
18	50	65	90	82	70	79
19	60	60	90	90	70	70
20	50	62	100	82	70	76
21	50	50	100	100	70	70
EDR average value, nSv/h	56	59	90	82	72	73

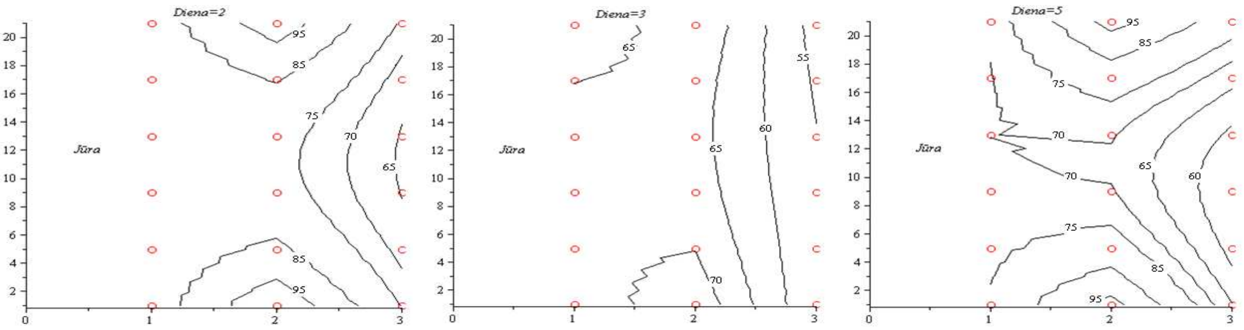

a b c

Fig. 6. EDR (nSv/h) field structure near ground surface: a – July 7 of 2008; b – July 9 of 2008; c – July 12 of 2008 (18 measurement points)

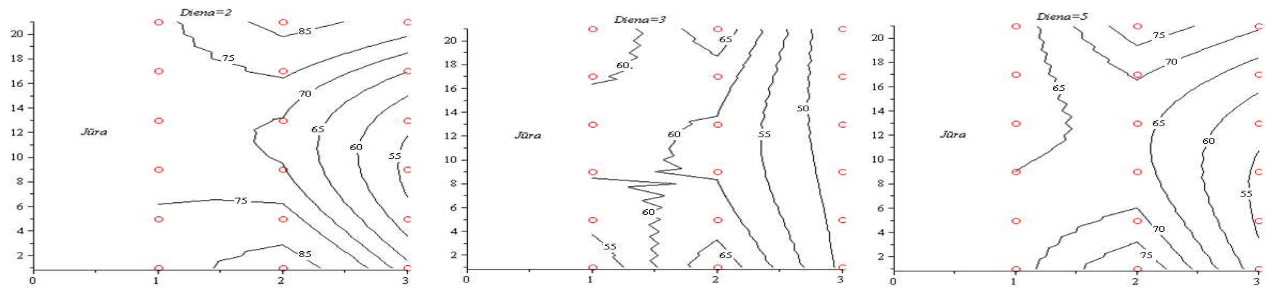

a b c

Fig. 7. EDR (nSv/h) field structure 1 meter above ground surface: a – July 7 of 2008; b – July 9 of 2008; c – July 12 of 2008 (18 measurement points)

Table 3

Comparison of the theoric and experimental values (nSv/h) 2008-07-07 1 meter above ground surface when 18 measurement points were used

Number of measurement point	EDR at sea coast, nSv/h		EDR at asphalt way, nSv/h		EDR at forest, nSv/h	
	Measured EDR value	Calculated EDR value	Measured EDR value	Calculated EDR value	Measured EDR value	Calculated EDR value
1	90	90	100	100	70	70
2	60	83	120	85	70	76
3	60	74	100	77	70	75
4	60	64	90	73	70	74
5	50	50	80	80	70	70
6	50	56	90	68	80	71
7	60	57	80	66	70	70
8	50	56	70	68	70	71
9	50	50	80	80	70	70
10	60	56	90	69	80	72
11	50	57	80	66	70	71
12	60	56	90	68	80	72
13	50	50	80	80	70	70
14	50	59	90	71	70	74
15	50	62	80	72	70	77
16	50	64	90	77	70	80
17	60	60	90	90	80	80
18	50	66	90	79	70	81
19	60	65	90	76	70	79
20	50	63	100	79	70	78
21	50	50	100	100	70	70
EDR average value, nSv/h	56	61	90	77	72	74

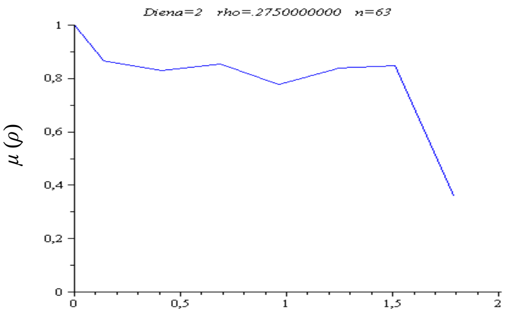

a

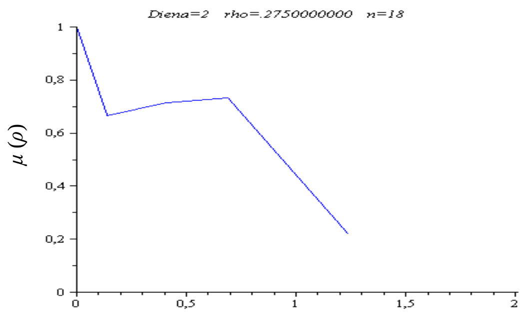

b

Fig. 8. a – EDR autocorrelation function of 1 meter above ground surface July 7 of 2008 (63 measurement points); b – EDR autocorrelation function of 1 m above ground surface July 7 of 2008 (18 measurement points)

Examples of EDR autocorrelation functions are given in Fig. 8 a, b.

The results in (Fig. 8 a, and b) show relatively strong correlation between EDR elements. It is evident, that the more experimental results are used, the correlation is stronger.

4. Conclusions

1. The wind of various directions changes the structure of EDR field.
2. It is found out that EDR values were greater near the ground surface.
3. Decreasing measurement number up to 33 and 18, the coincidence between measured and calculated EDR values was satisfactory. A difference between measured and calculated data is about 15%.
4. To get the similar structure of EDR field with accuracy of 15%, it is possible to decrease the measurement number 3.5 times using optimum interpolation method.

References

1. **Güngör Yener** and **Eşref Küçüktaş**. Concentration of radon and decay products in various underground mines in western Turkey and total effective dose equivalents. Analyst, January 1998, Vol. 123 (31-34).
2. **Imme G., La Delfa S., Lo Nigro S., Morelli D.** and **Patane G**. Gas radon emission related to geodynamics activity on Mt. Etna. Annals of Geophysics. Vol. 48. N. 1, February 2005.
3. **Papastefanou C**. Measuring radon in soil gas and groundwaters: a review. Annals of Geophysics. Vol. 50. No. 4. August 2007.
4. **Pienkowska H.** Radon exhalation from building materials and soil. Technical sciences, No. 8, 2005.
5. The map of researched territory [December 1 of 2008]. http://www.maps.lt/lt/zemelapis
6. **Луянас, В.** Космогенные радионуклиды в атмосфере. Вильнюс, Мокслас, 1979, 196 с.
7. **Нелепо Б. А.** 1970. Ядерная гидрофизика. Москва: Атомиздат. 224 с.
8. **Стыро, Д. Б.** Вопросы ядерной гидрофизики. Ленинград, Гидрометеоиздат, 1989, 256 с.

Proceedings of 4th International Conference ITELMS'2009

The Investigation of Bridge's Type Cranes with Settled Movement

P. Barzdėnas*, J. Kleiza, B. Spruogis*****

**Vilnius Gediminas Technical University, Plytines str. 27, LT-10105 Vilnius, Lithuania, E-mail: pbarzdenas@yahoo.com*
***Vilnius Gediminas Technical University, Sauletekio al. 11, LT-10223 Vilnius, Lithuania, E-mail: kleizajonas@gmail.com*
****Vilnius Gediminas Technical University, Plytines str. 27, LT-10105 Vilnius, Lithuania, E-mail: bs@ti.vtu.lt*

Abstract

In this article the gravitation's strength of driving wheels from concrete bridge's type goat crane is investigated. It is obtained the system of equations that fully describes the movement of crane whine turning on and allows solving the problem about location of the strength of gravitation when there is regime of settled working.
KEY WORDS: *dynamic, cranes of bridge type, settled movement, crossing mechanism.*

1. Introduction

When analyzing dynamical processes that accurs in cranes, it is necessary to estimate the peculiarity of constructial cranes crossings mechanisms, where the main is the type of cranes crossings mechanisms, the type of motion wheels, the number and scheme of motion wheels, the type and fixing version of under crane rails, type of gear‘s engine. In some cases there is need to estimate the peculiarity of crane‘s metal construction [1-5]. When making complex analysis of bridge‘s type cranes with settled movement, there is necessary to estimate: the mechanic of cranes settled movement and the whell rolling on rail mechanic, the force of attraction of driving wheels, the dynamic of cranes settled movement, when edges of driving wheels do not contact rails and when they do contact rails; the load on cranes in regime of setlled rectilinear case and etc. It is quite difficult task that depends on row of factors. In this article we widely estimate the forces of driving wheels in specific crane of bridge‘s type, goat‘s crane.

2. The Gravitation Forces of Driving Wheels

The gravitation force – is managed moving force, that is created when wheels of force gear contact with rails and is plused with direction of rim‘s movement.

It is difficult to describe the dipendence of gravitation forces in driving wheels when there are to engines. Usually when calculating the gravitation forces in moving mechanisms is keeped, that they are in proportion to opposition forces in moving crane. However there are different opinions. M.Shefler claims, that the gravitation force in driving wheels must to become clear from conditions where we see the proportional relative speed corresponding wheels elastic movement, but he does not present the final appearance of gravitation force [4].

Let‘s agree, that crane, which centre of mass is in geometrical bridge centre (Fig. 1), has equal driving wheels and is moving with the same speed along axle. Gaps, that are in both sides of mechanism‘s elements, are equal. So the opposition for movement is equal, there are equal forces that exists in driving wheels.

If now the heavyweight cart moves to the left, then the resistance (of left crane side) for movement is increasing when increasing vertical load on the wheels, but to the right – decreasing, the moment of inside force will appear, that will call movement from left crane side that reflects right and causing the turn of bridge and deformation of crane tempera.

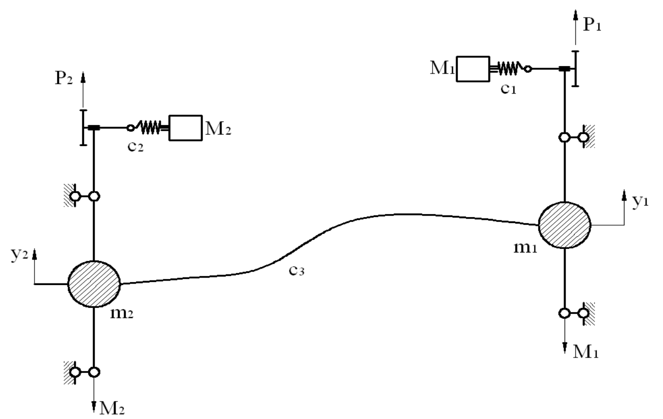

Fig. 1. The calculating scheme of crane

As turn of crane is possible only having tempera wheel movement and occurs enough slowly, we will not consider it when taking into consideration the tempera of bridge deformation and transmissions when exposing the gravitation forces of driving wheels. So the equation of crane movement is:

$$\begin{cases} J\,\ddot{\tau} + B\,\dot{\tau} + c_1\left(\tau - \theta_1\right) = M_0^{(1)} \\ J\,\ddot{\theta} + B\,\dot{\theta} + c_2\left(\theta - \theta_2\right) = M_0^{(2)} \\ m_1\,\ddot{y}_1 + c_3\left(y_1 - y_2\right) - \dfrac{c_1\left(\tau - \theta_1\right)}{r_1} = -W_1 \\ m_2\,\ddot{y}_2 + c_3\left(y_2 - y_1\right) - \dfrac{c_2\left(\tau - \theta_2\right)}{r_2} = -W_2 \end{cases} \tag{1}$$

where c_1 and c_2 – the stiffing of left and right sides in mechanism movement, N/m; θ – the corner of one engine shaft turn, rad; B – the coefficient of stiffing of engine; θ_1, θ_2 and r_1, r_2 – the corners of turn and ray of left and right driving wheels turning; $M_0^{(1)}$ – the moment of the first engine, Nm; $M_0^{(2)}$ – the moment of the second engine, Nm; m_1 – the mass of crane‘s right side, kg; m_2 – the mass of crane‘s left side and the mass of cart without load, kg; y_1 and y_2 – the movement of crane‘s left and right side, m; c_3 – the tempera of bridge when there is curve, N/m; W_1 and W_2 – The left and right side of crane resistance to the wind, N.

The two lacking equation we can get from these relations:

$$P_1 r_1 = c_1\left(\tau - \theta_1\right), \quad P_2 r_2 = c_2\left(\theta - \theta_2\right). \tag{2}$$

Because of driving wheels lengthwise tempera movement, their centres‘road is not equal to the road of clean wheel turning:

$$y_1 \neq r_1 \int_0^t \dot{\tau}_1\,dt \tag{3}$$

$$y_2 \neq r_2 \int_0^t \dot{\theta}_2\,dt\,. \tag{4}$$

According to tempera moving theory, the driving wheels gravitation forces P_1 and P_2 are proportional to correspondence speed of lengthwise tempera movement ε_1 and ε_2 for specific wheels:

$$P_1 = -K_1 \varepsilon_1, \quad P_2 = -K_2 \varepsilon_2 \qquad 5)$$

There K_1 and K_2 coefficients of correspondence driving wheels tempera movement.

Driving wheels speeds when they are turning:

$$v_1 = r_1\,\dot{\tau}_1, \quad v_2 = r_2\,\dot{\theta}_2\,. \tag{6}$$

Existing their speed $\dot{y}_1$ and $\dot{y}_2$. Dividing the difference between existing speed and turning speed:

$$\varepsilon_1 = 1 - r_1\,\dot{\tau}_1/\dot{y}_1\,, \quad \varepsilon_2 = 1 - r_2\,\dot{\theta}_2/\dot{y}_2\,. \tag{7}$$

While putting expressions (5), (7) in to (2) formulas, we get expression of missing connection equation between corner and rectilinear movement that are investigating in the system:

$$\begin{cases} c_1\left(\tau - \theta_1\right) + K_1\,r_1\left(1 - r_1\,\dot{\tau}_1/\dot{y}_1\right) = 0 \\ c_2\left(\theta - \theta_2\right) + K_2\,r_2\left(1 - r_2\,\dot{\theta}_2/\dot{y}_2\right) = 0 \end{cases} \tag{8}$$

Not rectilinear equation systems (1) and (8) totally describe the specific crane movement when switching on (Fig. 2) and allow solving task about gravitation forces location, when there is settled regime.

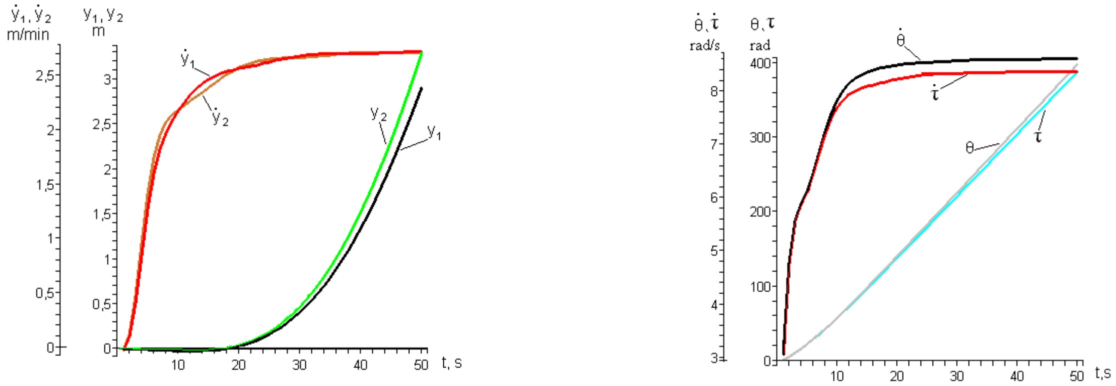

a b

Fig. 2. Specific goat crane with separate gears switching on dependence: a) The movement of left and right crane side and movement speed; b) The crane‘s engine shafts speed and their turning corners

Formatted crane movement parameters are described by solving equation systems (1) and (8), when $t \to \infty$. It is possible to show that when movement appears $\theta_1 = \theta = \omega_0^{(1)} = const$, $\theta_2 = \tau = \omega_0^{(2)} = const$ and $\dot{y}_1 = \dot{y}_1 = v_0 = const$ and putting these figures in to equations (1) and (8) we get formulas:

$$v_0 = \frac{K_1 r_1 \omega_0^{(1)} + K_2 r_2 \omega_0^{(2)}}{W + K_1 + K_2} \tag{9}$$

where $W = W_1 + W_2$.

Analogical we get formulas that describe rest figures characterising appearing crane movement:

$$\varepsilon_1^0 = 1 - \frac{r_1\, \omega_0^{(1)}}{v_0}, \qquad \varepsilon_2^0 = 1 - \frac{r_2\, \omega_0^{(2)}}{v_0} \tag{10}$$

Driving wheels gravitation forces:

$$P_1^0 = K_1 \left(r_1 \frac{\omega_0^{(1)}}{v_0} - 1 \right), \qquad P_2^0 = K_2 \left(r_2 \frac{\omega_0^{(2)}}{v_0} - 1 \right) \tag{11}$$

That means that when there is symmetrical transmission ($c_1 = c_2$), equal engines ($M_1 = M_2$) and wheels ($r_1 = r_2 = r$) the gravitation forces will be equal for each other. That allow saying that from switching crane of till occurring settled movement the distribution of gravitation forces till figures showed in (11) occurs.

3. Conclusions

1. The not rectilinear equation systems are took out, that totally describes specific crane movement when switching on and allows solving task about gravitation forces distribution when there is transitional or settled work regime.
2. When there is symmetric goat crane transmission, equal engines and wheels, the gravitation forces between each other are equal. In the moment *t* switching on crane, the dynamical processes occur, that later, when gravitation forces evenly distributes, ensures the settled movement of crane.

References

1. Standart LST EN 13001-2. Kranai. Bendrasis projektavimas. 2-oji dalis. Apkrovų veikimas. 2005.
2. **Spruogis B.** Pakrovimo ir iškrovimo įrenginiai bei mašinos. Vilnius: Technika. 1994. 207 p.
3. **Moore.R,** Gantry Crane: Analysis, Visualization, Experimentation and Control Mathematics. Department Macquarie University, Sydney. 1999
4. **Лобов Н. А.** Динамика грузоподьемных кранов. М.: Машиностроение, 1987. 160 с
5. **Казак С. А**. Динамика мостовых кранов. Машиностроение, 1968. 472 с.

Finite Element Analysis of Capacitive Micromachined Ultrasonic Transducers for Flow Measurements in Gases and Fluids

M. Mikolajūnas*, G. Vanagas*, D. Viržonis**

** Kaunas University of Technology, Institute of Physical Electronics, Savanorių 271, LT-50131 Kaunas, Lithuania, E-mail: gailius@minatech.lt; marius.mikolajunas@ktu.lt*
*** Kaunas University of Technology, Panevežys Institute, Daukanto 12, LT-35212, Panevėžys, Lithuania, E-mail: darius.virzonis@ktu.lt*

Abstract

Capacitive micromachined ultrasound transducer (cMUT) concept based device for measuring fluids and gases flow ratio is described and simulated. Employing cMUTs to work for a flow measurement allows minimizing the influence on the hydrodynamic resistance of the flow meter. The effect was achieved by obtaining the oblique front of the ultrasound wave without physically tilting the transducer's aperture. This became possible by introducing a special way of transducer segmentation and distribution along the wall of a measurement tube. Our solution allows obtaining required dynamical focusing and refusing from electronic delay lines at the same time. This lowers the price and simplifies the electronic part of device. For design verification a finite element model was developed. The transient analysis was used to simulate the ultrasound wave front. Simulation results showed the most concentration of the energy of transmitted ultrasound beam to propagate at an angle of 35^{o} to the plane of the transducer assembly and thus to a side wall of a measurement tube to which the transducer assembly is mounted.
KEY WORDS: *capacitive micromachined ultrasound transducer, flow meter, finite element analysis*

1. Introduction

The measurement of a fluid or gas flow velocity and rate is greatly important in latter-day science and industry. Flow measurement is necessary for control and monitoring of operations, in which liquids and gases are fabricated, transported or dosed.

The existing flow meters can be classified into several different categories: mechanical, electromagnetic, ultrasonic and optical [1]. In the last years, ultrasonic technique greatly improved in flow measurement accuracy and extended fields of use. The ultrasonic flow measurement offers many potential advantages over other flow measurement techniques. The instrumentation can be more accurate not only in static conditions, but in dynamic ones as well; and a most important point: ultrasound is cost-effective long term solution for flow measurement installations [5].

Capacitive Micromachined Ultrasonic Transducers (cMUT) concept came to the research in the past two decades as a branch of evolving microelectromechanical systems (MEMS) industry. Methods of cMUT fabrication are described widely [3, 4].

Most flow meters are designed to measure a flow that follows a certain flow velocity profile; therefore the information about the flow profile in a measurement duct is critically important. The exact character of the velocity profile will depend on many factors, one of which is the meter installation effect [5]. For ultrasonic flow measurement an ultrasound wave propagation direction must be parallel or have non-square angle in respect to the flow direction (Fig. 1). Radiation direction of simple ultrasonic transducer is perpendicular to the emitting surface; therefore they require tilting or using tilted mirrors/prisms to form an ultrasonic beam of required direction. Fig. 1 schematically shows the more or less traditional way of positioning the ultrasound transducers within the flow measuring tube. Here the ultrasound transmitter is transmitting ultrasound energy towards an oppositely placed receiver, which receives the ultrasound energy and converts it to the electrical signal. Signal attenuation, distortion or protrusion of transducer elements to the inner space of a measurement tube is unavoidable and the later distorts the flow. In the case of segmented transducers, angle path of an ultrasound beam to the emitting surface can be obtained (Fig. 2). Thus the transducer can be mounted substantially parallel to the sidewall of a measurement tube, eliminating the need of protruding/reflecting/attenuating elements. This is preventing from introduction of additional flow disturbances which affect the measurement data. However, fabrication of segmented piezoelectric transducers with high level of accuracy is problematic and expensive. Moreover, special matching layers in order to couple ultrasound into liquid or gas medium are required and these layers need to be manufactured to tight mechanical tolerances. Therefore we think cMUT concept here is to have potential advantages. An additional advantage of cMUT is the possibility of operation in high temperatures, at which the piezoelectric devices lose their properties. This creates new niche potential; eg. gas flow meters in internal combustion engines, exhoust gases flow meters, etc. So, this study was targeted to explore the effect of introducing cMUTs in ultrasonic flow meters.

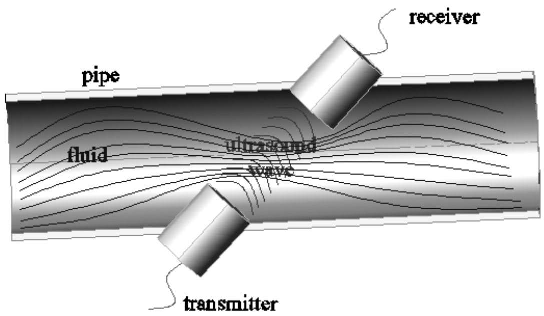

Fig. 1.Ultrasound transducer arranged at the angle to the tube wall.

2. Design of a Transducer

To obtain required radiation characteristics of a transducer, which is flush-mounted to the measurement tube wall, we designed bended segmented arrays of cMUT cells. Oblique front of ultrasonic wave was obtained by choosing different distances between the transducer elements. The special way of the excitation of transducer elements, using reversed biasing, was used [17]. This gives a potential of putting down the unit price and simplification of electronic part of the device.

The ultrasonic flow meter operates with a pair of transducers, where transmitting transducer excites an ultrasound beam, which is inclined to the flow at an angle to the plane of the transducer assembly and to the side wall (Fig. 2). We performed analysis for the angle $\varphi = 35°$, but other angles are equally conceivable. The exact path of the beam depends on the transducer design/operation mode and the measuring tube configuration.

For measuring fluid flow the ultrasound beam may be a pulsed beam. The flowing liquid or gases causes time differences, frequency variations and phase shifts in ultrasonic signals, which are subsequently captured and processed by the flow meter electronics. The time-flight flow meter detects the difference between the travel times of ultrasound in flowing and in stagnant fluids as [2]:

$$\Delta t = l \cos\varphi \frac{v}{c^2} \tag{1}$$

where l is a distance between the transducers; φ stands for an angle between the ultrasound beam path and direction of flow, v denotes the fluid flow velocity, c stands for velocity of sound.

The concept of a transducer design is shown in (Fig. 3), were both dimensions l_1 and l_2 kept equal to about 15 mm. Such a transducer is suitable for operation with an ultrasound frequency of about 1 MHz in measurement tubes

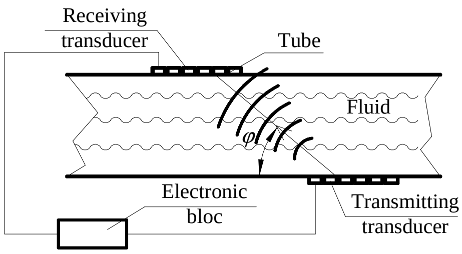

Fig. 2. Schematic view of ultrasonic flow meter with direct reception

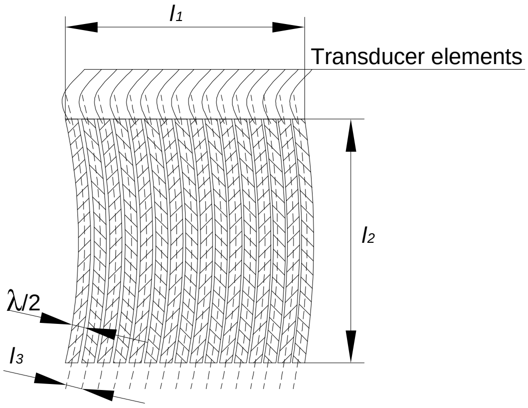

Fig. 3. Schematic view of a transducer assembly

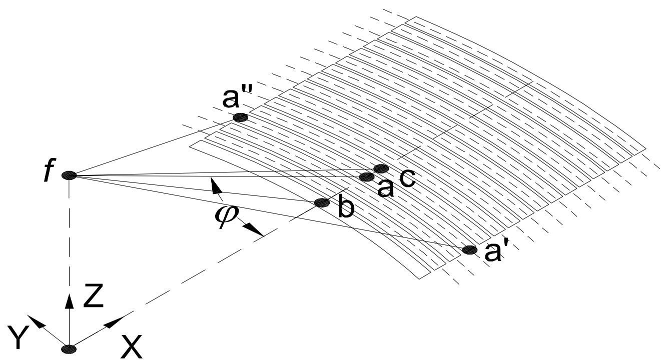

Fig. 4. A 3-dimensional view of the transducer of Fig. 2. illustrating its operation

with approximately 25-32mm cross-sectional diameters. Larger measurement tubes may be fitted with substantially equal or larger sized transducer assemblies. The transducer elements in Figs. 3 and 4 are sized to have a width of λ/2, λ being the wave length of the ultrasound waves to be generated. The transducer elements are arranged in mutually adjacent curved beams, in a substantially concentric circular pattern. The arrangement maintains substantially the same distance (Fig. 4) between each point within one element to the focal spot.

The distances from the centres a, b, c, of the transducer elements to the focal point *f* arranged according to the following equation:

$$2(d_i\text{-}d_0)=n\lambda \tag{2}$$

in which *d* is the distance between the front most transducer element and the focal spot *f*; d_i is the distance between the *i-th* transducer element of the transducer assembly and the focal spot; λ is the wave length of the ultrasound wave and *n* is a natural number (n = 1, 2, 3, etc.).

Applying (2) for the centres of substantially straight rows (e.g. arranged substantially in the Y-direction) of transducer elements, a linear focus is obtained parallel to the orientation of the transducer elements.

In case of each individual transducer unit within each transducer element (e.g. extending along the curved row a', a, a") is arranged substantially according to equation (2), (i.e. with d_i referring to the i-th individual transducer unit) the substantially circular arrangement of Fig. 4 is obtained, which may provide an ultrasound beam focused to a focal point *f*.

The separation between two adjacent transducer elements l_3 (Fig. 3) is chosen so that according to equation (2), the difference of the distances between adjacent transducer elements and the focal spot would equal λ/2. The separation between adjacent transducer elements decreases slightly with increasing number of the transducer element (i.e. increasing distance from the front most transducer element along the direction X in Fig. 4) to keep the above formulated criteria satisfied. Such a design of the transducer assembly simplifies the forming the ultrasound and allows keeping the driving electronics at maximum simplicity.

To form an inclined beam, elements of a transducer assembly are to be excited in a sequence with time delay with respect to each other. The specific design of the transducer described above with respect to Figs. 3 and 4 allows supplying exciting pulses to each transducer element with a constant time interval. This allows providing the exciting pulses from a pulse train produced by an ordinary generator of square pulses with a desired pulse duration and period.

3. Finite Element Modeling and Results

For verifying a design of ultrasonic transducer the finite element model was developed. The commercially available FEA software (ANSYS) was used. We have chosen 2D model for reduced simulation time. Coupled field simulation was performed including structure field of cMUT and acoustic field of fluid. As difference between the travel times of ultrasound in flowing and in stagnant fluids can be found analytically according (1), we limited calculations of direction acoustic wave in time domain. Features of acoustic fields computation in moving media conditions are widely analyzed and described [16]. In order not complicate the model we did not included a simulation of capacitive transducer cells. Simulation of a single transducer cell is described in our earlier work [15].

Acoustic wave equation in homogeneous media can be written as:

$$\Delta p-\frac{1}{c^2}\frac{\partial^2 p}{\partial t^2}=0 \tag{4}$$

where *p* is an acoustic pressure, *t* is time, Δ is Laplace operator.

Discretizing and solutions methods of (4) are described in [13, 14] and ANSYS documentation.

In our model structure elements were divided by PLANE42 elements, the ambient medium was modeled as hemisphere, consisting of FLUID29. The size of ultrasound propagation medium divisions is limited by the wavelength of the sound wave: for representative results with uncertainty less than 3%, as much as 10 elements are supposed to fit within the one wavelength. So the ultrasound propagation medium was divided in 0.15 mm elements, and this limited the maximum of frequencies available for analysis to 1.0 MHz (λ = 1.5 mm for the speed of sound in water c = 1500). The time-domain FEA with digitizing period of 50 ns was applied to simulate the pressure front of an acoustic wave.

Simulation results are graphically shown in Fig. 5. Fig. 5, a is an intensity distribution plot of an exemplary ultrasound beam generated by a transducer assembly extending s along the horizontal (*X*) axis and being centered about position 34 (*X* = 0.005 m). From Fig. 5a, it may be apparent that the generated ultrasound beam propagates at an angle of about 35^{o} to the plane of the transducer assembly and thus to a side wall to which the transducer assembly is mounted parallel. It may further be seen that the phase relation between adjacent transducer elements produces stray waves. However, these waves are not directed towards the receiver and are supposed not to affect the measurement.

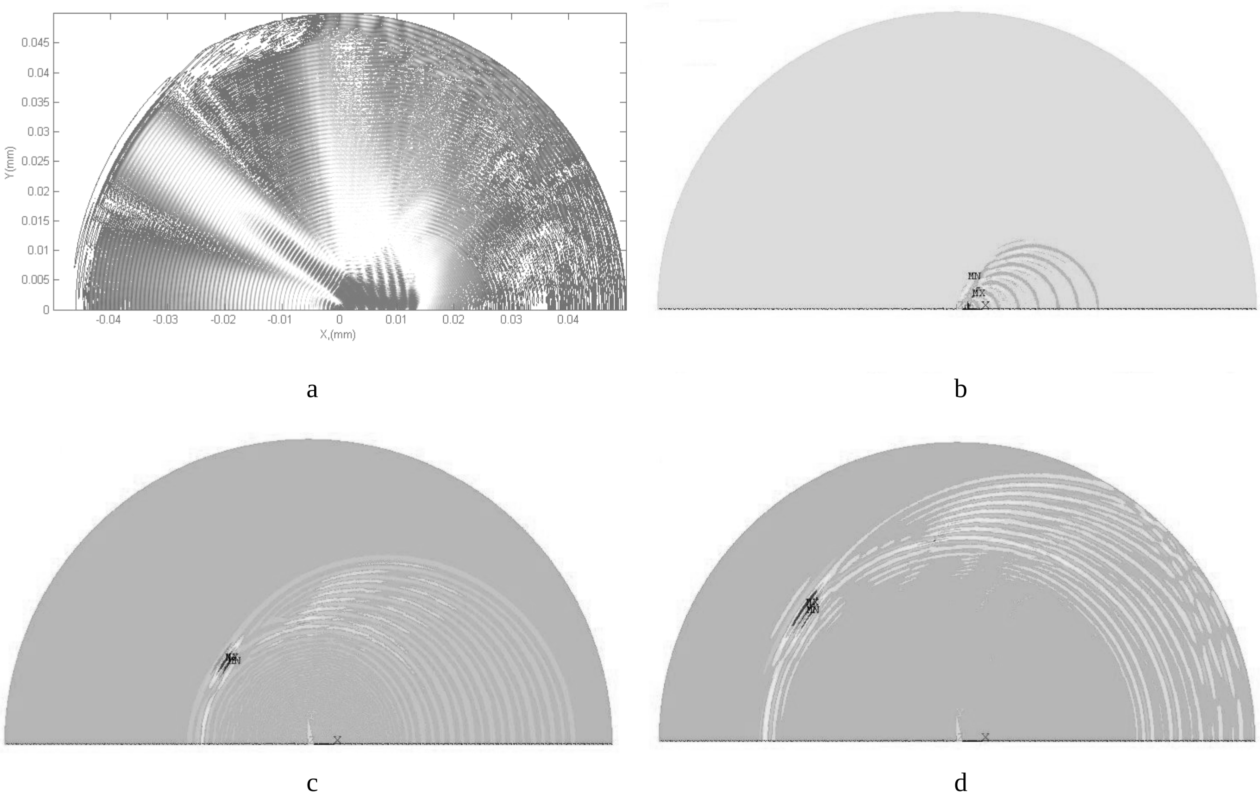

Fig. 5. Ultrasound beam generated transducer located parallel and propagating in a direction oriented at an angle to the horizontal axis: a – acoustic beam; b, c and d – stages formation of acoustic pulse

Conclusions

Described flow meter, based on cMUT concept, is supposed to have minimal influence on the hydrodynamic resistance of the flow meter and minimum flow distortions. The transducer designed for the said flow meter is having no matching layers or mechanical beam forming elements. Therefore it is being thought as advantageous over the existing transducer concepts.

Slightly bended segmented arrays of CMUT cells are used to improve the required focusing of the ultrasonic beam. Oblique front of ultrasonic wave was obtained choosing different distances between sections of transducer and specific way of exciting the transducer cells. Finite element analysis for this design shows the generated ultrasound beam to propagate at an angle of about 35^{o} to the plane of the transducer and to a side wall to which the transducer is mounted parallel.

Such a flow meter, having great advantages of exploiting cMUT properties in beamforming, is thought to be suitable for high operating temperatures of gases and fluids and therefore creates a niche potential for gas flow monitoring in internal combustion engines, exhoust gases monitoring and others.

References

1. **Pavlovic V., Stojcev M., Dimitrijevic B., Golubovic L., Zivkovic M. , Stankovic L.** Ultrasonic pulse-phase method applied in fluid flow measurements**.** Science, Measurement and Technology, IEE Proceedings, vol.143, 1996, p. 327 – 333.

2. **Gessner U.,** The Performance of the Ultrasonic Flowmeter in Complex Velocity Profiles. Biomedical Engineering, IEEE Transactions , 1969 Page(s):139 - 142 vol. BME-16
3. **Ergun A. S., Yaralioglu G. G. and Khuri-Yakub B. T.** Capacitive micromachined ultrasonic transducers: Theory and Technology. Journal of Aerospace Engineering, 2003;16 No.2
4. **Ergun A. S, Huang Y., Zhuang X., Orlkan O., Yarahoglu G., Khuri-Yakub B.T.** Capacitive Micromachined Ultrasonic Transducers: Fabrication Technology. Transactions on ultrasonic, ferroelectrics and frequency control, vol. 52, 2005.
5. **Bagdonas A., Daubaris G., Petkus V., Ragauskas A.** Triangular cross section duct for ultrasonic flow rate measurement. Ultragarsas, vol. 57, 2005.
6. **Soh H. T, Ladabaum I., Atalar A., Quate C. F., Khuri-Yakub B. T.** Silicon micromachined ultrasonic immersion transducers. Appl. Phys. Lett., vol. 69, 1996.
7. **Vontz T.** Device for ultrasonic flow measurement. Patent No. US 5,650,572 1997-07-22.
8. **Masamichi I., Hiroshi M., Shigeru T**. Ultrasonic flow meter. Patent No. JP2002071409. 2002-03-08.
9. **Ragauskas A., Daubaris G., Petkus V**. Ultrasonic flow meter with triangular cross section. Patent No. EP1742024. 2008-06-02.
10. **Bierl R, Lesser M., Meyer A., Steuber F.** Method and device for measuring an air mass flow by means of ultrasound. Patent No. WO 2008/000577. 2008-01-03.
11. **Schroder A., Kupnik M., O'Leary P., Benes E., Groschl M**. A Capacitance Ultrasonic Transducer With Micromachined Backplate for fast Flow Measurements in Hot Pulsating Gases. IEEE Sensors Journal 2006 Page(s):898 - 905 vol.6 No.4
12. **Khuri-Yakub B.T., Degertekin L. F.** Fluidic device with integrated capacitive micromachined ultrasonic transducers Patent No. US6854338. 2005-02-15.
13. **Zienkiewicz O. C., Taylor R. L**. The Finite Element Method. Fluid Dynamics Butterworrth-Heineman 2000. Pages: 348.
14. **Ihlenburg F.** The Finite Element Analysis of Acoustic Scattering. Springer 1998. Pages: 238
15. **Vanagas G., Mikolajūnas M., Grigaliūnas V, Jarimavičiūtė-Žvalionienė R., Ivašauskas A., Viržonis, D.** Investigation of dynamic parameters of multilayered microelectromechanical membranes with finite element modeling. Medžiagotyra Kaunas University of Technology, Academy of Sciences of Lithuania. 2008; 14: 175-178 p.
16. **Bezdek M., Landes H., Rieder A, Lerch R.** A Coupled Finite-Element, Boundary-Integral Method for Simulating Ultrasonic Flowmeters. IEEE Transactions on Ultrasonic, Ferroelectrics, and Frequency Control, vol. 54, no. 3, March 2007.
17. **Ragauskas, A. Viržonis D., Vanagas G., Repečka V.** Ultrasonic flow meter and method. European patent application No. 08160615.0–5236, Date of filing: 2008.08.20.

Proceedings of 4th International Conference ITELMS'2009

Determination of Frost Penetration in the Ground Taking into Aaccount Ground Water Flow

L. Furmonavičius*, V. Stasiukaitis*, S. Sušinskas**

**Geotechnic Group, Sunrise Valley, Saulėtekio al., 15, Vilnius, Lithuania, E-mail: liufu@st.vgtu.lt*
***Kaunas University of Technology, Panevėžys Institute, Klaipėdos str.1, LT352509,Panevėžys, Lithuania, E-mail: pamatas@takas.lt*

Abstract

This paper presents an analysis of influence of ground water flow on frost penetration depth during constant frost action under real ground and hydrological conditions.
Field observations and theoretical analysis show that dominant factors controlling depth of frost penetration are the intensity and duration of freezing period. Variation in soil type, density and water content may account for penetration depth variations by a factor of two.
KEY WORDS: *frost penetration depth, ground water flow, ground conditions, soil thermal properties, frost heaving.*

1. Introduction

The building of "Klaipedos Smelte" refrigerator is located just near the Kursiu Marios. Foundations of a building - driven piles with tips at 10-12 m depth from the ground floor level. Until 2001 freezing rooms of ground floor were used for storage of light frozen products – such as ice-cream, etc. On the upper two floors the freezing rooms had a temperature of minus (-) 20 ºC. Administration decided to use ground floor with the same freezing temperature without any additional isolation of the ground

It was necessary to check frost penetration depth in the ground under the new temperature regime and assure that penetration depth will not reach a morain clay in which during freezing ice lenses might occur. As a result of this frost heaving take place and piles will start to move up. Preliminary calculations not including ground water flow showed that critical frost penetration depth will be achieved during 6.5 years.
Because of hydrological conditions showing continous ground water flow the influence of it was analyzed.

2. Ground Conditions

As was mentioned before, "Klaipedos Smelte" territory is in Klaipeda harbour on a shore of Kursiu Marios. The refrigerator building is in about 20 m distance from the harbour quay wall.

The ground profile of the refrigerator consists of 0.3 m reinforced concrete floor; 0.6 m isolation layer-slag; 2.3 m – moderate wet gravelly sand, dense, 6.8 m - saturated gravelly sand bedded by moraine clay - very dense, stiff to very stiff (silty sandy clay with cobbles and gravel).

Refrigerator was constructed in 1967. According to existing pile driving data, for this building pile tips are 0.5 - 1.5 m embedded in moraine clay.

3. Analysis Philosophy

The geometry of refrigerator building is 36×36 m. According to geotechnical data ground water table level has a hydraulic gradient 0.01 (0.3 m at distance 30 m). The hydraulic permeability was assumed to be 30 m/day. There was no accurate estimation of it. Hydraulic permeability was estimated according to grain size distribution of gravelly sand. Thickness of water layer was assumed to be constant - 6.8 m. Taking into account this data it could be calculated that during one day and night through 1.0 m of freezing room width 2.04 m^3 ground water will come. This amount of water will bring some amount of heat which will have effect on velocity and depth of frost penetration.

The main ground water flow parameters are: soil permeability, hydraulic gradient, ground water temperature, etc. There was an assumption that these parameters are constant, however in reality they are not constant.

Table 1.

Thermal properties of soils

No.	Soil	Layer thickness, m	Water content *w*, %	Thermal conductivity λ, Wt/(m ºC)	Volumetric heat *C*, MJ/(m^3 ºC)
1	Dry slag	0 – 0.56	2	0.37	1.9
2	Gravelly sand, wet	0.56 – 2.9	5	1.50	2.0
3	Gravelly sand saturated	2.9 – 9.7	25	2.70	3.0
4	moraine clay	>9.7	20	1.35	3.0

It was assumed that ground water flow has constant parameters. Later in the analysis of data the influence of changes of hydraulic parameters will be shown.

4. Analysis of Influence of Ground Water Flow

Thermal continuity and conservation of thermal energy require that the rate of change in thermal energy of an element plus the rate of the heat transfer into the element equal zero. In our case it could be expressed:

$$\left(C+\frac{w}{1+w}\rho\frac{\partial\tilde{\mathcal{H}}}{\partial\,\mathrm{T}}\right)\frac{\partial\,\mathrm{T}}{\partial\boldsymbol{t}}=div(\lambda\cdot grad\,\mathrm{T})-div(\tilde{c}\,\mathrm{T}\boldsymbol{J}) \tag{1}$$

where T [°*C*] – temperature, *t* [s] – time, ρ [kg/m^3] – soil density, *C* [J/m^3 °*C*] – volumetric heat of soil, $\tilde{c}=4200$ [J/kg °*C*] – water heat capacity, w [unit] – water content, λ [Wt/(m °*C*)] – thermal conductivity of soil, $\tilde{\mathcal{H}}=334000$ [J/kg] – latent heat, J [kg/m^2 s] – intensity of ground water flow.

Freezing or thawing of water is under temperature T=0 °*C*, thus $\frac{\partial\,\mathrm{T}}{\partial\boldsymbol{t}}$ equal zero. Value of integral of this equation from some negative to some positive temperatures is finite value and equal to $\tilde{\mathcal{H}}=334000$ [J/kg]. Such function is δ -function. It can not be used directly for numerical solutions. It is convenient to make approximation by function:

$$\tilde{\mathcal{H}}=\frac{334000}{2}(\mathrm{th}(\mathrm{T}/\beta)+1)\,, \tag{2}$$

derivation by temperature of which equal:

$$\frac{\partial\tilde{\mathcal{H}}}{\partial\,\mathrm{T}}=\frac{334000}{2\beta\mathrm{ch}^2(\mathrm{T}/\beta)}\;. \tag{3}$$

This is continual finite function which has narrow but finite width with the same value of integral latent heat value- 340000 [J/kg]. When β approach to 0, the function approach to δ-function. For following calculations it was assumed β equals 0.2.

For simplification of the task it was assumed that ground water flow intensity has a constant value and constant direction. In reality when frost penetrates deeper, the height of flow crossection starts to be smaller. Implementation of this phenomenon complicates an analysis. So, just for simplicity it was used equation (1) with one unknown function T, the temperature.

During seasons of the year temperature of the upper layers of the ground varies. For simplicity it was not taken into account and mean value of temperature +7 °*C* was assessed.

In absence of ground water flow for prediction the duration during which temperature becomes constant, dimensionless parameter τ might be used.

$$\tau=\frac{\lambda t}{CA}\,. \tag{4}$$

where *A* – area of refrigerator floor, *C* – volumetric heat of soil (including latent heat).

Change of temperature in the soil is exponential with τ as exponential indicator. If τ > 1 it might be assumed that freezing process is stabilized, that means:

$$t>\frac{C\;A}{\lambda}\,.$$

If there is ground water flow the depth of frost penetration will be less and temperature stabilization process takes less time.

The equation (1) in Decart system of coordinates can be expressed:

$$\left(C+\frac{w}{1+w}\rho\frac{\partial\tilde{\mathcal{H}}}{\partial\,\mathrm{T}}\right)\frac{\partial\,\mathrm{T}}{\partial\boldsymbol{t}}=\frac{\partial}{\partial x}\left(\lambda\frac{\partial T}{\partial x}\right)+\frac{\partial}{\partial y}\left(\lambda\frac{\partial T}{\partial y}\right)+\frac{\partial}{\partial z}\left(\lambda\frac{\partial T}{\partial z}\right)-\tilde{c}\,J\frac{\partial T}{\partial x}\,, \tag{5}$$

where x – axis horizontal, parallel to ground water flow, y – horizontal axis perpendicular to ground water flow, z – vertical axis, perpendicular to refrigerator floor.

For numerical solution of the problem equation (6) was approximated by a system of discrete equations. To obtain high accuracy and employ smaller number of equations new coordinate system was implemented for creation of variable me:

$$\xi = \xi(x), \qquad \eta = \eta(y), \qquad \zeta = \zeta(z)\,. \tag{6}$$

These functions represent variable scale. They were chosen in a manner to avoid areas with drastic changes of temperature. In the areas where change of temperature is sharp, the axis is elongated and opposite, where change of temperature is slow, the axis is constrained.

After implementation this into equation (6) the foloing expression is obtained:

$$\left(C + \frac{w}{1+w}\rho\frac{\partial\tilde{\mathcal{H}}}{\partial\,\mathrm{T}}\right)\frac{\partial\,\mathrm{T}}{\partial\boldsymbol{t}} = \frac{\partial}{\partial\xi}\left(\lambda\frac{\partial\xi}{\partial x}\cdot\frac{\partial T}{\partial\xi}\right)\frac{\partial\xi}{\partial x} + \frac{\partial}{\partial\eta}\left(\lambda\frac{\partial\eta}{\partial y}\cdot\frac{\partial T}{\partial\eta}\right)\frac{\partial\eta}{\partial y} + \frac{\partial}{\partial\zeta}\left(\lambda\frac{\partial\zeta}{\partial z}\cdot\frac{\partial T}{\partial\zeta}\right)\frac{\partial\zeta}{\partial z} - \tilde{c}\,J\,\frac{\partial\xi}{\partial x}\cdot\frac{\partial T}{\partial\xi}\,. \tag{7}$$

Giving a symbol f for the equation left side in brackets:

$$\left(C + \frac{w}{1+w}\rho\frac{\partial\tilde{\mathcal{H}}}{\partial\,\mathrm{T}}\right) = f\,,$$

temperature T becomes a function of coordinates and time:

$$\mathrm{T} = \mathrm{T}(\xi,\,\eta,\,\zeta) \tag{8}$$

By the approximation employing finite elements, differential equation (8) is transformed into a system of discrete equations for which ξ, η, ζ a real number values are prescribed:

$$\begin{aligned}
& f(i,j,k)\frac{\mathrm{T(i,j,k)} - \mathrm{T}_{\mathrm{t=t\text{-}\Delta t}}\mathrm{(i,j,k)}}{\Delta\boldsymbol{t}} = \\
& = U_{i+1/2}[\mathrm{T(i+1,j,k)} - \mathrm{T(i,j,k)}] - U_{i-1/2}[\mathrm{T(i,j,k)} - \mathrm{T(i\text{-}1,j,k)}] + \\
& + V_{j+1/2}[\mathrm{T(i,j+1,k)} - \mathrm{T(i,j,k)}] - \mathrm{V}_{j-1/2}[\mathrm{T(i,j,k)} - \mathrm{T(i,j\text{-}1,k)}] + \\
& + W_{k+1/2}[\mathrm{T(i,j,k+1)} - \mathrm{T(i,j,k)}] - \mathrm{W}_{k-1/2}[\mathrm{T(i,j,k)} - \mathrm{T(i,j,k\text{-}1)}] + \\
& + Q_i[\mathrm{T(i,j,k)} - \mathrm{T(i\text{-}1,j,k)}]
\end{aligned} \tag{9}$$

where $i = 1,2,3,...,I,\ j = 1,2,3,...,J,\ k = 1,2,3,...,K.$

$$\begin{aligned}
& U_{i+1/2} = \left(\frac{\partial\xi}{\partial x}\right)_{\xi=i}\left(\lambda\frac{\partial\xi}{\partial x}\right)_{\xi=i+1/2}, \quad U_{i-1/2} = \left(\frac{\partial\xi}{\partial x}\right)_{\xi=i}\left(\lambda\frac{\partial\xi}{\partial x}\right)_{\xi=i-1/2}, \\
& V_{j+1/2} = \left(\frac{\partial\eta}{\partial y}\right)_{\eta=j}\left(\lambda\frac{\partial\eta}{\partial y}\right)_{\eta=j+1/2}, \quad V_{j-1/2} = \left(\frac{\partial\eta}{\partial y}\right)_{\eta=j}\left(\lambda\frac{\partial\eta}{\partial y}\right)_{\eta=j-1/2}, \\
& W_{k+1/2} = \left(\frac{\partial\zeta}{\partial z}\right)_{\zeta=k}\left(\lambda\frac{\partial\zeta}{\partial z}\right)_{\zeta=k+1/2}, \quad W_{k-1/2} = \left(\frac{\partial\zeta}{\partial z}\right)_{\zeta=k}\left(\lambda\frac{\partial\zeta}{\partial z}\right)_{\zeta=k-1/2}, \\
& Q_i = \tilde{c}\,J\left(\frac{\partial\xi}{\partial x}\right)_{\xi=i-1/2}
\end{aligned} \tag{10}$$

At the edges of calculation area, instead of (10) boundary conditions are implemented, i.e. $T=7^0$C. Boundary conditions are implemented, i.e. T = 7^0C. For analysis such boundaries of soil area were taken:

$$-100 \le x \le 100\ [m], \qquad 0 \le y \le 100\ [m], \qquad 0 \le x \le 50\ [m]. \tag{11}$$

Number of mods of mesh:

$$I = 100 \div 150, \qquad J = 50 \div 75, \qquad K = 80 \div 120. \tag{12}$$

The problem was solved by implementing the iteration procedure for each time step. Equation system (10) was solved by separating one strip from the system of matrix in the dissection of one axis. When calculation of all strips for one axis was finished, strips of other axis were analysed. This procedure was adopted until required accuracy was achieved. Then procedure was repeated for another step of time.

4. Results and Discussions

The practical conclusion for Klaipedos Smelte administration was positive. If assumptions on ground water flow are realistic (flow intensity 200 kg/m^2/day), the maximum frost penetration depth 4,0 m. This means that frost penetration will stop in the ground which is not frost susceptible and danger for building structures is avoided.

Having solutions it was very interesting to analyze what is going to happen if hydraulic properties of the ground are different from those which were accepted according to existing geotechnical information.

For the prediction of real penetration depth it was recommended to measure temperature at 1, 2 and 3 m depth at 2 locations: in a center and at the edge of freezing room results of which might be compared with calculations.

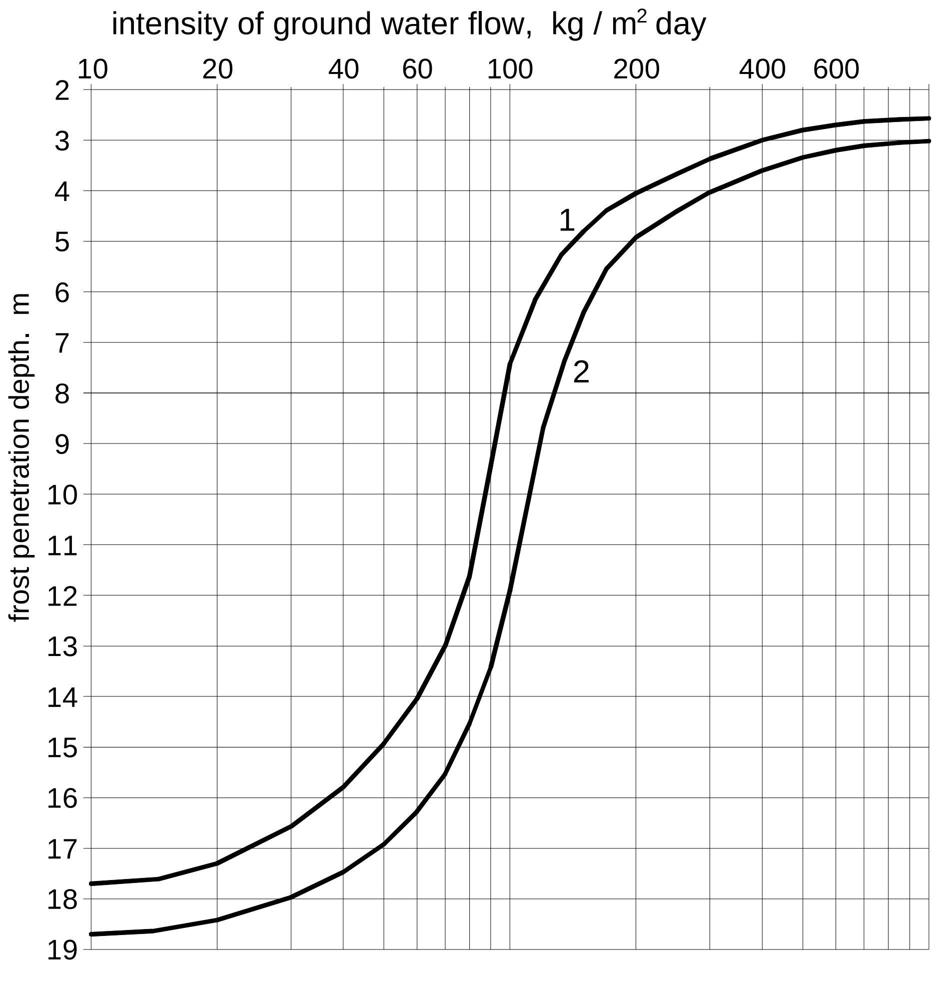

Fig.1. Influence of ground water flow on frost penetration depth of the ground: 1 − slag, thermal conductivity $\lambda = 0.37$ Wt/(m ^{O}C) , 2 − slag, thermal conductivity $\lambda = 0.74$ Wt/(m ^{O}C) .

Fig.1. shows that there is some critical value of flow intensity, about 50 kg/m^{2}day, increase or decrease from which has a significant effect or very small effect on frost penetration depth.
The time, during which frost penetration depth reach the maximum values is very influenced by ground water flow intensity (Fig. 2, 3).

Distribution of ground temperature beneath the freezing room floor is asymmetrical and depends on ground water flow direction as it is shown in Fig. 4 (a – thermal conductivity of slag-0.37 Wt/m^{o}C; b – 0.74 Wt/m^{o}C). Comparing depth of 0 temperature isotherm might be found the great influence of insulation layer.

Measured values of temperatures in the ground of freezing rooms at the edge and centre confirm asymmetry of thermal contours (Fig. 5). Comparison of predictions with measured values revealed that hydraulic conductivity of cohesionless soils of the refrigerator ground is less than accepted for analysis. This means that ground water flow intensity is less. The measured values of ground temperature correspond to water flow intensity about 100 kg/m^{2}day.

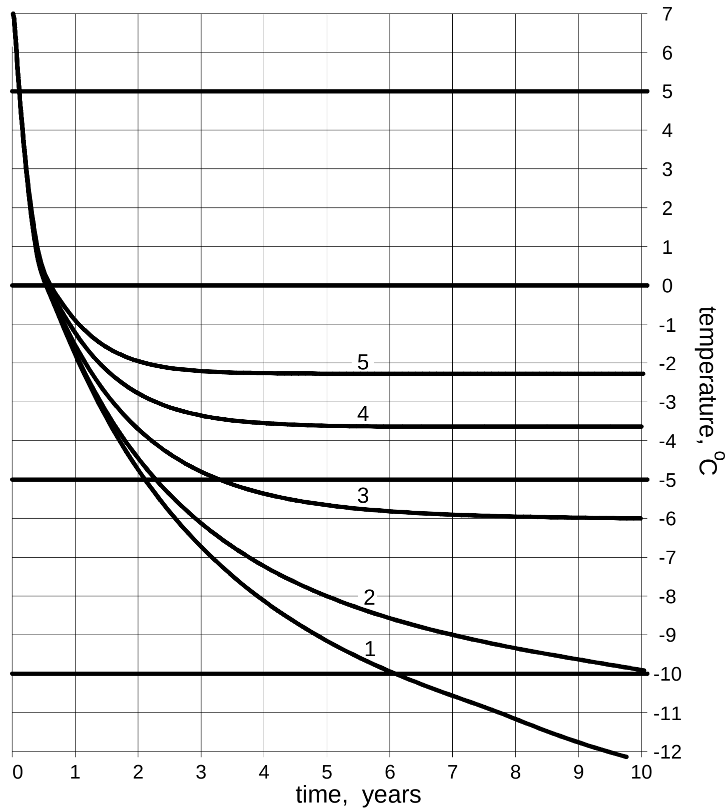

Fig. 2. Influence of ground water flow intensity to freezing temperature at 3.0 m depth: 1, 2, 3, 4, 5 coresponds intensity of ground water flow: 0, 50, 100, 150, 200 kg / m^2 day.

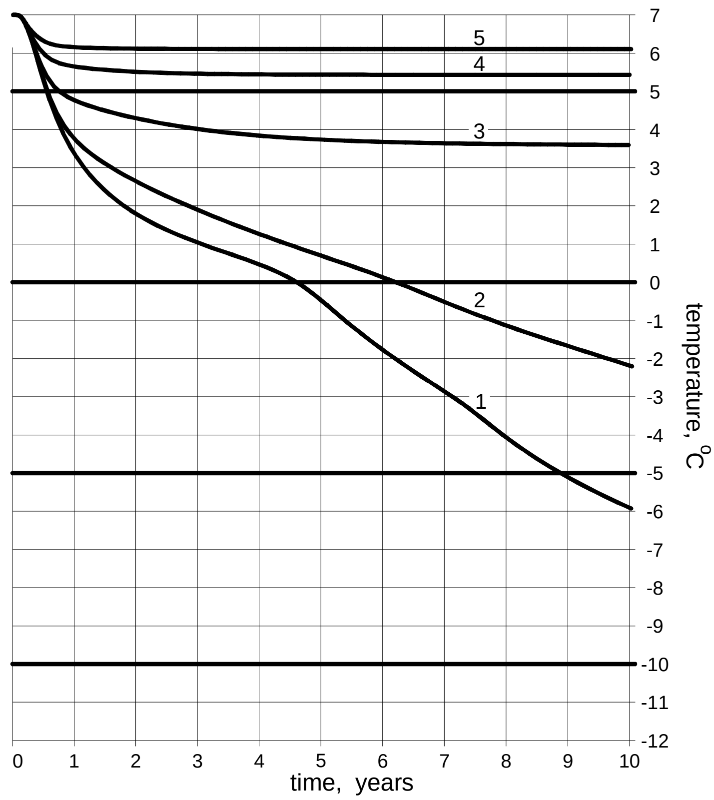

Fig. 3. Influence of ground water flow to freezing temperature at 7.6 m depth: 1, 2, 3, 4, 5 coresponds intensity of ground water flow 0, 50, 100, 150, 200 kg / m^2 day

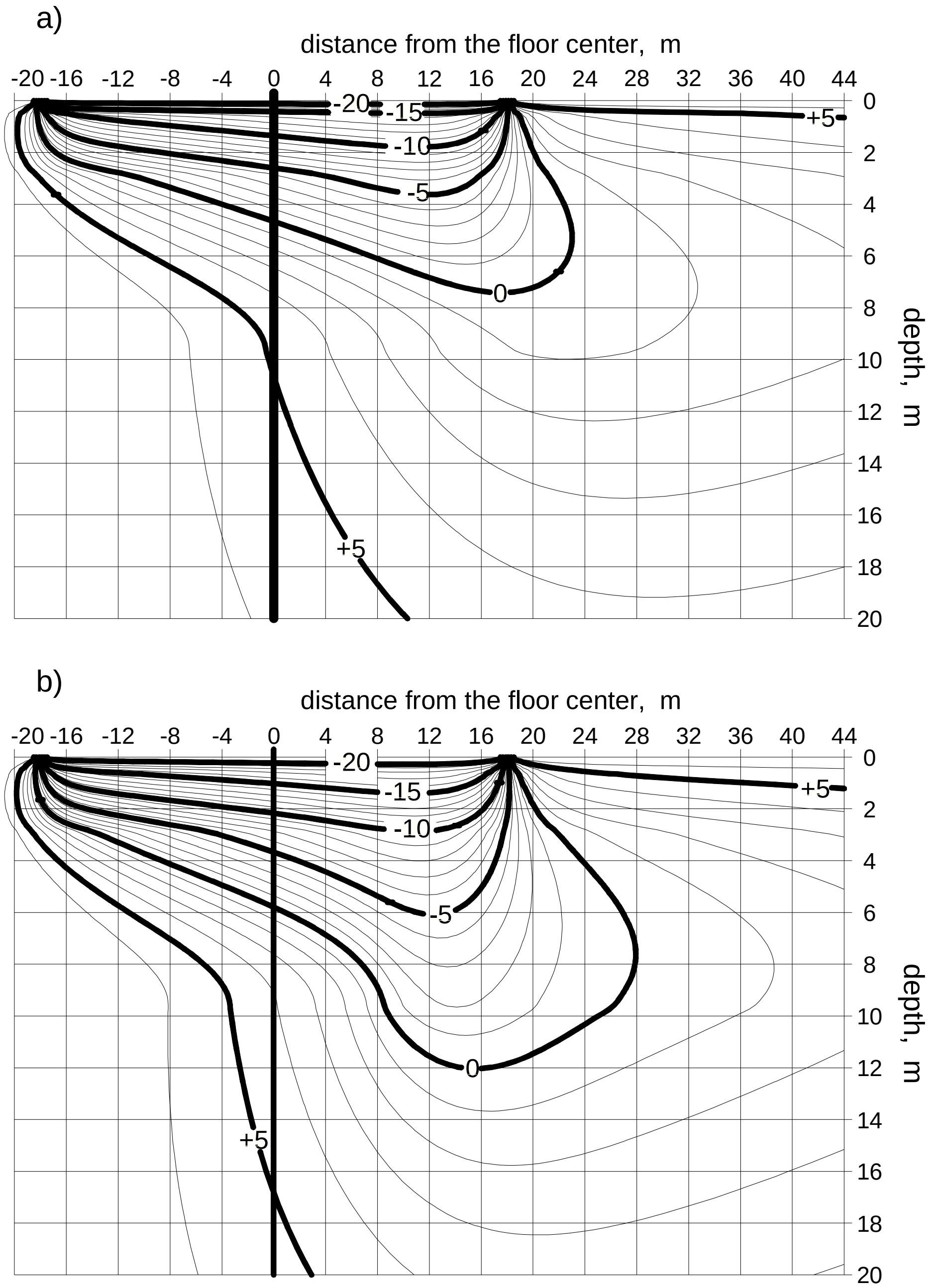

Fig. 4. Distribution of temperature in the ground beneath refrigerator floor centre (cross section parallel to ground water flow direction)

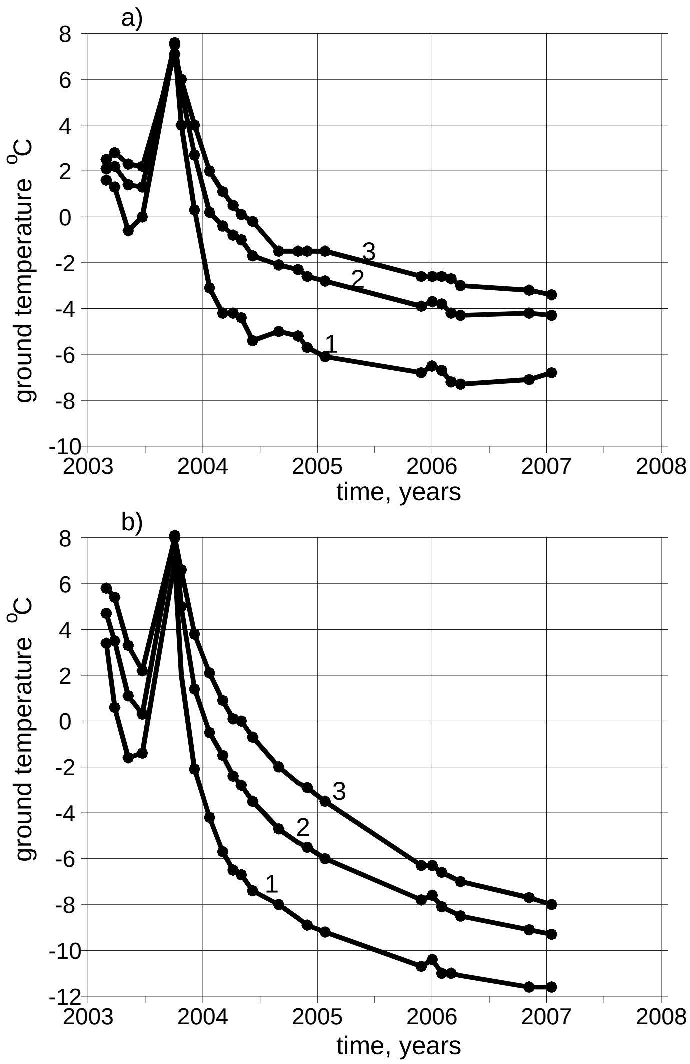

Fig. 5. Measured temperature in the ground at constant temperature (-20 °C) in the freezing room: a) in the edge of room, b) in the centre of two rooms: 1 − 1 m depth, 2 − 2 m depth, 3 − 3 m depth.

References

1. **Mitchell J. K**. Fundamentals of soil behaviour. John Willy & Sons, Inc. New York. 1976.

Proceedings of 4th International Conference ITELMS'2009

Models for Optimization of Total Assembly Time and Assembly Line Balancing

V. Kleiza*, J. Tilindis**

**Kaunas University of Technology, Klaipedos 1, LT-35209 Panevėžys, Lithuania, E-mail: vytautas.kleiza@ktu.lt*
***Kaunas University of Technology, Daukanto 12, 35212 Panevėžys, Lithuania, E-mail: jtjlt@yahoo.com*

Abstract

We present two different optimization formulations and give an example of an optimized workstation layout. Moving assembly lines have played a central role in mass automotive and other production. The assembly line where the final product assembly process is performed typically consists of 300 to 500 workstations (also known as cells or workcells).
KEY WORDS: assembly line, queueing time, optimization, mathematical model, aggregation.

1. Parallel Assembly Structure

We will study assembly organization form, when final product [2, 3] is split to certain number of parts. These parts are being assembled simultaneously at different assembly stations and then all parts assembled together to final product at the last assembly station (Fig. 1). This problem was considered while studying assembly process of wiring harness products assembly in [1]. Wiring harness components are especially suitable for this kind of assembly organization, because they contain a lot of small parts that have similar mounting and assembly times. So the statements made and solving methods discovered could be applied to any similar assembly process. The main goal of this paper is to represent assembly process in such way, that whole assembly time (queueing time included) would be the minimal.

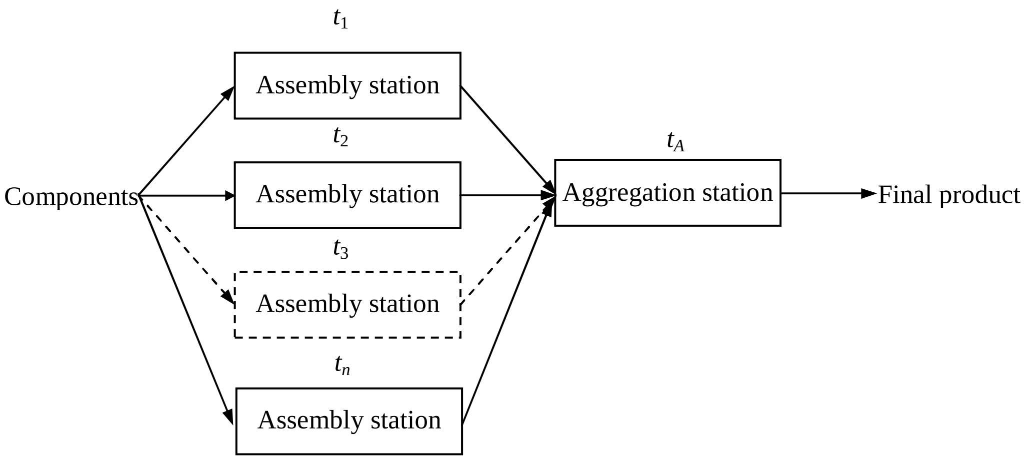

Fig. 1. Parallel assembly line

It was found [1] that utmost importance to whole assembly time has number of parts, in which we split final product. The function between number of parts and assembly time:

$$T_1(n) = \frac{T_S - A(n)}{n} + A(n), \tag{1}$$

where T_S - assembly time of not split product, n – number of parts, $A(n)$ - aggregation time.

We can use this function only after assuming these statements:

- Sum of assembly times of all parts and aggregation time is equal to assembly time of not spit product assembled in one station;

$$T_S = t_A + \sum_{i=1}^{n} t_i, \text{where } t_A = A(n),$$

- Assembly time consumed to assemble certain parts does not contain aggregation time. This is why is needed to subtract aggregation time form whole assembly time.
- Assembly time of each part is the same. This is why we can divide assembly time by number of parts.

$$t_1 = t_2 = ... = t_n ,$$

It was proved (by using correlation analysis methods) that aggregation function is linear [1]:

$$A(n) = kn + b \tag{2}$$

where k and b - aggregation time coefficients $(k > 0,\ 0 \le b < T_S)$, and they depend on certain product, and they can be found by analyzing this product.

2. Total Assembly Time Optimization

The main result of the project [1] is that that the function (1) has the unique global minimum at point $n_1 > 0$ i.e.

$$\arg\min_n T_1(n) = n_1 \tag{3}$$

While using function (1) we reduce total assembly time, but we do not consider queueing time $Q(n)$ which will appear between assembly stations and aggregation station. This time will appear when assembly time at the stations is lower than aggregation time. In this way aggregation station will become bottleneck [4] and parts will have to wait to be aggregated. Queueing time $Q(n)$ could be expressed as absolute value of difference between aggregation and part assembly times (queueing time) could be expressed:

$$Q(n) = \left| A(n) - \frac{T_S - A(n)}{n} \right| \tag{4}$$

Therefore function (total assembly time, queueing time included)

$$T_2(n) = \frac{T_S - A(n)}{n} + A(n) + Q(n) \tag{5}$$

has to be minimized, i.e. need to find point n_2

$$\arg\min_n T_2(n) = n_2 \tag{6}$$

This minimum point n_2 will be not the same as for model one (3). It was proved that n_2 is equal to positive root (if $k > 0,\ 0 \le b < T_s$)

$$n_2 = \frac{1}{2k}\left(-(k+b) + \sqrt{(k+b)^2 + 4k(T_S - b)}\right) \tag{7}$$

of equation

$$Q(n) = 0 . \tag{8}$$

So we found function between number of parts we split the product and whole assembly time with respect to queueing time.

To illustrate results of realizing the above models we represent the example (Fig. 2.) in which $T_S = 1.05$ h, $k = 0.076,\ b = 0.119$ and dependence of root n_2 of equation (8) on parameters k, b, i. e.

$$n_2(k,b) = \frac{1}{2k}\left(-(k+b) + \sqrt{(k+b)^2 + 4k(T_S - b)}\right).$$

These dependences are represented in Fig. 3. and Fig. 4.

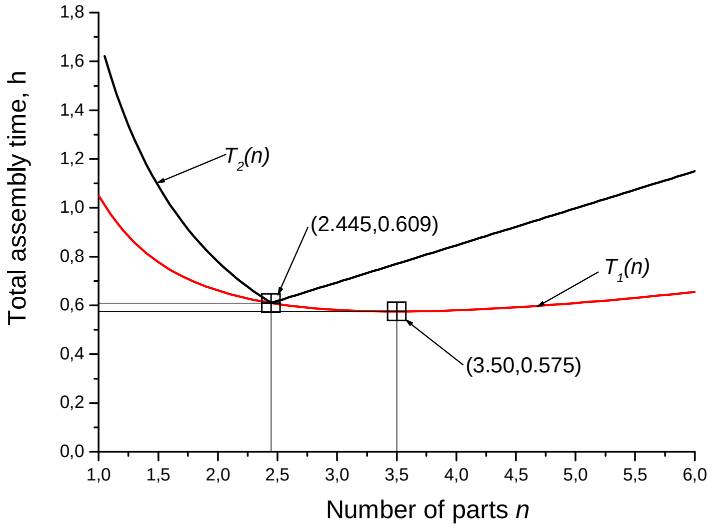

Fig. 2. Total assembly time by using the first and the second model. Coordinates of global minimum points (3.50, 0,575) and (2.445; 0.609).

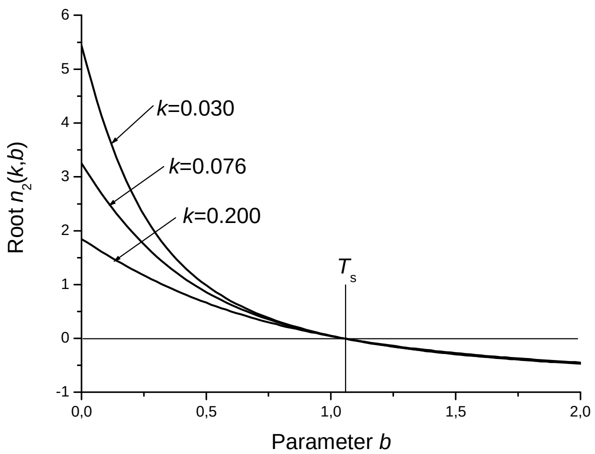

Fig. 3. Dependences of root $n_2(k,b)$ on parameter b.

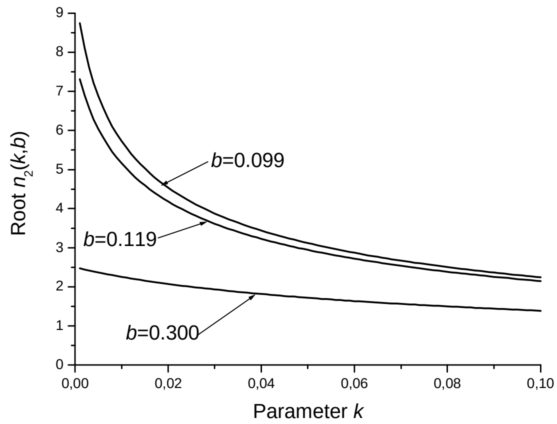

Fig. 4. Dependences of root $n_2(k,b)$ on parameter k.

3. Conclusions

1. Represented assembly time calculation model which evaluates queueing time appearing in assembly line between part assembly stations and aggregation station.

2. The method to calculate optimum point in which total assembly time with respect to queueing time is minimal was presented.

3. One example was calculated by two assembly time calculation models and the comparison between both solutions was made and noticed that both minimum points are different.

References

1. **J. Tilindis.** Technological process and optimization of the automotive wiring harness production. 2009. 50 p. (manuscript)
2. **Boysen, N., M. Fliedner, and A. Scholl**. Assembly line balancing: Which model to use when? // International Journal of Production Economics, 2008. Vol. 111(2), p. 509-528.
3. **Süer, G.A.** Designing Parallel Assembly Lines // Computers Ind. Eng, 1998. Vol. 35(3-4), p. 467-470.
4. **Anupindi R., Chopra S.** Managing business process flows. Upper Saddle River: Prentice-Hall Inc. 1999.

Proceedings of 4th International Conference ITELMS'2009

Research of Mobile Robots Antenna Pointing System

A. Papšys, V. Sinkevičius, L. Šumskienė

Kaunas University of Technology, S.Daukanto str.12, 35212 Panevėžys, Lithuania, E–mail: vytenis@elekta.lt

Abstract

The requirements of the mobile robot bandwidth antenna pointing system were estimated during the research work. All the paths of the mobile robot motion on a plane were approximated to the rectilinear motion or to gyration. The motional path, mobile robot speed and the distance to the receiving antenna are presented as the functions of the rotation speed of the transmitting antenna in this paper. The control system of the robot motion must work according these functions to make sure the good connection between antennas.
KEY WORDS: *mobile robot, antenna pointing system*

1. Introduction

Some times it is impossible for the human to reach the research place. In such situation the mobile robot can be sent for the realization of the task. Such robots are controlled by the control station analyzing the view from the video camera [1]. Therefore it is important to have a good connection between moving robot and the control station. The directive antennas are used to keep up such connection. They are controlled pointing them always to the receiving antenna of the control station. The energy recourse of the mobile robot limiting the size of the directive antenna and the quick-acting of it's pointing. Therefore the antenna must be as small as possible, but also it must be orientated to the receiving antenna straightly. There are two main effects the pointing system of the robot antenna must react to: a) the form of controlled motional path and the headway, b) the effect of the uncontrolled motion under the sway of small shoals (rough road, small stones et cetera) to the truck and also to the orientation of antenna [2, 3, 4].

2. Typical Path of the Mobile Robot Motion on the Plane

The bandwidth antenna of the mobile robot must be perpendicular to the vector pointed to the receiving antenna. The antenna is oriented on the horizontal plane rotating it vertically. Therefore the path of the mobile robot motion will be analyzed as the projection on *XY* plane (Fig. 1.). All the paths of the mobile robot can be reduced to the segments of linear and curvilinear motion [4]. The radius of minimal turn of the mobile robot depends on the type and the measurement of the truck. Also there is the minimal speed of the stabile robot motion in such path space. Consequently, the segments of the curvilinear motion path can be approximated to the circular arcs. The typical path of robot-explorer is shown on Fig. 1. On the segments *1-2*, *3-4* and *6-7* the path of the robot is linear. The curvilinear segments *2-3*, *4-5* and *5-6* are approximated to the circular arcs.

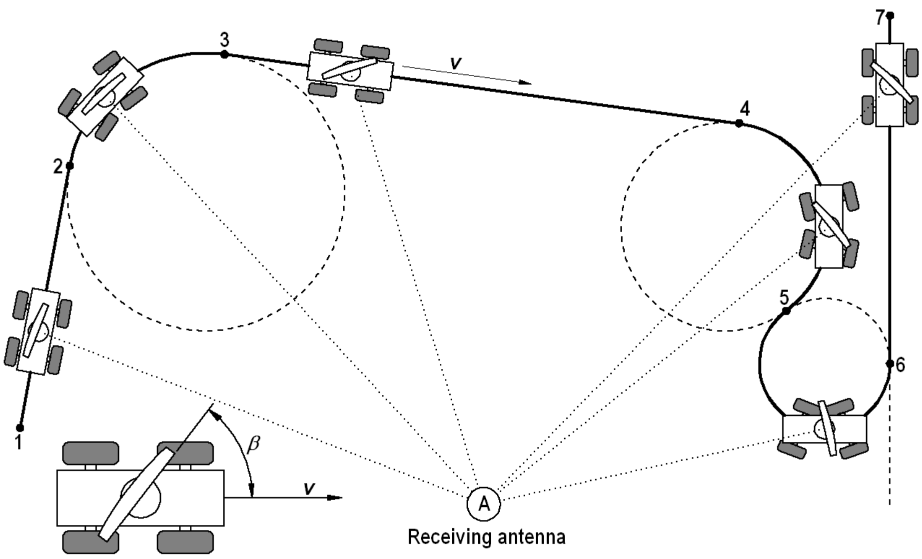

Fig. 1. Typical path of the mobile robot motion

When the robot is moving, the antenna is changing it's rotation angle β. The antenna must be perpendicular to the section connecting the receiving antenna and the center of robot antenna plane. The azimuth rate ω is the angular velocity of β. It depends on the linear speed of the robot v, distance to the receiving antenna H and the rotating radius r. These dependences for the linear and curvilinear motion were estimated for the analysis of servo drive quick-acting of the antenna rotating angle.

3. The Linear Motion of the Mobile Robot

The mobile robot moves on a level plane at speed v. Let us assume that the motion path of the mobile robot doesn't cross the central point A of the receiving antenna. Consequently, it is always possible to draw a perpendicular AB of the length L from the receiving antenna to the linear motion line of the mobile robot (Fig. 2, a). The length of the perpendicular L will be the shortest distance the mobile robot would reach to the receiving antenna.

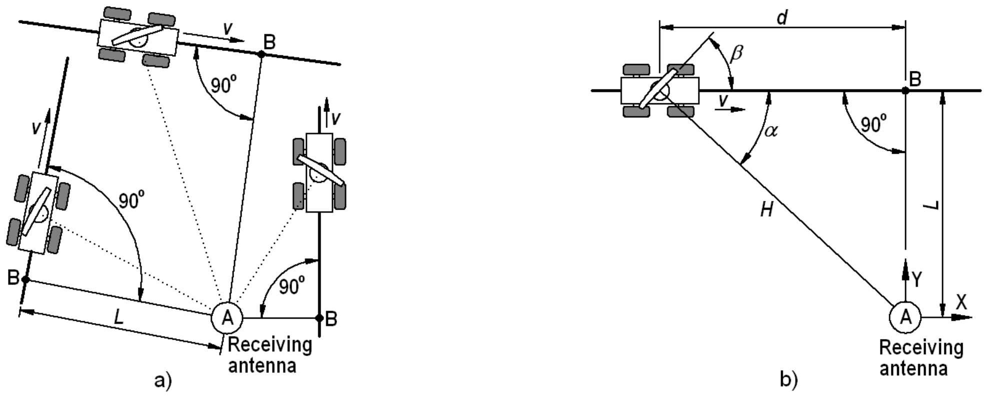

Fig. 2. The linear motion of the mobile robot: a – the motion to the various directions, b – calculation scheme

The calculation scheme was used for the calculation of the changing rate of the antenna rotation angle β (Fig. 2, b). The antenna rotation angle β depends on the distance d between the mobile robot and the point B and the distance L as follows:

$$\beta(L,t,v) = \operatorname{arctg}\left(\frac{d}{L}\right) = \operatorname{arctg}\left(\frac{vt}{L}\right). \tag{1}$$

According to the equation (1) the robot is at the point B at the time t=0. The antenna azimuth rate ω can be written from the equation (1) as follows:

$$\omega(L,t,v) = \frac{d}{dt}\beta(L,t,v) = \frac{v}{L\left(1+v^2\frac{t^2}{L^2}\right)}. \tag{2}$$

The graphs of the antenna azimuth rate are shown in Fig. 3. We can see that the maximum azimuth rate of the antenna is at the time t=0. It is a moment when the distance between the mobile robot and the receiving antenna is the shortest (at the point B).

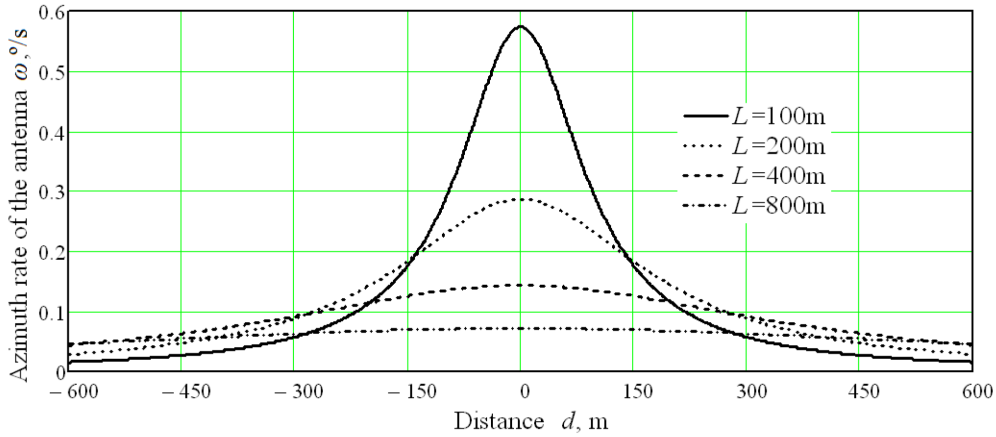

Fig. 3. The azimuth rate of the antenna as the function of the distance L and the linear speed v

Now it is possible to write the equation of the maximum azimuth rate ω_{max} considering the results before. The azimuth rate depends on the distance L and the linear speed v as follows:

$$\omega_{max}(L,v) = \frac{v}{L}. \tag{3}$$

The maximum azimuth rates ω_{max} of the mobile robot antenna calculated using the equation (3). They are shown in Fig. 4. The maximum azimuth rate is less than 0.3°/s, when the distance to the receiving antenna is L>1000 m.

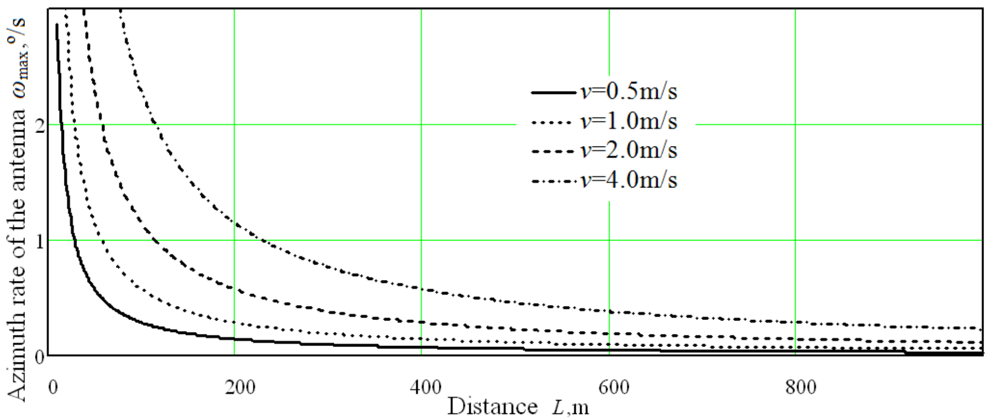

Fig. 4. The maximum azimuth rate ω_{max} as the function of the distance L and the linear speed v

4. The Curvilinear Motion of the Mobile Robot

The mobile robot moves on a level plane and strikes a snag. It changes the motion direction and starts to move in circle [2, 3]. Now we have a motion in circular path. Let us as assume that the mobile robot moves in circle always of the same radius r and it starts to move in the circle of the other radius only if the turn angle of the truck is changed. Consequently, the curvilinear path of the mobile robot can be approximated by the circular arcs of known radius r.

Next the antenna rotation angle β and the azimuth rate ω as the functions of circle radius r, motion speed v and the distance to the receiving antenna L will be estimated (Fig. 5.).

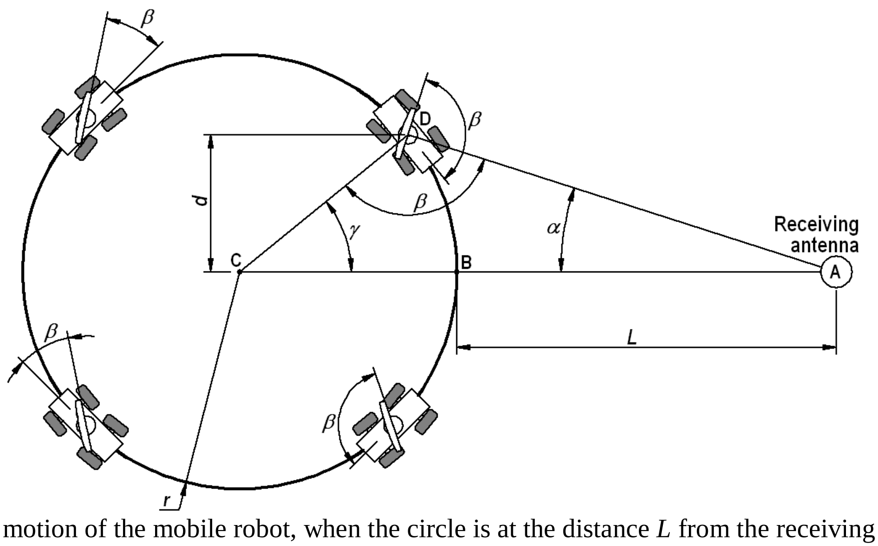

Fig. 5. The circular motion of the mobile robot, when the circle is at the distance L from the receiving antenna

The point B of the circular path is on the line conjunctive the centre of the circle and the receiving antenna point A. The distance between points A and B is the equal of L. γ is the turn angle of the vector conjunctive the rotation center C with the rotation center of the mobile robot antenna. Taking into account that the robot is at the point B at the time t=0, the equation of turn angle can be written as follows:

$$\gamma(r,v,t) = \frac{vt}{r}. \tag{4}$$

Then the distance H between mobile robot and the receiving antenna is equal to:

$$H(r,v,t)=\sqrt{2r(r+L)(1-\cos\gamma(r,v,t))+L}. \tag{5}$$

The turn angle β of the mobile robot antenna is calculated from the triangle *ACD* as follows:

$$\beta(r,v,t)=\arccos\frac{r^2-(r+L)^2+(H(r,v,t))^2}{2rH(r,v,t)}. \tag{6}$$

The equation of the azimuth rate ω is quite cumbersome, but when the $L>>r$ it can be written as follows:

$$\omega(L,t,v)=\frac{d}{dt}\beta(L,t,v)\approx\frac{v}{r}. \tag{7}$$

The equation (7) shows that the azimuth rate of the moving mobile robot is the constant and depends only on the linear speed v and the rotation radius r, when the $L>>r$. The graphs of the azimuth rate are shown in Fig. 6. The azimuth rate is growing up when the circular radius becomes smaller. This is the main characteristic choosing the size, mobility of the robot and the ability to keep the transmitting antenna pointed to the receiving antenna. The rotation radius of the small robots is very small too, but the speed is quit high. Unfortunately, such robot can't transport the antenna pointing system with the quick-acting of 60÷180º/s rate.

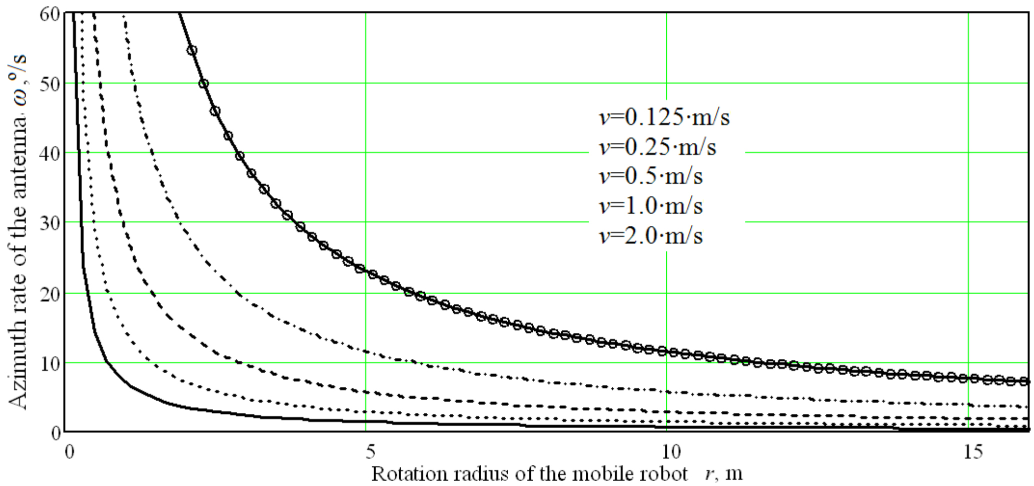

Fig. 6. The azimuth rate of the antenna, when the mobile robot moves in circle

5. Conclusions

If the mobile robot moves directly at the distance of 1 km from the receiving antenna, the quick-acting of the mobile robot pointing system can be 0.3º/s only. However, the speed of the robot must be very low to make sure good connection between antennas.

The antenna azimuth rate of the mobile robot moving in circle depends on rotation radius and motion speed, but not on the distance between robot and the receiving antenna. The quick-acting of the antenna must be taken into account in the algorithm of the speed control of the robot.

It is recommended to use two stages antenna pointing system, if the short circular arcs are dominating in the path of the robot and the turn angles of the antenna are 1÷3º only. The first stage can be relatively slow-acting with the electric motor, and the second stage must be quick-acting with the piezoelectric drives and with the pointing of 1÷3º range.

References

1. **Bapna D., Rollins E., Foessel A., Whittaker R.** Antenna pointing for high bandwidth communications from mobile robots. Robotics and Automation, 1998. Proceedings. 1998 IEEE International Conference on Volume 4, Issue , 16-20 May 1998, p.3468 – 3473.
2. **Patricia Mellodge, Pushkin Kachroo**. Model Abstraction in Dynamical Systems. Application to Mobile Robot Control. – Springer, 2008.-116p.
3. **Shuzhi Sam Ge, Frank L Lewis**. Autonomous Mobile Robots. - CRC Press, 2006.-696p.
4. **Farbod Fahimi**. Autonomous Robots. Modeling, Path Planning, and Control. – Springer, 2009. 339p.

Proceedings of 4th International Conference ITELMS'2009

Regression Models for Predicting Loads Transfer Time in Automatic Warehouse Palletizing System

V. V. Janilionis*, V. Janilionis**

**Dematic Ltd., Dematic Ltd. office in Kaunas, Raudondvario pl. 107, 47186, Kaunas, Lithuania,*
E-mail: vytautas.janilionis@dematic.com
***Kaunas University of Technology, Donelaičio str. 73, 44029, Kaunas, Lithuania, E-mail: vytautas.janilionis@ktu.lt*

Abstract

The purpose of this study is to develop models to support warehouse designers in choosing the most suitable parameters for automatic warehouse palletising systems. Loads transfer time in automatic warehouse palletising system depends on the loads input rate, system structure, control algorithms, and parameters of the equipment. The design of automatic palletising system has to ensure system resources to be used at the most optimum way and average loads transfer time in system would not be greater than required. This research proposes integration of simulation, visualization and statistical analysis for warehouse palletizing system analysis and supporting design tasks. The simulation model of one automatic load palletising system and using simulation model run results developed nonlinear regression models for predicting the average loads transfer time in system with different equipment parameters and loads input rates in this paper are presented. The results show that proposed models could be very useful for designing automatic warehouse palletizing system.
KEY WORDS: *palletizing system, automatic warehouse, logistics, simulation, regression analysis.*

1. Introduction

The performance of automatic warehouse is highly influenced by the equipment technical parameters and control algorithms. The research and development of logistics future factory is mainly concerned with robotics-logistics and informatics-logistics. Robotics-logistics can be understood as the field of activities where applications of industrial robot technologies are offered and demanded in order to ensure the optimization of internal material flows [1]. The intra-logistic robots are mainly used for palletizing and packing.

The purpose of this study is to develop models to support warehouse designers in choosing parameters for automatic warehouse palletizing systems. At present most warehouse systems are designed on the basis of insights, experience and sometimes on a detailed simulation. There is a need for design methodology requiring less detailed data and shorter designing time [2, 3].

Analytical models for predicting loads transfer time in automatic warehouse are applicable only in simple systems [4]. It is almost impossible to guarantee that complicated systems will operate properly only by doing analytic calculations. Complicated system models are developed using approach based on integration of analytical methods and Monte Carlo simulation [5].

In practice simulation models allowing testing the system on different operating scenarios, technical parameters, layouts etc. before it is actually being build are created. Simulation technique enable to identify and solve the problems associated with automatic warehouse palletizing systems in designing, launching, and operating phases of the automatic warehouse [2, 8].

An increasing demand of simulation as a modelling and analysis tool has resulted in a growing number of simulation software products in the market. Most widely used simulators are: ProModel, AutoMod, Workspace, HyperMesh, and ProcessModel [3, 6, 7]. They are very powerful at simulation, but their experimentation performance and statistical analysis facilities are poor. Evaluation of simulation software, described in [7], rates these features only satisfactorily, 5-6 out of 10 shows that application of advanced statistical methods to simulation results is complicated.

Our experience has indicated that model visualization provides a more comprehensive view of simulation analysis. It can help to spot the problem areas easier and guide quicker to the problem solving. Our claim is that visualization can be our common sense guide in experimentation with a simulation model.

In this research we propose integration of simulation, visualization and statistical analysis for warehouse palletizing system analysis. Therefore, the simulation software Automod [9] is integrated with the statistical analysis software SPSS [10].

2. Automatic Loads Palletizing System Description

The purpose of automatic warehouse palletizing system is to pick a pallet in a certain order as quickly as possible using warehouse equipment (conveyors, de-trayer and robots) and its control algorithms. This system functions as a part of the warehouse and connects storage and dispatch areas. Fig. 1 shows the investigated automatic loads palletizing system.

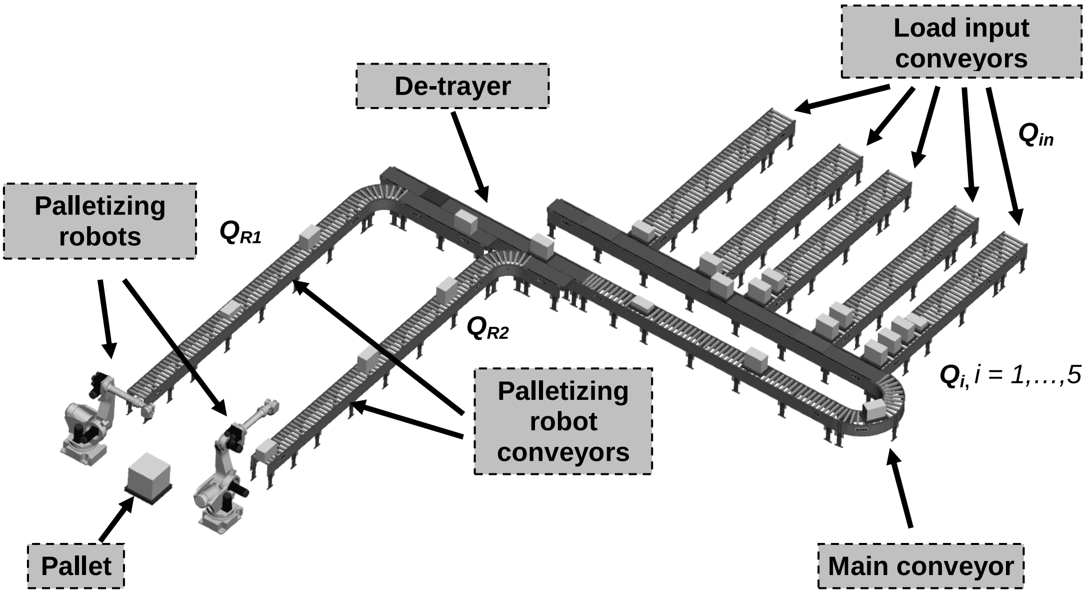

Fig.1. Automatic loads palletizing system

Loads arrive to the palletizing system from the other system in the warehouse and are put to the input queue Q_{in} before they get onto loads input conveyors. Load is put on the conveyor, if the required loads input conveyor queues Q_i of size k_i (i = 1, …, 5) has enough remaining capacity, otherwise it stays in queue Q_{in}. The main conveyor claims and merges loads in the right sequence and transports them to de-trayer, where loads are removed from trays. Then loads are pushed to palletizing robot conveyors and wait in the queue Q_{Ri} of size k_{Ri} (i = 1, 2) until the palletizing robots pick them. Robots take the loads from the conveyors and put them on a pallet. Every picked pallet has n loads. The pallet leaves the automatic palletizing system and travels to the other system in the warehouse after it is picked.

The main conveyor is the bottle neck of the system, because it has to maintain arriving loads in the right sequence. The palletizing robots receive a list of loads, labelled l_1, l_2, …, l_n, l_{n+1}, ..., which they have to pick for a particular pallet before each pallet is being built. The list of load labels is generated so that the loads are put on the pallet of size n in the most optimum way and also taking into account the specification (weight, dimensions, content, etc.) of each load. Since two robots R_1 and R_2 work in parallel, the de-trayer splits the sequence of loads with labels l_1, l_2,…, l_n., l_{n+1},…into two sequences of loads with even and odd label numbers (l_1, l_3, …, l_{2k-1} and l_2, l_4, …, l_{2k}) and sent them respectively to robots R_1 and R_2.

In this research, it is assumed that loads arrive on input conveyors from the other system in the warehouse already sorted in increasing order according to their label number (e.g., the load input conveyor Q_3 can have the sequence of loads with labels l_{m+3}, l_{m+4} ,l_{m+7} , l_{m+12}, but cannot have sequence of loads with labels l_{m+4} , l_{m+3}, l_{m+7} and l_{m+12}). The main conveyor prevents the robots from the lock-up and controls the difference between the label numbers of loads in even and odd subsequences. Then merging loads on the main conveyor are controlled by the function

$$In(k) = \begin{cases} 0\,, & if \quad \left| k - last_{k \bmod 2+1} \right| > \Delta k, \\ 1\,, & otherwise, \end{cases}$$

where k is the load label number, $last_1$ is the last load with odd label number merged on the main conveyor, $last_2$ is the same with the even label number, Δk - maximum allowed difference between label numbers of loads in even and odd subsequences.

In order to pick a pallet according to the specified list, robots have to receive loads in perfect sequence maintained on the man conveyor using the previously mentioned function. The following sequence control strategies, such as: S_0 - perfect sequence ($\Delta k = 1$), S_1 - one insert is allowed ($\Delta k = 3$), S_2 - two inserts are allowed ($\Delta k = 5$) are investigated in this research.

3. Simulation Model of Automatic Palletizing System

A simulation model allowing to estimate the average loads transfer time in system with different equipment parameters, control algorithms and loads input rates in order to design loads palletizing system is needed.

The simulation of the system has been undertaken using AutoMod simulation software. The AutoMod software has been developed for over 20 years specifically to model material handling systems. There are no limitations on model size, complexity, or level of detail for operational rules. The built models are highly accurate and use three dimensional true to scale virtual reality graphics.

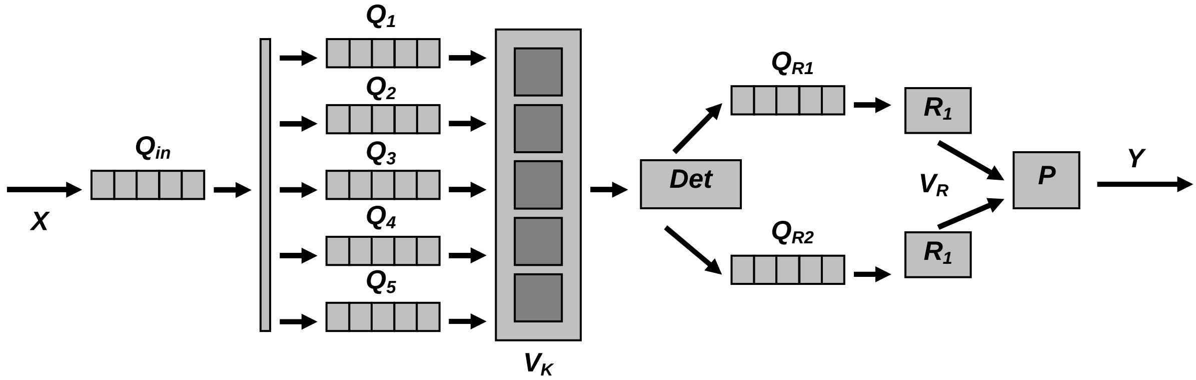

Fig. 2. Model flow diagram

Fig.2. shows a flow diagram of the loads palletizing system simulation model with the following parameters:

- X – average input rate of loads (loads/h); interarrival time between loads have a distribution $F \in \{N, U, E\}$, where N-normal, U-uniform, E-exponential;
- Y – average loads transfer time in the system (sec.); this is time interval from load entering queue Q_{in} to being put on the pallet;
- Q_{in} – input queue with infinity capacity, where the load enters system;
- Q_i - queues of size k_i before the main conveyor, where loads wait until being claimed and merged by the main conveyor, i=1,…,5;
- V_K – the main conveyor speed (loads/h);
- Q_{Ri} - queues of size k_{Ri} before the palletizing robots, where load waits until picking by the palletizing robots, i=1,2;
- V_R - picking speed of robots R_1 and R_2 (loads/h);
- n - pallet size (load).

It should be noted that only parameters, that have a significant influence to the average loads transfer time in the system, are considered in this research. It is possible to define the conveyor acceleration, deceleration, the kinematics' movements of the palletizing robots, etc. in developed simulation model.

4. Regression Models for Predicting Average Loads Transfer Time

Results presented in this paper were generated by performing simulation runs with robots' speed V_R = 720 (loads/h), conveyor speed V_K = 700 (loads/h), average loads input rate $X \in \{200, 250, 300, \dots, 500\}$, sequencing control strategies $S \in \{S_0, S_1, S_2\}$, and interarrival time between loads had an exponential distribution. The SPSS [10] software was used for analysis of simulation results and development of regression models.

In order to get the best fit regression model of the average load transfer time in the system (Y) against average loads input rate (X) various nonlinear regression models

$$Y = f\left(\tilde{X}_1, \tilde{X}_2, ..., \tilde{X}_r, \beta_0, \beta_1, ..., \beta_r\right) + \varepsilon ,$$

were tested. $\tilde{X}_i$ is nonlinear transformation of X. We compared logarithmic and polynomial models where regression function is a nonlinear function of the X but is the linear function of the unknown parameters. The best fit was obtained by using polynomial regression models

$$Y = \beta_0 + \beta_1 X + \beta_2 X^2 + ... + \beta_r X^r + \varepsilon$$

where *r* is the highest power of X that included in regression, ε is the regression error term. The polynomial regression model is similar to the multiple regression models, where powers of the same dependent variable X are regressors, that are

$$\tilde{X}_1 = X, \tilde{X}_2 = X^2, \tilde{X}_3 = X^3, ..., \tilde{X}_r = X^r .$$

After defining new regressors $\tilde{X}_i$ that are nonlinear transformations of the original X, regression function is linear in unknown parameters

$$\mathbf{Y} = \tilde{\mathbf{X}}\boldsymbol{\beta} + \boldsymbol{\varepsilon} \quad ,$$

which can be estimated by ordinary least squares method

$$\hat{\boldsymbol{\beta}} = \left(\tilde{\mathbf{X}}^{\mathrm{T}}\tilde{\mathbf{X}}\right)^{-1} \tilde{\mathbf{X}}^{\mathrm{T}}\mathbf{Y} .$$

Which degree polynomial should we use? The answer balances between flexibility and statistical precision. The increase of the degree r introduces more flexibility into the regression function, but increasing r means adding more regressors, which can reduce the precision of the estimated coefficients. We used sequential hypothesis testing procedure in order to determinate the degree of the polynomial. This procedure sequentially tests individual hypothesis

$$H_0 : \beta_i = 0,\ H_a : \beta_i \neq 0 \qquad , \ t = \frac{\hat{\beta}_i}{SE(\hat{\beta}_i)} \sim T\left(n-r-1\right),\ \ i = r, r-1,...,1 .$$

Using sequential testing procedure we determinated that the coefficients on X^r in polynomial regression model were zero when $r > 4$. The best obtained model for predicting average load transfer time in system (Y) against average load input rate (X) is

$$Y = \beta_0 + \beta_1 X + \beta_2 X^2 + \beta_3 X^4 + \varepsilon.$$

Hypothesis about normal distribution of error term $H_0 : \varepsilon \sim N(0, \sigma_e^2)$ were tested for all models.

Table 1

Regression models for predicting average loads transfer time in automatic warehouse palletizing system

S	Regression equations	Measures of fit		Hypothesis testing results	
		R^2_{adj}	S_e	$H_0 : \beta_i = 0$ $H_a : \beta_i \neq 0$	$H_0 : \varepsilon \sim N(0, \sigma_e^2)$
S_0	$Y = 21.3 + 0.398X - 0.001 \cdot X^2 + 1.86 \cdot 10^{-9} \cdot X^4$	92.5	2.68	$\beta_0^{*}, \beta_i^{***}$ $i = 1,3$	$p = 0.051$
S_1	$Y = 57.94 + 0.049X - 8.46 \cdot 10^{-5} \cdot X^2 + 2.21 \cdot 10^{-10} \cdot X^4$	98.2	0.462	$\beta_0^{***}, \beta_1^{*}$ $\beta_2^{*}, \beta_3^{***}$	$p = 0.567$
S_2	$Y = 57.6 + 0.053X - 9.41 \cdot 10^{-5} \cdot X^2 + 2.46 \cdot 10^{-10} \cdot X^4$	98.1	0.502	β_0^{*}, β_1^{*} $\beta_2^{*}, \beta_3^{***}$	$p = 0.818$

Notes: $*p < 0.1$, $**\,p < 0.05$, $***p < 0.01$.

Table 1 gives the best fit of regression models for predicting average loads transfer time in automatic warehouse palletizing system, when sequencing control strategies $S \in \{S_0, S_1, S_2\}$, robots speed V_R = 720 (loads/h) and conveyor speed V_K = 700 (loads/h). The results in Table 1 conclude that values of adjusted R-Square (R^2_{adj}) are greater than 92% and models are good at predicting the average values of the loads transfer time in automatic warehouse palletizing system; hypothesis testing indicates that regression coefficients β_i are different from zero (p<0.1), regression coefficients are statistical significant; regression errors are normally distributed (p>0.5) and all models satisfy regression assumptions.

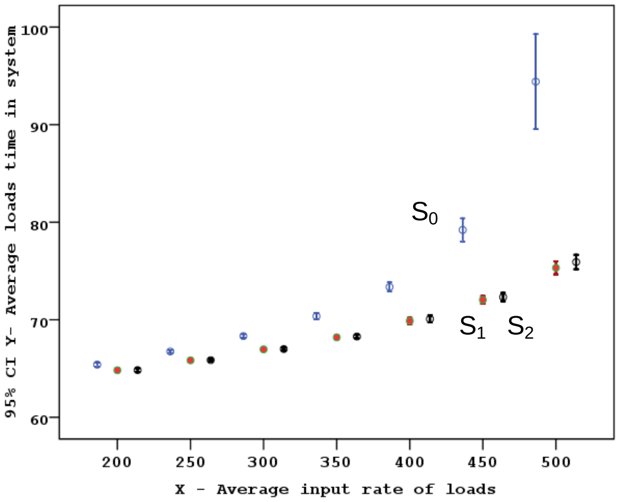

a

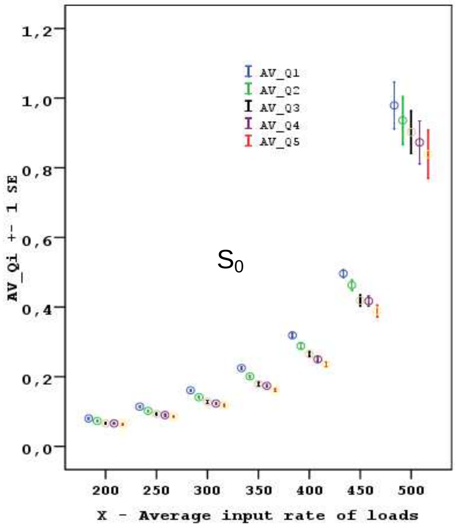

b

Fig. 3. a) Average loads transfer time in system for different load input rates and sequencing control strategies S_0 ,S_1, S_2, V_R = 720 loads/h; b) Average lengths of queues Q_i (i = 1,…,5) for different load input rates and sequencing control strategy S_0 , V_R = 700 loads/h.

Fig. 3. represents some graphical analysis results: Fig. 3 a shows the values of average load transfer time in the system and 95% confidence intervals of mean for different load input rates and sequencing strategies; Fig.3, b points the average queues Q_i length ± 1 SE (standard error of mean), i =1, …, 5 for different load input rates and sequencing control strategy S_0. The average load transfer time in the system reduces from 82 to 71.9 sec. (12.3%), for sequence control strategy S_1 and average load input rate of 450 loads/h compared to strategy S_0. Similarly the average load transfer time in the system reduces from 96.2 to 75.1 sec. (21.9%), for sequence control strategy S_1 and average load input rate of 500 loads/h compared to strategy S_0.

The results show that proposed models could be useful tools for designing automatic warehouse palletizing system.

5. Conclusions

It was developed the simulation model of automatic loads palletizing system with visualization allowing to testing the influence of different load input rates, equipment parameters and control strategies on the system performance.

Simulation results were used to develop the nonlinear regression models for the predicting average load transfer time in the system. Various nonlinear regression models were compared and it was determinated that a polynomial regression model of degree 4 is the best. The R-Square values vary from 0.92 to 0.98, models satisfy regression assumptions and are good at predicting the average values of the loads transfer time in automatic warehouse palletizing system.

Analysis results showed that the average load transfer time in the system reduces significantly for sequence control strategies, S_1 , S_2 and average load input rates greater than 400 loads/h, compared to strategy S_0 . The developed regression models can be used in designing the automatic palletizing systems in the warehouses.

The usage of proposed approach for warehouse palletizing system analysis showed that the integration of simulation, visualization and statistical methods improve the quality of exploratory data analysis by supporting the creative tasks of the analyst.

References

1. **Echelmeyer W., Kirchheim A., Wellbrock E.** Robotics-Logistics: Challenges for Automation of Logistic Processes. - Proceedings of the IEEE International Conference on Automation and Logistics. 2008, pp. 2099-2103.
2. **Dallari F., Marchet G., Melacini M.** Design of order picking system, The International Journal of Advanced Manufacturing Technology, 2009, 42(1-2) , pp. 1-12.
3. **Johari N. A.M., Haron H., Jaya A. S. M**. Robotic modelling and simulation of palletizer robot using Workspace5. Computer Graphics, Imaging and Visualisation (CGIV 2007).-IEEE Computer Society. 2007, vol. 7. pp. 217 – 222.
4. **Lerher T., Sraml M., Kramberger J., Potrc I., Borovinsek M., Zmazek B.** Analytical travel time models for multi aisle automated storage and retrieval systems. The International Journal of Advanced Manufacturing Technology, 2006, 30(3-4), pp. 340-356.

5. **Alzbutas R., Janilionis V.** Integration of Analytical and Monte Carlo methods for Dynamic System Safety Analysis // Advances in Safety and reliability. Proceedings of the European safety and reliability conference. Taylor&Francis Group, London, 2005, vol. 1, pp. 61-67.
6. Rohrer M.W. Maximizing simulation ROI with Automod. - Proceedings of the 2003 Winter Simulation conference. 2003, vol. 1, p. 201 – 209.
7. **Verma R., Gupta A., Singh K.** A critical evaluation and comparison of four manufacturing simulation softwares. Kathmandu University Journal of science, engineering and technology, 2009, 5(1), p. 104 – 120.
8. **Siromiatnikov V. S., Ortega M. G. R., Oleinikova L. N., García J. M., Sandoval F. G.** Using Simulation to Support Optimization of Conveyor System. ACIT-Automation, Control, and Applications. ACTA Press, 2005, p. 36 – 45.
9. Applied AutoMod 12.2.1.-Santa Clara:-Applied Materials Inc., 2008, 1076 p.
10. **Norušis M. J.** Advanced Statistical Procedures Companion. SPSS 15.0. Prentice Hall, 2007, 432 p.

Proceedings of 4th International Conference ITELMS'2009

The Research Cars Salons Parameters Power for Human

L. Pelenytė–Vyšniauskienė*, R. Viltrakis**

**Kaunas University of Technology, Panevėžys Institute, Klaipėdos g. 1, LT-35209 Panevėžys, Lithuania,
E-mail: linapelenyte@gmail.com
**Kaunas University of Technology, Panevėžys Institute, Klaipėdos g. 1, LT-35209 Panevėžys, Lithuania,
E-mail: ramunas.viltrakis@gmail.com*

Abstract

This article deals with processes during the collision of vehicles as well as occupant's dynamics inside the vehicle. The research is being done on what the occupant motion depends on and what the power balance between the occupant and safety means is. The article offers a way of evaluating injuries, measuring occupant acceleration and velocity, taking into account different distances inside the vehicle during the accident.
KEY WORDS: *occupants, frontal crash, deceleration, speed, HIC.*

1. Introduction

More than a million casualties and seriously injured, several tens of thousands of victims - this is an annual European Road Statistics. These figures are identical and can be adapted to the traffic situation in Lithuania scratches. Every year the country recorded about 6 thousand, traffic accidents, which have killed or injured people. In 2007, motor vehicle killed 739 people. This is the highest rate in recent years in Lithuania and one of the largest in the European Union. Although traffic accidents in 2008 decreased significantly (498 killed people), the problem remains no less important [1].

As the main causes of deaths in traffic accidents the European Commission, on the basis of detailed studies, identified the allowable speeding, driving while being drunk and non-safety belt. These reasons particularly relevant for Lithuania.

Due to intensification of traffic, high-speed automotive and non-use of safety measures, at the time of accident severity of injuries acquired increasing the number of deaths on the ground. The analysis of injuries per 1000 people showed that most suffer head injuries - 86.6%, face - 90.6% and chest - 60.4% (Fig. 1).

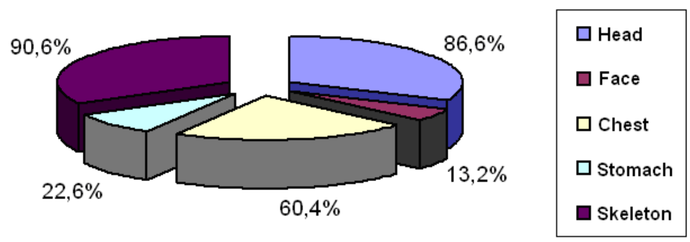

Fig. 1. Injuries in the accidents distributions

The easiest way of human movement in a car accident is to investigate the aid of computer programs. In this case, the imposition of the initial parameters: the car make, model, year, speed before the collision, the human weight, height, position, we can obtain various interesting results: the movement trajectory after a collision, deformation rates, development, acceleration, etc. However, computer programs are expensive and complex for simple users, because this purpose of the study - an analysis of human movement trajectory by using mathematical calculations and analysis aid.

2. Human Motion during the Frontal Crash

Analysing any car collision in time interval it is possible to differentiate two phases since the beginning of collision till its complete stop.

The first collision phase is when cars crash into each other or into immovable object and get deformed.

A car crashes with a certain acceleration. It sharply decreases and its direction changes. Meanwhile human body by inertia moves in the moving direction of the car. During the collision a man is affected by the impact power, which is directly proportionate to crash acceleration. The crash impact is transferred through bordering systems: safety belt, air bag, seat, etc. So while calculating it is important to evaluate their indirect action characteristics. They appear because of ineffective safety belt deformation, inadequate tension, sometimes because of clothes. While using air bag ineffective deformation occurs because of the distance between air bag and a person [2].

The second colliding phase is when cars or a car and an obstacle start pushing each other and separate. A car gets deformed till a certain limit and under the influence of elasticity and centrifugal force bounces back from the object. At this moment air bag becomes flat and belt tension decreases. The passenger's acceleration direction coincide with car acceleration, i.e. operator strikes against the seatback.

If the collision force is eccentric, i. e. appear angular acceleration and tangential force, then vehicles change their moving direction or spin. As the contact is extremely brief it is considered that the position hardly changes, consequently general direction of deformations as a rule coincides with adequate relative speed direction or slightly deviate. If the direction of deforming forces is precisely determined it is possible to set the collision (attack) angle. This fact is of high importance in technical expertise.

At the collision moment kinetic energy is absorbed by the car contacted part. In case the collision is very strong, part of energy is transmitted to interior. The larger deformation area cause's the smaller probability to get injuries.

3. Deceleration, Speed, Times and *HIC* Dependence of Cars Salons Parameters

On purpose to find out, more about occupant's dynamism and its affecting forces, simplified model of occupant mass centres.

While analysing occupant motion in a car during the crash we accept the facts that:

1. Car acceleration deceleration does not depend on occupant acceleration deceleration

   a car >> a occupant

2. Car deformation does not depend on occupant and safety systems.

Let us analyse an uncomplicated frontal collision when car interior stays non-deformed and decreas of general occupant energy is invariable measure and equals to kinetic energy existing at the beginning of collision.

While applying mathematical motion model it has become clear that after calculating occupant travel s and necessary body travel srea, the following versions are possible:

$s > s_{req}$ – passenger suffers, safety increases, if s decreases;

$s < s_{req}$ – passenger does not suffer, safety increase;

$s \approx s_{req}$ – passenger does not suffer.

Such simplifications allow us to analytically analyse characteristics of car deformations and the lowest possible occupant's head, thorax and pelvis acceleration deceleration during collisions. The essence of analyses is setting constants of the smallest possible occupant's acceleration deceleration using total occupant's forward displacement [3, 4]:

$$s = s_{interior\,total} + s_{Fz}\left(t_{thorax\,rebound}\right) - s_{thorax}\left(t_{start}\right), \tag{1}$$

where:

$s_{\mathrm{int}erior\,total}$ – obstacle, distance in a car from thorax (body) until the closest obstacle, where occupant can be displaced.;

$s_{Fz}\left(t_{thorax\,rebound}\right)$ – distance, that the car covers, until the collision moment when thorax hits an obstacle;

$s_{thorax}\left(t_{start}\right)$ – distance that thorax (body) covers at the initial moment of collision.

In Calculations used this formula:

Time, required to reach the final point and kinetic energy disappearance is equal:

$$t_{end} = t_{start} + \left(\frac{2s_{req}}{a_{const}}\right)^{0.5} \tag{2}$$

where:

$t_{start} = t_1 = 0$ - time when the accident begins;

$t_{end} = t_2$ - time when the accident ends;

sreq - distance, required for the body not to be injured during the accident. It is calculated after the following formula:

$$s_{req} = \frac{1}{2}vt = \frac{1}{2}at^2 \tag{3}$$

Calculations are done under the asumption that frontal impact is ideal, occupant body is one-piece and in accidents moves rectillineally. It is also assumed that occupant acceleration is invariable (*a*=const). Motion acceleration can be expressed by ratio $a_t = a/g$, where g = 9.8 m/s^2, a – acceleration, which is freely chosen on the basis of studies [3]. Occupant's velocity during his impact is calculated by formula $v = at_2$.

Head injury coefficient can be calculated using formula [5]:

$$HIC = \left[\frac{1}{t_2 - t_1} \int_{t_1}^{t_2} a_t dt \right]^{2.5} (t_2 - t_1) \tag{5}$$

where:

t_1 and t_2 - any time moments during impact between the earlier mentioned tstart and end tend times;

a- acceleration in time interval $t_1 - t_2$.

The parameters of this research:

- It is assumed that the driver is 186 cm tall and 88 kg of weight, and do not use any of the car safety systems. Assumed, that at the moment of impact, the head will reach the car's cabin components of no less than 25% of its total area.
- Studied completely frontal collision when during a car accident the interior of a car is not deformed and does not affect the dynamics of human movements (in some cases, this type of collision can be equated to sudden braking).
- Selected for the analysis of 2 different classes of cars: compact class of 1991 "Mazda 323" and minivans Class of 1999 "Opel Zafira A".

According to the given procedure we will count all measured cars a, m/s^2; t_2, s; v, m/s and HIC, when distance s between driver and steering wheel is minimal, medium and maximal. Calculation in a few cases is given as

$a_1 = 10g, 20g, 30g, 40g, 50g, 60g$.

Received results are included into Table 1 and Fig. 2 – 7.

According to the schedule, we can see that the lower the speed, the lower the head injury coefficient *HIC*. It is also the shorter time the accident takes place and t_2 is lower, the speed and the HIC is less.

Study showed that all the characteristics of a smaller car are lower. However, when the speed exceeds 20 m/s, and the distance is s_{ever}, the head injury coefficient exceeds a critical *HIC* threshold in both cars, and such injury is considered to be very dangerous or even fatal.

Table 1

The results of calculations

Opel Zafira A (1999)						Mazda 323 (1991)				
s, m		a, m/s^2	t_2 ,ms	v, m/s	*HIC*	s, m	a, m/s^2	t_2 ,ms	v, m/s	*HIC*
s_{min}	0.4	98	90	9	29	0.31	98	78	8	25
		196	64	13	114		196	55	11	99
		294	52	15	257		294	45	13	223
		490	40	20	714		490	35	17	618
		588	37	22	1028		588	32	19	890
s_{ever}	0.54	98	103	10	33	0.41	98	90	9	29
		196	73	14	131		196	64	13	114
		294	60	18	294		294	52	15	257
		490	46	23	818		490	40	20	714
		588	42	25	1178		588	37	22	1028
s_{max}	0.67	98	115	11	38	0.5	98	101	10	32
		196	81	16	149		196	71	14	128
		294	66	20	332		294	58	17	287
		490	51	25	918		490	45	22	798
		588	47	28	1320		588	41	24	1150

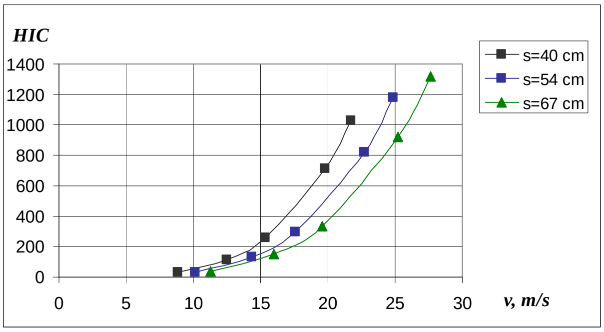

Fig. 2. *HIC* dependability on velocity “Opel Zafira A“

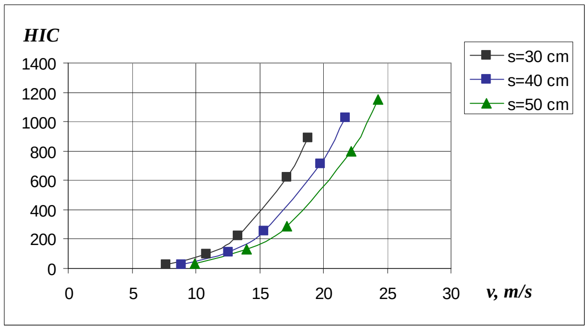

Fig. 3. *HIC* dependability on velocity “Mazda 323”

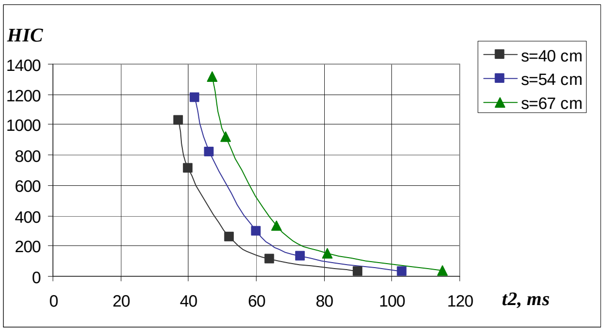

Fig. 3. *HIC* dependability on time “Opel Zafira A“

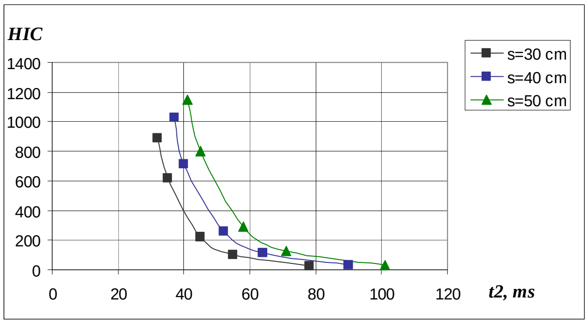

Fig. 6. *HIC* dependability on time “Mazda 323”

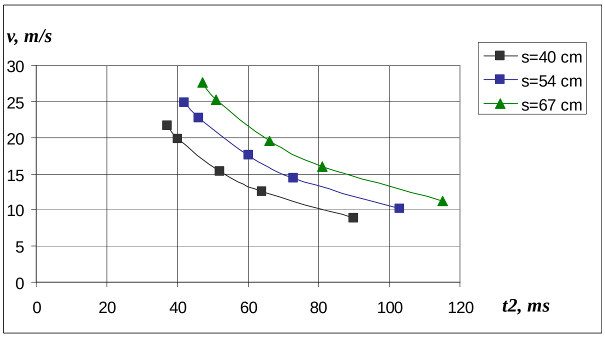

Fig. 4. Velosity dependability on time “Opel Zafira A“

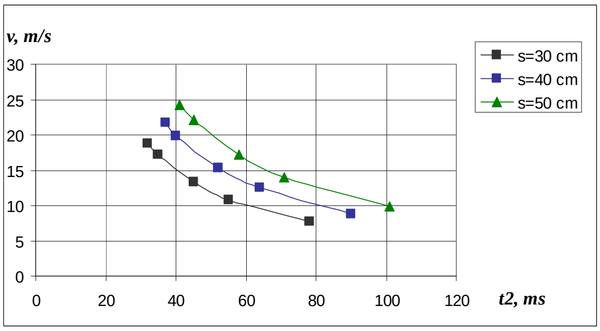

Fig. 7. Velosity dependability on time “Mazda 323”

4. Conclusions

1. Making further analyses when passenger suffers and gets injured, velocity and acceleration dependability on time has been surveyed, taking into account different distance to the obstacle in the car. It has been set that the larger $s_{obstacle}$ the higher velocity the body reaches.
2. The study found that the smaller car cabin dimensions are smaller, and the characteristics are also significantly lower.
3. In the case of cars in the “Opel Zafira A” and “Mazda 323” showed that the death zone, where the *HIC* ≥ 1000, is reached when the speed is 22 m/s, and the duration t_2 of the accident of “Opel Zafira A” aims to 115 ms, and the “Mazda 323” – 101 ms.

References

1. Lietuvos automobilių kelių direkcija prie susisiekimo ministerijos. Prieiga per internetą: <http://www.lra.lt/lt.php/eismo_saugumas/eismo_ivykiu_statistika> .
1. **Koshiro, O., Munekazu, K..** Influences of the physical parameters on the risk to injuries in low impact speed. Accident Analysis & Prevention, July 2004, Vol. 28, Issue 4, p. 265–271.
2. **Hülsmann J.** Sensor Study for Frontal Impacts. 7th International Symposium on Automotive Occupant Restraint Systems. Germany 24th, April 2002, p. 6-10.
3. **Pelenytė-Vyšniauskienė, L., Jurkauskas, A..** Research into Occupant‘s motion in cars during crashes. Transport. Vilnius: Technika, 2004, Vol XIX, No 4. p. 184–190.
4. **Raymond D., Begeman P., Hai-Chun Chien, Bir C.** The Effect of Occupant Size on Head Displacement in Frontal Collisions. SAE 2006 Transactions Journal of Passenger Cars - Mechanical Systems, Volume 45, August 2008, p. 208-214.

Proceedings of 4th International Conference ITELMS'2009

Optimization of Energy Consumption for Light Rail Electric Transport with Supercapacitor System Using Neural Network Controllers

V. Brazis*, M. Gorobetz, L. Grigans***, L. Latkovskis****, A. Levchenkov*******

***** *Riga Technical University, Kronvalda bulv.1-207, LV 1010, Riga, Latvia, E-mail: viesturs.brazis@rtu.lv*
*** Riga Technical University, Kronvalda bulv.1-202, LV 1010, Riga, Latvia, E-mail: mihails.gorobecs@rtu.lv*
**** Institute of Physical Energetics, Aizkraukles iela 21, LV 1006, Riga, Latvia, E-mail:linardsgrigans@gmail.com*
***** Institute of Physical Energetics, Aizkraukles iela 21, LV 1006, Riga, Latvia,E-mail: leonsl@edi.lv*
****** Riga Technical University, Kronvalda bulv.1-202, LV-1010, Riga, Latvia, E-mail: anatolijs.levcenkovs@rtu.lv*

Abstract

In this paper the solution of energy saving problem is proposed. To achieve useful utilisation of regenerative energy and reduce the overall energy consumption, the braking energy should be temporarily saved in an energy storage system ESS, based on supercapcitor, until another power consumer is connected to the overhead line. Such a storage system is able to cope with the common task of peak power reduction and overhead voltage stabilization. ESSs could be installed stationary at substations, weak spots of network or on-board vehicle.
The purpose of this paper is to develop model for transport control system is to coordinate energy consumption of multiple various participants of traffic. The transport system is a cooperative system, where behaviour of one participant depends on other. Therefore, the negotiation process between vehicles is necessary. Each vehicle has electronic device which controls his own object sending data to the control centre, which is responsible for optimization and coordination of negotiation process.
Controller for speed prediction of electric transport is based on nonlinear autoregressive neural network with exogenous inputs. Inputs of controller are current tram speed, distance from the beginning of the route, type of next speed change point, light upon arrival to the traffic light on the way, time interval between current time and directive time. Training set for the controller is received from the simulation model of T3A tram, moving on the part of route containing two passenger stops and traffic light. Neural network is trained and results of its workability are proposed. Usage of neural network gives possibility to predict actions of all participants of electric transport flow and allow using ESS more efficiently.
KEY WORDS: *energy saving, light rail electric transport, neural network controller*

1. Introduction

The most efficient and low emission kind of public transport is a rail transport. Tram based light rail transit (LRT) has been chosen by a lot of city municipalities as the main urban passenger transportation solution.

The renewed tramcars acquired regenerative braking capability, thus providing up to 40% reduction in the energy consumption. However, the regenerative braking energy cannot be completely used in typical existing traction drive systems because none of the LRT substations is equipped with a reversible rectifier. The real energy saving strongly depends on other trams connected to the same section of overhead line. If a number of trams are connected to the DC overhead line, a portion of the regenerative braking energy could be transferred to other trams when they are operated in the traction mode, but in the case when several trams are simultaneously braking, this energy cannot be utilised and is wasted in a brake rheostat. It is often impossible for the tramcars to instantly consume regenerative energy at low traffic density in the off-peak hours and on easily loaded lines, since in the overhead supplying zone of a single traction substation at one tram's braking other trams not often can simultaneously utilise the energy in the traction mode [1] or even are not located in this overhead line section.

To achieve useful utilisation of regenerative energy and reduce the overall energy consumption, the braking energy should be temporarily saved in an ESS until another power consumer is connected to the overhead line. Such a storage system is able to cope with the common task of peak power reduction and overhead voltage stabilization. ESSs could be installed stationary at substations, weak spots of network or on-board vehicle.

As distinguished from the heavy rail transport with predictable acceleration and deceleration areas mostly near stations, curves, hills, semaphores, switches, etc., the city traffic with its low speeds, frequent accelerations and sudden brakings is characterised by starting and braking zones distributed along the LRT network. The energy transfer from a tramcar to another vehicle or substation at a distance from several hundred metres up to few kilometres is associated with considerable energy losses, which decrease the power saving up to 10% [2]. Therefore, the most effective way of utilising the regenerative energy without transfer losses is installation of on-board ESSs.

Modern LRT vehicles have good dynamical properties and increased average speed, which impose the highest current constraints on the overhead line and lead to large line voltage drops in the traction mode [3]. The starting power peaks present a problem of availability of enough power at a feeding network, otherwise the mentioned voltage drops occur that significantly impair a tram's dynamic performance. The overhead line resistance increases with distance from a substation. If ESS is installed in substation it cannot eliminate undervoltage away from this substation. At the same time, an on-board ESS makes possible direct utilisation of stored energy at the place of consumption, which improves the dynamic behaviour of a vehicle having the same acceleration in a weaker network or a higher acceleration in well-fed overhead lines. Such an on-board ESS allows increasing the number of trams without resort to building new expensive substations, which is important in the cases when traffic should periodically be intensified for a limited time.

One of the most promising energy storage devices is a supercapacitor battery chosen for a tram ESS. In comparison with chemical accumulator batteries and rotating flywheels, the supercapacitors have better charge and discharge dynamic power characteristics despite the smaller total energy capacity. The advantage of supercapacitor is also independence of its parameters from the environment temperature.

Therefore, most attention has been paid to store as much as possible regenerative energy, applying as simple as possible technical solutions, which would allow the least rise in the cost of traction equipment without decreasing the tramcar operation safety. Such storage is achieved using a single-stage pulse converter without intermediate DC conversions [4]. Owing to the lack of a speed sensor and difficult access to the traction and braking signal outputs of a large fleet of existing renovated T3A trams, the control system of ESS has been developed independent of the tram controller. As distinguished from an ESS with a speed sensor [1], which should be recommended for brand new vehicles, the proposed solution with an independent control system of the ESS could easily be applied to the existing tram without reengineering its traction circuit and control system's hardware and software.

The straightforward ESS charging with a constant current has compatibility problems with the line parameters [5]. The charging of a supercapacitor with constant power requires that the ESS control system be incorporated into the vehicle traction drive with its modification [6]. The proposed charging algorithm with constant filter capacitor voltage provides the automatic whole braking energy saving without significant modification of the existing tram power circuit.

The lack of running-braking mode and speed signal in virtue of the autonomous ESS conception complicates the switch design, because information about the tram drive mode should be extracted from the available measurements of currents and voltages. This problem is solvable by relatively simple integrating the ESS control system in LRT traffic control intelligent neural network control system, which calculates the optimal vehicle moving mode. As the neural network controller calculates traction and braking mode parameters for multiple vehicles, the energy consumption and regeneration power could be predicted, thus allowing preparing the ESS for more energy storing and peak energy shaving. The intelligent LRT control system could more discharge the supercapacitor before multiple tram braking and prevent ESS deep discharge before simultaneous start of few trams. By setting the ESS operation mode in dependence from whole tram line vehicle traffic conditions by outboard intelligent control system, the parasitic energy distribution between a number of ESS are eliminated. The energy storing in other tram supercapacitor and peak energy shaving is fully controlled and accepted only if single tram ESS capacity limits are reached.

2. Power Circuit of Energy Storage System and T3A Tramcar Traction Drive

While connecting a supercapacitor energy storage system (ESS) to the existing T3A tramcar power scheme it is necessary to take into account that it should provide:

- two-way voltage boost/buck energy interchange between the T3A power circuit and the supercapacitor,
- smoothed charge/discharge current of the supercapacitor,
- smoothed and radio-frequency filtered line current,
- controllable initial charge of the supercapacitor,
- protection of the supercapacitor against overcurrents caused by overhead short circuits.

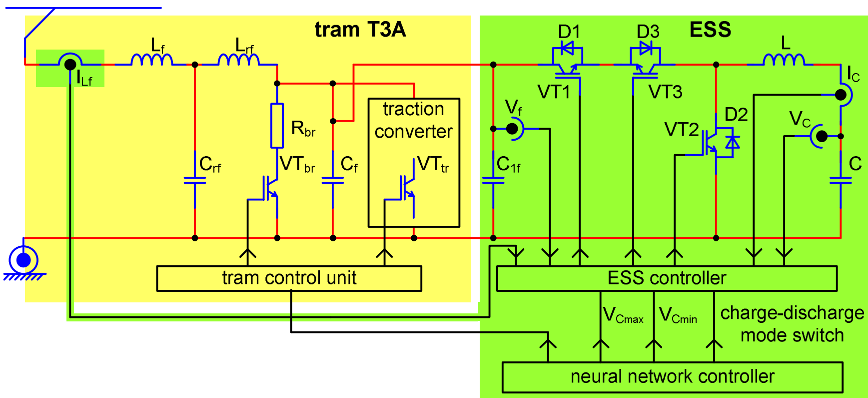

Fig. 1. A simplified circuit diagram of ESS and its connection to the T3A tramcar power circuit

A simple solution for the ESS power stage can be achieved by connecting it to the tram filter capacitor [4] at supercapacitor's voltage always being lower than that of the filter capacitor V_{Cf} [7, 8]. A simplified circuit diagram [9] of the energy storage system and its connection to the T3A tramcar power circuit is shown in Fig. 1.

The ESS under consideration consists of supercapacitor *C* and bidirectional DC/DC power converter. The IGBT *VT1* with diode *D2* makes a voltage buck converter in the supercapacitor's charging mode, whereas *VT2* and diode *D1* at the IGBT *VT3* switched on – a voltage boost converter in the supercapacitor's discharging mode. The *VT3* is needed for protection of the supercapacitor in the cases when short circuit or undervoltage occurs on the overhead line or in the tram traction converter. To prevent overcurrents and uncontrolled discharge of supercapacitor, *VT3* is switched off when the ESS input voltage is lower than that of supercapacitor [10].

The ESS is connected to the tram's filter capacitor C_f =5100 μF, which is therefore used also as a basic element for the buck/boost converter of ESS. Capacitor C_{1f} only compensates inductances of the connecting cables and must be placed as close as possible to the *VT1*, *VT2*, *VT3* and *C*; its capacitance is considerably lower than that of C_f. Such a connection allows exploitation of tram's radio-frequency filter L_{rf}, C_{rf} and input choke L_f for smoothing the pulsed currents flowing from the ESS to the overhead line.

The ESS has been developed as an entirely autonomous device having no links to the tram control unit. Two current and two voltage sensors are used for the ESS control purposes. Three of them are placed inside the ESS, and only the input current sensor of a tram should be installed in its power circuit.

The main task of the ESS controller is to store whole tramcar braking energy not allowing its dissipation in a braking rheostat. To store the energy, a capacitor must be discharged to voltage V_{Cmin} at the beginning of braking. As the braking energy depends on the tramcar speed, the processes of charging and discharging the supercapacitor may be controlled in compliance with the tramcar's real speed.

The following two voltages and two currents are measured for the ESS control purposes: filter capacitor voltage V_f, supercapacitor voltage V_C, supercapacitor current I_C, and tram input filter current I_{Lf}.

The charge-discharge mode switch is a very important part of the controller for stable operation of an ESS. The lack of running-braking mode signal in virtue of the autonomous ESS conception complicates the switch design, because information about the tram drive mode should be extracted from the available measurements of currents and voltages [9]. The choice of a proper charge-discharge switch solution is determined by the following:

- simultaneous setting of both the modes is not permissible,
- the circuit L_f, C_f, *L* and *C* (Fig. 1) has a low damping factor, so fast switching from one mode to the other can cause rising oscillations in it,
- a neutral position – no mode is set – is permissible, and is a good choice for achieving stable operation of the system,
- the tram drive mode cannot be determined by current I_{Lf}, so filter voltage V_f should be used for this purpose.

The charge mode is allowed when V_{Cf} >700 V, and the discharge mode is set when the voltage falls down to 600V.

The commonly used minimum supercapacitor voltage is V_{Cmin}=0.5V_{Cmax} (see, e. g. [1]) and is recommended by manufacturers of supercapacitors. In this case 75% of its energy capacity is utilised at the power capability $V_{Cmin}I_{Cref}$ varying from 0.5P_{max} to P_{max}. However, as is discussed in [4], the braking power is maximal at the beginning of tram braking when the ESS has its minimum power capability. Therefore a narrower voltage range was chosen - V_{Cmin}≈0.67V_{Cmax} , which gives 55% utilisation of the supercapacitor energy capacity at power capability 0.67P_{max} at the beginning of tram braking. However narrower ESS voltage range restricts the peak power shaving.

The charge mode is disabled when the supercapacitor voltage reaches V_{Cmax}, and is resumed when it falls down to V'_{Cmax} (see Fig. 2). The discharge is disabled when this voltage falls down to V_{Cmin}, and is permitted again when it rises up to V'_{Cmin}. As the V_{Cmax} and V'_{Cmax} could not be raised by supercapacitor construction limitations, the V_{Cmin} and V'_{Cmin} could be varied for improving ESS performance. The roman number in indexes (Fig. 1) shows the number of LRT car in two vehicle traffic control example.

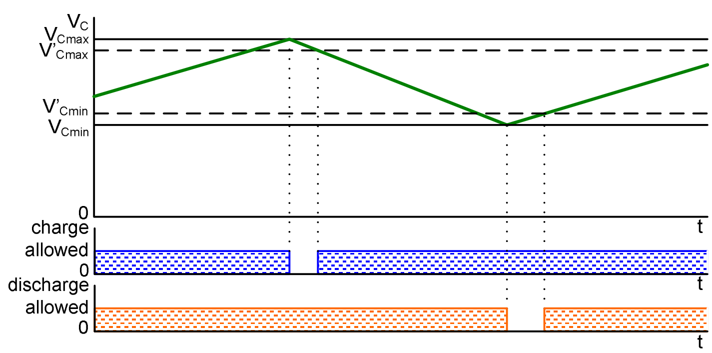

Fig. 2. Signal diagrams of supercapacitor voltage limiter

3. Structure of Public Electric Transport Control System

The purpose of transport control system is to coordinate actions of multiple various participants of traffic. The transport system is a cooperative system, where behaviour of one participant depends on other. That is why the negotiation process between vehicles is necessary. Each vehicle has electronic device which controls his own object sending data to the superagent, which is responsible for optimization and coordination of negotiation process.

It follows that coordination centre is needed to control public electric transport and predict its movement.

Therefore, the following objects can be defined for intelligent public electric transport control system.

- TR – electric vehicles:
  - D_{tr} – electric drives of electric vehicles;
  - M_{tr} – sensors of electric vehicles;
  - R_{tr} – transmitters of electric vehicles;
  - A_{tr} – power converter;
  - ESS_{tr} - energy storage system;
  - N_{tr} – navigational device that controls position of the vehicle on the route
  - V_{tr} – own electronic control devices of electric vehicles;
- CC – centre of intelligent control of electric transport:
  - V_{cc} – electronic control devices of control centre;
  - Db_{cc} – data base of intelligent agent of control centre;
  - Pg_{cc} – software with artificial intelligence procedures for intelligent agent of control centre;
  - R_{cc} – transmitters of control centre;
- L – traffic lights, as electric transport flow control devices:
  - E_L – electrical part of traffic lights;
  - V_L – electronic control devices of traffic light;
  - A_L – actuators for control signal transfer to electric part of traffic lights;
  - M_L – sensors of traffic lights;
  - R_L – transmitters of traffic lights;

Interaction between abovementioned objects is shown in Fig. 3.

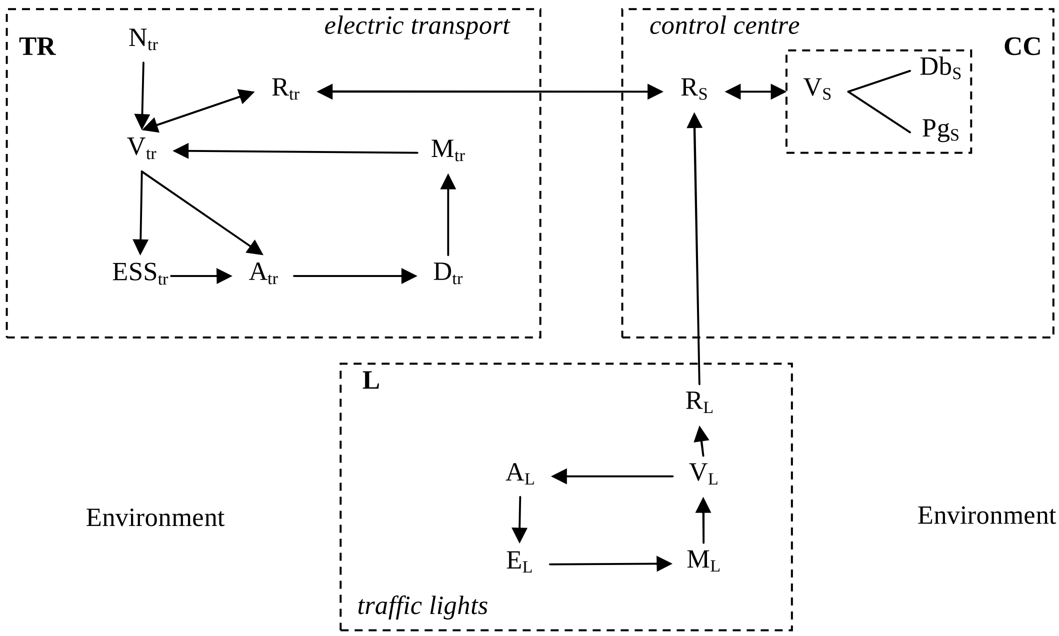

Fig. 3. Public electric transport control system

In addition to other electronic devices, navigational device is proposed to be installed on each public electric vehicle. The purpose of this device is to get geographical coordinates of transport unit, as well it can be used as speed meter. It may be based on satellite systems, like GPS, GALILEO, GLONASS etc., as well as GSM, GSM-R or other wireless navigation technologies. For city transport it is useful to use combined devices, because straight signal from the satellite may be corrupted or interrupted by high buildings, narrow streets or tunnels. In this case additional antennas, located on the open-sky positions, like rooftops, should be used to transfer signal from the satellite to public transport vehicle.

4. Mathematical Model for Public Electric Transport Control System

Mathematical model for control centre software of public transport network should represent all objects and elements presented in real system, including abstract objects such routes, schedules etc.

PTN = {GN, DC } – public electric transport network, where

- GN – geographical transport network;
- DC – contact network of public electric transport;

Geographical network is a set GN = {G_1, G_2, G_3}, where

- G_1 – roads and streets;
- G_2 – crossroads;
- G_3 – passengers stops.

For each $g \in GN$ geographical coordinates of beginning and end are known:

- $x^g{}_1$, $y^g{}_1$ – coordinates of the beginning;
- $x^g{}_2$, $y^g{}_2$ – coordinates of the end.

Contact network may be described as a set of objects DC = { SC, ST }, where

- SC – sections in which contact network is divided;
- ST – substations for power supply.

For each $s \in SC$ geographical coordinates of beginning and end are known too:

- $x^s{}_1$, $y^s{}_1$ – coordinates of the beginning;
- $x^s{}_2$, $y^s{}_2$ – coordinates of the end.

Each public electric transport unit $tr \in TR$ has following parameters:

- M_{tr} = {$m^{tr}{}_1$, $m^{tr}{}_2$, …, $m^{tr}{}_n$} - route, where $m \in GN$;
- S_{tr} = { $d^{tr}{}_1$, $d^{tr}{}_2$, …, $d^{tr}{}_k$} – schedule as a set of directive times for each passenger stop from the route $m \in G_3$;

For each section $s \in SC$ of contact network the appropriate element $g \in GN$ from geographical network may be found:

- SC $\rightarrow$ GN,

therefore, the electrical route for each public electric transport unit $tr \in TR$ can be found:

- Me_{tr} = {$me^{tr}{}_1$, $me^{tr}{}_2$, …, $me^{tr}{}_q$}, where $me \in SC$.

These data are saved in data base of control centre and are constant.

Each vehicle $tr \in TR$ has following parameters:

- $v_{tr} \in \Re$– current speed, received by navigation device;
- $x_{tr}, y_{tr} \in \Re$ – geographical coordinates received by navigation device.
- $d_{tr} \in \Re$– current directive time for next passenger stop;
- $l_{tr} \in$ GN - location in geographical network;
- $le_{tr} \in$ SC – appropriate section in electrical network;

Each traffic light $tl \in G_2$ has following parameters:

- $x_{tl}, y_{tl} \in \Re$ – geographical coordinates of location;
- $l_{tl} \in G_2$ – location in geographic network;
- $W_{tl} \in \{0, 1\}$ – current light on the traffic light (0 – red, 1 – green};
- $D_{tl} \in$ {$d^{tl}{}_0$, $d^{tl}{}_1$} – duration of red light and green light.

Taking in account received data, prediction system of control centre calculates following values:

- $TR_s = \{tr_1, …, tr_n\}$ – public transport vehicles located in section $s \in SC$ of contact network, that gives possibility to exchange by electrical energy;
- $l_{tr} = f(x_{tr}, y_{tr}, x_d, y_d, M\} \in \Re$ – distance between current position of $tr \in TR_s$ and next possible crossroad or passenger stop;
- $t_{tr} = f(v, l\}$ – time moment when acceleration or braking will occur;
- $vt_{tr} = f(W, D\}$ - target speed to reach after acceleration or braking;
- $w_{tr} = f(v, v_t , t\}$ - duration of acceleration or braking;
- $A_{tr} = f(v, v_t, w_t\}$- energy should be consumed during acceleration or generated during the braking.

5. Mathematical Model of Prediction Neural Network Controller

Neural network mathematical model is based on neuron structure. Each neuron has input data set, weight for each input data, activation or transfer function and output. Neural network consists of several layers. Each layer may have definite or indefinite number of neurons. Neural networks give possibility to analyse an object by input parameter set and to detect predefined class of the object on the output. That means, neural network should be trained to detect classes and classes are predefined.

General mathematical model of neural network is following:

- Input data set for neural network: $X = \{x_1, x_2, \ldots, x_n\}$
- Set of neural network hidden layers: $L = \{l_1, l_2, \ldots, l_k\}$
- Set of neurons for each j-th hidden layer: $P^j = \{p_1, p_2, \ldots, p_r\}$
- Set of neural network outputs: $C = \{c_1, c_2, \ldots, c_m\}$
- Set of time delay for j-th layer input: $TDL^j = \{tdl_1, tdl_2, \ldots, tdl_{in}\}$
- Weights for each input of i-th neuron of j-th layer: $W_i^j = \{w_{i1}, w_{i2}, \ldots, w_{in}\}$
- Bias for each i-th neuron of j-th layer: b_i^j
- Input summation function for each i-th neuron of j-th layer: $s_i^j = \sum(W_i^j * X) + b_i^j$
- Transfer function for all neurons of j-th layer: $F^j(s^j)$

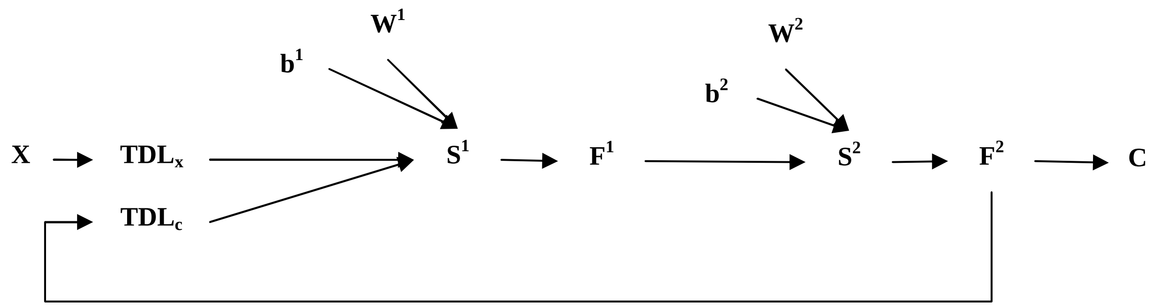

Fig. 4. Nonlinear autoregressive neural network structure

For prediction controller nonlinear autoregressive neural network (Fig. 4.) with exogenous inputs is proposed. It’s main advantage is regressive input from the output with time delay that give possibility to use it for prediction.

6. Algorithms for Public Electric Transport Control System

Algorithm of control of ESS by neural network is following. Let us assume that there is 1 tram with ESS, but all other participants are equipped by devices to send requests for

Algorithm for discharge of supercapacitor for multiple vehicles

Step 1. Getting request for use of amount A_{req} of energy for t_{req} seconds
Step 2. Predicts next speed changes $v = f(t_0, t_1)$ using prediction neural network in time interval of next $t_1 > t_{req}$ seconds
Step 3. Validate changes of speed:
If $dv/dt < 0$ then Step 4.
If $dv/dt > 0$ then refuse request.
Step 4. Calculate status of supercapacitor voltage after discharge $V_c = f(A_{req}, t_{req})$
Step 5. Validate ESS
If $V_c > 320$ and $V_c < 430$ then accept to use energy;
If $V_c < 320$ then accept to use energy until $V_c = 320$

Algorithm for charge of supercapacitor for multiple vehicles

Step 1. Getting request for give amount A_{req} of energy for t_{req} seconds
Step 2. Predicts next speed changes $v = f(t_0, t_1)$ using prediction neural network in time interval of next $t_1 > t_{req}$ seconds
Step 3. Calculate status of supercapacitor voltage after charge $V_c = f(A_{req}, t_{req})$
Step 4. Validate ESS
If $V_c > 320$ and $V_c < 430$ then accept to take all energy
If $V_c > 430$ then accept to take energy until $V_c = 430$.

7. Computer Experiment of Neural Network Training for Speed Prediction

Computer experiment of speed prediction of electric transport is based on nonlinear autoregressive neural network with exogenous inputs.

Inputs of controller are proposed as following:

$$X = \{v, s, p, l, d\},$$

where

- $v \in \Re$ - real - current speed
- $s \in \Re$ - real - distance from the beginning of the route (1D coordinate)
- $p \in [0\ 1]$ – binary - type of next speed change point (1 – stop, 0 – crossroad)
- $l \in [0\ 1]$ – binary - light of traffic light on the way (0 – red, 1 – green)
- $d \in \Re$ - real - time interval between current time and directive time

Training set for the controller is received from the model of T3A tram (Fig. 5), moving on the part of route containing 2 passenger stops and 1 traffic light.

The model is run for 3 times with different states of traffic lights and schedules. Results of modelling are saved to database and the following data set of 475 elements is received as it is shown on Table 1.

Table 1

Example of training data

v	s	p	l	d
…				
21.5108	291.788	0	0	147
21.1317	297.692	0	0	146
20.5233	306.958	1	0	145
20.1444	312.6	1	0	144
23.3609	318.458	1	0	143
27.8059	325.577	1	0	142
…				

Nonlinear autoregressive neural network with exogenous inputs network is created with following parameters:

- 2 layers
- 10 neurons with F1 = tansig(u);
- 1 neuron with F2 = tansig(u);

Created network is trained using Levenberg-Marquardt algorithm. The results of training are shown on Fig. 6 and Fig. 7.

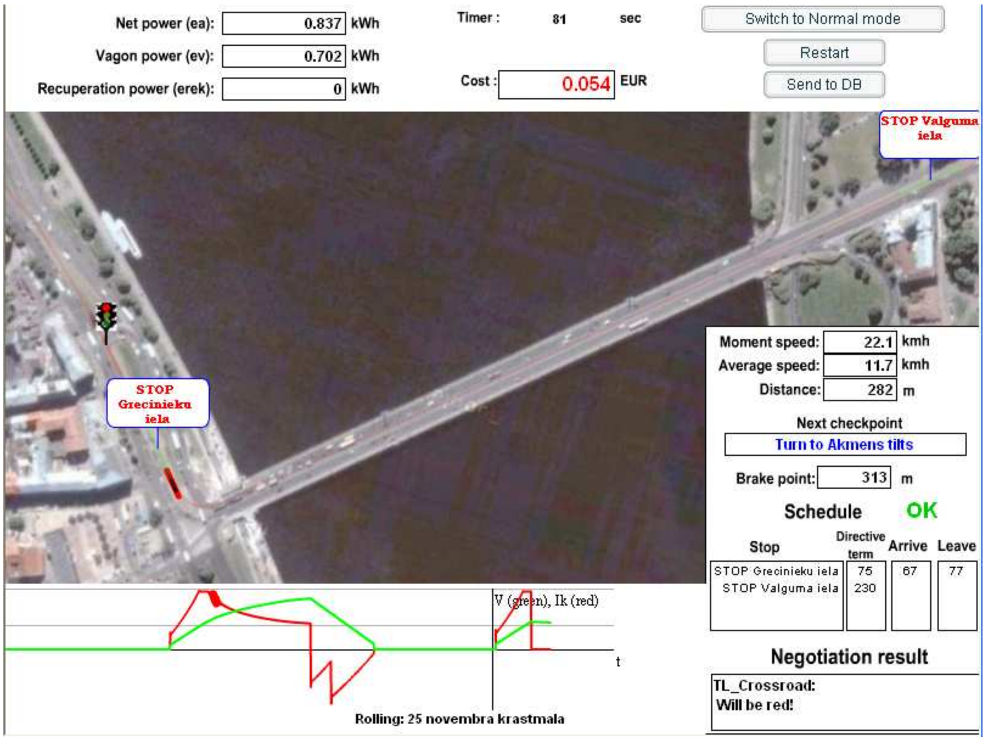

Fig. 5. Model of tram T3A route for training data collection

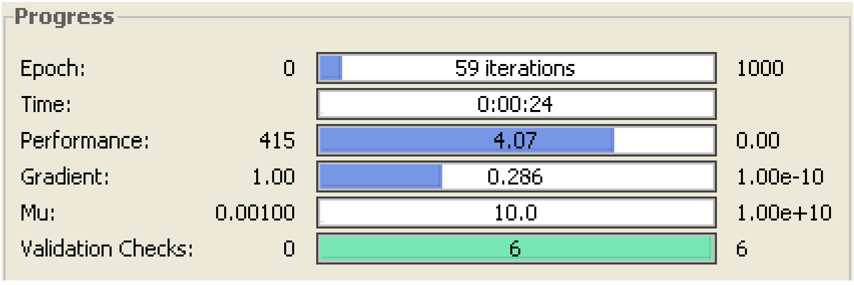

Fig. 6. Neural network training results

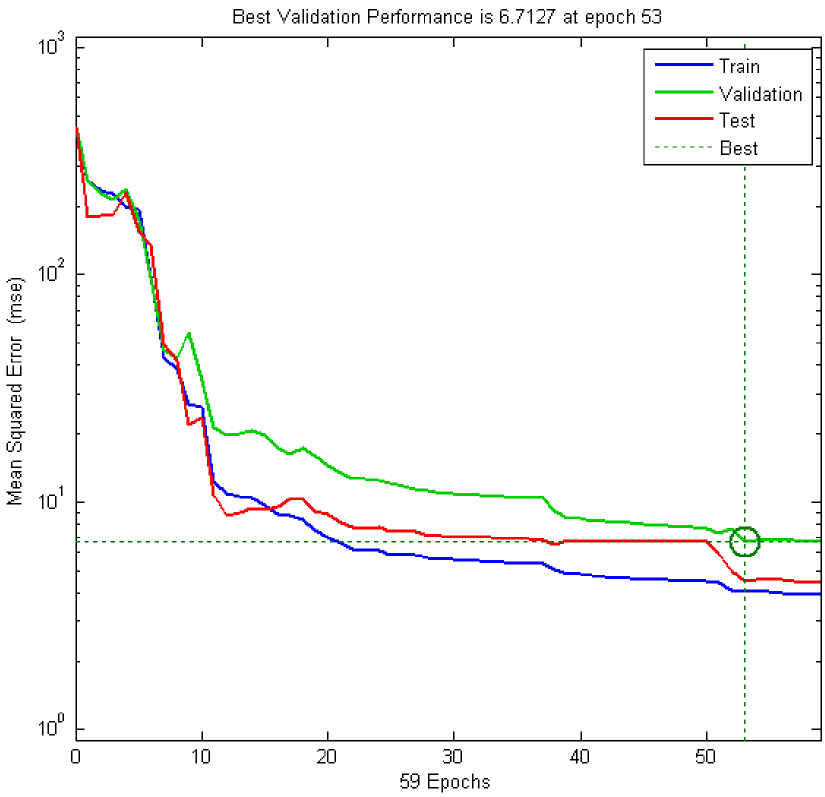

Fig. 7. Neural network training performance graph

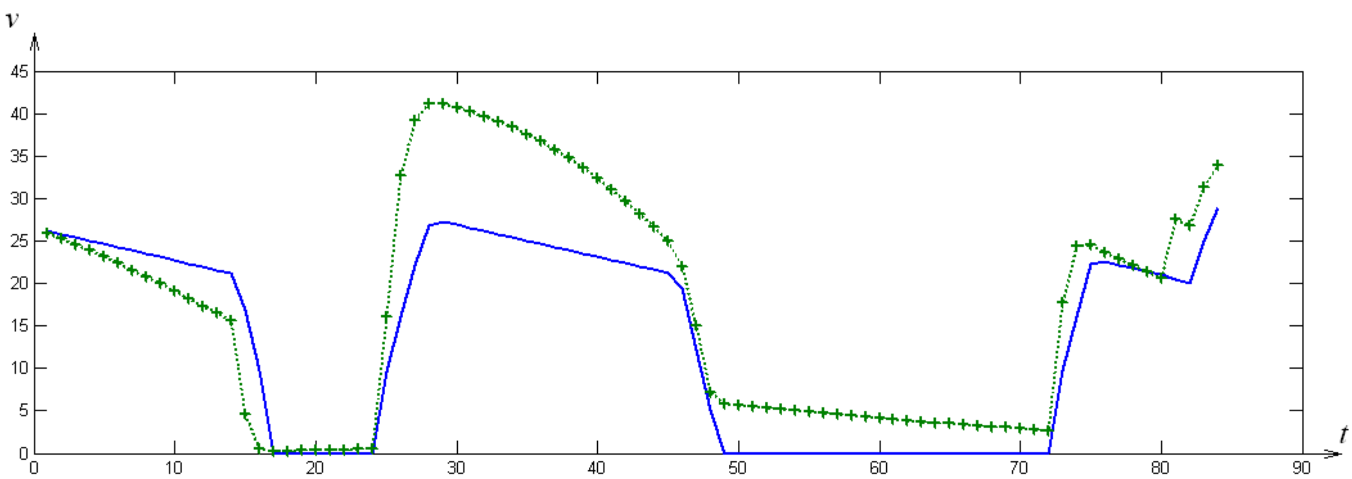

Fig. 8. Neural network training performance graph

After training test data have been generated from the model, and neural network has been simulated to predict speed changes with new data. The result of prediction is shown on Fig. 8. Speed is presented as a solid line, but speed prediction as a result of neural network controller is dotted line.

8. Conclusion

1. The independent operation of the control systems of ESS and tram traction converters makes however the operation algorithms of ESS control system complicated, which reduces its stability margin.
2. For better performance of tram driving modes and oscillation dampening it is advisable to fit the ESS control system with a speed measuring system. Synchronisation of the ESS and traction converters is recommended for brand-new tramcars with upgraded ESSs. In this case a tram's control system and ESS controller should be linked.
3. The integration of the ESS and tram controllers into the automatic traffic control and signalisation system would make possible to gather and forecast information on the braking energy amount and even manage the optimal multiple tram ESS operation.
4. Usage of neural network gives possibility to predict actions of all participants of electric transport flow and allow to use ESS more efficiently.

References

1. **Barrero R., Tackoen X., Van Mierlo J.** Analysis and configuration of super-capacitor based energy storage system on-board light rail vehicles. Proceedings of the 13th International Power Electronics and Motion Control Conference EPE-PEMC 2008, Poznan, 1-3 September 2008, p. 1535-1540.
2. **Rankis I., Brazis V.** Simulation of tramcar's energy balance. 2nd Intern. Conf. "Simulation, Gaming, Training and Business Process Reengineering in Operations", Riga, p. 160–163.
3. **Destraz B., Barrade P., Rufer A., Klohr M.** Study and simulation of the energy balance of an urban transportation network. European Conference on Power Electronics and Applications, EPE 2007, 2-5 Sept. 2007, Pages: 1 - 10 Digital Object Identifier 10.1109/EPE.2007.4417349.
4. **Latkovskis L., Bražis V.** Application of supercapacitors for storage of regenerative energy in T3A tramcars. Latvian Journal of Physics and Technical Sciences, Riga, N5, p. 23-33, ISSN 0868-8257.
5. **Sejin N., Jaeho Ch., Hyung-Cheol K., Eun-Kyu L.** PSiM based electric modeling of supercapacitors for line voltage regulation of electric train system. Power and Energy Conference, PECon 2008. IEEE 2nd International Date: 1-3 Dec. 2008, p. 855 – 859.
6. **Szenasy I.** Improvement the energy storage with ultracapacitor in metro railcar by modeling and simulation. Vehicle Power and Propulsion Conference, VPPC '08. IEEEDate: 3-5 Sept. 2008, p. 1 – 5.
7. **Rufer A.** Power-Electronic Interface for a Supercapacitor-Based Energy-Storage Substation in DC-Transportation Networks. EPE Conference proceedings Toulouse, pp. D1–D8.
8. **Barrero R., Tackoen X., Van Mierlo J.** Improving energy efficiency in public transport: Stationary supercapacitor based Energy Storage Systems for a metro network Vehicle Power and Propulsion Conference, VPPC '08. IEEEDate: 3-5 Sept. 2008, p. 1 – 8.
9. **Latkovskis L., Brazis V., Grigans L.** Simulation of On-Board Supercapacitor Energy Storage System for Tatra T3A Type Tramcars. Modelling, Simulation and Optimization, ISBN 978-953-7619-36-7. – in print.
10. **Latkovskis L., Bražis V.** Simulation of the Regenerative Energy Storage with Supercapacitors in Tatra T3A Type Trams. Proceedings of the Tenth International Conference on Computer Modeling and Simulation (UKSIM 2008), Cambridge, UK, 1-3 April 2008, pp. 398-403.
11. **J. Greivulis, A. Levchenkov, M. Gorobetz.** Modelling Of Artificial Neural Network Controller For Electric Drive with Linear Torque Load Function // In Proceedings of 7th International Conference Engineering for Rural Development 2008, Jelgava, Latvia, p. 81-87.
12. **Gorobetz M., Ribickis L., Balckars P., Greivulis J., Levchenkov A.** Method of Accident Prevention Using Intelligent Control System for Railway Transport. // In Proceedings of 6th International Conference TRANSBALTICA 2009, Vilnius, Lithuania, 2009, p. 51-56.
13. **M. Gorobetz, P. Balckars, A. Levchenkov, L. Ribickis.** Modelling of Neural Network Controller for Scheduling Task in Intelligent Transport Systems // In Proceedings of 16th International Symposium "Towards more competitive European rail system", Zilina, Slovakia, 4-5 June 2008, p. 279-289.
14. **M. Gorobetz, A. Levchenkov.** Modelling Of Artificial Neural Network Controller For Electric Drive //In Proceedings of 10th International Conference on Computer Modelling and Simulation (UKSIM), Cambridge, UK 1-3 Aprīlis 2008, p. 198-203.
15. **M. Gorobetz, A. Levchenkov**. Multiple Criteria Decision-Making Using Genetic Algorithms for Transportation Systems. //In Proceedings of International Conference on Multiple Criteria Decion-Making, January 7-12, 2008, Auckland, New Zealand.
16. **J. Greivulis, M. Gorobetz, A. Levchenkovs**. Modelling of Clustering Analysis with Special Grid Function in Mechatronics Systems for Rural Development // In Proceedings of 6th International Conference Engineering for Rural Development 2007, Jelgava, Latvija.
17. **M. Gorobetz, A. Levchenkov, L. Ribickis.** Intelligent Electric Vehicle Motion And Crossroad Control // In Proceedings of 12th International Power Electronics and Motion Control Conference. Portoroz, Slovenia, 2006, p. 1239 - 1246.
18. **I. Rankis, M. Gorobetz, A. Levchenkov.** Optimal Electric Vehicle Speed Control By Intelligent Devices. Rīgas Tehniskās universitātes raksti. Energetika un Elektrotehnika. Serija 4, Sejums 16. 2006. p. 127-137.

Proceedings of 4th International Conference ITELMS'2009

Mathematical Formulation of Public Electric Transport Scheduling Task for Artificial Immune Systems

M. Gorobetz*, I. Alps, A. Levchenkov*****

**Riga Technical University, Riga, Latvia, E-mail: mgorobetz@gmail.com*
***Riga Technical University, Riga, Latvia, E-mail: ivars.alps@rtu.lv*
****Riga Technical University, Riga, Latvia, E-mail: levas@gmail.com*

Abstract

This paper describes mathematical formulation and application of artificial immune system for scheduling tasks for public electric transport. Artificial immune system is inspired by human immune system to simulate process of interaction between antigens and antibodies. The task of scheduling in transport system is represented as a one of the most well-known flow shop problem. Artificial immune system as a genetic based method is used to solve such task. Mathematical model and algorithm is proposed to create optimal schedule for public electric transport for minimization of electric energy consumption and time. Numerical example shows several steps of algorithm for artificial immune system for scheduling task solution.

1. Introduction

Nowadays in metropolis number of vehicles is increasing day by day. It is a reason for a lot of problems for public transport, causing traffic jams, schedule violation, etc. Unexpected standing on crossroads is reason for often braking with following accelerations myriad times. This is cause for electric power overconsumption and public transport delay. To provide quick, cheap and comfortable passengers delivery with public electric transport in metropolis there was and will be topical problem. On the one hand, amount of vehicles on the streets and electricity expenses are going up day by day, traffic jams become from bad to worse, public transport stays in traffic jams longer time and use electricity increasingly, but on the other hand citizens require public transport as fast and as cheap as possible. Optimal traffic organization, traffic lights working coordination with transport moving on the routes according optimal schedule will help to solve this actual problem for any big city worldwide.

This paper describes the new application of artificial immune algorithm, to create coordinated traffic lights working schedule for optimal electric transport flow on routes. In terms of artificial immune systems, multi-criteria target function is defined as antigen. Schedules which are solutions of the problem are defined as a set of antibodies. Each antibody represents a sequence of processor to perform all operations of each vehicle on public transport route. Randomly generated schedule is evaluated according target affinity function. As genetic based methods, artificial immune systems create new population of antibodies using specific procedures as diversification, clonal proliferation and hypermutation, which imitate features of biological immune system. Processing continues until solution is found or predefined stopping criteria is achieved.

2. Problem Formulation

To organize optimal red green lighting schedule on crossroads is very important for standby time decreasing in public transport. Currently traffic lights in the Riga city are working basically separate from each other. They have not shared control system and have not coordinated red green lighting time along public transport routes.

In this paper is proposed to use immune algorithm and scheduling theory to create optimal schedule for traffic lights working time on crossroads as solution of traffic jams eliminating in the city. If traffic lights will work coordinated according optimal schedule, this could decrease electric transport standby time, eliminate often breaking and acceleration, finally save electricity.

Traffic lights electrical process and electric transport mechanic and electric process modeling are describing below. Traffic lights electrical process control model consist of logical control scheme, switches, transmitter and lamps scheme as shown in Fig. 2. Artificial immune system is proposed for traffic light control device to optimize traffic flow on the set of crossroads.

Traffic lights electrical process and electric transport mechanic and electric process modeling are describing below. Traffic lights electrical process control model consist of logical control scheme, switches, transmitter and lamps scheme as shown in Fig. 2. Artificial immune system is proposed for traffic light control device to optimize traffic flow on the set of crossroads.

Electric transport control model consists of vehicle control scheme, model of ANN and DC drive model as shown in Fig. 3. Electric transport units send signal about current location, schedule etc. to control centre. Artificial immune system of the control centre creates optimal traffic lights working schedule and through transmitter sends signal to traffic lights and in same time relevant information to vehicle's controller which accelerate or brake DC drive according received signal.

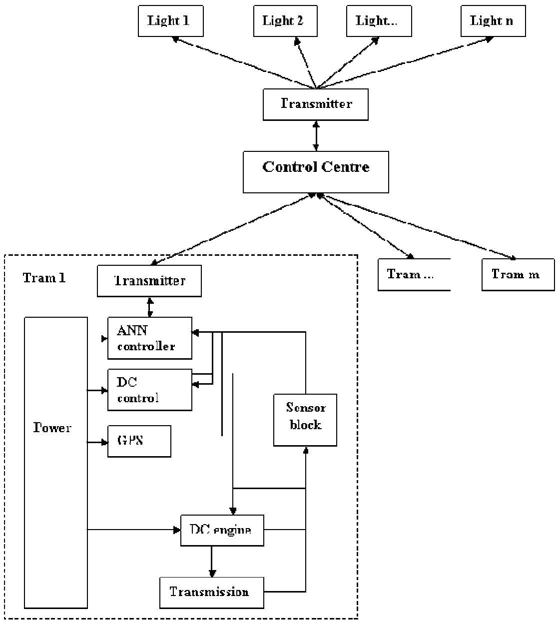

Fig. 1. Structure of intelligent control system of electric transport and traffic light

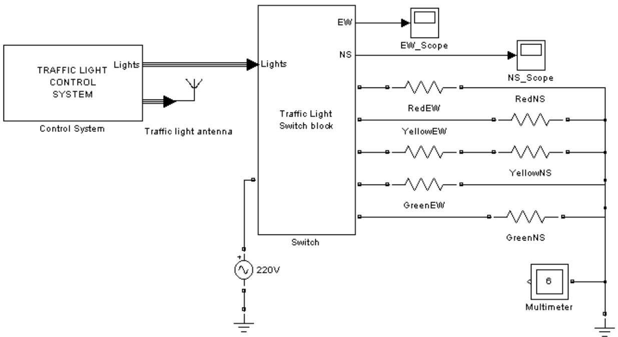

Fig. 2. Scheme of traffic lights control system

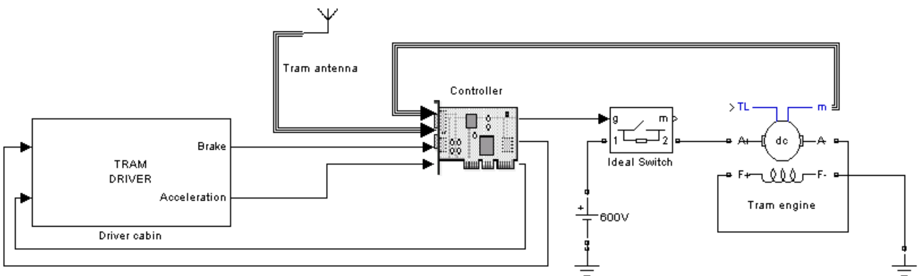

Fig.3. Scheme of intelligent transport control system

3. Mathematical Model for Artificial Immune System of Traffic Control

A. Nomenclature

Following definitions are proposed for mathematical model of artificial immune system:

– Processors – $P = \{p_1, ..., p_n\}$ - crossroads and streets;

– Jobs - $TR = \{TR_1, ..., TR_m\}$ - vehicles;

– Set of sequences - $S = \{R_1, ..., R_b\}$ routes, where
  for each route $R \in S$, $R = \{o_1, ..., o_{k_r}\}$, where
  - $k_R \le n$ - Number of operations for route r;
  - $o_i \in P$ - Processor to perform operation i;

- Set of prior operations of each route – $PR = \{0, o_1, o_2, ..., o_{k_r - 1}\}$, $PR \to R$
- Each vehicle $t \in TR$ has a route R^t assigned to it, where $R^t \in S$;
- Duration for each operation $o \in R^t$ for each vehicle $t \in TR$ $D^t = \{d_1^t, ..., d_{k_{R^t}}^t\}$, $D^t \to R^t$, $d \in D^t$, $d \in \Re$;
- Antibody – $AB = \{g_1, ..., g_q\}$ - the schedule for all vehicles, where
- $q = |R^{TR_1}| + |R^{TR_2}| + ... + |R^{TR_m}|$ - size of antibody is a number of operations in each route of each vehicle;
- $g_i = o_\alpha \in R^t$, $g_j = o_\beta \in R^t$, $i < j \Rightarrow \alpha < \beta$ - sequence of operations, which can not be disarranged for each route $R^t \in S$ of vehicle $t \in TR$
- Each gene $g \in AB$ is represented as a following tuple: $g = < tr, p, p', d >$, where
  - o tr - vehicle, which performs operation of gene *g*
  - o p - crossroad or street on which vehicle *tr*, performs operation of gene *g*;
  - o p' - prior crossroad or street, where vehicle *tr* has performed its previous operation;
  - o d - duration of operation of gene g, which performs vehicle *tr* on processor *p*.
- Each antibody $AB = \{g_1, ..., g_q\}$ is represented as a following lists combined with elements of genes tuples:
  - o $JL = \{tr_1, ..., tr_q\}$ - job list, which consists of vehicles operation of each gene in antibody;
  - o $ML = \{p_1, ..., p_q\}$ - machine list, which consists of crossroad or streets to perform operation of each gene in antibody;
  - o $PML = \{p'_1, ..., p'_q\}$ - predecessor machine list, which contains prior crossroad or street for operation of each gene in antibody;
  - o $TL = \{d_1, ..., d_q\}$ - time list, which contains duration of each operation in antibody;

- Antigen – target function
- $$\begin{cases} F = f(T, E) \to \min \\ T = f(AB) = \sum_{i=1}^{m} T_m \to \min \\ E = f(AB) = \sum_{i=1}^{m} E_m \to \min \end{cases}$$
- where
- $T(AB)$ – total time to fulfil all operations of each vehicle according to schedule AB;
- $E(AB)$ – total electrical energy consumed during fulfilment all operations of each vehicle according to schedule *AB*;
- $F(T, E)$ – multi-criteria target function, depending on T and E.

B. Parameters for Immune System

Antibody population size – z
Memory pool size - M
Replacement rate – ρ
Clonal proliferation rate – κ
Hypermutation rate – ψ
Donor rate – δ
Tournament pressure - γ
Inducing rate – λ
Diversity probability - σ
Bit number in Gene shift - θ
Bit number of nucleotide - β
Number of proliferation - η

C. Additional Conditions for Traffic Control Task

Each electric vehicle $u \in TR$ has following parameters, which depends on time t:
Current – $I_u(t)$
Torque - $\tau_u(I_u)$
Acceleration – $a_u(\tau_u)$

Deceleration – $b_u(\tau_u)$

Velocity – $v_u(a_u, b_u)$

Therefore, duration of each operation of vehicle $u \in TR$ depends on velocity v_u : $D^u = \{d_1^u(v_u),...,d_{k_{R^t}}^u(v_u)\}$.

The difference between usual flow-shop scheduling task and traffic control task is that duration of each operation is not predefined and is in functional dependency on the performance of other operations as well as criterions such as conditions of the streets surface, weather conditions, distance considering ratio among two contiguous vehicles, drivers acquirements, etc.

Due to this reason evaluation of the schedule may be solved using simulation of each result of artificial immune system for public transport system model, which takes in account following variable parameters:

- green light duration limits,
- relative number of electric transport in the traffic flow, initial street fullness,
- average length of a vehicle,
- minimal distance between vehicles in traffic jam,
- maximal speed,
- weather – clear, cloudy with rain and heavy rain with reduced visibility, that has influence on
- driver’s reaction time,
- acceleration time to maximal speed.

4. Algorithm for Artificial Immune System for Task Solution

A. General Steps of Immune Algorithm

Step 1. Random schedule initialization. According immune algorithm operation sequence, first step is random initialization of possible antibody (schedule) population.

Generate initial population $G^0 = \{AB_1, AB_2,..., AB_z\}$, where $AB_i = \{g_1^i,..., g_q^i\}$,

$g_j^i = rand(R^{TR_1} \cup R^{TR_2} \cup ... \cup R^{TR_m})$, $g_j^i \neq g_k^i$,

$i = \overline{1, z}, \quad j, k = \overline{1, q}$

Step 2. Procedure for simulation of transport system according to schedule. The results of simulation is total time and total energy spent by all vehicles according to schedules:

$\exists AB \in G^0, \quad T(AB_i), \quad E(AB_i), \quad i = \overline{1, z}$

Step 3. Evaluation of schedule affinity to target function.

Each schedule is evaluated by target function using results of simulation

$\exists AB \in G^0, \quad F_i(T(AB_i), E(AB_i)), \quad i = \overline{1, z}$

Step 4. Clonal proliferation of the most matched schedule. In the IA scheme, the most matched (Maximum affinity value) schedule derived from the earlier step is chosen for hypermutation after clonal proliferation process.

Step 4.1. Selecting schedule with best affinity for clonal proliferation: $F^*(AB^*) = \max(F_1(AB_1),..., F_z(AB_z)) \Rightarrow AB_0^*$

Step 4.2. Proliferating selected schedule AB_0^* according to proliferation number:

$CP = \{AB_1^*, AB_2^*,..., AB_\kappa^*\}$, $AB_i^* = AB_0^*, \quad i = \overline{1, \kappa}$

Step 4.3. Light chain hypermutation in each schedule

Step 4.4. Simulation of hypermutated schedules

Step 4.5. Affinity evaluation for each hypermutated schedules

Step 4.6. Preliminary donor schedule set creation

Step 4.7. Memory pool update

Step 5. Tournament selection for donor schedule. Several schedules according to the predefined tournament size are chosen randomly for competition with the surviving winner being turning into a donor schedule.

Step 5.1. Select schedules from preliminary donor schedule set

Step 5.2. Tournament stage

Step 5.3. If defined number of schedules is selected, than finish, else go to step 5.2

Step 6. Germ-line DNA library construction. In IA components from the memory schedules and the donor schedules construct the germ-line DNA library.

Step 7. Gene fragment rearrangement. In IA new schedules are created via gene fragments rearrangement process.

Step 8. Schedule diversification. Matching a large variety of antigens/tasks requires an equal level of diversity in schedule type. In the IA this was achieved by mimicking the following six diversification mechanisms.

point mutation
recombination
conversion,
inversion
shift
nucleotide addition

Step 9. Stop criterion. The whole process will stop when the generation equals to a pre-defined number. Otherwise the process reverts to Step 2 for iteration. Finally the best and most diverse solutions are stored in the memory pool.

Numerical example is proposed to show several steps of immune algorithm for scheduling of traffic light. Therefore this example is simplified and duration of each operation is constant.

Let us assume that three crossing streets are given as shown in Fig. 4. Streets are split into parts with two types such as crossroads C2 and C4 and parts of the streets between crossroads S1, S3, S5, S6, S7, S8, S9. Three public electric transport routes are given and three electric transport vehicles TR1 TR2 and TR3 moving by these routes.

The task is to create optimal traffic lights working schedule for crossroads C2 and C4 to minimize total time spent by all vehicles to complete their routes.

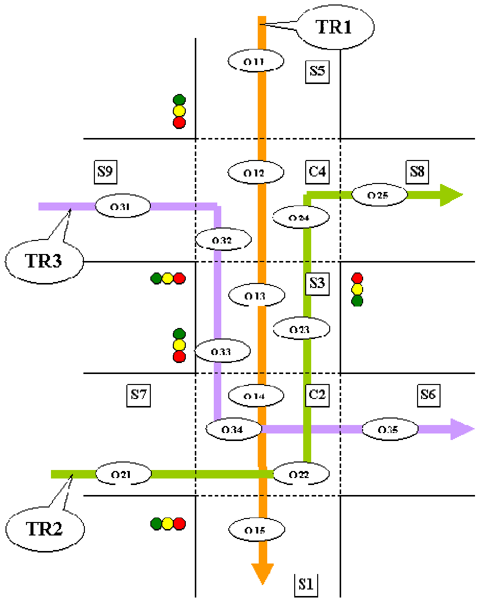

Fig. 4. Vehicles moving directions and streets scheme

According scheduling theory terms,

Processors – S1,S3,S5,S6,S7,S8,S9 and C2,C4; streets and crossroads

Jobs – TR1, TR2, TR3

Each job has 5 operations – routes

O(TR1)={o11, …, o15} and ML(TR1)={S5,C4,S3,C2,S1} where operation o11 is processed by S5, etc.

O(TR2)={o21,…,o2,5} and ML(TR2) = {S7,C2,S3,C4,S8} where operation o21 is processed by S7, etc.

O(TR3)={o31,…,o35} and ML(TR3) = {S9,C4,S3,C2,S6} where operation o31 is processed by S9, etc.

Operations sequence for transport units are shown in Table 1.

Table 1

Order	O1	O2	O3	O4	O5
TR1	5	4	3	2	1
TR2	7	2	3	4	8
TR3	9	4	3	2	6

This operations passing duration are shown in Table 2.

Table 2

Duration	O1	O2	O3	O4	O5
TR1	6	6	5	2	3
TR2	4	1	7	2	6
TR3	5	2	3	4	7

As shown in Fig. 4, C2 and C4 are crossroads and therefore they have restrictions. Through P2 simultaneously can move vehicles coming from S3 and S1, but vehicles coming from S3 and S7 moving in same time is restricted. Similar restrictions are for crossroad C4. Through C4 simultaneously can move vehicles coming from S3 and S5, but can't move vehicles coming from S3 and S9. Set of „friendly" and „conflict" operators are shown in Table 3.

Table 3

S2	**3**	**1**	<>	**7**	**6**
S4	**3**	**5**	<>	**9**	**8**

Step 1. According immune algorithm operation sequence, first step is random initialization of possible antibody (schedule) population. Schedule contains n*m genes for *n* transport units and m operations. In this task schedule contains 15 genes and randomly generated four schedules AB1, AB2, AB3 and AB4 as shown in Table 4. Each transport unit appears in the schedule *m* times.

Table 4

RANDOMLY GENERATED SCHEDULES

AB1	1	2	3	3	2	2	1	1	3	2	1	3	1	2	3
AB2	1	1	1	1	1	3	2	2	2	2	2	3	3	3	3
AB3	2	2	3	3	1	1	2	1	3	3	2	1	1	2	3
AB4	1	2	1	3	3	2	3	1	3	2	3	2	1	2	1

Step 2. Next step is to create related machine list (ML) for each schedule. Related machine lists and corresponding passing time lists (TL) are shown in. and Table 6.

Table 5

RELATED MACHINE LIST

ML1	5	7	9	4	2	3	4	3	3	4	2	2	1	8	6
ML2	5	4	3	2	1	9	7	2	3	4	8	4	3	2	6
ML3	7	2	9	4	5	4	3	3	3	2	4	2	1	8	6
ML4	5	7	4	9	4	2	3	3	2	3	6	4	2	8	1

Table 6

RELATED TIME LIST

TL1	6	4	5	2	1	7	6	5	3	2	2	4	3	6	7
TL2	6	6	5	2	3	5	4	1	7	2	6	2	3	4	7
TL3	4	1	5	2	6	6	7	5	3	4	2	2	3	6	7
TL4	6	4	6	5	2	1	3	5	4	7	7	2	2	6	3

Table 7

PREDECESSOR MACHINE LIST

PML1	0	0	0	9	7	2	5	4	4	3	3	3	2	4	2
PML2	0	5	4	3	2	0	0	7	2	3	4	9	4	3	2
PML3	0	7	0	9	0	5	2	4	4	3	3	3	2	4	2
PML4	0	0	5	0	9	7	4	4	3	2	2	3	3	4	2

According restrictions is created predecessor machine list, set of previous operators, which from TR1, TR2 and TR3 are coming. Predecessor machine list dates are use calculating value of makespan. Predecessor machine list is shown in Table 7.

$$AB_i = \frac{obj_i}{SC_i} \quad \text{and} \quad obj_i = \frac{\min\{makespan_i \mid i = 1,2\ldots, N_{Ab}\}}{makespan_i}$$

where $makespan_i$ indicates makespan value of the i^{th} schedule and obj_i is its associated normalized value. To find value min makespan are necessary create Gantt chart for each schedule. As shown in Table 8 min makespan to operate schedule complete is 24 seconds.

Table 8

MIN MAKESPAN CALCULATING

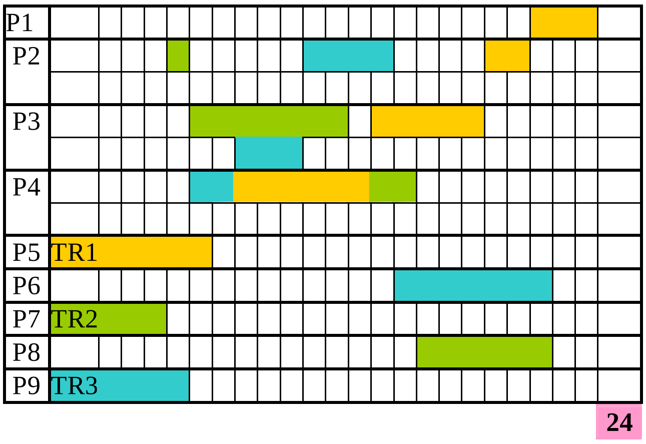

The relationship among schedules is evaluated according to the similarity count SCi expressed as

$$SC_i = \frac{\sum_{j=1}^{N_{Ab}} count_{ij}}{N_{Ab}}, \; i, j = 1,2,\ldots, N_{Ab};$$

with

$$count_{ij} = \frac{\sum_{k}^{nm} Ab_{ij}^{k}}{n*m}$$

where the similarity count at the k locus among schedules Ab_i and Ab_j is expressed as

$$AB_{ij}^{k} = \begin{cases} 1 \text{ if the jobs at the k locus of } Ab_i \text{ and } Ab_j \text{ are identical} \\ 0 \text{ else} \end{cases}$$

Ab_{ij}^{k} calculating results, values of $count_{ij}$ are shown in Table 9. Values of obj_i and Ab_i are shown in Table 10.

Table 9

ABIJK CALCULATING AND VALUES OF COUNTIJ

Ab similar																sum	count
AB1#AB2	1	0	0	0	0	0	0	0	0	1	0	1	0	0	1	4	0.266667
AB1#AB3	0	1	1	1	0	0	0	1	1	0	0	0	1	0	1	7	0.466667
AB1#AB4	1	1	0	1	0	1	0	1	1	1	0	0	1	1	0	9	0.6
AB2#AB3	0	0	0	0	1	0	1	0	0	0	1	0	0	0	1	4	0.266667
AB2#AB4	1	0	1	0	0	0	0	0	0	0	0	0	0	0	0	2	0.133333
AB3#AB4	0	1	0	1	0	0	0	1	0	0	0	0	1	1	0	5	0.333333

Table 10

VALUES OF OBJI AND ABI

	SC	obj	AgAb
SC1	0.333333	0.96	2.88
SC2	**0.166667**	**0.77**	**4.62**
SC3	0.266667	1	3.75
SC4	0.266667	0.83	3.1125

A higher affinity means that the schedule has a higher activation with an antigen ant a lower similarity with the other schedules. Consequently, highest affinity has second populated schedule AB2.

5. Conclusions

Application of artificial immune algorithm in scheduling tasks show great promise. To solve multi-criteria scheduling problem for public electric transport flow optimization with artificial immune algorithm application is plan for nearest future and expecting goal of this investigation is decreasing make span time.

Create mathematical formulation and investigate immune algorithm application for scheduling tasks conclusions for the present are:

- On biological immune system based artificial immune algorithm can be applied to create coordinated optimal traffic lights working schedule
- Transport flow optimization tasks solving result mostly will approximate, due to several transport flow dependent criterions could not be defined unequivocal
- Artificial immune algorithm can be applied to solve multi criteria transport flow optimization tasks
- Coordinated optimal traffic lights working schedule can be applied for minimize electricity consumption and tasks for transport units standby time decreasing.

References

1. **L. Ribickis, M. Gorobetz, A. Levchenkov.** Intelligent Electric Vehicle Motion And Crossroad Control // In Proceedings of 12th International Power Electronics and Motion Control Conference. Portoroz, Slovenia, 2006, p. 1239 - 1244.
2. **J. Greivulis, A. Levchenkov, M. Gorobetz**. Modelling Of Artificial Neural Network Controller For Electric Drive with Linear Torque Load Function // In Proceedings of 7th International Conference Engineering for Rural Development 2008, Jelgava, Latvia, p. 81-87.
3. **I. Rankis, M. Gorobetz, A. Levchenkov.** Optimal Electric Vehicle Speed Control By Intelligent Devices. Rīgas Tehniskās universitātes raksti. Enerģētika un Elektrotehnika. Sērija 4, Sējums 16. 2006, p. 127-137.
4. **M. Gorobetz, A. Levchenkov**. Evolutionary Algorithms and Dynamic Parameters for Public Electric Transport Modeling // In Proceedings of 16th Mediterranean Conference on Control and Automation, Ajaccio, France, 25-27 June 2008, p. 215-219.
5. **M. Gorobetz, A. Levchenkov.** Modelling of Stochastic Parameters for Control of City Electric Transport Systems Using Evolutionary Algorithm // In Proceedings of International Workshop on 22th European Conference on Modelling and Simulation, Nicosia, Cyprus, 3-6 June 2008, p. 207-212.
6. **A. Levchenkov. M. Gorobetz.** Multiple Criteria Decision-Making Using Genetic Algorithms for Transportation Systems // In Proceedings of International Conference on Multiple Criteria Decion-Making, January 7-12, 2008, Auckland, New Zealand, 41 p.
7. **M. Gorobetz, P. Balckars, A. Levchenkov, L. Ribickis**. Modelling of Neural Network Controller for Scheduling Task in Intelligent Transport Systems // In Proceedings of 16th International Symposium „Towards more competitive European rail system", Zilina, Slovakia, 4-5 June 2008, p. 279-289.
8. **M. Gorobetz.** Research of Genetic Algorithms For Optimal Control of Electric Transport. Doctorate work, 2008, 189 p.
9. **P. Musilek, A. Lau, M. Reformat, L Wayard-Scott**. Immune programming // Proceedings of Elsiever information sciences 179, 2006, p. 972-1002.
10. **Guan-Chun Luh, Chung-Huei Chueh**. multi-modal immune algorithm for the job-shop scheduling problem // Proceedings of Elsiever information sciences 179, 2009, p. 1516-1532.

Proceedings of 4th International Conference ITELMS'2009

Modeling of Electric Engine Starting and Electric Transport Uniform Motion

M. Gorobetz*, A. Levchenkov, V. Skopis*****

**Riga Technical University, Riga, Latvia, E-mail: mgorobetz@gmail.com*
***Riga Technical University, Riga, Latvia, E-mai: levas@gmail.com*
****Riga Technical University, Riga, Latvia, E-mail: vskopis@gmail.com*

1. Introduction

This article describes the electric motor operations (here its launch, the vehicle acceleration to optimal velocity and further uniform motion). The model can be related to different means of electric transport, such as tram, trolley-bus and electric train. The author already regarded modeling electric motor with the help of Simulink in a previous article, but here attention is paid to a new Simulink extension – Simscape that combines electrical, mechanical, hydraulic, physical signal and thermal blocks, among which the author is interested in electrical and mechanical blocks, so this article is about modeling electromechanical system, which is enclosed into mechatronics, where control is also integrated, and this control will be modeled in continuation and described in the author's further articles. Blocks of Simscape which help to simulate operation of an electric motor and to show its parameters on scopes are regarded in this article.

2. Problem Formulation

The purpose of this work was to simulate electric motor which converts electrical energy into mechanical that helps to move electrical vehicle, e.g. tram. This motion had to be shown on a chart. In our real live electric motors have rotating parts (rotors), so rotational motion is going on there. This rotation should be converted into vehicle's motion, so, the vehicle's wheels have to rotate to get translational motion of the object. The change of this motion parameters has to be shown on the screen in order to understand the processes going on while operating the motor and to see what happens if the motor is controlled using different signals which will be realized in further works because the motor should not only be launched, but also it has to be controlled as any mechatronic system combines not only electromechanical components, but also control blocks. But the task of concrete work was to model electrical energy into motion of a vehicle and to show this motion.

3. Methods of Solution and Mathematical Formulation

a) Used formulas:

Voltage value of the resistor dependence on current and active resistance values	$U = IR$
Voltage value of the inductive element dependence on current and inductance values	$U = L\dfrac{di}{dt}$
Force value dependence on current and constant of proportionality values	$F = KI$
Voltage value dependence on velocity and constant of proportionality values	$U = Kv$
Rotational torque value dependence on current and constant of proportionality values	$M = KI$
Voltage value dependence on angular velocity and constant of proportionality values	$U = K\omega$
Force value dependence on velocity derivative time and constant of proportionality values	$F = m\dfrac{dv}{dt}$
Rotational torque value dependence on angular velocity derivative time and constant of proportionality values	$M = J\dfrac{d\omega}{dt}$
Rotational torque value dependence on radius of the wheel, force and mechanism orientation indicator	$M = r\,F\,o_r$
Velocity value dependence on radius of the wheel, angular velocity and mechanism orientation indicator	$v = r\,\omega\,o_r$
Force value dependence on damping (viscous friction) coefficient and velocity values	$F = Dv$
Relative velocity dependence on absolute velocities of terminals *R* and *C* values	$v = v_R - v_C$
Rotational torque value dependence on damping (viscous friction) coefficient and angular velocity values	$M = D\,\omega$
Relative angular velocity dependence on absolute angular velocities of terminals *R* and *C* values	$\omega = \omega_R - \omega_C$

b) Symbols:

U – Voltage, V (volt)
I – Current, A (ampere)
R – Resistance, Ω (Ohm)
L – Inductance, H (Henry)
t – Time, s (second)
F – Force, N (Newton)
v – velocity/relative velocity, m/s (meter per second)
K – Constant of proportionality
M – Rotational torque, N·m (Newton per meter)
ω – angular velocity/relative angular velocity, rad/s (radian per second)
m – Mass, kg (kilogram)
J – Inertia, kg·m^2 (kilogram per square meter)
r – Radius of the wheel, m (meter)
o_r – Mechanism orientation indicator. The variable assumes +1 value if axle rotation in the globally assigned positive direction is converted into translational motion in positive direction, and –1 if positive rotation results in translational motion in negative direction.
D – Damping (viscous friction) coefficient, N·s/m - in translational motion, N·m·s/rad - in rotational motion
v_R, v_C – absolute velocities of terminals R and C, respectively, m/s (meter per second)
ω_R, ω_C – absolute angular velocities of terminals R and C, respectively, rad/s (radian per second)

The scheme operation is described then.

4. Scheme Operation

Firstly the working scheme is made.

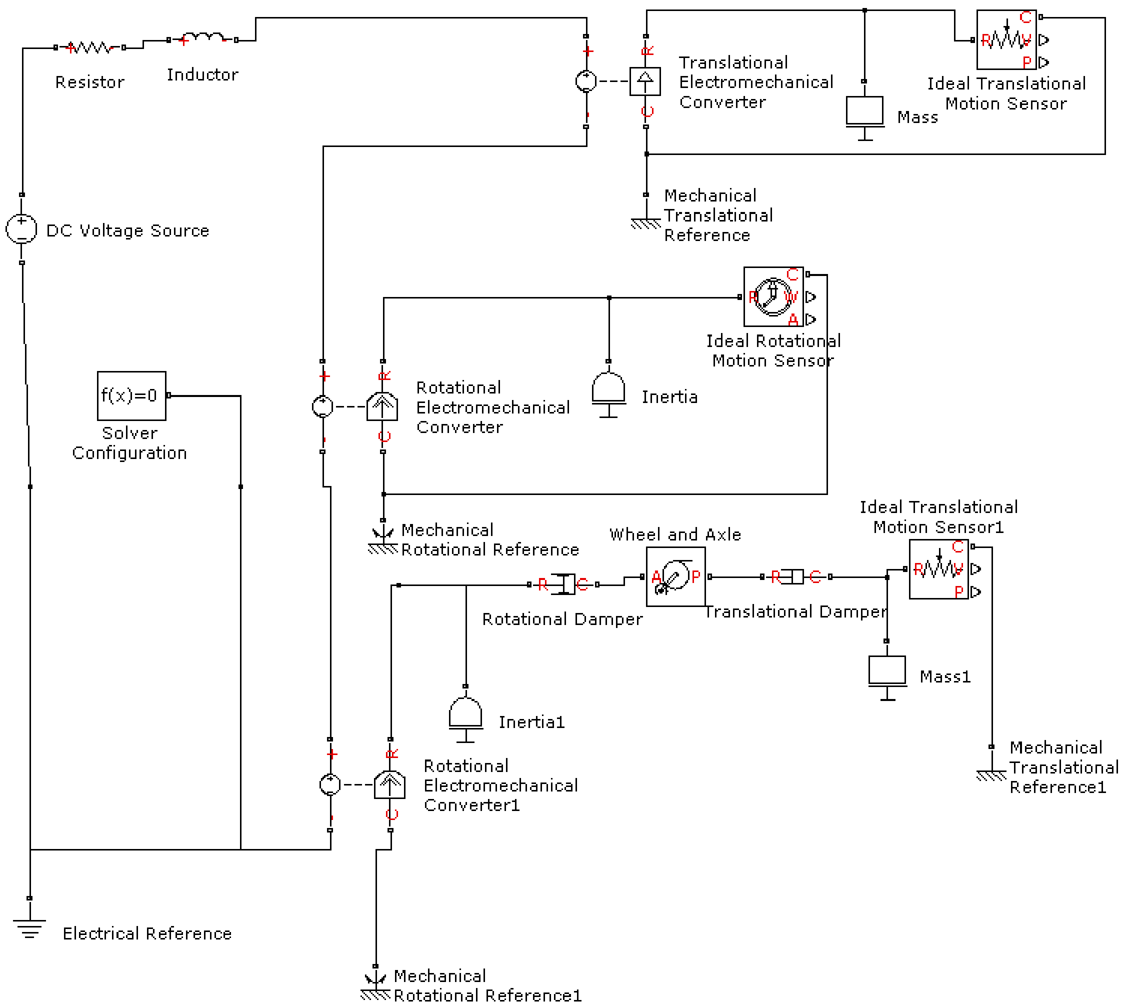

Fig. 1. Working scheme

Electric motor which is examined in the model is equivalently replaced with Simscape blocks *Resistor* (representing active resistance) and *Inductor* (representing inductance). To covert electrical energy into mechanical blocks *Translational Electromechanical Converter* and *Rotational Electromechanical Converter* are used. To model load blocks *Mass* (for translational motion) and *Inertia* (for rotational motion) are connected to the motor. It is an opportunity for both blocks to set not only the load value, but also initial velocity. To show the change of the vehicle's velocity and position according to time block *Ideal Translational Motion Sensor* is used (the opportunity to set the object's initial position is available). To show the change of rotational motion parameters (angular velocity and angular position) *Ideal Rotational Motion Sensor* is used. To show all this with the help of element *Scope* which is the block of Simulink core, the physical signal taken from Simscape blocks is converted into Simulink signal using *PS-Simulink Converter*. *Solver Configuration* block is connected to the scheme because it is necessary for the usage of Simscape elements in the simulation. There are also used electrical and mechanical Simscape blocks which represent ground in the scheme - *Electrical Reference, Mechanical Translational Reference* and *Mechanical Rotational Reference.*

In first two cases two types of mechanical motion are simulated: translational motion and rotational motion. The parameters of rotational motion are analogical to translational motion. Angular velocity (rad/s) is analogical to velocity (m/s), angular position (rad) is analogical to position (m). So, the charts representing the changes of parameters of both types of motion should be similar.

Translational and rotational motion charts:

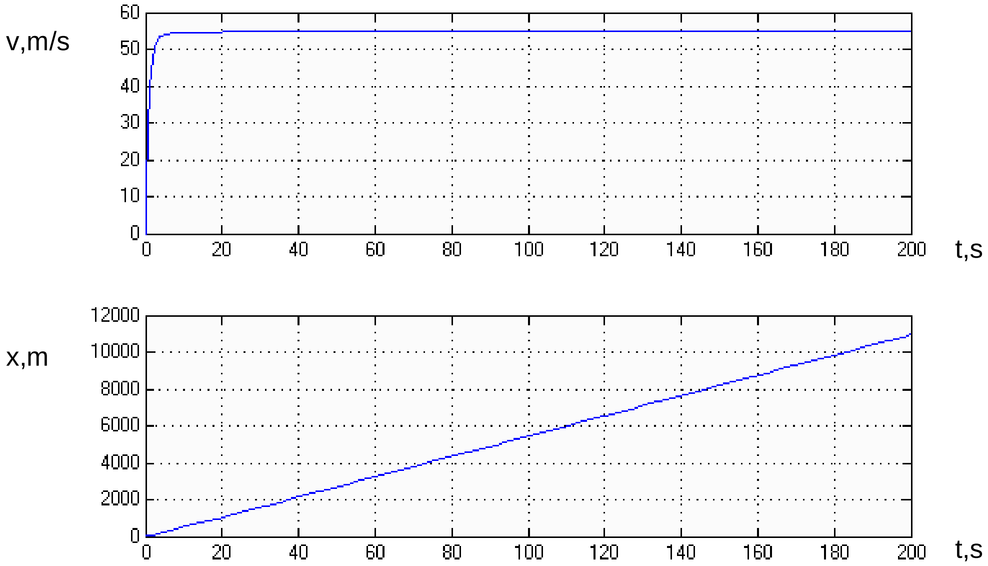

Fig. 2. Translational motion charts

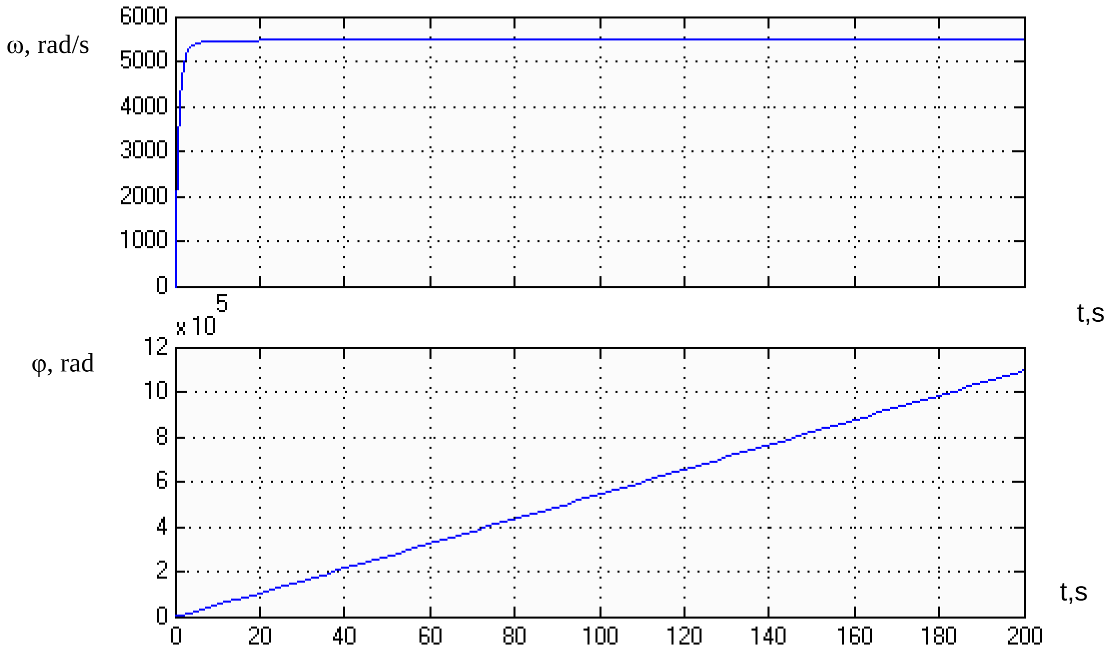

Fig. 3. Rotational motion charts

Charts of both types of motion show that velocity (in translational motion) and angular velocity (in rotational motion) are changing for some short time period before reaching a constant value, which is the uniform velocity of the tram (in translational motion) or the uniform angular velocity of the motor rotation (in rotational motion) – so, uniform motion is held. The uniform change of position (angular position) also shows that the motion is uniform, the diagram has to be a straight line. As the simulation time is rather long (here 200 seconds) in comparison to time in which uniform velocity is reached, the graphs of position change are straight lines in this work.

So, the graphs of translational and rotational motion are similar in their forms, but differ in parameter's physical sense (they are analogical) and in their numerical values.

Also rotational motion conversion into translation motion is simulated in this work. Block *Wheel and Axle* is used for this purpose. Dampers (*Rotational Damper, Translational Damper*) are used to simulate viscous friction. As there are more some different loads connected to the motor and friction is used, the tram has to cope with larger counterforce to reach the uniform velocity and this velocity is less if the load is larger because this speed is limited by the motor power. That is why the change of position according to time during longer period is not uniform (the graph during this period should be parabolic).

Lower the charts for the point where rotational motion is changed into translational motion using dampers are presented (the first chart is velocity change, the second – the change of position).

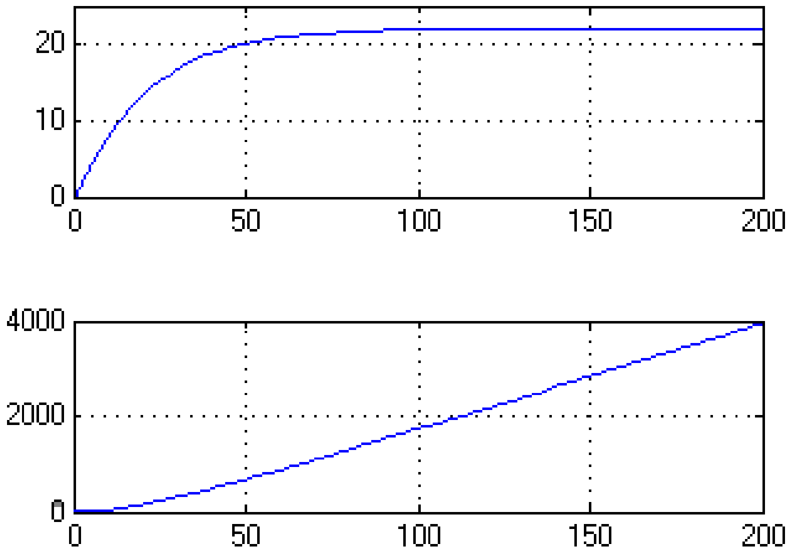

Fig. 4. Charts of motion, converting rotational motion into translational, using dampers

As it is shown on charts, velocity doesn't reach the constant value at once, but it takes rather long time to reach it because of larger load and the presence of friction. This happens in real life too as the motor has to reach the nominal rotational velocity after launch overcoming friction. The constant linear velocity also is less as the force is the same but the load is larger. The change of position is parabolic at first, but when the velocity becomes constant (v=const) the graph of position change is approximately a straight line as it has to be during uniform motion. (But the position reaches less value in the same time than in the first case where simple translational motion is researched).

5. Conclusions

As this work has shown, electrical and mechanical parts are easily combined, and this is electric transport operating principle. Modeling of electric transport motion also showed that vehicles, for example, trams, don't reach their uniform (average) velocity after starting at once, but some time is necessary to reach it. This time depends on load which is connected to the motor (in our case the tram with driver and passengers) and friction both in rotating mechanisms and between wheels and ground. This is going on in real time as it has been shown in the model (using the charts representing the motion processes). The change of tram's position is proportional to time and velocity (if the motion is not uniform – to initial velocity and acceleration) and this is seen on charts. So, the results we have got after modeling coincide with theory and practice.

References

1. **L. Ribickis, A. Ļevčenkovs, M. Gorobetz**. Sistēmu teorijas pamati industriālās elektronikas modelēšanā. -Rīga: RTU, 2008, 102 p.
2. **Дьяконов В. П.** Simulink 5/6/7. -М.: ДМК-Пресс, 2008. 784 с.
3. **Дьяконов В. П., В. В. Круглов.** Matlab 6.5 SP1/7/7 SP1/7 SP2 + Simulink 5/6. Инструменты искусственного интеллекта и информатики. – М.: Солон-Пресс, 2006, 456 с.

4. **Герман-Галкин С. Г.** Компьютерное моделирование полупроводниковых систем в MATLAB 6.0 – СПб.: Корона Принт, 2001. - 320 с.
5. **Б. Я. Лурье, П. Дж. Энрайт**. Классические методы автоматического управления . – СПб. : БХВ-Петербург, 2004. - 624 с.
6. **L. Ribickis, Jю Valeinis**. Elektriskā piedziņa mehatronikas sistēmās. – Rīga: RTU, 2008. Apjoms 286 p.
7. J. Dirba, K. Ketners. Elektriskās mašīnas. – Rīga: RTU, 2007. Apjoms 517 p.
8. **Вольдек А. И.** Электрические машины Ленинград : Энергия. Ленингр. отд-ние, 1974. – 839 с.
9. **Zviedris A.** Elektriskās mašīnas. - R: Zvaigzne, 1984. – 367 p.

Proceedings of 4th International Conference ITELMS'2009

Cycle Strength of Cast Stainless Steel 08Cr18Ni10NiTi

B. Timofeev*, S. Timofeeva*, Z. Bazaras**

**CentalResearch Institute of Structural Materials "Prometey", 49 Shpalernaya str, 191015 St. Petersburg, Russia, E-mail: prometey@pop3.rcom.ru*
***Kaunas University of Technology Panevezys Institute, Daukanto str. 12, LT–35212 Panevezys, Lithuania. E–mail: Zilvinas.Bazaras@ktu.lt*

Abstract

Experimental data on low cycle fatigue and fatigue crack growth rate of cast stainless steel type 08Cr18Ni10NiTi and also the values of the limit of this material endurance at room and elevated temperatures on the basis10^7 cycles are submitted. It is shown, that fatigue strength in the range of endurance from 10^2 to 10^8 cycles for cast steel is less, than at deformed (forging, plate, tube) metal of same composition.
KEY WORDS: *cast, cycle strength, stainless steel, endurance, values of the limit, fatigue, crack growth rate.*

1. Introduction

High alloyed stainless steels are used in the nuclear industry at creation of the main equipment of pipelines of the nuclear power plant (NPP) as various semi-products (plate or sheet, forging, cast, tube). These materials possess high plastic properties (elongation, reduction of area, impact strength), however after prolonged operation at the elevated temperatures can be embrittlement by thermal ageing [1]. First of all it concerns to semi-products from the cast steel with austenite and ferrite microstructure. The amount of ferrite in a microstructure is limited 10-20% that is effective means of the prevention cracks in metal.

A lot of works for Cr-Ni steel of domestic and foreign researchers is devoted to studying of processes of thermal ageing. This theme is rather actual especially for the equipment of the NPP, which long time is exposed to influence of the elevated temperatures. The urgency of such works is connected to change of mechanical properties at operation and first of all with decreasing of plasticity and impact strength of metal with austenite-ferrite microstructure. On change of impact strength in the majority of works the estimation of propensity such steel to thermal embrittlement also is made.

2. Tensile Strength

Cast semi-products from stainless steel are used for units of valves and pumps of the NPP. The composition of a cast material is chosen so that in a microstructure containing basically austenite, there was such minimum quantity of δ-ferrite which would allow improving foundry properties of a material, weld ability and plastic properties. The common contents of δ-ferrite in not stabilized cast stainless steel is usual less, than 20%, and for the stabilized cast stainless steel - are less, than 10%. For not stabilized stainless steel degradation of mechanical properties takes place at long ageing in conditions of operational temperatures for the atomic power station about 250°C. Degradation occurs owing to disintegration spinoidal formations in δ- ferrite to a phase, result of that is increase of hardness of δ-ferrite and reduction in viscosity of a material as a whole. Researches have shown that degradation of mechanical properties owing to disintegration formations can be restored at short-term annealing at 550°C (one hour). Properties of cast stainless steels at long operation can change also because of growth carbides and/or nitrides, is especial on borders аустенита with d-ferrite and in the δ-ferrite, and also at allocation of the G-phase rich with harmful impurity. However in the References there is an insufficient amount of the data describing behaviors cast stabilized corrosion-proof austenite steel at thermal ageing. Believe that degradation of mechanical properties of cast preparations from this steel at long operation in conditions of the atomic power station is less, than not stabilized because of the smaller contents of δ-ferrite.

3. Cyclic Strength

Investigation of fatigue strength of cast stainless steel was spent on a complex cast semi-products, external and which internal diameter were 750 and 140 mm accordingly and height 350 mm. The level of mechanical properties for cast in an initial condition were UTS = 480 MPa, YS = 250 MPa, EL = 41%, RA = 61% at 20°C and UTS = 345 MPa, YS = 180 MPa, EL = 58%, RA = 30% at 350°C. The submitted values of properties corresponded to the requirement Tu-108.17.1039-79. After thermal ageing at 400°C during 3000 h the level of properties practically has not changed in comparison with initial metal of casting after heat treatment at 1100°C with cooling on air (austenization). For the investigated metal resistance of low cycle fatigue in a range of durability of 10^2-10^4 cycles has been appreciated at 20 and 350°C, and also the limit of endurance is determined on the basis of 10^7 cycles at the same temperatures. Experimental data are presented in Fig. 1.

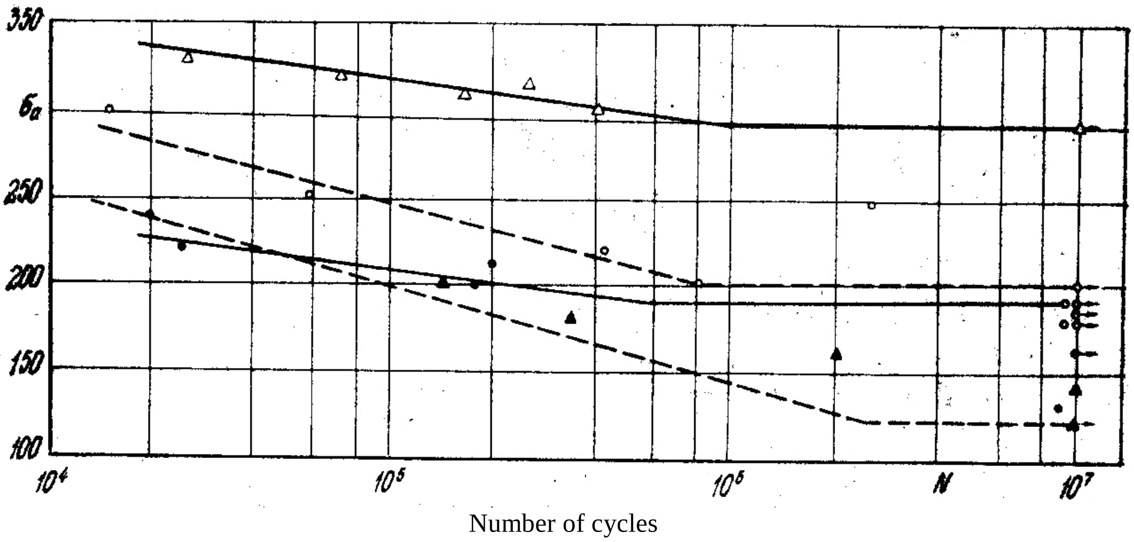

Fig. 1. Cyclic strength of 08Cr18Ni10Ti in air at 20°C (Δ, o) and 350°C (Δ,•): solid line – plate, dashed line – cast

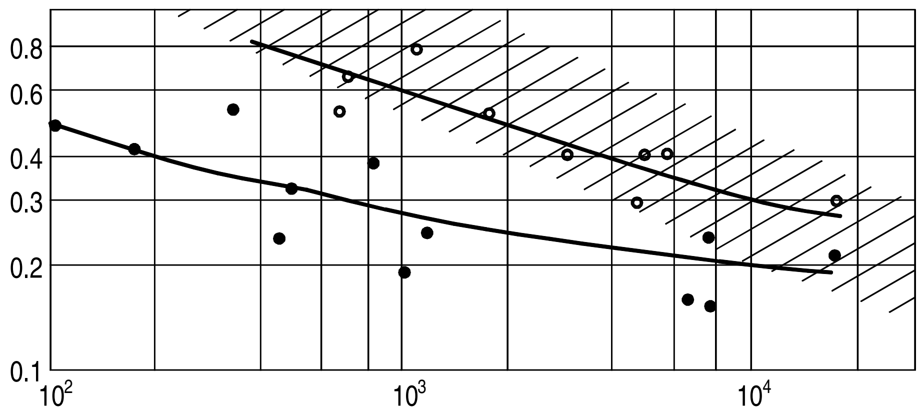

Fig. 2. Low cycle fatigue of 08Cr18Ni10Ti steel cast at 20 (o) и 350 (•): scatter band for the deformed metal is shaded

As strength properties at ageing change insignificantly also the limit of endurance of cast metal in both conditions appeared practically identical and equal 200 MPa at 20^{o}C and 120 MPa at 350^{o}C. For the deformed stainless steel approximately with the same level of a yield strength Weller curve is located above, and the limit of endurance at 350^{o}C made 190 MPa.

In the field of low cycle fatigue at temperature 20^{o}C the experimental dots reflecting resistance to destruction after ageing and in an initial condition are practically in one area of disorder and coincide with the deformed material. At the elevated temperature (350^{o}C) in the field of durability of 10^2-10^3 cycles the strain amplitude approximately twice is less in comparison with the deformed stainless steel that is connected to similar decrease in reduction of area. Thus the microstructure of cast steel differs from deformed in larger size of grain (3-4 point at cast metal in comparison with 5-6 point at the deformed metal). Besides grains of cast metal are bordered by δ-ferrite that is not present in deformed austenite some steel.

For cast stainless steel the estimation of fatigue durability and at a stage of growth of a crack on valve metal after 12 years of operation was spent. The fatigue crack growth rate on air at the room and elevated temperatures is submitted on Fig. 3 and 4, accordingly. From the submitted data follows, that growth rate of a crack for deformable metal is a little bit more, than for cast. Probably, the austenite grains, bordered by δ-ferrite, are some an obstacle for the accelerated growth of a fatigue crack.

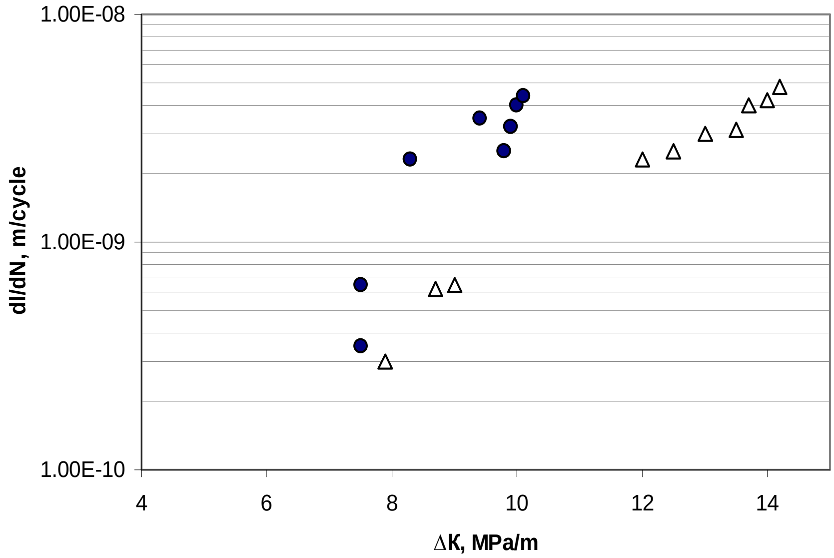

Fig. 3. Fatigue crack growth rate of 10Cr18Ni10Ti steel in air at T=20°C and R=0.1: ● - plate and Δ - cast metal

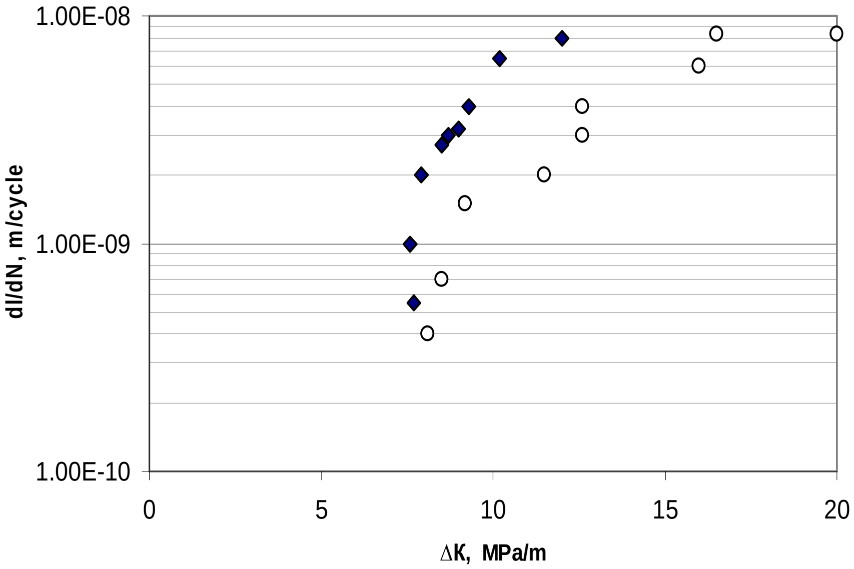

Fig.4. Fatigue crack growth rate of 10Cr18Ni10Ti steel in air at T=350°C and *R*=0.1: ♦ - plate and o – cast metal

Conclusion

2. Fatigue strength in the range of endurance from 10^2 to 10^8 cycles for cast stainless steel is less, than at deformed (forging, plate, tube) metal of same composition.
3. Fatigue crack growth rate of deformable stainless steel is a little bit more, than for cast metal of same composition with austenite-ferrite microstructure.

References

1. **Balandin Yu. F., Gorynin I. V., Zvezdin Yu. I. Markov V. G.** Structural materials for NPP. Moscow, Energoatomizdat, 1984, 280 p.
2. **Timofeev B. T., Nikolaev Yu. K.** About the prediction and assessment of thermal embitterment of Cr-Ni austenitic-ferritic weld and casting at the ageing temperatures 260-425oC. International Journal of Pressure Vessels and Piping, vol.76, No.12, October 1999, p. 849-856.
3. **Ehrnsten U., Karjalainen-Roikonen P., Aaltonen P., Ahlstrand R., Hietanen O., Timofeev B., Bloomin A.** The effects of long-term operation on properties of cast titanium stabilized stainless steel. The 8-th International Symposium on Environmental Degradation of Materials in Nuclear Power Systems Water Reactors. Amelia Island, Florida, USA, 10-14 August 1997, p.1025-1030.

4. **Ehrnsten U., Karjalainen-Roikonen P., Nenonen P., Ahlstrand R., Hietanen O., Timofeev B., Bloomin A**. Properties of cast Ti-stabilised stainless steel after long-term ageing. Proceedings of the Sixth International Conference on "Material Issues in Design, Manufacturing and Operation of Nuclear Power Plants Equipment", Volume 1, 19-23 June 2000, St.Petersburg, p. 104-112.
5. **Karjalainen-Roikonen P., Ehrnsten U., Nenonen P., Aaltonen P**. Ageing of cast Ti-stabilised stainless steel. Report VAL62-11/2000. Espoo, Finland, 47 p.
6. **Ondrouch J.** Mechanical properties of dissimilar weldment after long term ageing. Proceedings of International Seminar "Dissimilar Welded Joints in NPP Equipment and Piping: Problems and Means to Solve Them". 18-22 September 1995, St. Petersburg, Russia, p. 70-76.
7. **Alikin A. P., Kolosov I. E., Orlova V. N., Timofeev B. T.** Microstructure and mechanical properties of cast semi-products from steel types 20 and 08Cr18Ni10Ti. Voprosy sudostroenija. Issues: Metal Science, No..31, 1980, p. 26-32.
8. **Kuzmina S. E., Timofeev B. T.** Assessment of mechanical properties degradation for austenitic stainless steels and their weldments during the thermal ageing. Proceedings of the Tenth International Conference on "Material Issues in Design, Manufacturing and Operation of Nuclear Power Plants Equipment", Volume 2, 7-9 October 2008, St. Petersburg, p. 97-117.
9. **Timofeev B. T., Bazaras Zh. L**. Low Cycle Fatigue of the Equipment of Nuclear Power Plants Made of 15Kh2MFA Steel. Materials Science, Vol. 41, No. 3, 2005, p. 410-417.
10. **Timofeev B. T., Karzov G. P.** Assessment of WWER-1000 Reactor State. International Journal of Pressure Vessels and Piping. Vol.83, No.6, 2006, p. 464-473.
11. **Timofeev B. T.** Low Cycle Fatigue Consideration in NPP Equipment Design. Proceedings of the Fifth International Conference "Material Issues in Design, Manufacturing and Operation of NPP Equipment", 7-14 June 1998, Pushkin, vol.1, p. 210-230.
12. **Timofeev B. T., Bazaras Zh. L**. Low Cycle Fatigue of Welded Joints of 08Kh18N10T Steel. Materials Science, Vol. 43, No. 1, 2007, p. 117-123.
13. **Timofeev B. T., Bazaras Zh. L**. Cyclic Strength of the Equipment of Nuclear Power Plants Made of 22K Steel. Materials Science, Vol. 41, No. 5, 2005, p. 680-685.

Proceedings of 4th International Conference ITELMS'2009

Aspects of the Multilayer Structural Element Cross Section Kern Calculation in the Heterogeneous Case

J. Bareisis*, V. Kleiza**

**Kaunas University of Technology, Panevezys Institute, Daukanto 12, LT-350209 Panevezys, Lithuania,*
E-mail: jonas.bareisis@ktu.lt
***Kaunas University of Technology, Panevezys Institute, Daukanto 12, LT-350209 Panevezys, Lithuania,*
E-mail: vytautas.kleiza@ktu.lt

Abstract

The paper deals with such a cross-section zone of a multilayer structural element (called a kern) in which the existing axial compressing loads cause only compression stresses. The general solution has been obtained when the shape of cross-section is any polygon. Analytical and numerical methods are presented when cross-section is a connected or disconnected domain and a part or the whole contour of cross-section is an integrable curve(s). The method of finding the kern geometry and its localization requires only coordinate values of polygon vertices. Geometries containing curved parts are analyzed by approximating the curves that correspond to line segments or by applying the analytical method proposed. Several examples of cross-section geometries are given, as well as the numerical and graphical results obtained.
KEY WORDS: *beam section, kern, compression stress zone, core, limit zone, foundation analysis, compression member.*

1. Introduction

The concept of cross-section kern (CSK) is wide used in various fields of construction, navy and material mechanics. It is often required that there would be no or limited tension stresses in plates, prestressed concrete beams and concrete dams. That is why establishment of CSK as a zone in which an applied axial load does not invoke tension stresses is rather important.

If the compressing axial load acts on a homogeneous structural element at its centroid, then the entire cross-section is uniformly compressed. Axial compressing and bending cause excentrically acting load, therefore the axial load acting at a certain distance from the centroid can cause tension stresses.

In the CSK determining methods reviewed, only homogeneous structural elements are explored, however recently multilayer, i.e. heterogeneous structural elements formed by using the various materials and combinations of their arrangement, have been used ever more widely in the construction.

Heterogeneous structural elements are frequently affected by excentrical loads (e. g. building structures meant for work in seismic zones). In those cases, it is of most importance to define load arrangement zones that ensure either the absence of tension stresses or precise estimation of the latter values. This is especially important for the materials whose strength for tension is considerably lower than that for compressing.

2. The Heterogeneous Case

A method of determining CSK for a heterogeneous bar is proposed and grounded in this section. Let the cross-section K of a heterogeneous bar, its contour ∂K, and its convex hull $Q = \mathrm{conv}(K)$ [6, 7] as well as the contour ∂Q be given in the principal stiffness coordinate system $\{x_{ss}, y_{ss}\}$ [1]. A multilayer bar is composed of n layers with the elasticity moduli $E_1, E_2, ..., E_n$, while the respective cross-sections take up connective and non overlapping domains K_i along the entire length of a bar. Such a bar is cross heterogeneous; however it is homogeneous in the longitudinal direction. The whole cross-section of a bar is

$$K = \bigcup_{i=1}^{n} K_i,\ K_i \cap K_j = \varnothing,\ i \neq j\ , \tag{1}$$

and we can define the axial stiffness density function in the system $\{x_{ss}, y_{ss}\}$ [1]

$$E(x, y) = \sum_{i=1}^{n} E_i I_i(x, y) \tag{2}$$

where

$$I_i(x,y)=\begin{cases}0, & (x,y)\notin K_i\\ 1, & (x,y)\in K_i\end{cases}.$$

Function (2) is piecewise constant and it is defined on the entire cross-section K, and if the point (x,y) belongs to the *i* - th layer, then $E(x,y)$ is equal to the elasticity modulus E_i of layer K_i, i.e.

$$E(x,y)=E_i \text{ if } (x,y)\in K_i. \tag{3}$$

Let (x_F, y_F) be the resultant of a point affected by load $F<0$, perpendicular to the bar cross-section, and (x_C, y_C) of a point at which stresses are calculated in the system $\{x_{ss}, y_{ss}\}$. Then the distribution of stresses in the cross-section of a heterogeneous bar [1], [2]

$$\left.\begin{aligned}&\sigma(x_F, y_F, x_C, y_C)=\\ &\frac{F}{B}E(x_C,y_C)\left(1+\frac{B}{D_x}y_C y_F+\frac{B}{D_y}x_C x_F\right)\end{aligned}\right\}, \tag{4}$$

where [26]: *B* is the axial stiffness of a heterogeneous bar

$$B=\iint_K E(x,y)dxdy, \tag{5}$$

D_x and D_y are extreme bending stiffnesses of a heterogeneous bar

$$D_x=\iint_{K_{ss}} x^2E(x,y)dxdy,\ D_y=\iint_{K_{ss}} y^2E(x,y)dxdy \tag{6}$$

We denote the domain K_{ss}, i.e., the image of the domain K in the system $\{x_{ss}, y_{ss}\}$, by K, as before.

Note that in the case of a heterogeneous bar, function (4) that defines stresses is piecewise linear (in the homogeneous case it is linear), because, if the point (x_F, y_F) is fixed, then the latter is only the function of the variables *x* and *y*, and its part

$$\left(1+\frac{B}{D_x}y_C y_F+\frac{B}{D_y}x_C x_F\right) \tag{7}$$

is a linear function, while the other part

$$\frac{F}{B}E(x_C,y_C) \tag{8}$$

is a piecewise constant function (see (3)).

Taking into consideration that function (7) is positive, and function (8) is negative, determination of CSK of a heterogeneous bar is reduced to the following problem: find a set $\mathrm{kern}(K, E_1, E_2, ..., E_n)$ of all the points (x_F, y_F) so that at all the points of cross-section K only compressing stresses appeared, i.e., that function (4) were negative or

$$\left(1+\frac{B}{D_x}y_C y_F+\frac{B}{D_y}x_C x_F\right)>0. \tag{26}$$

Thus the problem of finding CSK of a heterogeneous bar is reduced to an analogous problem for a homogeneous bar [3 - 5].

We present below a numerical algorithm for finding the CSK geometry and its localization. It is precise if cross-section is any polygon, and approximate if the cross-section is any domain. Let as consider the case (Fig. 1), where the polygons K_i that approximate all domains are convex or concave. Note that this kind of limiting of domains does not restrict the CSK finding problem on principle, since the every domain can be approximated by polygon with a high accuracy.

3. Calculation Method

Let $P_i^{(j)}$ be the sequences of polygons K_i vertices ordered (counterclockwise). Then the contour of any polygon K_i is

$$\partial K_i = \bigcup_{k=1}^{j_i} \left\{ P_i^{(j)} P_i^{(j+1)} \right\}. \tag{10}$$

We show that in such case, all the moments

$$m_{pq} = \iint_K x^p y^q E(x,y) dxdy$$

could be expressed in algebraic form.

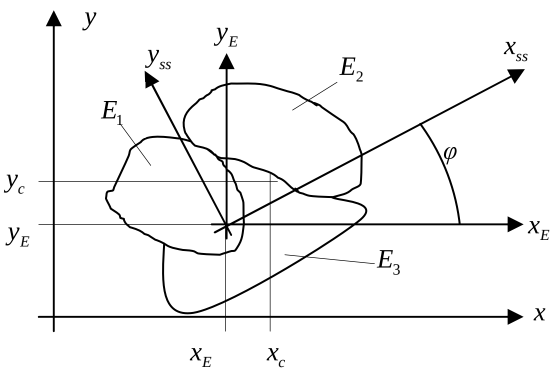

Fig. 1. Geometry of a multilayer structural element, global and principal stiffness coordinate systems.

Indeed, any sides of i - th polygon is

$$\begin{aligned} &P_i^{(j)}(x_{ij},\, y_{ij}) P_i^{(j+1)}(x_{i(j+1)},\, y_{i(j+1)}), \\ &i = 1,2,...n, \quad j = 1,2,...j_i \end{aligned}, \tag{11}$$

and those equations are:

$$\begin{cases} x_{ij}(t) = x_{ij} + \overline{x}_{ij}\, t \\ y_{ij}(t) = y_{ij} + \overline{y}_{ij}\, t \end{cases}, \ (0 \le t \le 1), \tag{12}$$

where $\overline{x}_{ij} = x_{i(j+1)} - x_{ij}$, $\overline{y}_{ij} = y_{i(j+1)} - y_{ij}$. Then, applying the Green theorem we have:

$$\begin{aligned} m_{pq} &= -\frac{1}{q+1} \sum_{i=1}^{n} E_i \sum_{j=1}^{j_i} \overline{x}_{ij} \int_0^1 \left(x_{ij}(t) \right)^p \left(y_{ij}(t) \right)^{q+1} dt = \\ &- \frac{1}{q+1} \sum_{i=1}^{n} E_i \sum_{j=1}^{j_i} \overline{x}_{ij} s_{pq}^{(ij)} \end{aligned} \tag{13}$$

or

$$\begin{aligned} m_{pq} &= \frac{1}{p+1} \sum_{i=1}^{n} E_i \sum_{j=1}^{j_i} \overline{y}_{ij} \int_0^1 \left(x_{ij}(t) \right)^{p+1} \left(y_{ij}(t) \right)^{q} dt = \\ &\frac{1}{p+1} \sum_{i=1}^{n} E_i \sum_{j=1}^{j_i} \overline{y}_{ij} \overline{s}_{pq}^{(ij)} \end{aligned}, \tag{14}$$

and the integrals $s_{pq}^{(ij)}$ and $\overline{s}_{pq}^{(ij)}$

$$s_{pq}^{(ij)} = \int_0^1 \left(x_{ij}(t)\right)^p \left(y_{ij}(t)\right)^{q+1} dt\,, \tag{15}$$

$$\overline{s}_{pq}^{(ij)} = \int_0^1 \left(x_{ij}(t)\right)^{p+1} \left(y_{ij}(t)\right)^{q} dt\,, \tag{16}$$

for $p \geq 0, q \geq 0,\ p+q \leq 2$, can be expressed infinite form

$$\left.\begin{aligned}
&s_{00}^{(ij)} = y_{ij} + \frac{1}{2}\overline{y}_{ij}\,,\\
&\overline{s}_{10}^{(ij)} = x_{ij}^2 + x_{ij}\overline{x}_{ij} + \frac{1}{3}\overline{x}_{ij}^2\,,\\
&s_{01}^{(ij)} = y_{ij}^2 + y_{ij}\overline{y}_{ij} + \frac{1}{3}\overline{y}_{ij}^2\,,\\
&\overline{s}_{20}^{(ij)} = x_{ij}^3 + \frac{3}{2}x_{ij}^2\overline{x}_{ij} + x_{ij}\overline{x}_{ij}^2 + \frac{1}{4}\overline{x}_{ij}^3\,,\\
&s_{02}^{(ij)} = y_{ij}^3 + \frac{3}{2}y_{ij}^2\overline{y}_{ij} + y_{ij}\overline{y}_{ij}^2 + y_{ij}^3\,,\\
&\overline{s}_{11}^{(ij)} = \frac{1}{4}\overline{y}_{ij}\left(\overline{x}_{ij}^2 + 2x_{ij}^2\right) + \frac{1}{3}\overline{x}_{ij}\left(2x_{ij}\overline{y}_{ij} + \overline{x}_{ij}y_{ij}\right) +\\
&+x_{ij}y_{ij}\left(\overline{x}_{ij} + x_{ij}\right)
\end{aligned}\right\}. \tag{17}$$

Thus the parameters B, D_x, D_y, necessary to calculate CSK, are expressed by integrals (15) and (16). By employing expressions (13) or (14) and (17) we finally have

$$B = m_{00} = \sum_{i=1}^{n} E_i \sum_{j=1}^{j_i} \overline{y}_{ij}\overline{s}_{pq}^{(ij)} = \sum_{i=1}^{n} E_i \sum_{j=1}^{j_i} \overline{y}_{ij}\left(y_{ij} + \frac{1}{2}\overline{y}_{ij}\right),$$

$$\begin{aligned}
&D_x = m_{20} = \frac{1}{3}\sum_{i=1}^{n} E_i \sum_{j=1}^{j_i} \overline{y}_{ij}\overline{s}_{20}^{(ij)} =\\
&\frac{1}{3}\sum_{i=1}^{n} E_i \sum_{j=1}^{j_i} \overline{y}_{ij}\left(x_{ij}^3 + \frac{3}{2}x_{ij}^2\overline{x}_{ij} + x_{ij}\overline{x}_{ij}^2 + \frac{1}{4}\overline{x}_{ij}^3\right),
\end{aligned}$$

$$\begin{aligned}
&D_y = m_{20} = -\frac{1}{3}\sum_{i=1}^{n} E_i \sum_{j=1}^{j_i} \overline{x}_{ij}s_{20}^{(ij)} =\\
&-\frac{1}{3}\sum_{i=1}^{n} E_i \sum_{j=1}^{j_i} \overline{x}_{ij}\left(y_{ij}^3 + \frac{3}{2}y_{ij}^2\overline{y}_{ij} + y_{ij}\overline{y}_{ij}^2 + y_{ij}^3\right).
\end{aligned}$$

4. Numerical Results

The initial results of application of the CSK calculation method proposed are presented in Fig. 2. A multilayer column has been considered, the cross-section of which is of an asymmetric T shape with four (1, 2, 3, 4) reinforcement bars (RB) in the horizontal direction and three (2, 5, 6) in the vertical direction (Fig. 2). The total cross-section area $A = \mathrm{mes}(K)$ of a column (e.g. reinforcement concrete) was assumed to be constant in all the cases. The elasticity modulus E_m of the matrix is equal to 1, while the elasticity modulus E_r of the RB was changed from 1 up to 500. Considering the entire area $A_r = \sum_{i=1}^{6}\mathrm{mes}(K_i)$ occupied by RB on the CSK are $A_{ck} = \mathrm{mes}(\mathrm{kern(K)})$, the ratio E_r/E_m was equal to 10, which corresponds to the reinforcement-concrete case.

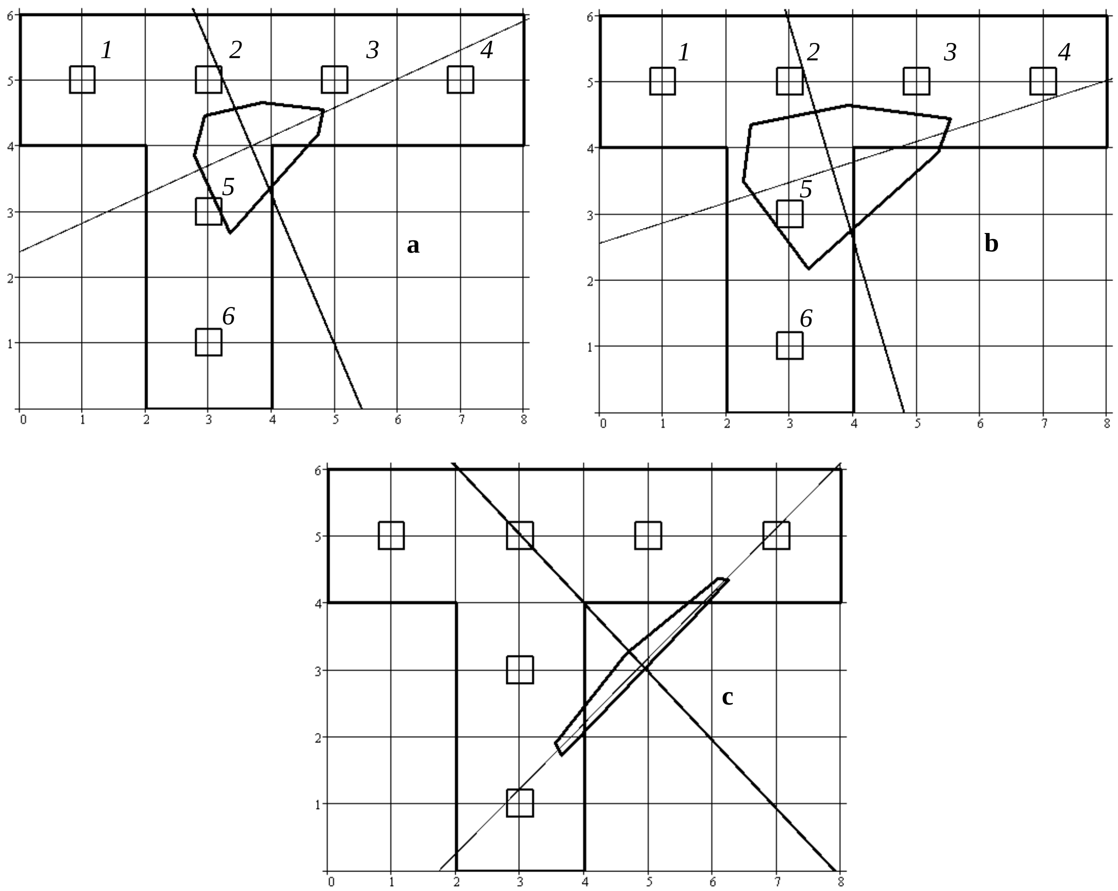

Fig. 2. Analysis of the column cross-section kern for: **a** - the ratio of reinforcing elements and matrix elasticity modulus is E_r / E_m = 1 (homogeneous structure); **b** – stiffness of the border reinforcing elements 1, 4, and 6 is 50 times higher than that of reinforcing elements 2, 3, and 5; **c** - stiffness of the border reinforcing elements 4 and 6 is 50 times higher than that of the remaining ones.

Alteration of the area A_{ck} of the heterogeneous bar was calculated in percent by comparing it with the CSK area of the homogeneous bar the value of which is equated to 100%. In the case of a homogeneous bar (Fig. 2, a), the CSK area is $A_{ck} = 2.32$, its ratio with the total cross-section area is $A_{ck}/A = 0.097$, and its centroid coordinates are $x_c = 3.66,\ y_c = 4.00$. Alterations in the CSK geometric parameters were calculated with regard to these quantities.

The figures presented below illustrate the possibilities of proposed method.

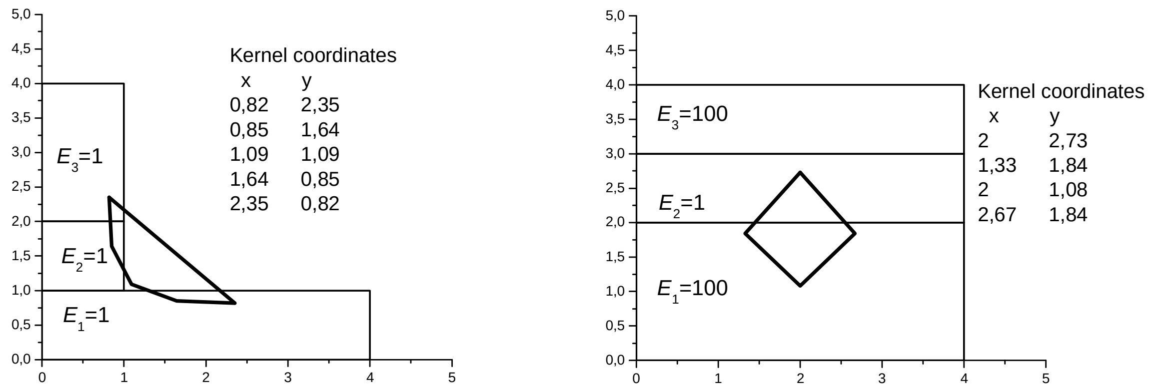

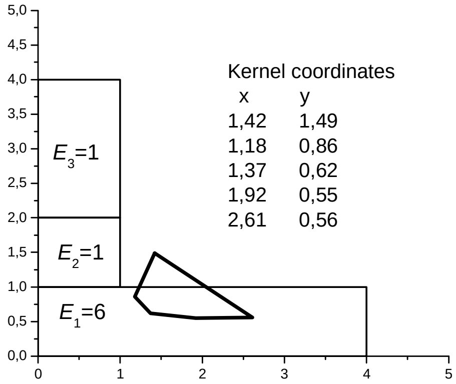

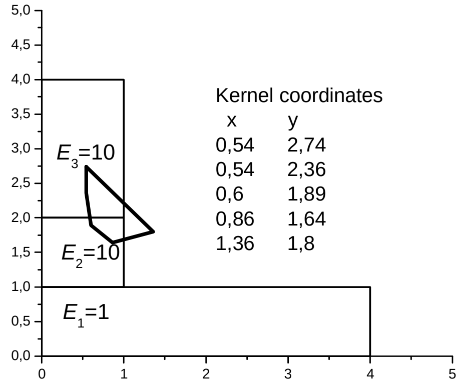

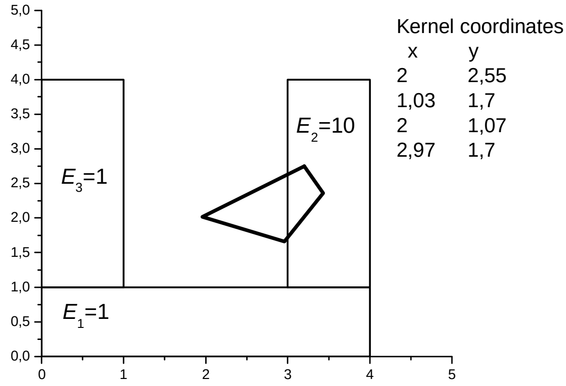

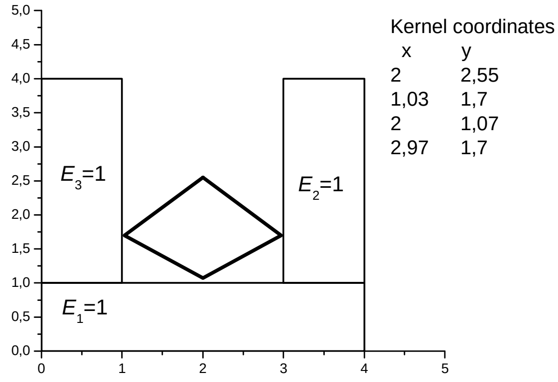

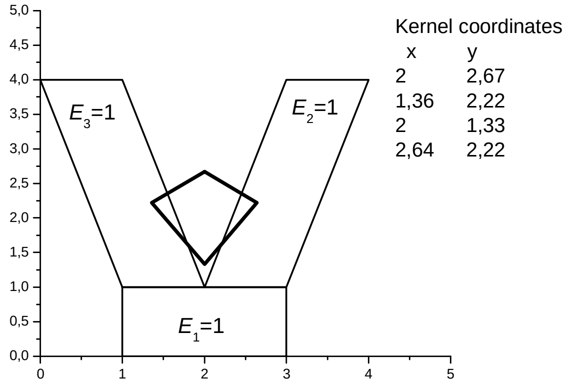

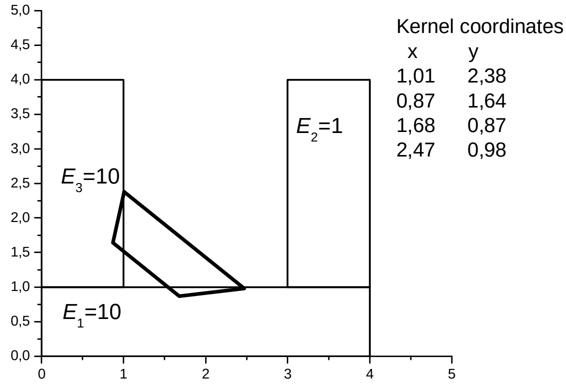

5. Conclusions

1. A new method for determining the cross-section kern geometry and its localization of multilayer column has been presented.

2. An efficient calculation algorithm has also been presented that enables us to calculate heterogeneous cross-section moments of every order without using the integration procedure.

3. The cross-section parameters have been calculated, applying the algorithm proposed for a asymmetric T-shaped column with non-uniformly arranged reinforcement elements varying their geometric and stiffness parameters.

4. The investigated cases allow us to argue that the ratio between the heterogeneous column cross-section kern area and that the entire structure cross-section can be up to two times higher or lower that much as compared with the that kind ratio of a homogeneous columns.

5. The primary investigations corroborate the efficiency of the methods proposed as well as a possibility for structure designers to optimally arrange reinforcement elements and select their stiffness so as to ensure the required stress distribution in a multilayer column.

References

1. **Bareisis, J.** Stiffness and Strength of Multilayer Beams. Journal of Composite Materials, No. 5 (38), 2004, p. 389-397.
2. **Bareisis, J.** Design and Stress State of Tensions in Multilayer Bars. Journal of Composite Materials, No. 6 (40), 2006, p. 515-531.
3. **Mofid M., Yavari A.** On the kern of a general section. International Journal of Solids and Structures. 17(37), 2000, p. 2377–2403.
4. **Mofid, M., Shadnam, M. R., McCabe, S. L.** On a new approach for finding the kern of a beam section. Engineering Structures. 9(23), 2001, p. 1080-1084.
5. **Mofid M., Alizadegan R., Ashori B., Yavari.** A. Computing the kern of a general cross-section. Advances in Engineering Software. 12(32), 2001, p. 949-955.
6. **Jarvis A.** On the identification of the convex hull of a finite set of points in the plane. Information Processing Letters. 1(2), 1973, p.18–21.
7. **Graham R. L.** An efficient algorithm for determining the convex hull of a finite planar set. Information Processing Letters. 4(1), 1972, p. 132–133.

Proceedings of 4th International Conference ITELMS'2009

Investigation and Assembling of One Fiber Reflection Optopair Sensor

V. Kleiza*, J. Verkelis**

**Kaunas University of Technology, Panevezys Institute, Klaipėdos str. 1, LT-35209 Panevezys, Lithuania, E-mail: vytautas.kleiza@ktu.lt*
***Institute of Semiconductor Physics, Gostauto str. 11, LT-LT-01108 Vilnius, Lithuania, E-mail: jverk@pfi.lt*

Abstract

Mechanical-optical equipment was created and manufactured for an investigating and assembling one fiber reflection optopair (OFROP) and sensor. It enables positioning of the active fiber tips along *XYZ* coordinates manually (accuracy ± 0.5 μm) and by step motor controlled by electronics (accuracy 0.1 μm). An angle between the fiber axes was controlled in the range 0-180^o with the accuracy ± 0.5^o. The output power of light transmitted from the receiving fiber was measured by energy meter LP-5025 (accuracy 4%, resolution 0.01%).

A non-contact nano-micro reflection mirror positioning system was created for measuring fiber-optical sensor output signal *U* dependent on displacement *h* from the mirror (*U-h* characteristics), sensitivity of the sensor as well as resolution. Construction and technology of the OFROP sensor, and signal processing electronics were created.

The output signal *U* of OFROP dependences on the mirror displacement *h* and angle 2θ between the axes of the fibers regularities, being *b* (the distance between active fiber tips) minimal were researched by experiment and modeling. *U-h* parameters, such as the maximal sensitivity S_{max}, positions of *U* inflection points h_1^-, h_1^+, peak value of U and its position h_1, position of interval Δh in which *U-h* characteristic is linear and their dependences on θ and *h* were determined. Experimental results are consistent with those obtained by modeling.

KEYWORDS: *fiber reflection optical pair, mirror positioning system, sensor sensitivity*.

1. Mathematical Model

The Gauss type light beam power is concentrated in a narrow cone, and the electromagnetic field distribution in any perpendicular plane of the fiber axis is radial symmetric and completely defined [1], [2] by the following parameters: radiation intensity

$$I(\rho, z) = I_0 \left(\frac{R_0}{R(z)} \right)^2 \exp\left\{ -\frac{2\rho^2}{R^2(z)} \right\}, \ \rho = \sqrt{x^2 + y^2} ,$$

beam power

$$P = \int_0^\infty I(\rho, z) 2\pi\rho d\rho ,$$

beam divergence

$$R(z) = R_0 \sqrt{1 + \left(\frac{z}{z_0} \right)^2} .$$

The optical system (Fig. 1), that consists of light-emitting fiber **L**, a mirror and plane **P**, which the position of which is completely defined by the angle θ and distance *b*, of light reflected power in plane **P** is indicated by the function [3]:

$$U = \frac{C_0}{\pi R^2 (Z(h,\theta))} \exp\left\{ -\frac{\left(x(h,\theta) - d \right)^2}{R^2 (Z(h,\theta))} \right\}. \tag{1}$$

Here *d* is the distance from the point *p* to a point (in plane **P)**, in which the received power is calculated (Fig. 1), $R(Z)$ is the effective radius of the Gaussian beam in addition to

$$h_0(b,\theta) = \frac{b}{2\tan\theta}, \tag{2}$$

$$Z(h,\theta) = z(h,\theta) + z'(h,\theta), \tag{3}$$

$$z(h,\theta) = \frac{h}{\cos\theta}, \tag{4}$$

$$z'(h,\theta) = 2h\cos\theta + b\sin\theta - z(h,\theta) \equiv h\frac{\cos 2\theta}{\cos\theta} + \sin\theta, \tag{5}$$

$$x(b,h,\theta) = 2h\sin(\theta) - b\cos(\theta), \tag{6}$$

$$R(Z) = a_0 + Z^m k\tan\theta_c. \tag{7}$$

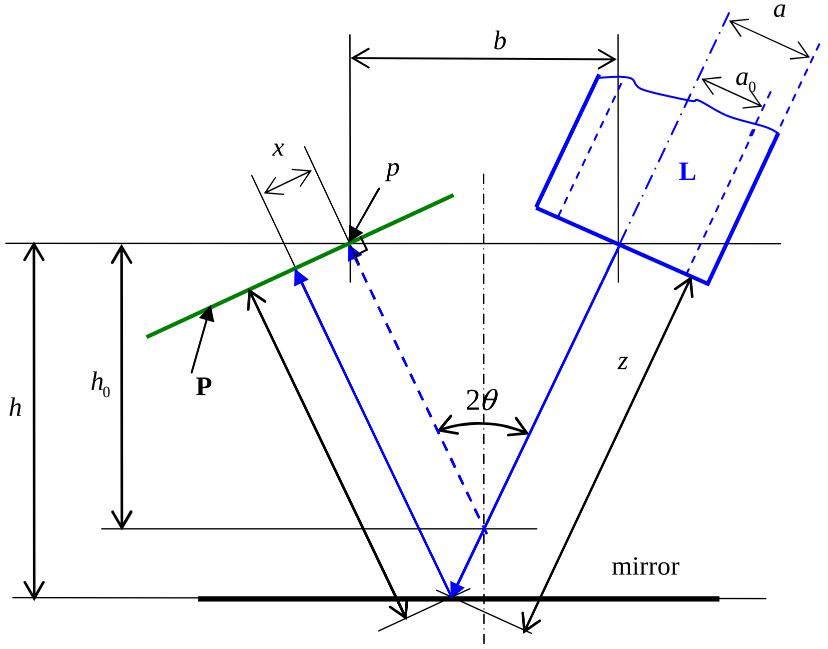

Fig. 1. The scheme of the detection of reflected Gaussian beam power.

Fig. 2 presents the calculations of reflected light power, performed using expression (1) for three positions $h = h_1, h_0, h_2$ of the reflection mirror, and for three positions $d = d_1, 0, d_2$ of the points (of plane **P**) at which the power is calculated.

Curves *1, 3, 4* defined the dependences of reflected light power on the distance *h* at three fixed points $d = d_1, 0, d_2$, and curves *2, 4, 6* define analogous dependences dependent on the distance *d* at three fixed distances to the mirror $h = h_1, h_0, h_2$. Note that curves *2, 4, 6* are symmetric, while curves *1, 3, 4* are asymmetric. This method enables us to calculate the dependences of reflected light power on *h* at any point of plane **P**, i.e., on the whole plane **P.**

We have used expression (1) for constructing a mathematical model of one fiber optopair (OFROP). In order to determine OFROP *U-h* characteristics (UHC) in theory (Fig. 3), we explore the case where the distance $b(\theta)$ between the centers of active fiber tips **A** (light receiving) and **L** (light emitting) is minimal $b(\theta) = b_{\min}(\theta) = 2a\cos\theta$ and the parameter $d = 0$ (Fig. 4). Note that the value of $b_{\min}(\theta)$ is defined by the diameter 2*a* of fiber cladding and the angle θ. If 2θ ($0 < \theta < \pi/2$) is the angle between fiber **A** and **L** axes, then the optopair *U-h* characteristic (a signal emerging in fiber **A**) is expressed by function (1), with the parameters:

$$h_0(\theta) = \frac{a}{\sin\theta} - \sin\theta, \tag{8}$$

$$z(h,\theta)=\frac{h}{\cos\theta}, \tag{9}$$

$$z'(h,\theta)=h\frac{\cos 2\theta}{\cos\theta}+a\sin 2\theta, \tag{10}$$

$$Z(h,\theta)=2h\cos\theta+a\sin 2\theta \quad , \tag{11}$$

$$x(h,\theta)=2(h\sin\theta-a\cos^2\theta), \tag{12}$$

$$R(Z)=a_0+Z^m k\tan\theta_c. \tag{13}$$

Here a is the radius of fiber cladding, a_0 is the radius of fiber core, θ_c is the angle of fiber aperture, and k,m are constants defined in the experiment. $C_0=QK_AK_MK_TI_L$, where Q is the area of fiber core, K_A is light loss in the receiving fiber, K_T is light loss in the medium, and U_L is the power lead in the emitting fiber **L**.

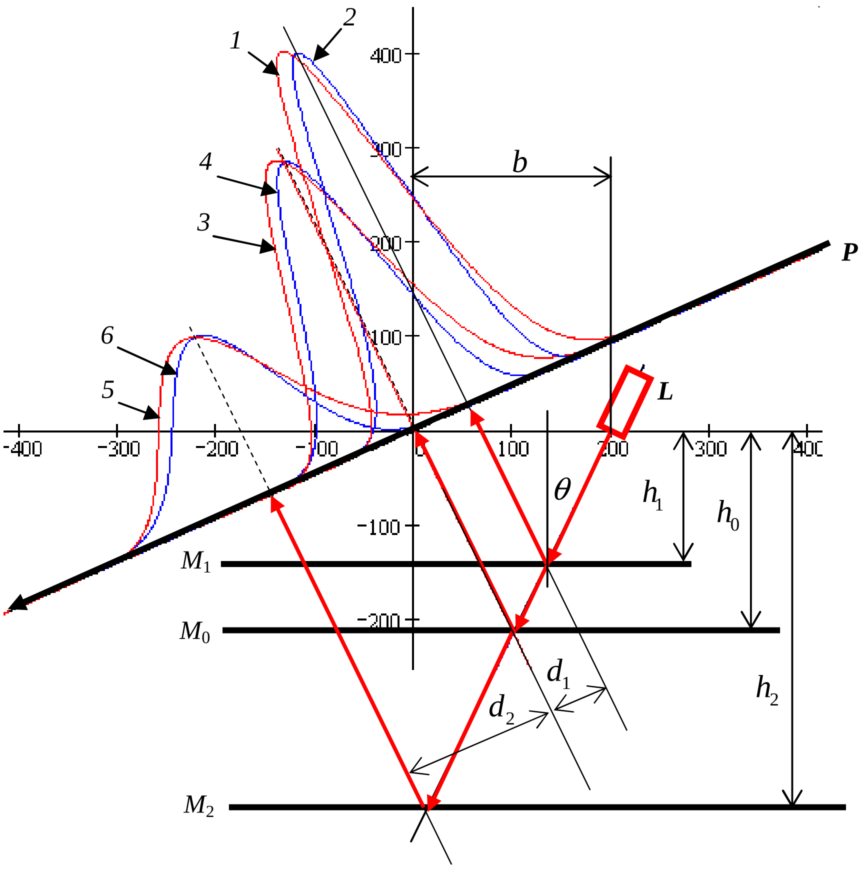

Fig. 2. The scheme of light beam power calculation according expression (1).

Note that function $U(h)$ is positive and has a single maximum for all the positive h values. Naturally, sensitivity of an optopair is equal to derivative

$$S(h)=\frac{\partial U}{\partial h}, \tag{14}$$

and the maximal value of signal is achieved at the point h_1, which is a unique solution of the equation

$$\frac{\partial U}{\partial h}=0. \tag{15}$$

It is easy to see that sensitivity $S(h)$ (Fig. 6) has two local extrema (at the points $h_1^- > h_1^+$), at which $S(h_1^-) < 0$, $S(h_1^+) > 0$. These two points are unique solution of the equation

$$\frac{\partial^2 U}{\partial h^2} = 0. \tag{16}$$

Of course, in the neighbourhood of the points h_1^-, h_1^+ the function $U(h)$ is closest to a linear one, i. e., dependences of signal $U(h)$ on h are almost linear.

When calculating the sensitivity and maximal sensitivity along the entire h variation interval, one ought to know the analytic expressions of derivatives $\frac{\partial U}{\partial h}$ and $\frac{\partial^2 U}{\partial h^2}$, however, it is possible to find them in a convenient form only if the parameter $m = 1$ [3], therefore in calculations we have used efficient numerical differentiation algorithms that stabilize errors. To solve equations (15) and (16), the unconditionally convergent Newtom method was used. Note that we need to solve these equations for various sets of optopair parameters.

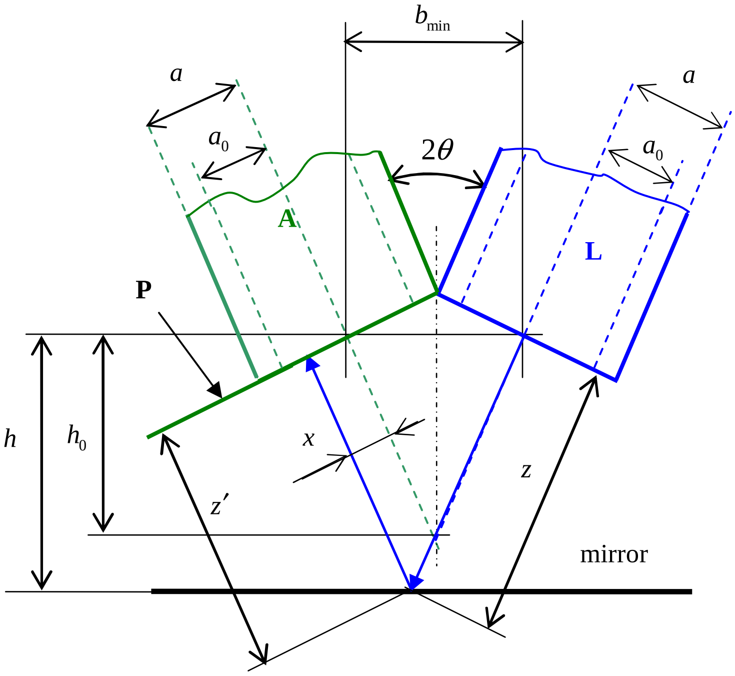

Fig. 3. Geometry of one optopair.

2. Experimental Set-up

Output signal *U*-*h* characteristics were measured by using a scheme shown in Fig. 3. Fibers **A**, **L (**WF50/125P0.22; WF100/125 P0.22; WF200/230 P0.22) were installed in SMA 905 connectors. The angle between fiber axes is 2θ. The maximal output signal and minimal distance b_{min} were controlled by a special mounting desk (Fig. 4). SMA emitter (H22E4020IR), of 15 dBm power, λ_{max}=850 nm and a stabilized current supply 80 mA were used. Output power of the sensor was measured by a precise fiber emission gauge LP-5025-8. Fibers **A**, **L** and the mirror (Au) were fastened on a precise *XYZ* positioning device under a microscope. The positioning step was controlled by an electronic device and, in addition, by a micrometer (±0.5 µm). The angle 2θ between the axes of active fiber tips was defined by the microscope scale indices (Fig. 4).

3. Results and Discussion

Experimental measurement points (X, +, |) of *U*-*h* UHC of the one fiber reflection optopair as well as modeling results (continuous curves) are presented in Fig. 5. As we can see, the results obtained experimentally are congruent with the modeling results. UHC has a peak at the position of which is denoted as h_1 and amplitude as $A(h_1) = U(h_1)$. Steeper parts of all the curves $A(h)$ are up to the peak and more sloping after it. The results indicate, that with an increase of the diameter $2a_0$ values are linearly increasing (Fig. 7, 9), while $A(h_1)$ is increasing exponentially (Fig. 7, 8). The increase of h_1 can be accounted for the fact that with an increase in the diameter of fiber core, the dimensions of OFROP also increase and therefore the distance between the centers of active fiber tips is increasing as well. The value of $A(h_1)$ increases due to an increase in the effective area of fibers.

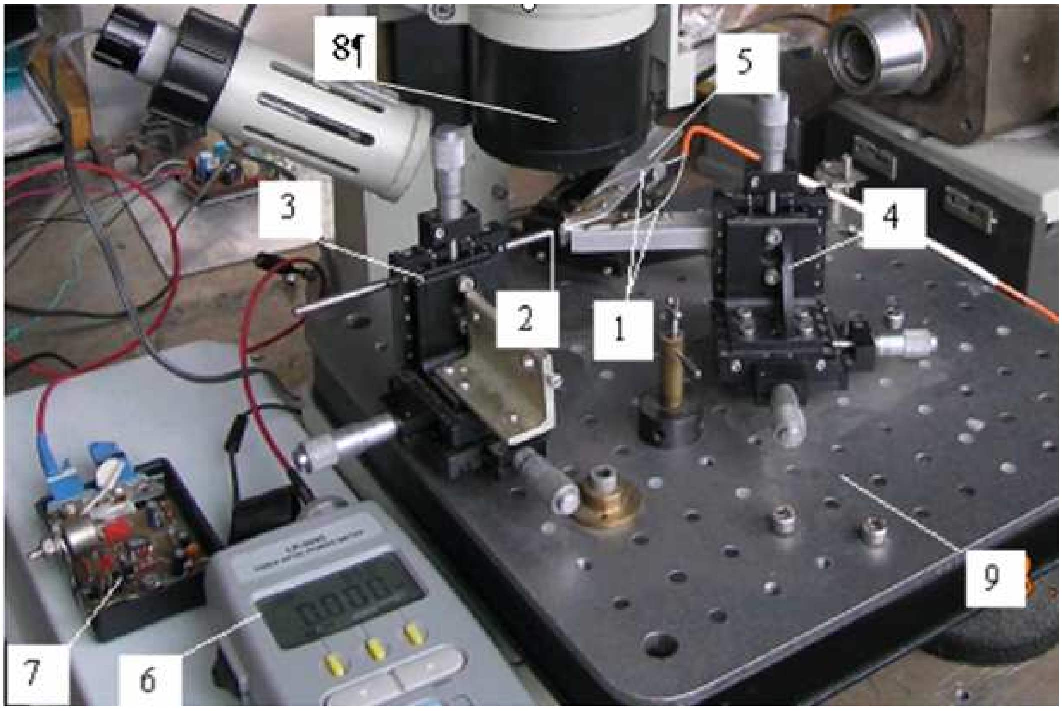

Fig. 4. The fiber optopair set-up: *1*- fibers, *2* – mirror, *3* – translator of the mirror (XYZ ± 0,5 µm), *4*, *5* – translator of fiber light power meter (XYZ ± 0,5 µm, θ ± 0,5º), 6 – receiving optical fiber power meter , *7* – stabililized source of power supply (80 mA), *8* – optical microscope to monitoring the fiber tips relatively to the mirror, *9* – optical plate for fastening translators.

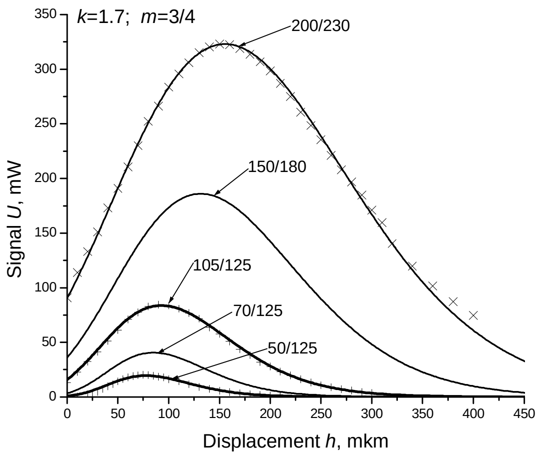

Fig. 5. Calculated and experimental (+, x and |) dependences of signal U_A on the displacement *h*. The parameters *k*=1.7; *m*=3/4 for all graphs. The curves correspond to fibers a_0 / a .

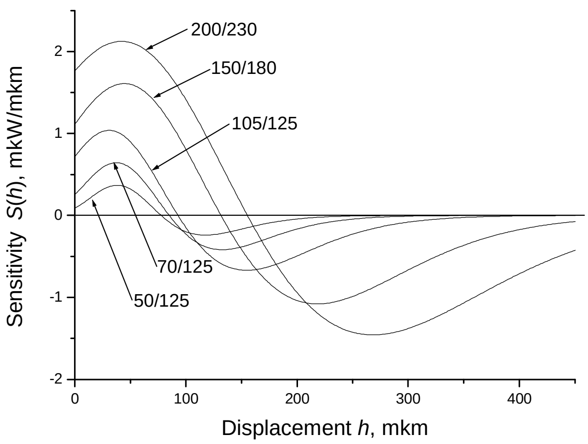

Fig. 6. Calculated dependences of the sensor sensitivity (dU_A/dh) on the displacement *h*. The parameters *k*=1.7; *m*=3/4 for all graphs. The curves correspond to fibers a_0 / a .

The maximal sensitivities $S^+_{\max}$ and $S^-_{\max}$ of OFROP sensor and the h values corresponding to them (h_1^+ and h_1^-) are of great importance. The sensitivity $S(h)$ is a derivative of signal $A(h)$ according to h ($S(h) = dA/dh$). As mentioned above (16), $S^+_{\max}$ and $S^-_{\max}$ are solutions to the equation $\partial^2 A / \partial h^2 = 0$. The values of these parameters are given in Table 1. The calculation results show that with an increase in the diameter of fibers, the values of both h_1^+, h_1^- (Fig. 9) and $S_{\max}^+$, $S_{\max}^-$ (Fig. 10) are increasing linearly. Fig.11 illustrates the dependence of constant (1) $C_0 = QK_A K_M K_T I_L$ on the diameter of fiber core.

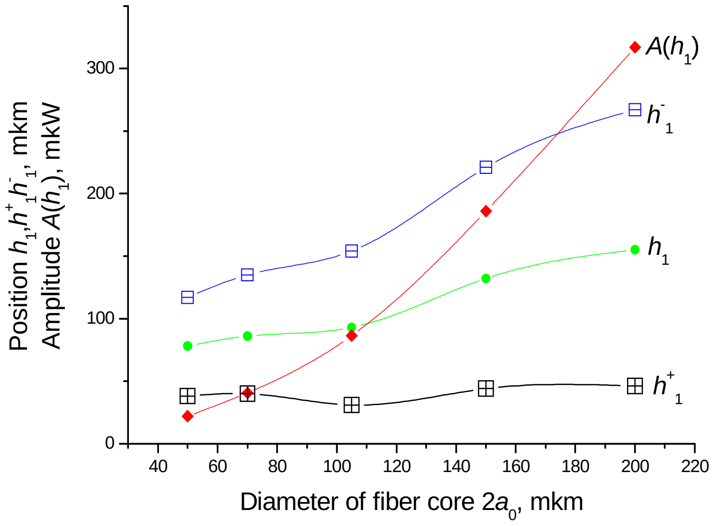

Fig. 7. Dependence of some UHC characteristic points of OFROP on the diameter $2a_0$ of fiber core (experimental points an interpolation of splines). $A(h_1)$ are values of signal amplitude, h_1 are positions of signal amplitude, h_1^+ and h_1^- are positions of the maximal sensitivity of sensor.

Table 1.

FIBER a_0 / a	$S(h_1)=0$		$\max\lvert S^-(h)\rvert = S(h_1^-)$		$\max S^+(h) = S(h_1^+)$		$C_0 \times 10^{-5}$
	h_1 [μm]	$\max A(h) = A(h_1)$, [μW]	h_1^- [μm]	$S(h_1^-)$ [μW/μm]	h_1^+ [μm]	$S(h_1^+)$ [μW/μm]	
50/125	78	22	117	0.368	38	0.240	1.5
70/125	86	41	135	0.640	40	0.418	4.5
105/125	93	86	154	1.071	31	0.691	15.5
150/180	132	186	221	1.610	44	1.108	67.0
200/230	155	317	267	2.125	46	1.457	195.0

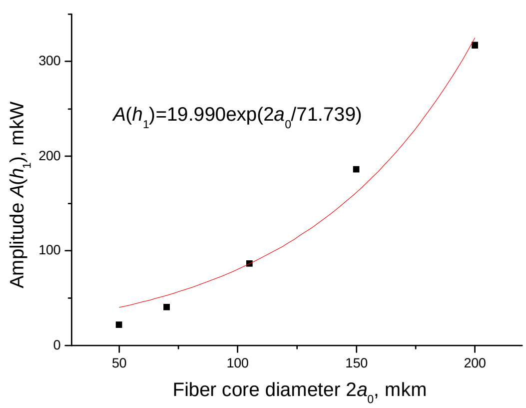

Fig. 8. Dependence of the amplitude value $A(h_1)$ of OFROP output signal on the diameter $2a_0$ of fiber core (experimental points and approximation by the exponential function).

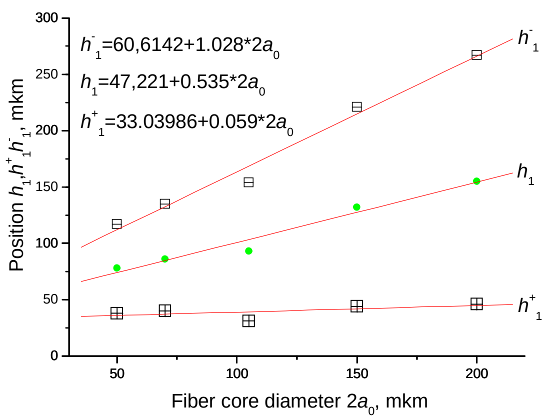

Fig. 9. Dependences of positions of the OFROP output signal amplitude (h_1) and maximal sensitivity (h_1^+ and h_1^-) on $2a_0$ (experimental points and approximation by least squares lines).

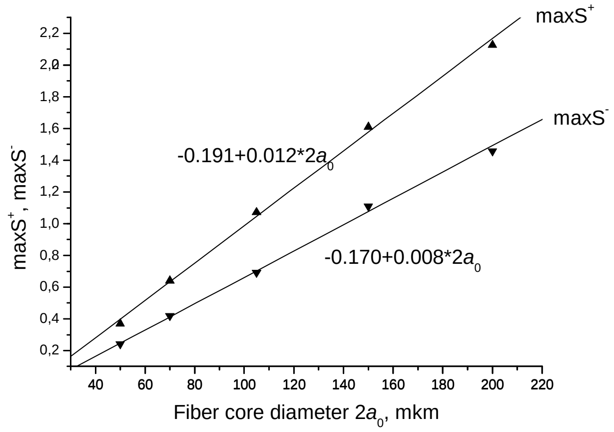

Fig. 10. Dependences of the maximal sensitivity $\max S^{+}$ and $\left|\max S^{-}\right|$ values of OFROP on the diameter $2a_0$ of fiber core (experimental points and approximation by least squares lines).

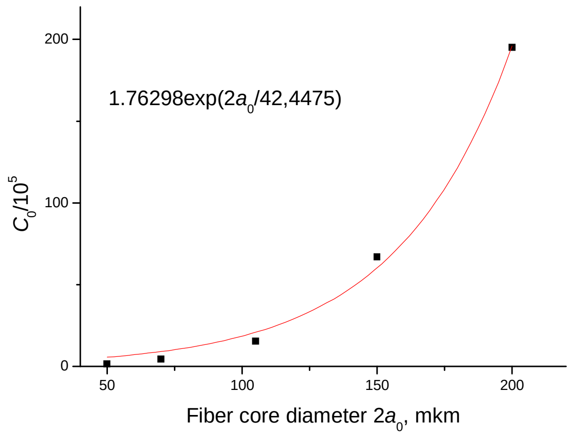

Fig.. 11. Dependence of the constants C_0 of model (1) on the diameter $2a_0$ of fiber core (experimental points and approximation by the exponential function).

4. Conclusions

Dependences (*U-h* characteristics) of output signal *U* of one-fiber pair on the distance *h* between active fiber tips and the light reflecting mirror and on the diameter ($2a_0$=50, 70, 105, 150, 200 μm) of fiber core have been explored experimentally and by modeling, the angle θ=27° being optimal (the angle between the active fiber tips axes 2θ), the distance $b = b_{min}$ between the centres of active fiber tips being minimal.

We have shown that with an increase of the diameter of fibers, the maximal sensitivity values $\max S^{+}$ and $\max S^{-}$ are increasing linearly. This leads to conclusion that the optimal fiber diameter for non-contact fiber reflection displacement sensors and actuators is $100 \div 105\,\mu\text{m}$, because their diameter with cladding $2a$=125, which is the diameter of the cheapest multimode fibers most, frequently used for communication. Other regularities of the *U-h* characteristics which depend on *h* and on the diameter $2a_0$ of fiber core are also pointed out. The experimental and modeling results are well congruent.

Sensors and transducers were proposed to Kaunas Technology University for measurement and indication nanometric displacement and vibration of mechatronic elements. KEMEK Engenineering UAB for fabrication process automatization and for weighing and dosing equipment, Linoma UAB for manufacturing signal processing electronics, having digital indication, security organizations for application fiber-optical microphones.

Acknowledgements

This work is supported by Lithuanian State Science Foundation (Grant No. T-104/08).

The authors are much obliged to the Lithuanian Semiconductor Physics Institute in which the experiments have been carried out, as well as to the companies AndaOpteck for fiber-optic sensors supplied free of charge, and Skaidula that provided the measurement equipment and produced fiber pigtails.

References

4. **A. Siegman.** Lasers. Maplewood, NJ: Univ. Sci. Books. 1986. p. 663-681.
5. **H. Kogelnik, T. Li.** Laser beams and resonators. Appl. Opt., vol. 5, No. 10. 1966. p. 1550-1566.
6. **V. Kleiza, J. Verkelis.** The Fiber-Optic Non-Contact Piezomechanical Nano-Micro Positioning, Manipulating and Measurement System // Journal of Vibroengineering. 2008. Vol. 10, No. 2, p. 180-183.
7. **V. Kleiza, J.Verkelis.** Investigation and Comparison of Modelling and Experimental Results for the Fiber Optopair Reflection non Contact Displacement Sensor // Proceedings of SPIE. 2007, Vol. 6596. p. OV 1-6.

Proceedings of 4th International Conference ITELMS'2009

Military Specialist Preparation Features in Nowadays Environment

S. Bekešienė*, V. Kleiza, A. Malovikas***

**Gen. J. Žemaitis Military Academy of Lithuania, Šilo 5A, LT-10322 Vilnius, Lithuania,
E-mail: svajone.vosteriene@lka.lt
** Intitute of Mathematics and Informatics, Akademijos str. 4, LT-08663 Vilnius, E-mail: vytautas.kleiza@ktl.mii.lt*

Abstract

Traditionally the leading attention to leader education preparing to leader as administrator, which can organize any kind of fighting action, combat arrangement, thorough equipage for soldiers and other, without including the psychological, the emotional, the individual and the other peculiarities. Also the main changes in view to army performance in nowadays situations when we must fighting with terrorism, prevent the armed conflicts, the changes in armed forces performance in inside political and the others increasingly request a higher competent in professional, moral-psychological, humanity for army control for various administrative level leaders.

The reviews of best practices in leadership development (LD) have concluded that the key to effective LD in organizations is the systematic application of tools and practices. In recent years, the Lithuanian Military Academy (LMA) has embarked on an effort to systematize leadership in its training and education system. This study describes the development of a survey measure that is based on a model of the "system components of LD" that has guided the LMA's efforts to design systematic leadership development practices across different military training courses and schools. Data is collected on the "leadership climate" across training companies of officer cadets ($N = 111$). A confirmatory factor analysis is performed which provides evidence for the construct validity of the measure. Scale reliabilities are also reported. The findings are discussed on context of the value of the measure and the "systems model of LD", with regard to the challenges of systematic leadership in military organizations. Also in this article the algorithm scheme for test program of the leader abilities and possibilities is presented.

KEY WORDS: *leader, army, leadership, geopolitics, algorithm schema, test.*

1. Introduction

To qualify as a military specialist we need a complex attitude to this process content and goals. The effective influence for preparation content are doing such as government military-politically interests, public and requirements for military practice for military specialists, the pedagogical and psychological condition of education, the manning methods of army personal (officers and soldiers), the military-professionals manning for army and others. All this factors are by influence of the global military range, geostrategy and geopolitical environment.

The fundamental changes in global military environment and in every state society in regional level deep increase the enforcements for military commanding personnel. This process seeks to see that peculiarity of low levels and high levels are not the same. The low levels necessitate direct style of leadership and the high level requires the indirect leadership. The process is important because develops in political, diplomatically, economical, cultural and regulation fields, that dimensions all time transform. This processes influence military environment development and necessitate the leaders, which will be good professionals and will solve a difficulties. In nowadays for military commanding leadership personal are significant not only the professional skills.

The analysis of leadership literature shows a range of leader approaches such as: the official training, the organizational individual resource approach, person-psychological approach, and the best exercitation approach [3, 6, 11]. These approaches differ in their use of leadership practices, processes, tools and content.

The official preparation approach for leadership includes workshops or classroom teaching of leadership theories and principles. The official training can be positive, especially if the education is linked directly to the occupation experiences or used as a supplement experience to provide learning opportunities (e.g., in simulations, action learning), there is little real confirmation to demonstrate the actual reassign of such training on the occupation. In an extensive field study of different proposals for official leadership grounding and expansion are the effective leadership guidance that included elements of theoretical development, personal growth including: the proof, the risk taking and the individual-discovery, mastery-building and feedback. Eventually, the primary contribution of formal leadership training is insight development. Time and actual on-the-job leadership experience are needed for mastery of leadership. The leadership training also depends on the individual motivations, skill and chance to learn, ponder and alter.

The organizational individual resource attitude to leadership combines issues such as selection, recruitment, training and succession planning to prepare and equip leaders to be effective to transit to the next level of leadership. Leaders must conceptualize what each passage entails the knowledge, the skills or abilities a leader must have and the challenges involved in making each move to the next higher level. The strength of this idea is that it differentiates the leadership demands required at different levels of leadership in the organization [4]. There can be noticed, that each leader have a wish to became better then colleges. In the foreground is the leader's person. So, there are several questions: what must know nowadays leader about leadership, what requirements are raise for leader and how the leader became.

The personal-psychological advances to leadership related on individual alter in terms of how one thinks of oneself. There are contended that three critical psychological processes are the key to being an effective leader in today's context. These are self-insight, self-regulation and self-identity. Leaders must find their own individual way of being effective through understandings of their own strengths and weaknesses, of the context, of other people and their needs in the situation, and of how these three components relate to each other. In this attitude the leader should therefore facilitate the systematic development of these psychological processes through the use of feedback processes such as multi-source feedback, coaching, and self-reflection.

The best practices approach influence not only at the individual's growth and learning, but also attempts to align leadership to organization strategies. Best practices can embody any number of developmental processes and components including talent identification and management, individual development planning, management development, succession planning, mentoring and coaching. The best practices approach to leadership is basically still a training intervention even though the practices, tools and processes are integrated to provide a holistic developmental experience for the individual participant in the program.

2. Leadership Development in the Lithuanian Military Academy

As was stated in the introduction the effective leadership consists of many components that are thoughtfully integrated into a coherent system to develop the individual. Many leadership initiatives combine two or more of the leadership practices, but these initiatives should be functioned consummately the whole organization. The backbone of most leadership development systems is the formal program, which serves as a shell under which a variety of practices can be introduced to address the desired training objectives. One method of making leadership development more systematic is to design and implement an array of developmental experiences that are meaningfully integrated with one another.

The Lithuanian Military Academy personal has a big potential to solve leadership problems. The requirements, as demonstrated by accomplished experiments, for military and public specialists regularly are the same, only in activity are disagreements as inside as in outside. This conclusion takes possibility to organize military and academic research interconnection, also to achieve better results. Such type interaction must take the possibility to use the academic ground to solve military problems in the future in the military practice. For leadership feelings implantation are explore every avenues such as society, army an own Lithuanian Military Academy.

The methods of making leadership in the Lithuanian Military Academy are [6]:

1. Inculcate the estimation that in future practice to become the leader is only one way to be the professional of own area;

2. Teaching the cadet – future officer form the inside leader characteristics studying military also academic courses.

To reach these particularize goals are possible in such courses:

1. Organizational – regulative direction projects:
   - consistent study organization;
   - size up particular study goals (object, each lecture, seminar and practical prosecution);
   - constantly workable seminars, including the cadets activity character and the cadets-leaders requirements subject to theirs exercise duty and course;
   - differentiation for each discipline earmark hours for practical and theoretical practice;
   - the backups of particular questions avoidance in studying objects;
   - the particular requirements formulation for cadets and students;
   - military and academicals objects interaction organization.
2. Social – psychological direction envisages:
   - the cadets innate leader characteristics estimation and psychological help for its elaboration;
   - psychological support for cadets from enter studies in academy to finishing;
   - individual work with cadets;
   - objects, in which are studying leadership psychological aspects and work with subalterns features;
   - to work closely with army cohorts, where are serve academy graduates, and full-scale analysis of reciprocations about theirs post faults and achievements (reciprocations from cohorts and their own).
3. Scientific – technical direction:
   - the new pedagogical technologies use;
   - the automotive studies results evaluation system installation;
   - the scientifically studies organization (studies planning and regulation; studies places organize and development; professors qualification in-service training.

The effective leadership resulted from the systematic design of leadership practices and tools into a learning process. Simply providing stand-alone training or tools is not effective as the learning are not reinforced or integrated into the overall training program. Leadership development is not about delivering a program or administering a feedback tool or making people go through a developmental experience. Instead, effective LD ensures that such leadership development practices and tools are used consistently throughout the training. LD should be implemented as a systemic process because development occurs over time and a single training event or program is not sufficed.

3. The Leader Abilities Investigations System

So, for the leader abilities investigations in the Lithuanian Military Academy was used the methods such as tests - questionnaires and mathematical statistical methods. The investigations were accomplished in the teaching management objects in the Lithuanian Military Academy throughout the 2003/2004 – 2004/2005 academicals years [2]. The results of investigations was used to highlight the abilities as for leaders as for leaders groups.

The leader‘s regularity, as is known, characterize the qualification and competence. The ground of these features is the abilities system. Very important is to know own and generally leaders competence. In these intentions, the teaching planes for personal training must be organized by ground of abilities analysis. Particularity it is actual using the informatics technologies in teaching and testing systems.

The designed questionnaires for test procedure were prearranged to take into consideration the eleven skills features analyzing (Table 1). The test procedure shows, that some time was need to answer to 110 questions of this test and for test results analyzing by special regulations, which are presented in Table 2 as individual abilities and possibilities test results analysis, was needed much more time as was planed [2]. Consequently this experience required the second goal of investigation of the leader’s skills. There was made the decision to prepare the test program using for testing and get results analyzing the intelligent technologies. The algorithm scheme in consonance with prepared methodic, which are brief described in this article below, was decided to prepare for personal computers on the top of Linux operating system using Maple 12 version programming environment [5, 12].

For each leader and especially for military environment leaders is important the professionalism, which characterizes a qualification and competency. As are known, these are the main educating features. The qualification is definable as result of process of learning, educating, and achieved competence usage. The competence is knowledge and the skills coordination and the capability in the practical use for particular factors. The competence are achieving by nurture, training and by experience. In the traditional personal management the competence notion associate with individual perspective, the development of competence associate with qualification advance, and with requirements for individuals, associates [9]. Forasmuch the ground of competence are the abilities, the adequate exclusive: the personal, the social and the professional. The main abilities of these competences are presented in the Table 1.

Table 1

The ability system for leader

The competence quality	The main abilities
1. The personality	A – ability manipulate himself B – individual worth system (clarity) C – individual goals clarity D – regular personality development
2. The social	G – possibility influences the peoples round about I – ability to lead J – ability to teach and train (subordinates) K – ability form and develop group (work)
3. The professional	E – ability to solve the problems F – creative and innovation management H – modern knowledge (management and others)

The biggest part of personality abilities can be native and the biggest part of professional abilities – educated. The majority of abilities are: native and educated parts. The abilities can be and are developing. Consequently the abilities layer of the leader is the ground of qualification higher.

The abroad scientists and also the Lithuanian scientists to investigate the problems of the personal management used the tests [1, 9]. There are a lot of the tests for investigation of the leader’s abilities, but commonly the leaders choosing for testing own abilities the English management consultants Mike Woodcock and Dave Francis development manual [10]. Also in LMA for leader’s abilities investigations was used adapted, formulated and approbated by this research methodic recommendations the specifically test [10].

The Table 2 is the ground for tested person analysis, because after questionnaire is calculating results by each direction and filling the 2-th colon of the Table 2. After that, the analysis of get results for each direction is giving the place-range in the 4-th colon and inverse range in the 5-th colon. The learning requirements are designated after analyzing own abilities also possibilities and designed main limitations. The inverse range shows the importance leader’s restrictions and necessary learning tendencies.

Table 2

Individual abilities and possibilities test results analysis

Direction	Results	Strong sides	Range	Inverse range	Restrictions
A		Ability manipulate himself		Insufficient ability manipulate himself	
B		Individual worth system		Personal valuables system obscurity	
C		Individual goals clarity		Personal goals obscurity	
D		Regular personality development		Steady person suspended development	
E		Ability to solve the problems		Insufficient skills for problems solving	
F		Creative and innovation management		Insufficient creative	
G		Possibility influence the peoples round about		Insufficient ability to influence folk	
H		Modern management knowledge		Insufficient management intelligence	
I		Ability to lead		Weak leadership skills	
J		Ability to teach and train subordinates		Inadequate education abilities	
K		Possibility to influence the peoples round about		Low ability to form and develop the collective	

By this represented methodic in Lithuanian Military Academy was performed the investigations of management abilities and education requirements for over 100 cadets. The get results are presented in anonymity, don't indicating the names and the platoon of the tested cadets. The each cadet measured own abilities and possibilities after answering to all questions. Below in Table 3 are shown one case of questionnaire calculated results. In this example we can see that the lower result is two points reached on the professional competence quality, specifically on E – ability to solve the problems.

Table 3

The results for personal abilities and possibilities

Direction	A	B	C	D	E	F	G	H	I	J	K
Results	10	5	8	7	2	4	7	8	4	5	3

The get results also let us to form the abilities and possibilities sections for every one cadet in graphical view as shown in Fig. 1. To analyze tests results in graphical type was used the simple Microsoft Excel program. The graphical expressions of the get values let correctly to know in which directions must be developing the abilities, and this let to estimate the directions of the education priorities.

The group (flock, team) basics limitations can be estimating analogically as individual and herewith necessary education directions. In this way in the second colon of the Table 2 are laying the calculated and averaged the test results of all tested members of group. Then using investigated results of the test of abilities and possibilities is determined the education requirement. Instance, for example bring up the qualification, are preparing the education torrents from several groups, which education requirements are different, but the education process is organized by conjoint program and schedule.

In these cases the individual education requirements must be sum and highlight the profile of common requirements. For this goal are using the results of personal tests of abilities and possibilities. The underlying education directions of each member are summing. The torrent of education requirements profile shows underlying educational directions (Fig. 2).

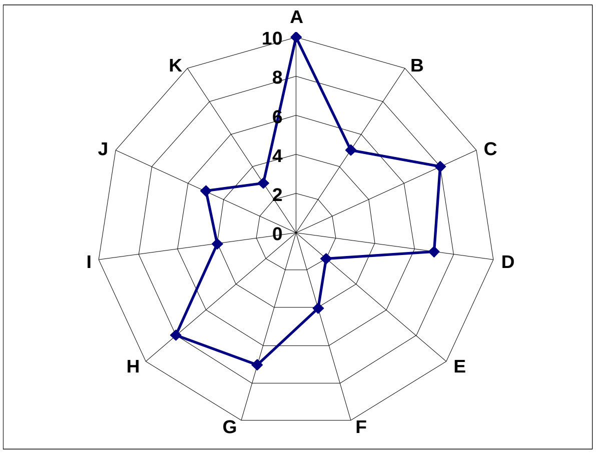

Fig. 1. Personal profile of abilities and possibilities (example from investigations)

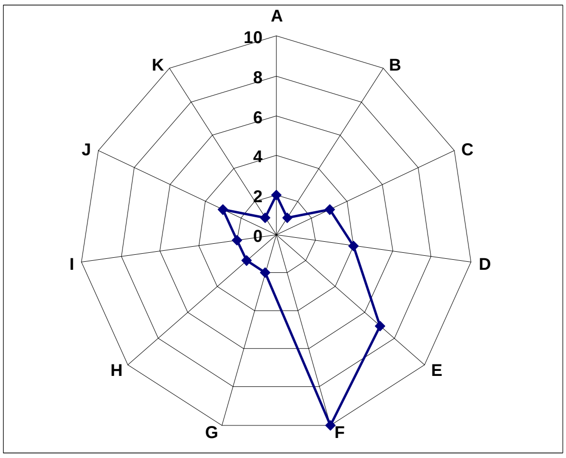

Fig. 2. The diagram of education torrent underlying profile (in all 111 members)

In this way using the individual and groups results of tests of abilities and possibilities are planning profiles for abilities and education requirements. The sectional education profiles help rationally form torrent education especially highly qualification programs and rationally to use the education time.

4. Study and Analyze of Leader Skills Use of Informatics Technologies

As was said before, the effective usage of investigation methodic can be reach by using informatics technologies. The leader's skills tests system must be prepared by solving such problems:

1. Prepare the tests system for abilities investigations and analysis;
2. Prepare test program and methodic for personal computer use;
3. Prepare the leader's skills self-control and education system by using distance teaching;
4. Prepare group skills control and educate system using informatics' technologies.

The referred problems can be solved by prepared leader's skills: investigates, education requirement and education algorithm, in education system. This is a large scale of propositions that must be solving to integrate the study and analyze of leaders' abilities into test program.

In the third paragraph of this article was described the first step prepared in Lithuanian Military Academy, the methodic for abilities investigations and analysis, which was used for the second step realization. There was made-up the algorithm, by prepared test program and methodic, for personal computer with Linux operating system [5]. Also was foreseeing to use for leader's skills test program realization for personal computer the Maple 12 version programming environment and one of its possibilities such as maplet [12, 8]. The schema of the test algorithm is presented in Fig. 3 below. The prepared construction was realized in 37-th blocs and is the direct visualization of testing methodic for leadership analysis used for investigations in Lithuanian Military Academy [2]. All recommendations how to analyze cadet's skills in presented algorithm schema are included. So, this tests schema by the three competence qualities for eleven main features for leader's abilities investigations is constructed to draw the individual abilities and possibilities for the chosen eleven features. As scores, the test program gives the calculated points, and also shows diagrammatical visualization of get results. The visualization is very viewable for analyzing; in this you can ascertain to compare presented test results in Table 2 and in Fig. 3.

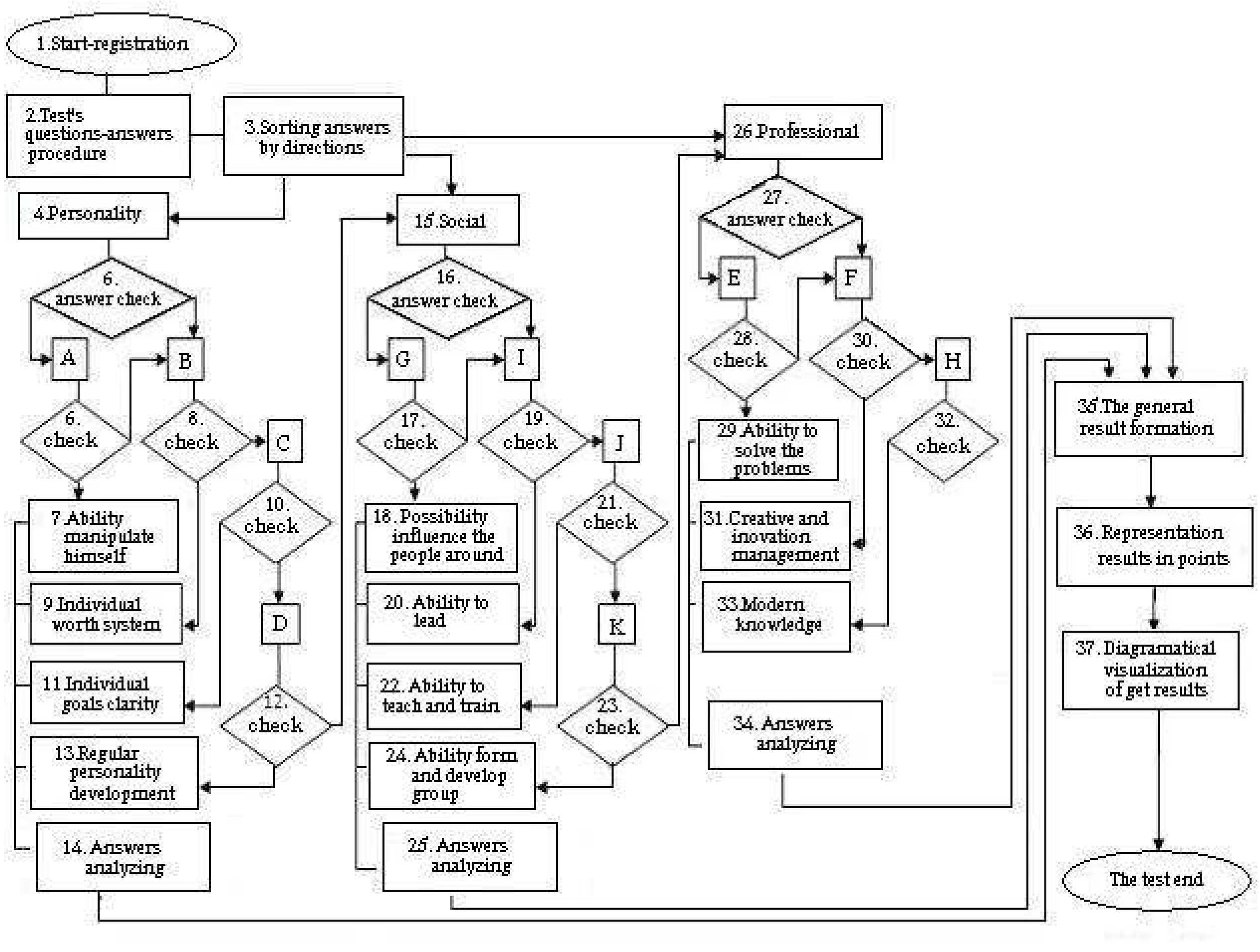

Fig. 3. The schema of the test algorithm

Traditionally existing such type programs are required information for tracking the progress, so the start is in 1-th bloc - personal information of a cadet. After registration the process goes to 2-th bloc, where are the test's tasks and assignments which a cadet has to do. The 1-th and 2-th blocs are the testing cadet's direct work with test program. The test user can see the tasks in appear the program windows and must chose the answer "Yes" or "No". The answers are moving to 3-th bloc where are sorting by directions of investigating abilities. Then all answers are checking in the 4-th, 15-th, and 26-th bloc's sub blocs. The competence quality as personality (from 4-th to 14-th blocs) are analyzing by four features: A – ability manipulate himself; B – individual worth system (clarity); C – individual goals clarity; D – regular personality development. In each direction high score 10 points. The competence quality as social (from 15-th to 25-th blocs) are checking by four features: G – possibility influences the peoples round about; I – ability to lead; J – ability to teach and train (subordinates); K – ability form and develop group (work). Also was choosing for this investigation the competence quality as professional and from 26-th to 34-th blocs is analyzing: E – ability to solve the problems; F – creative and innovation management; H – modern knowledge (management and others).

The each competence quality test's answers analyzing are processing in 14-th, 25-th and 34-th blocs. All calculated results information fall into 35-th bloc, where is forming the general test results. The 36-th bloc is forming the test score where the expressions of the value are points. But for us was very important that get results be clarity understand by tested cadets, and was decided that the test can inform user about get scores by diagrammatical visualization. This last step is the 37-th bloc.

The test program end is performed after passing all blocs, and get results are using for leader development.

5. Conclusions

The leader's professionalism characterizes qualification and competence. There are different competency types, but in our investigations was chosen: individual, social and professional. The ground of competency is abilities. In this article was presented the methodic for study and analyze of eleven main features of leaders skills.

Nowadays successful work of leader requirements gives attention not only for leader as for good administrator and hand training, but also for adequate psychological training. The essence revelation for leader is necessary. So by these investigations was resolved the test system helping to know what type of knowledge we must to give, what leader features form and considered to cadets individual features help them eliminate or improve own abilities to became the leaders.

The leader features education in Lithuanian Military Academy require the systemically view to cadets and academy all levels personal work, which must guaranty higher level of the well-rounded training for future officers. This goal can be reached continually improving interaction in different academy layers. The pedagogical technology let regiment and logic for pedagogical process for military specialist preparation. The study results are the algorithm for test program of study and analyze of leaders skills. The realization of this algorithm helps to successfully measure the individual abilities, and lets the creative use of pedagogical technologies, which guarantee the professors' training process realization development, the betterment of quality of military specialist. The informatic technologies will let to make the analysis in much shorter time.

References

1. **Ariane Lussato**. Les tests de recrutement (leurs limites). Presses Universitaires de France, 1998. 127 p.
2. **Baležentis A**. Vado (vadovo) gebėjimų tyrimai ir analizė naudojant informacines technologijas // Personalo vadybos teorijos ir praktikos aktualijos. Vilnius: LKA, 2004.
3. **Huntington Samuel P.** The Soldier and the State: The Theory and Politics of Civi-Military Relations/Cambridge: Harvard University Press, 1957, 83-85 and passim.
4. Lietuvos Respublikos krašto apsaugos sistemos organizavimo ir karo tarnybos įstatymas. Vilnius: Žin., 1998, Nr 49-1325.
5. Linux-based operating system. http://www.ubuntu.com/ . (2009-04 15).
6. **Malovikas A., Prakapienė D.** Karybos specialisto rengimo aktualijos globalizacijos salygomis// Vadybos šiuolaikinės tendencijos (Modern tendencies of management). Vilnius: LKA, 2008.
7. Maple 12. http://www.bu.edu/systems-support/software/maple.html . (2009-04 15).
8. Maplets Beginner's Guide. http://valle.fciencias.unam.mx/~hector/mapletsguide.pdf . (2009-04 15).
9. **Martinkus B., Neverauskas B., Sakalas A.** Vadyba specialistų rengimo kiekybinis ir kokybinis aspektas. – Kaunas: Technologija, 2002. 173 p.
10. **M. Woodcock, D. Francis.** The unblocked manager. A practical guide to self development. Vildwood House, 1982. 300 p.
11. Vadovavimas jūrų pėstininkams. Jūrų pajėgų departamentas. JAV jūrų pėstinikų štabas. Vašingtonas. DC. 20380-1775. 1995-01-03.
12. **K. Geddes, G. Labahn, M. Monagan.** Maple 12 Introductory Programming Guide, Maplesoft, 2008.

Proceedings of 4th International Conference ITELMS'2009

The Intelligent Technologies Application for Artillery Control

S. Bekešienė*, R. Baušys, V. Kleiza***, A. Pincevičius***

**Military Akademy of Lithuania, Šilo srt. 5a, LT-10322 Vilnius, E-mail: svajone.bekesiene@lkat.lt*
**Military Akademy of Lithuania, Šilo srt. 5a, LT-10322 Vilnius, E-mail pincev@cablenet.lt*
*** Vilnius Gediminas Ttechnical University, Saulėtekio ave. 11, LT-10223 Vilnius, E-mail: romas@fm.vtu.lt*
****Intitute of Mathematics and Informatics, Akademijos str. 4, LT-08663 Vilnius, E-mail:vytautas.kleiza@ktl.mii.lt*

Abstract

A mortar is a close battle piece of ordnance designed for shooting with high trajectories ($\alpha > 45°$) and is used as a mobile, powerful "infantry artillery". This weapon possesses the capability to destroy enemy soldiers and fire positions, concealed behind hills or in a settlement, boasts simple construction and maintenance, has a small mass and mobility (they can be transported by a small cross-country vehicle). Due to these qualities mortars can be effectively employed on mountainous terrains for surprise effect. At present 60, 80 and 120 mm mortars are most popular. These weapons manage to retain popularity and are being perfected. Since a mortar is a relatively cheap gun, its control is not yet computerized. This study presents possibilities of the computerized control of this weapon and planned representation of combat results that might aid in taking decisions concerning further actions.

1. Solution of the Ballistic Problem

For a mine to hit the designated point, it is necessary to solve problems of its trajectory control. It is necessary to establish the aiming setting (the angle of the throw in thousandth parts), the main direction of firing (the angle with which the muzzle of the mortar is tilted referencing from the north direction) and the number of the charge (the initial velocity of the mine) under known target coordinates and meteorological conditions. Such a movement is described using a system of equations

$$\begin{cases} m\dfrac{d^2x}{dt^2} = -k\dfrac{dx}{dt} + F_1\cos\phi \\ m\dfrac{d^2y}{dt^2} = -k\dfrac{dy}{dt} + F_1\sin\phi \\ m\dfrac{d^2z}{dt^2} = -k\dfrac{dz}{dt} + mg \end{cases}, \tag{1}$$

with initial conditions

$$\begin{cases} x(0) = 0,\ x'(0) = v_0\cos\alpha_1\cos\alpha_2 \\ y(0) = 0,\ y'(0) = v_0\cos\alpha_1\sin\alpha_2 \\ z(0) = 0,\ z'(0) = v_0\sin\alpha_1 \end{cases}.$$

where m – mass of the mine (shell), g – free fall acceleration, k – resistance to movement quotient, v_0 – the initial velocity, α_1 – the angle of the throw, α_2 – direction setting, i. e. the angle between the north direction and the direction to the target (main firing direction), F_1 (frontal), F_2 (side) – wind impact force and ϕ – the angle of wind direction and main firing direction.

In the system of equations (1), resistance to movement quotient k is a variable that is hard to choose and experimentally determine. This variable depends on the velocity of the mine and meteorological conditions: atmospheric pressure, temperature of the air, humidity in the points of the trajectory. All these parameters change during the movement since the device rises to a great height.

In studies [1, 2] proposed methodology makes it possible to approximately solve the non-linear differential equations system which describes the movement of the mine on the trajectory. A non-linear problem, which "rectifies" at individual intervals, is being solved. For various target distances constant k is chosen so as to make the data of firing tables and computations coincide. Then the obtained points are approximated with the help of the polynomial and the analytical dependence of the resistance-to-movement quotient k on the distance of the target is obtained. Fig.1.The discontinuity of the curve corresponds to the transition of the mine velocity to the supersonic movement interval.

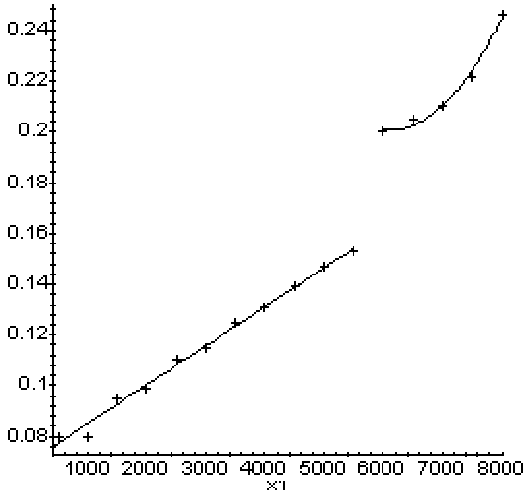

Fig.1. Dependence of the resistance quotient *k* on the distance to the target

Then, the system of equations with initial conditions (1) and target distance being defined can already be solved analytically. After numerical values of the quotients and parameters of initial conditions are entered into these solutions, they become functions of angles α_1, α_2 and time t. We obtain a corresponding system of non-linear algebraic equations:

$$\begin{cases} x(\alpha_1,\alpha_2,t) = L \\ y(\alpha_1,\alpha_2,t) = 0 \\ z(\alpha_1,\alpha_2,t) = \Delta h \end{cases} \tag{2}$$

where L is the distance of the target, Δh – difference between the heights of the mortar and the target with reference to sea level. If the distance of the target L =1500 m and the difference in heights Δh = 0, we can obtain these firing and transit trajectory parameters: initial velocity is 163 m (charge No. 2), firing setting – 571000, angle of fall – 73°, fall velocity – 152 m/s, flight time – 30 s, trajectory height – 1137 m.

2. Finding of Target Parameters

For finding firing parameters these initial data are necessary: target distance and direction. Target coordinates on the map might also be indicated. Since distances are not great (up to 8000 m), we can make use of the qualities of the rectangular Cartesian coordinates system. Knowing Δx, Δy and Δz, we easily find the distance of the target "main firing direction" $\alpha_2 = \arctan\frac{dy}{dx}$. Signs/signatures of the values, i. e. positive or negative, should be taken into consideration.

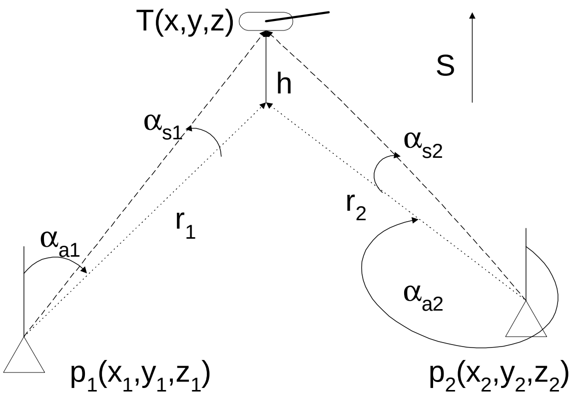

Fig. 2. Measurement scheme of the distance to the target, azimuth and the angles of the site (location)

Here α_{a1}, α_{a2} – azimuth angles are referenced from the north direction clockwise, α_{s1}, α_{s2} angles of the site/location – from the plane xy, r_1, r_2 are distances to the target, x, y, z –target coordinates, x_i, y_i, z_i – coordinates of the observation posts.

Reconnaissance data can be transmitted from the observation post: target distance from the observation post r is indicated and the direction to the target. Coordinates of the observation post $[x_s, y_s]$ are usually known. Differences in coordinates are found according to formula (having verified signs of the values) $\Delta x = x_s + r \cos \gamma$, $\Delta y = y_s + r \sin \gamma$.

If the difference between the heights of the mortar and the target is not very significant, it can be estimated with the help of the map. If fighting goes on in a mountainous terrain, the difference in heights should be estimated most accurately to avoid fatal mistakes. In that case, the most necessary data about the target is received from two observation posts (see Fig. 2).

Further we solve the optimization problem. We find the most suitable target coordinates by minimizing the polynomial of errors. Absolute errors: ε_a – the error of the azimuth angle, ε_r – the error of the distance and ε_s – the error of the site angles can be written down as follows:

$$\left.\begin{aligned}
\varepsilon_a &= \sum_{i=1}^{2}\left[\arctan\left(\frac{x-x_i}{y-y_i}-\alpha_{ai}\right)\right] \\
\varepsilon_s &= \sum_{i=1}^{2}\left[\arcsin\left(\frac{z-z_i}{\sqrt{(x-x_i)^2+(y-y_i)^2+(z-z_i)^2}}-\alpha_{si}\right)\right] \\
\varepsilon_r &= \sum_{i=1}^{2}\left[\sqrt{(x-x_i)^2+(y-y_i)^2+(z-z_i)^2}-r_i\right].
\end{aligned}\right\} \tag{3}$$

By comparing errors of measurements, described in (3), the system of equations and absolute errors of corresponding measurement devices (rangefinder, angle measuring devices), we will obtain the “polynomial of errors”:

$$s = \left(\frac{\varepsilon_a}{\Delta\varepsilon_a}\right)^2 + \left(\frac{\varepsilon_s}{\Delta\varepsilon_s}\right)^2 + \left(\frac{\varepsilon_r}{\Delta\varepsilon_r}\right)^2. \tag{4}$$

Further we find such target coordinates x, y, z with which functional (4) reaches the minimum and meanwhile find the site of the target with a desired reliance probability. Having solved the problem by using observation posts data presented in

Table 1

α_{ai}	α_{si}	r_i	$\Delta\varepsilon_a$	$\Delta\varepsilon_s$	Δr
51	4.5	6400	0.5	0.5	30
34	8	3600	0.5	0.5	20

We will obtain these target parameters with reference to the mortar (distance, difference in heights and direction (azimuth) angle).

$$L = 7800 \text{ m}, \quad \Delta h = 500 \text{ m}, \quad \alpha_a = 750000.$$

With the indicated data available, it is possible to use the standard program for the computation of target settings. Conducting firing on a mountainous terrain, such computations can be very useful.

3. Individual and Group Target Destruction Probability

Dispersion of artillery shells and mines is described by a bivariate normal distribution:

$$P = \frac{1}{2\pi\sigma_x\sigma_y}\int_{x_1}^{x_2}\int_{y_1}^{y_2} e^{-\frac{(x-x_m)^2}{2\sigma_x^2}} e^{-\frac{(y-y_m)^2}{2\sigma_y^2}}\, dxdy\,. \tag{5}$$

Where $[x_1, x_2]$, $[y_1, y_2]$ are target measurements, $[x_m, y_m]$ – aiming point coordinates, σ_x, σ_y – mean standard deviations. If we miss and fire several shots to the same target, the hit probability is computed according to the formula:

$$P_n = 1-(1-P)^n,$$

where $(1–P)$ is a probability to miss during each individual trial. This probability does not change. Hit probability of the tank in the distance of 1 km $P \approx 0.136$. In order to destroy this tank with the reliance probability of 0.85, it is necessary to fire 13 times. While firing with low trajectories, chances of hitting the target considerably increase (an artillery shell or a grenade, moving with a low trajectory, has a much greater chance of hitting the target). A mortar is in essence a very effective weapon in destroying group targets and was designed as such.

The system of equations (1) with initial conditions can be solved when random values of the initial velocity and other parameters are provided:

$$v_0 + random[normald]\Delta v_0 \quad , \quad k + random[normald]\Delta k \, , \qquad (6)$$

$$F_1 + random[normald]\Delta F_1 \quad , F_2 + random[normald]\Delta F_2 \, ,$$

where *random[normald]* is a random value distributed according to the standard normal distribution $N(0, 1)$, Δv_0 , Δk , ΔF_1, ΔF_2 are maximum errors of the initial velocity v_0 , resistance quotient k, impact of the head wind F_1 or side wind F_2.

For example, the possible difference of the initial velocity of a 120 mm mortar mine in tables [3] is indicated as 0.5%. While firing the barrel is not completely still and this error increases. Accidental fluctuations in atmosphere pressure and temperature determine ≈ 1% difference of the resistance quotient k. If we compute 10000 shots to a target within the chosen distance with random parameter values, we will be able to rather accurately estimate mean standard deviations σ_x, σ_y.

Usually, a group target (the adversary in the assembly area of 200x300 m) is fired upon by a six-mortar group. In executing one salvo, each mortar fires three times, correspondingly changing the angle of the barrel. Thus, during one salvo, 18 shots are fired. Because of firing errors, explosives though aimed at the same point $[x_i, y_i]$ fall at ever different spots. Knowing σ_x, σ_y deviations can be estimated:

$$x_i = x_i + 3\sigma_x \times random[normald],$$
$$y_i = y_i + 3\sigma_y \times random[normald].$$

A random dispersion of mines with the six-mortar battery having fired 10 salvos (ten shots to each point of aiming) is represented in Fig. 3.

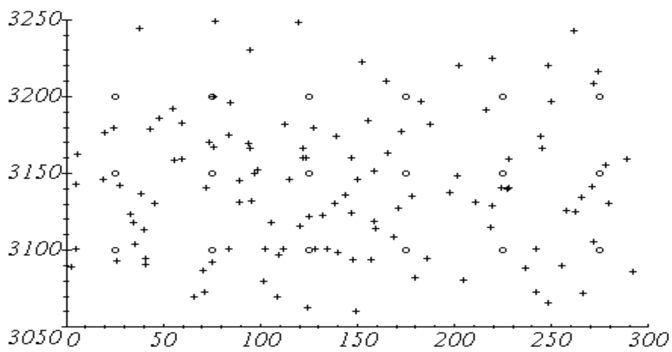

Fig. 3. Scheme of targets when firing at a group target and mine dispersion after 10 salvos. L =3050 m, σ_x = 26 m, σ_y=18 m. o → points of aiming, + → points of mine fall.

Granted that each mine destroys enemy soldiers within the radius of 15 m, it is possible to estimate what part of the enemy soldiers will be destroyed. Since mine dispersion is random, this process, that is the computation of losses caused by ten salvos, must be performed a 1000 and more times (1000 realizations). Having counted the average of the results of realizations, we will get a true-to-life result. The number of salvos is increased until the desired level of group target destruction is reached. It is possible to change the arrangement of group target aiming points and optimize artillery fighting upon a group target.

4. Representation of Results. Information Interface (Glyph)

We shall discuss the concept of information interface (glyph). By employing the possibilities of the Geographical Information Systems (GIS), a “tool” able to supply additional information about capabilities of an object in the future time was created. Possibilities of future actions of this object are analyzed in relation to the real position of the object. The position of the object is visualized not just estimating its spatial position (point on the map). The program, which estimates the capabilities of the object for a certain action and represents them on the map (what the object or its parameters will look after a certain action), is provided.

The created “tool” makes it possible to represent group target destruction results on the map. Having activated the program describing the destruction of a group target, we receive percentage values, associated with a concrete place (coordinates of the location and matrix elements which indicate destruction probability during the foreseen firing).

Fig. 5 represents the area covered by enemy fortifications. The distance between the points in the horizontal direction is 10 m, in the vertical one – 16 m. When losses increase, the color darkness (it is possible to indicate destruction percentage on the color scale).

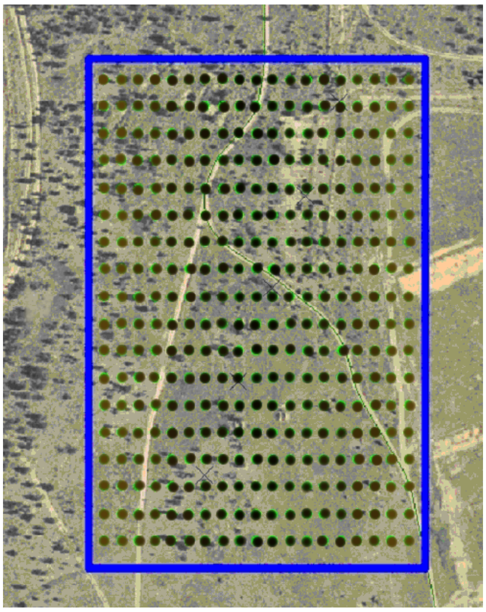

Fig. 4. Probables “sheet” of possible losses. Darkness of color indicates increasing losses

5. Conclusions

1. Using the created programs, in several seconds, it is possible to compute firing parameters:
   1.1. number of the charge;
   1.2. sight setting, including corrections because of pressure, temperature, charge temperature, impact of the wind, inadequacy of the mine mass;
   1.3. setting of the main firing direction;
   1.4. trajectory height, incidence/fall velocity, incidence/fall angle, etc.
2. To find the number of mines in order to destroy a target at a certain distance with a degree of reliability.
3. To find destruction parameters of a group target and represent the possible situation on the map.

Using these programs, a unit commander can analyze different would-be fighting scenarios; they can become a part of the decision taking system. Implementation of the proposed control programs will turn the mortar into a truly modern weapon.

References

1. **A. Pincevičius, R. J. Rakauskas, G. Misevičius.** The numerical simulation in ballistics //Nonlinear Analysis: Modelling and Control, 2001, vol. 6, No. 1, p. 89-104.
2. **A. Pincevičius, R. J. Rakauskas, G. Misevičius.** The numerical simulation of military skills // Liet. Matem. rink., T 42, spec.nr. Vilnius, 2002, p. 26-33.
3. Minosvaidžių padalinių kovos statutas. Lietuvos Respublikos kariuomenė, Divizijos Generolo ST. Raštikio Puskarininkių mokykla, Kaunas, 1997 m.

Proceedings of 4th International Conference ITELMS'2009

The Effective Use of the Intelligent Technologies in Planning Infantry Attacks

S. Bekešienė*, R. Baušys, V. Kleiza***, A. Pincevičius***

**Military Akademy of Lithuania, Šilo srt. 5a, LT-10322 Vilnius, E-mail: svajone.bekesiene@lkat.lt; pincev@cablenet.lt*
***Vilnius Gediminas Ttechnical University, Saulėtekio ave. 11, LT-10223 Vilnius, E-mail: romas@fm.vtu.lt*
****Intitute of Mathematics and Informatics, Akademijos str. 4, LT-08663 Vilnius, E-mail: vytautas.kleiza@ktl.mii.lt*

Abstract

A system of "program tools" created by using information bases of Geographic Information Systems (GIS) makes it possible to carry out the engineer estimation of the terrain, obtain data on the network of roads, water bodies, vegetation, building structures and qualities of the soil. A visibility instrument has been created which indicates visibility on the battlefield from several chosen terrain places. Actions of each individual soldier on the battlefield are modeled, the impact of random factors is estimated and a "digital experiment" of a would-be attack is carried out. Various possibilities of the representation of the obtained data are discussed. A program representing results of a would-be "attack variant" on the map has been created. This makes it possible to estimate capabilities of a military unit fighting on a concrete terrain and thus contributes to a better decision making on the part of the unit commander.
KEY WORDS: *modeling, military operations stochastic models, geographical information system.*

1. Engineer Estimation of the Terrain

Modern information technologies [1–4] are widely employed in planning military actions and estimating capabilities of a military unit to execute a certain task. The main information source about the terrain is sheets of a digital map with the scale of 1:10000. The entire standard information of the digital map is based on only slightly-associated integration between geographic information systems and relation data base packets. GIS information layers are created on the basis of spatial information of the terrain in accordance with the requirements for a concrete military operation. To this end the necessary "program tools" [5 - 7] were created.

The created tool of road analysis makes it possible to organize dynamic inquiries in order to find roads satisfying certain criteria. The necessary information is automatically provided by the electronic map. Having activated this tool, it is sufficient to circle the area of interest and the system points out all the roads of the chosen width. Road surface, number of lanes and other attributes inherent in the system are shown. Inquiry about a bridge brings forth complete bridge information: length, lifting capacity, etc.

All the terrain in the information system is divided according to the utilization type: settlement, arable land, forest. The tool of the forest analysis makes it possible to obtain information about the density of the forest, thickness of tree trunks. Having chosen the measurement tool, it is possible to estimate the width of the clearing and obtain information on the cross-country capacity on the terrain.

Each individual tool generates its own individual information layer. It is possible to obtain a map of the indicated terrain roads or forests, or to see a complete image of the "combined layers". Thus, it is possible to fast and without difficulty choose maps and obtain all the necessary *engineer information.*

GIS information bases hold data about the height of objects on the terrain. A height analysis tool has been created which automatically extracts the necessary data from electronic map bases and then provides information about the visibility in the designated terrain. Let's say that ten soldiers are fortified and are about to be attacked by a three times larger force – 30 soldiers. Having summoned the visibility tool, we indicate the coordinates of the tops of the square that we desire to see, the coordinates of the points from which we are going to observe the terrain and obtain the image of visible (green) and invisible (red) areas in Fig.1. At the same time a visibility matrix is created (visible points are designated by 1, the invisible ones – by 0) Fig. 2a.

In order to obtain the visibility matrix of the fortified adversary, it is sufficient to know visibility from 5 points (for each pair of soldiers) and create a generalized visibility matrix. The created program executes the generalized procedure, i.e. it creates the visibility matrix of all defending soldiers. Such results are presented in Fig. 2b.

The distance on the terrain between the visibility points in the horizontal direction (longitude coordinate) is equal to 10 m while in the vertical direction (latitude coordinate) it changes to 16 m (it is not difficult for the elements of the matrix to find the coordinates of the indicated point).

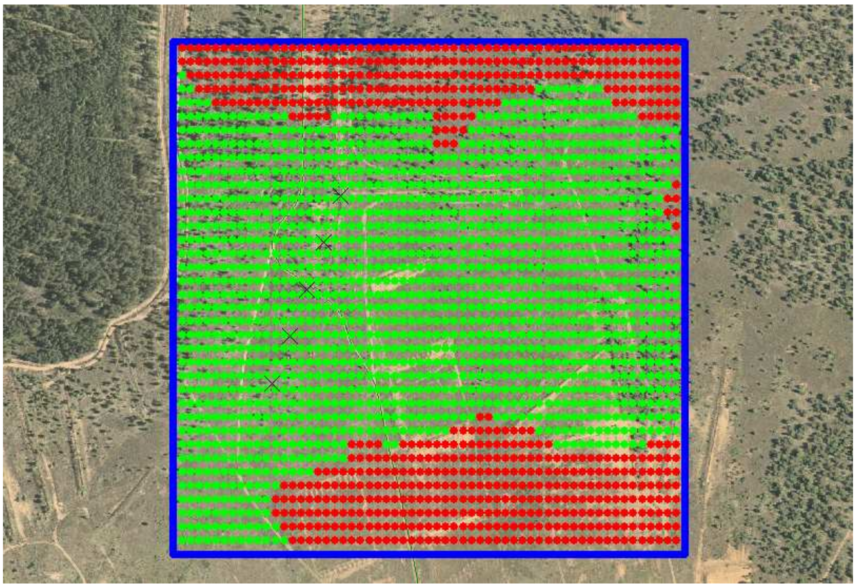

Fig. 1. Image of terrain and work of the visibility tool: visibility from the designated “X” point (at the bottom).

0000000000000000000000000000000000000000000000000000000000000
0000000000000000000000000000000000000000000000000000000000000
0000000000000000000000000000000000000000000000000000000000000
0000000000000000000000000000000000000000000000000000000000000
0000000000000000000000000000000000000000000000000000000000000
0000000000111111110000000000000000000000000000000000000000000
0000001111111111111111111100000000000111000000000000000000000
0000001111111111111111111111111000000011111000000000000000000
0000001111111111111111111111111111110011111111000000000000000
0000001111111111111111111111111111111110111111100000000000000
0000011111111111111111111111111111111110000001000000000000000
0000111111111111111111111111111111111110000000000000000000000
0000111111111111111111111111111111111110000000000000000000000
000011111111111111**8**111111111111111111111000000000000000000000
0001111111111111111111111111111111111111000000000000000000000
0111111111111111111111111111111111111111100000000000000000000
0111111111111111111111111110111111111111000000000000000000000
0111111111111111111111111000000000011110000000000000000000000
0111110000001111111111110000000000000000000000000000000000000
0111111000000111111111111100000000000000000000000000000000000
0111111100000111111111111110000000000000000000000000000000000
0111111110000111100000111111000000000000000000000000000000000
0111111111111111000000000000000000000000000000000000000000000
0111111111111111100000000000000000000000000000000000000000000
0111111111111111100000000000000000000000000000000000000000000
0111111111111111110000000000000000000000000000000000000000000
0111111111111111110000000000000000000000000000000000000000000
0111111111111111111000000000000000000000000000000000000000000
0111111111111111111100000000000000000000000000000000000000000
0111111111111111111100000000000000000000000000000000000000000
0111111111111111111000000000000000000000000000000000000000000
0111111111111111000000000000000000000000000000000000000000000
0111111111111111100000000000000000000000000000000000000000000
0111111111111111100000000000000000000000000000000000000000000
0111111111111111110000000000000000000000000000000000000000000
0111111111111111110000000000000000000000000000000000000000000

Fig. 2a. Results of the visibility tool analysis. The observer point was designated by “8”. The place visible to him – 1, the invisible – 0.

0000000000011000011111111111111111111111111111111111111111111
1000000011111000011111111111111111111111111111111111111111111x
1100000011111100011111111111111111111111111111111111111111111x
1111001111111111111111111111111111111111111111111111111111111x
1111111111111111111111111111111111111111111111111111111111111x
1111111111111111111111111111111111111111111111111111111111111x
1111111111111111111111111111111111111111111111111111111111111
1111111111111111111111111111111111111111111111111111111111111
1111111111111111111111111111111111111111111111111111111111111
1111111111111111111111111111111111111111111111111111111111111
11111111111111111111**8**1111111111111111111111111111111111111111
1111111111111111111111111111111111111111111111111111111111111
1111111111111111111111111111111111111111111111111111111111111
111111111111111111**8**111111111111111111111111111111111111111111
1111111111111111111111111111111111111111111111111111111111111
1111111111111111111111111111111111111111111111111111111111111x
1111111111111111111111111111111111111111111111111111111111111x
1111111111111111**8**11111111111111111111111111111111111111111111x
1111111111111111111111111111111111111111111111111111111111111x
1111111111111111111111111111111111111111111111111111111111111x
11111111111111**8**1111111111111111111111111111111111111111111111
1111111111111111111111111111111111111111111111111111111111111
1111111111111111111111111111111111111111111111111111111111111
1111111111111111111111111111111111111111111111111111111111111
111111111111**8**111111111111111111111111111111111111111111111111
1111111111111111111111111111111111111111111111111111111111111
1111111111111111111111111111111111111111111111111111111111111
1111111111111111111111111111111111111111111111111111111111111
1111111111111111111111111111111111111111111111111111111111111
1111111111111111111111111111111111111111111111111111111111111x
1111111111111111111111111111111111111111111111111111111111111x
1111111111111111111111111111111111111111111111111111111111111x
1111111111111111111111111111111111111111111111111111111111111x
1111111111111111111111111111111111111111111111111111111111111x
1111111111111111111111111111111111111111111111111111111111111
1111111111111111111111111111111111111111111111111111111111111

Fig. 2b. A generalized visibility matrix. Pairs of attacking soldiers designated by “x”, pairs of defenders bay “8”.

The available generalized information on battlefield visibility (the visibility matrix) is used in solving the attack or defense task by applying the stochastic method. The attacking soldiers move along the designated lines (the direction of the attack and tactics is designated). Then we get the information stating when the adversary can see and fire at a concrete soldier. It should be pointed out that on real terrain the visibility (objects of more than 1 m in height are visible) rarely exceeds 300–400 meters.

2. Modeling of Combat Actions

Combat actions, in a very complicated way, are affected by many random factors the description of which by using analytical representations is often practically impossible. To this end statistical models and the Monte-Carlo method are used. When the relationship between the modeled objects is unknown or very complex, this method makes it possible to find the result of their interaction [5, 6, 7]. These actions of soldiers are modeled: movement towards the adversary, observation and detection of the enemy, firing and the elimination of the adversary. Similar actions of the adversary are modeled: detection of the attackers and their elimination.

If the visibility scheme of soldiers fighting in defense corresponds to that in Fig. 2b, the attacking soldiers at such a short distance are spotted right away. They are visible provided the terrain features do not impede. The soldiers move towards the enemy maintaining $d \approx 8 \div 12$ m distance between one another. The visibility of the soldier in attack is indicated (see Fig. 2b) by the elements of the matrix (1 – the soldier is seen, 0 – the soldier is not seen).

Certainly, different scenarios of soldiers' movement on the battlefield are possible. For example, with the platoon in attack, two teams attack from the flanks and one remains in the center (see Fig. 2b). The soldiers move forward in bounds. The soldiers rise for the bound at $\Delta t_1 \approx 3 - 4$ s (leaving adversary no time to take aim) at a random moment of time $\Delta t_2 \approx 14 - 16$ s. We will analyze their movement changing the time at $\Delta t = \Delta t_1 + \Delta t_2 \approx 18 - 20$ s intervals. This type of movement can be described as a re-location to another square (the sides of the squares are $\approx 18 \times 10$ m).

Let's say that two inside pairs of each team (in defense, a soldier aims and becomes a target himself *for a longer time*) rise for a bound ($\Delta t_1 \approx 3 - 4$ s), the remaining pairs cover by fire. Then, the pairs in the back rise for a bound and those at the front cover them by fire (see Fig. 3).

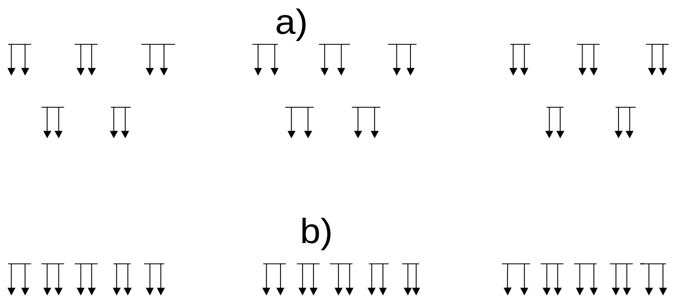

Fig. 3. Scheme: a) two inside pairs of each team rise for a bound, the remaining pairs cover by fire; b) pairs in the back rise for a bound and those at the front cover them by fire

In the studies [5, 6] the hit probability of the enemy in offence and defense were estimated. By using the method of least squares functions $P(r)$, estimating the hit probability with reference to the distance between fighters, were recorded. Graphic representation of these dependences is shown in Fig.4.

If a bound lasts 3–4 seconds, and the adversary needs 5 seconds to take aim, the hit probability decreases. Its change can be estimated by employing the formula that is widely used in the queuing theory:

$$P_i(r) = 1 - e^{\frac{P(r)\, t_i}{t_0}} \tag{1}$$

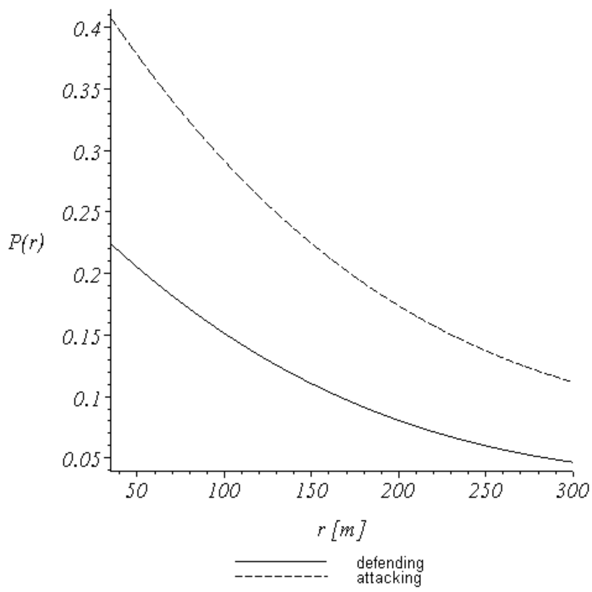

Fig. 4. Dependence of the hit probability on the distance between fighters.

where $P(r)$ is mean hit probability when target distance is r, t_1 is the average time during which a soldier manages to take aim (for example 5 s), t_i - stands for a random time interval (the time of the bound is 3–4 seconds).

Soldiers bearing automatic rifles choose enemy soldiers firing at them or those that are nearest to them and shoot by taking aim. Whether a concrete event has occurred is tested this way. For example, if hit probability in a concrete case, i. e. with the soldier being in a certain position, is equal to 0.4, the random variable R, distributed according to the uniform law within the interval [0; 1], is generated and the condition

$$R \le P_i\,(r) \tag{2}$$

is checked. If the inequality (2) is satisfied, it is considered that the event has taken place – “the target has been hit”, if it is not satisfied, the event has not taken place. The same model is used to check other events, for example “the enemy has been spotted”. Afterwards the results are summed up, casualties and numbers of personnel further participating in the attack are counted. This is repeated until the battle ends, i. e. the time allotted for the battle ends, more than half of the personnel are killed, etc. Thus the results of one realization are obtained. Such computations are repeated 100–200 times and the average of the results is found (each realization is different because ever different random variables are generated) for each computed time moment (point). The number of realizations is being increased until the obtained answer stops changing though the number of realizations is further increased with the indicated computation accuracy.

3. Information Interface (glyph)

We shall discuss the concept of information interface (glyph) [8]. By employing the possibilities of the Geographical Information Systems (GIS), a “tool” able to supply additional information about capabilities of an object in the future time was created. Possibilities of future actions of this object are analyzed in relation to the real position of the object. The position of the object is visualized not just estimating its spatial position (point on the map). A program, which estimates the capabilities of the object for a certain action and represents them on the map (what the object or its parameters will look after a certain action), is provided.

In more detail we shall describe the realization and application specificities of information interface in relation to a platoon that is ready to attack. The situation in this concrete case is provided in Fig. 4. Having activated the program describing the battle, we receive percentage values, associated with a concrete place (matrix point) with possible successes or losses during the foreseen battle. Possible losses are represented on the visibility scheme in different colors – the color darkens with increasing losses. This probable “sheet of possible losses” is supplied in Fig.5.

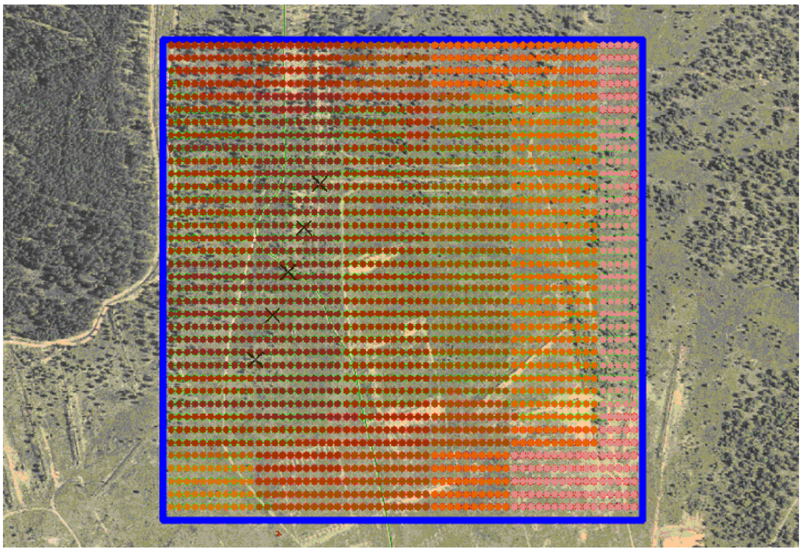

Fig.5. Probable “sheet” of possible losses. Darkening color indicates increasing losses.

4. Conclusions

Accurate and timely engineer estimation of the terrain by using GIS is a prerequisite for effective control of modern and rapid military operations. Employment of digital maps and digital terrain images, made by great resolution satellites, make it possible to perform an effective battlefield analysis by in advance more successfully choosing a location for the defense post.

The developed programs, employing stochastic models make it possible to describe combat actions of a concrete soldier and analyze the impact of numerous random factors on the course of the battle: the beginning of the attack, the duration of the bound, tactical elements (different movement types of soldiers on the battlefield, coverage by fire from the flank).

For individual fighting teams it is possible to choose the least dangerous movement direction on the battlefield. Computation results, by using information interface, can be represented on the map.

Employment of information interface can be an effective aid to the combat unit commander in decision making. This might be a part of a decision-making system.

It is possible to explore the impact of battle elements on the final result and use the programs in conducting classes and field training for cadets.

References

1. **M. Whelan, J. Loftus, D. Perme, R. Baldwin.** Reducing training costs through integration of simulations, C4I systems and expert systems // Proceedings of the 2002 Winter Simulation Conference, 2002.
2. **E. H. Page, W. H. Lunceford.** Architectural principles for the U.S. Army's simulation and modelling for acquisition, requirements and training (SMART) initiative // Proceedings of the 2001 Winter Simulation Conference, 2001.
3. **M. Rose.** A GIS-Enabled Expert System Approach to Military Training Area Scheduling and Management// Proceedings ESRI Int. User Conference, 2002, paper No. 765.
4. **G. W. King, C. T. Morrison, P. R. Cohen.** Action Models // Proceedings of the 2003 Winter Simulation Conference, 2003.
5. **A. Pincevičius, R. Baušys, P. Jankauskas.** Application of geographical information systems in the modeling of military operations // Aviation, Vol. 9, No. 3, 2005, p. 36-42.
6. **A. Pincevičius, R. Baušys, P. Jankauskas.** The simulation of an infantry attack using geographical information systems // Aviation, Vol. 9, No. 3, 2006, p. 30-36.
7. **A. Pincevičius, R. Baušys, S. Bekešienė, V. Kleiza.** Modelling of infantry attacks on real terrain, Nonlinear Analysis // Modeling and Control, 2008, Vol. 13, No. 4, p. 491-501.
8. **G. Kindlmann.** Superquadric Tensor Glyphs. Joint EUROGRAPHICS and IEEETCVG Symposium on Visualization. 2004.

Proceedings of 4th International Conference ITELMS'2009

European-Standard Railway Line between Vilnius and Kaunas

L. Černiauskaitė*, K. Sakalauskas**

**Kaunas University of Technology, Panevezys Institute, S. Daukanto g. 12, LT-35212 Panevėzys, Lithuania,*
E-mail: laucer@one.lt
****Vilnius Gediminas Technical University, Saulėtekio av. 11, LT-10223 Vilnius, Lithuania,*
E-mail: kazsak@ap.vgtu.lt,

Abstract

The article studies the possibilities for the enhancement of railway communication between Lithuania's two largest cities – Vilnius and Kaunas. Reviewing the political reasons and economic arguments behind the improvement of the transportation, it presents the theory of transport axle in the Vilnius-Kaunas dipole. Authors lay down arguments explaining why the transport axle should include a European-standard railway line like that of the Rail Baltica project. Two versions of building the European-standard railway line between Vilnius and Kaunas are proposed. Possibilities are discussed to modernize the existing railway line and adapt it to facilitate speeds for passenger train traffic up to 160 km/h. The article provides traction calculations, plans modernization works and calculates the investments required
KEY WORDS: *European-standard railway line, Vilnius and Kaunas dipole, transportation infrastructure, passenger transport railway, Rail Baltica, investments*

1. Introduction

After reaching population of half a million, cities, according to practices around the globe, start sharing the agglomeration – a complex accretion of urbanized territories, meshing around the old core in a dynamic and almost unstoppable process. If regulated in a rational way, it usually directs territorial development along the intensive traffic of transport, in most cases along main railway lines. Similar master plans have been developed in Stockholm, Copenhagen, Washington D.C. and many other cities similar to Vilnius in size. Our neighboring Poland, Belarus and Germany propose connecting largest cities by „axles", which are to become urban „skeleton", directing and regulating the oncoming expansion of city territories under the so-called theory of gravitational *urban* development. Territorial arrangement and urban framework of entire Europe and Lithuania – under the approved General Plan of the Republic of Lithuania – is based on the principle of „axles" and „spines" [1]. One of the key tasks of territory planning in this aspect is to render active the development of infrastructures that integrate the country into the European Union. Lithuania's strategic importance in the Baltic Sea region lies within the international transport corridors crossing its territory.

Lithuania's urban framework provides for top-level – interstate (European) and national – centers of Lithuania: multifunctional cities of Vilnius and Kaunas, which meet requirements for agglomerated metropolitan centers. Together they have enough potential; however, separately they lack and will continue to lack potential (especially demographic) for gaining recognition as centers on the European scale (*Euro City).* Such centers are important for the country's integration into the EU. The general plan stipulates forming a European-level center as an urban dipole of Vilnius and Kaunas, connecting the existing potentials of the two metropolitan centers. The status as Euro City guarantees far bigger EU support to the city and serves as a powerful magnet to attract foreign business and investments.

Consequently, absence of a Euro City-level metropolitan center would rank Lithuania among second-rate countries in the region, which would serve as a major obstacle for taking a due market position in the region and Europe. On the other hand, Lithuania is unlikely to acquire the status without a universally-accepted center with a population of at least a million people and a cluster of production, businesses, communications, international trade, banking, foreign tourism and a point of attraction of international relations [2].

A stretch with distinguishing parameters has been forming along the axle of the Vilnius-Kaunas dipole for many years. Firstly, 1.53 million people (38 percent of the country's overall population) reside in the territory of 30 kilometers on both sides of the axle connecting geometric centers of Vilnius and Kaunas; the density of population is 131.6 persons per km^2. The indicator is higher by a factor of 1.1 than the European Union's statistics (116.4 persons per km^2). The indicator puts the Lithuanian dipole region between Denmark (124/3 persons per km^2) and Luxembourg (170.9 persons per km^2) [3]. Studies of transport flows have shown that the majority of railway passengers leaving Vilnius in six directions from Vilnius on business days head towards Kaunas. A fourth of them reach Kaunas. Without doubt, the situation regarding railway passenger flows from Kaunas is similar.

The first priority, the first and mandatory condition for establishing a dipole is to create an actual potential of the two cities and, later, an urban link – a fast and convenient corridor of transportation.

The dipole will function in a lively and forceful way if a trip by rail between Vilnius and Kaunas takes 30-35 minutes at most. For this purpose, selection of locations for final passenger stops is of utmost importance – the locations should ensure fast and convenient communication with city public transportation, Rail Baltica stations and centers of both cities. In Vilnius, the final station should be located in consideration of the final stop of the planned high-speed tram route. Similar high-efficiency public transportation should be planned for Kaunas in the future [4].

Coordination of the region's economic development is a key factor in dipole economic growth, closely related with improvement of the transport system between Vilnius and Kaunas, as well as along the stretch between the two cities. This also involves encouragement of direct contacts, broad inclusion of business figures into the solution of dipole economic development matters and establishment of organizational structures to coordinate such actions [5, 6].

Practical observations suggest that an automobile highway is not suitable in this case because the speed limit tends to be reduced in small towns it crosses. The perfect axle for a dipole is high-speed railway or a combination of automobile highway, regular railway and high-speed railway. The route also connects two international airports and logistic centers.

Kaunas is located in the intersection of Lithuania's key roads of transportation: automobile roads of IX and I corridors, Moscow-Kaliningrad and Warsaw-Riga-Tallinn railways. These facts serve as preconditions for Kaunas to become a logistic and transport center [6].

Global practice shows that a modern public transportation system is the main factor in urban development [7]. The prepared scheme for Vilnius modern tram allows introduction of the progressive type of transport, thus building tough competition for cars and reducing environmental effects. The approved tram scheme provides for two new lines: "Stotis-Santariškės" and "Justiniškės-Centras-Lazdynai" [4, 8]. The main goal for developing communications, as stipulated in the Strategic Plan, is to improve conditions for international cargo and passenger transport. The following tasks are set out for achieving the goal:

- Modernization and development of international corridors to increase their capacity. Main instruments are as follows: *prioritizing railway transport*; building a European-track part of Corridor I from the Lithuanian-Polish border to Kaunas; modernizing the Vilnius-Kaunas section of IX B railway corridor; modernizing automobile roads, which are a part of the trans-European network; building lacking road connections in the cities of Vilnius and Kaunas; improving the infrastructure of international interior water roads.
- Creation of favorable conditions for expansion of international transport connections. Main instruments are as follows: modernizing Vilnius and Kaunas airports; designing and building logistics centers for intermodular logistics in Kaunas and Vilnius; modernizing existing railway stations for cargo and passengers; harmonize network of routes of all means of transportation and traffic schedules in the region [4, 6, 7].

In the effort to property organize passenger transport via railways, it is highly important to determine the demand for railways as a transport system in the society. Results of a survey carried out by J. Butkevičius show that merely two aspects of railway journeys have been identified as satisfactory by passengers – the possibility to reach the point of destination without transfer and low ticket prices. Merely 9–13 percent of passengers appreciate other advantages of railways, i.e., sufficient train speed, comfort, convenient schedules, safety and other. Without doubt, railway transportation has shortcomings. Biggest shortcomings include low transport speed and lack comfort [9, 10].

An analysis is provided of two possibilities to improve passenger communication between Vilnius and Kaunas: construction of a European-standard railway line and renovation of existing railways to increase speeds of passenger trains to 160 km/h.

2. European-Standard Railway Line Vilnius – Kaunas

Under the Rail Baltica project, the railway trunk-line should make a western bypass of Kaunas (Version I) or cross Kaunas suburbs in the east (Versions II and III) [11, 12]. Considering that the international line does not reach the Lithuanian capital, the shortcoming may be compensated by the building of a European-standard railway blind pass to Vilnius. Proper connection of the railway line with the Vilnius' modern tram would create a unique transport axle between the Vilnius and Kaunas dipole.

The European-standard railway line would start outside the Kaunas railway station where the existing railway forks in the Vilnius direction – close to the Palemonas station [7, 12]. Further on, route should continue on the common track formation all the way to Kaišiadorys where a platform for high-speed trains would have to be constructed. From the Kaišiadorys station to Rykantai, the new railway line should run close to the existing double-track railway or a combination track formation would be built on the common formation. From Rykantai, the line would go to the proposed modern European-standard railway station in Pilaitė where the final stop of the high-speed tram is also projected. The railway station would facilitate easy transfer to the tram or other means of transportation. From Pilaitė, there would be direct routes to the student campus in Saulėtekis, Santariškes, the central railway station and the international airport (with one transfer). To sum up the version, we see that the new European-standard railway line's 66.02 km (80% of the overall length) would run on the common formation all the way to Rykantai, with lines separated in sections where it is technically impossible (train separation points and low-radius curves). From Rykantai to Pilaitė (the final tram stop), the 12 km line would run on the new routes. Routing conditions are rather complex (the Paneriai forest) because of the nature reserve (Pit Geomorphologic Reserve) and the need to cross the Neris River valley.

As an alternative to the version, we can consider the possibility of routing to the Vilnius central railway station (as stipulated in the General Plan). The 27.76 km stretch from Rykantai to the Vilnius railway station is highly complicated due to the abundance of low-radius curves and the well-developed infrastructure of existing railway stations (Lentvaris, Paneriai). This causes extensive difficulties because the new railway line has to be placed in the existing track formation, while there is too little space due to dense territories and other railway equipment. Train speeds would be limited in the stretch, and construction costs of a new railway would be very high. This version is complicated in the technical and economic sense. Every kilometer of the European-standard railway line on a new track costs approximately 12 million litas. Every kilometer of the European-standard railway line on a combination track costs 9 million litas, while a kilometer of the European-standard railway line on an overhead track costs 15 million litas. More precise calculations would be made considering specific project characteristics. Additional assessment should be made of management and utilization costs [13]. A more precise economic and financial analysis requires calculation of *income* as well, with the majority of money coming from the infrastructure usage fee.

3. Research of Possibilities to Modernize the Existing Railway Line Infrastructure

The double-track stretch on the existing railway line Vilnius – Kaunas measures 103.3 km.

Overhaul repairs of the Vilnius – Kaunas railway line carried out in 2005 has enabled passenger trains to reach speeds of 100 – 120 km/h. Currently, a trip between Vilnius and Kaunas on an electric train ER-9 M takes 1 hour and 12 minutes (with 3 stops).

A study by Vilnius Technical University scientists calculated the speed limit at 160 km/h, therefore, the analyzed calculation versions are based on a locomotive TEP 70 with 4 and 7 passenger cars and gives an approximate simulation of possible electric trains version and special-construction rolling-stock Pendolino [14-16]. Summary of analysis of versions of train time results on the railway line Vilnius – Kaunas is provided in Table 1.

An analysis of results of the traction calculation, we may conclude that a trip from Vilnius to Kaunas on a locomotive TEP 70 will take 52 minutes (with a stop in Kaišiadorys only) when the locomotive traction force is used to the maximum and there are no speed limits on the route. As compared with the current fastest trip from Vilnius to Kaunas (trains now take a minimum of 1 hour 12 minutes), this means economy of 20 minutes.

Table 1

Summary of analysis of versions of train time results on the railway line Vilnius – Kaunas

Version No.	Locomotive, train	Number of stops	Stops	Duration of travel from Vilnius to Kaunas (hours:minutes)
I	TEP 70 (7 cars)	1	Kaišiadorys	0:57
II	TEP 70 (4 cars)	1	Kaišiadorys	0:52
III	TEP 70 (4 cars)	3	Lentvaris Kaišiadorys, Pravieniškės	1:03
IV	Electric train	1	Kaišiadorys	0:54
V	Electric train	3	Lentvaris Kaišiadorys, Pravieniškės	0:58
VI	Pendolino	1	Kaišiadorys	0:51

Summary of investments needed for renovation of the railway line Vilnius – Kaunas to increase the speed limit to 160 km/h until 2010 is provided in Fig 1.

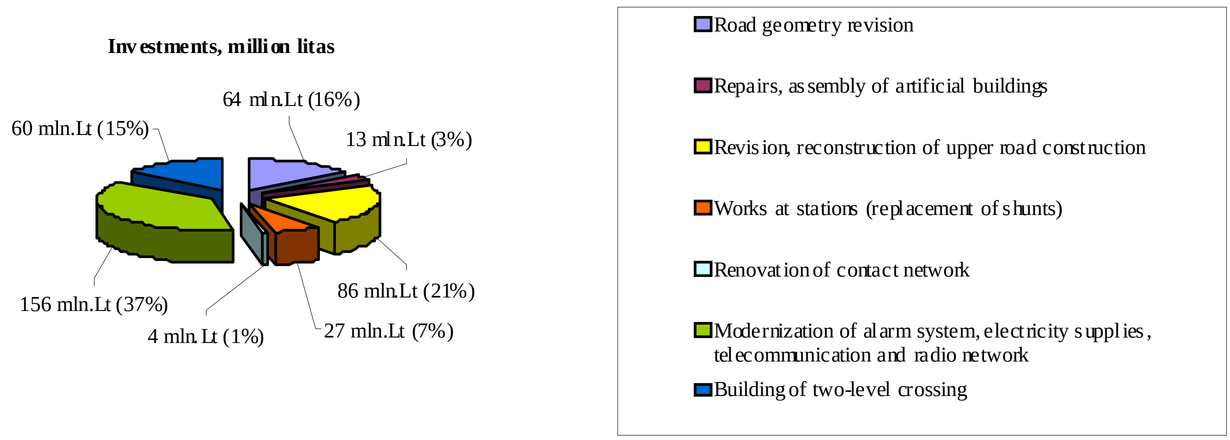

Fig. 1. Distribution of investment necessary for renovation of the railway line by types of work

4. Conclusions

The Vilnius-Kaunas dipole is a new-quality phenomenon in the development of the city network in Lithuania, which meets the most modern global urban tendencies and is an unavoidable process.

The core of the Vilnius-Kaunas dipole – the railway connection – should shaped as an organic part of the Rail Baltica network to not only serve the individual cities of Kaunas and Vilnius but also two of them as a unit treated as an integral urban arrangement. A modern high-speed railway should be the core of the dipole. The railway should be given priority, as the practice is in most European countries. Passengers value railways as a cheap, safe and comfortable way of reaching final destinations.

It is necessary to achieve that the trip between the final stations of the dipole took 30-35 minutes at most. This is the primary and most important condition for efficient functioning of the dipole as an organic connection between Vilnius and Kaunas. Location of the dipole's final stations should be in agreement with high-speed transport routes within Vilnius and Kaunas.

The European-standard railway line, as a branch of the Rail Baltica railway from Palemonas to Rykantai should be built in a single track formation, except for stretches of low-radius curves or train separation points. The railway line should go on a new route and cross the Neris river valley in the section between Rykantai and Pilaitė – the final passenger station of the railway and the high-speed tram.

Modernization of the existing railway line between Vilnius and Kaunas should be granted investments, which are necessary for elimination of main reasons that keep passenger train speeds under 160 km/h to ensure safe and high-speed communication. On a modernized railway line, a passenger train should make the trip from Vilnius to Kaunas with a single stop in Kaišiadorys in 52 minutes.

References

1. **Vanagas J.** Kaunas in Dipole: Benefits for the City // Build and Architecture (Statyba ir architektūra). 2005, No. 2, p. 21-23, No. 3, p, 36-38. (in Lithuanian)
2. **Vanagas J.** The Dipole of Vilnius and Kaunas: What is it Like? // Town Planning and Architecture (Urbanistika ir Architektūra), 2004, Vol. XXVIII, No. 4, p. 158-164. (in Lithuanian)
3. General Plan of the Territory of the Republic of Lithuania // Build and Architecture (Statyba ir architektūra), Vilnius: October 2002 (special edition), 56 p. (in Lithuanian)
4. Comprehensive plan of the territory of the Republic of Lithuania. The Ministry of Environment of the Republic of Lithuania. Vilnius, 2004. 68 p. (in Lithuanian)
5. Metropolitan Areas. Monograph – Interreg II C. Baltic Sea Region, Project No. 21, Potsdam, 2000. 90 p.
6. Study into Quality of Life in Region of Vilnius-Kaunas Dipole, Vilnius Gediminas Technical University, headed by **Vanagas J.**, 2004. 189 p. (in Lithuanian)
7. Strategic Plan for Vilnius-Kaunas Dipole. Vilnius City Municipality and Kaunas City Municipality. Vilniaus Planas and Kauno Planas, Vilnius: December 5, 2003. 38 p. (in Lithuanian)
8. Fesibility study of a tramway for Vilnius. GROUPE SYSTRA. Paris-Franse, 2002. 126 p.
9. **Butkevičius J.** Transportation of Passengers (Keleivių vežimai). Vilnius: Technika, 2002. 416. p. (in Lithuanian)
10. **Butkevičius J., Mazūra M., Ivankovas V., Mazūra S.** Analysis and forecast of the dynamics of passenger transportation by public land transport // Transport, 2004. Vol. XIX, No. 1, p. 3-8.
11. **Šeduikis A.** Rail Baltica in Lithuania // Build and Architecture (Statyba ir Architektūra), 2004, No. 4-5, p. 10-13. (in Lithuanian)
12. **Šeduikis A.** Rail Baltica to Reach Vilnius // Build and Architecture (Statyba ir Architektūra), 2004, No. 6, p. 20-21. (in Lithuanian)
13. New European-Track Railway Line from the Polish-Lithuanian Border to Kaunas and Multimodal Center. Final report by ALAnet GLOBAL. Vilnius, 2003. p. 122.
14. **Černiauskaitė L., Sakalauskas K., Milišiūnas A.** Technical and economic expedient research of modernisation railway line Vilnius – Kaunas // Material of the 4th International Conference „Transbaltica-03". Vilnius: Technika, 2003, p. 362 – 370. (in Lithuanian)
15. **Černiauskaitė L., Rezgaitis R.** Soliution of problems of train speed increment in Lithuanian railway lines. Journal of Civil Engineering and Management, 2003, Vol. IX, Supplement 1, p. 77-82.
16. **Černiauskaitė L., Sakalauskas K.** Technical and economical problems of the IX B and XI D international railway transport corridors integration into European railway transport network // Transport, 2003. Vol. XVIII, No 4, p. 143–152.

Authors index

INTELLIGENT TECHNOLOGIES IN LOGISTICS AND MECHATRONICS SYSTEMS (ITELMS'09).
Proceedings of the 4th International Conference. Held on June 4-5, 2009, Panevezys, Lithuania.

INTELEKTUALIOS TECHNOLOGIJOS LOGISTIKOJE IR MECHATRONINĖSE SISTEMOSE (ITELMS'09).
4-os tarptautinės konferencijos, įvykusios Panevėžyje 2009 m. birželio 4-5 d., pranešimų medžiaga (anglų kalba).

Maketavo D. Vaičiulis